

**Physiologically based pharmacokinetic modelling
to investigate the impact of aging
on drug pharmacokinetics
and drug-drug interaction magnitudes
in aging people living with HIV**

Inauguraldissertation

zur

Erlangung der Würde eines Doktors der Philosophie
vorgelegt der
Philosophisch-Naturwissenschaftlichen Fakultät
der Universität Basel

vorgelegt von

Felix Stader

aus

Radolfzell am Bodensee, Deutschland

Basel, 2020

Originaldokument gespeichert auf dem Dokumentenserver der Universität Basel
edoc.unibas.ch



Dieses Werk ist lizenziert unter einer Creative Commons Namensnennung – nicht kommerziell – keine
Bearbeitung 4.0 International Lizenz

Genehmigt von der Philosophisch-Naturwissenschaftlichen Fakultät

auf Antrag von:

Prof. Melissa A. Penny

Prof. Catia Marzolini

Prof. Manuel Battegay

Prof. Youssef Daali

Basel, 18.02.2020

Prof. Dr. Martin Spiess

Dekan

Table of Contents

Acknowledgment	Page 3
Publications contained in this thesis	Page 5
Abstract	Page 7
Chapter 1: General Introduction	Page 9
Chapter 2: Development of a Virtual Aging Population	Page 23
Chapter 3: Physiologically based Pharmacokinetic Model Development	Page 51
Chapter 4: Pharmacokinetic Changes in the Elderly	Page 87
Chapter 5: Antiretroviral Pharmacokinetics with Aging	Page 121
Chapter 6: Drug-Drug Interaction Magnitudes with Aging	Page 149
Chapter 7: Effective Method to Predict Drug Interactions	Page 199
Chapter 8: General Discussion	Page 221
References	Page 233
Appendix	Page 279

Acknowledgment

The three years journey of my PhD comes finally to an end and I would like to express by true gratefulness to all fellow travelers, who supported me during this exciting time.

Firstly, I would like to express my sincere gratitude to my supervisors Prof. Catia Marzolini, Prof. Melissa Penny, and Prof. Manuel Battegay, who were a brilliant, supportive team, leading to the success of this thesis. I would like to thank Prof. Catia Marzolini for her supportive supervision, her trust, and her granted freedom, which all allowed me to grow as a scientist and led to outstanding scientific results. I would like to thank Prof. Melissa Penny for all her advice and her introduction to the mathematical perspective of modelling and simulation. I was very grateful that Prof. Melissa Penny did not hesitate a single second to welcome me warmly and openly in her group. I would also like to thank Prof. Manuel Battegay for his valuable inputs to address important clinical aspects in HIV care. I am grateful for his constant scientific support and help through all times.

Secondly, I would like to thank Prof. Jürg Utzinger and the entire Swiss TPH, especially the group of Prof. Melissa Penny and Prof. Tom Smith, for giving me the possibility to conduct my scientific research in a very positive and inspiring work environment, which led clearly to the success of this work.

Thirdly, I would like to thank all my collaborators. Ms. Perrine Courlet, who provided the analytical method to measure all plasma concentrations from our conducted clinical study, and, Ms. Hannah Kinvig and Dr. Marco Siccardi for their scientific advice on active drug transporters and PBPK modelling.

Fourthly, I would like to thank the study participants, the clinic team of the University Hospitals Basel and Lausanne as well as the Swiss HIV Cohort Study, who supported the verification of my used modelling approach with clinically observed data.

Lastly and most importantly, I would like to thank my wife Barbara and my daughter Enya, who was born at the beginning of the PhD, for all their love, patience, and support during the entire time.

Basel, 20.01.2020

Felix Stader

Publications contained in this thesis

The provided list contains all publications that are used in this thesis. A full list containing all publications and conference presentations can be found in the appendix of this thesis.

Felix Stader has no conflict of interest to declare in any of the used publications contained in this thesis. The thesis was financially supported by the Swiss National Foundation (Grant No. 166204), the OPO Foundation, and the Isaac Dreyfuß Foundation. The co-authors provided valuable input regarding study design and data analyses, analytical techniques to measure in vitro parameters used for model development and plasma concentrations used for model verification, and revised the manuscripts. The author of this thesis was involved in the study design, data collection, data analysis, model development and verification, and writing of the manuscripts. Detailed information on the conflict of interest, funding sources, and contributions of co-authors can be found in each publication.

Stader F, Siccardi M, Battegay M, Kinvig H, Penny MA, & Marzolini C. Repository describing an aging population to inform physiologically based pharmacokinetic models considering anatomical, physiological, and biological age-dependent changes. *Clinical Pharmacokinetics*, **2019**. 58(4): 483-501.
DOI: 10.1007/s40262-018-0709-7
PMID: 30128967

Stader F, Penny MA, Siccardi M, & Marzolini C. A comprehensive framework for physiologically based pharmacokinetic modelling in Matlab®. *CPT Pharmacometrics & Systems Pharmacology*, **2019**. 8(7): 444-459.
DOI: 10.1002/psp4.12399
PMID: 30779335

Stader F, Kinvig H, Penny MA, Battegay M, Siccardi M, & Marzolini C. Physiologically based pharmacokinetic modelling to identify pharmacokinetic parameters driving drug exposure changes in the elderly. *Clinical Pharmacokinetics*, **2020**. 59(3): 383-401.
DOI: 10.1007/s40262-019-00822-9
PMID: 31583609

Stader F, Courlet P, Kinvig H, Battegay M, Decosterd LA, Penny MA, Siccardi M, & Marzolini C. Effect of ageing on antiretroviral drug pharmacokinetics using clinical data combined with modelling and simulation. *British Journal of Clinical Pharmacology*, **2020**. [Epub ahead of print].

DOI: 10.1111/bcp.14402

PMID: 32470203

Stader F, Decosterd LA, Stoeckle M, Cavassini M, Battegay M, Alves Saldanha S, Marzolini C, Courlet P, & the Swiss HIV Cohort Study. Aging does not impact drug-drug interaction magnitudes with antiretrovirals: a Swiss HIV Cohort Study. *AIDS*, **2020**. 34(6): 949-952.

DOI: 10.1097/QAD.0000000000002489

PMID: 32028327

Stader F, Courlet P, Kinvig H, Battegay M, Decosterd LA, Penny MA, Siccardi M, & Marzolini C. Clinical data combined with modelling indicate unchanged drug-drug interaction magnitudes in the elderly. *Clinical Pharmacokinetics & Therapeutics*, **2020**. [Epub ahead of print].

DOI: 10.1002/cpt.2017

PMID: 32772364

Stader F, Kinvig H, Battegay M, Khoo S, Owen M, Siccardi M, & Marzolini C. Analysis of clinical drug-drug interaction data to predict magnitudes of uncharacterized interactions between antiretroviral drugs and comedications. *Antimicrobial Agents & Chemotherapy*, **2018**. 62(7): 1-12.

DOI: 10.1128/AAC.00717-18

PMID: 29686151

Abstract

People living with HIV (PLWH) are aging but are often excluded from clinical studies because of pragmatical and ethical concerns. Therefore, the effect of aging on the pharmacokinetics and drug-drug interaction (DDI) magnitudes of antiretroviral drugs remain uncertain. Consequently, clinical guidance regarding dose adjustment for antiretroviral drugs and the clinical management of DDIs with advanced aging are missing.

Studies presented in this thesis combined clinically observed data with physiologically based pharmacokinetic (PBPK) modelling to investigate the continuous effect of aging on drug pharmacokinetics and DDI magnitudes. The PBPK model was developed in the mathematical programming language Matlab®. A virtual population considering age-related changes in demographics, physiology, and biology informed the model.

Clinically observed data of ten non-HIV drugs being commonly administered as comedications to aging PLWH were used to verify the predictive power of the PBPK model to simulate drug disposition in the elderly. Extrapolating the pharmacokinetics of all investigated ten drugs across adulthood (20 to 99 years) elucidated that the progressively decreasing drug clearance drove age-related pharmacokinetic changes, which itself was caused by the decline of the hepatic and renal blood flow and the glomerular filtration rate. Age-dependent pharmacokinetic alterations were independent of drug characteristics. Additional clinical data of 52 drugs obtained from young and elderly individuals verified this general model-based hypothesis.

Concentration-time profiles of ten antiretroviral drugs, belonging to the current first-line treatment, were obtained in two clinical studies including PLWH at least 55 years, who participated in the Swiss HIV Cohort Study. These clinically observed data were generally predicted within the 95% confidence interval of the PBPK model, demonstrating the ability of the used approach to predict real-life plasma concentrations from PLWH, who had a declined kidney function (e.g. the glomerular filtration rate was $65.6 \pm 19.2 \text{ mL/min/1.73m}^2$) and common comorbidities (e.g. hypertension). Age-related pharmacokinetic changes of antiretroviral drugs across adulthood were found to be similar to non-HIV drugs, indicating a marginal increase in antiretroviral drug exposure with advanced aging.

One of the conducted clinical studies in PLWH at least 55 years was designed to investigate DDI magnitudes between amlodipine, atorvastatin, or rosuvastatin and a dolutegravir (no interaction expected) or a boosted darunavir (high interaction potential) containing antiretroviral regimen. The comparison with historical data obtained in young PLWH aged 20 to 50 years yielded no changes in the DDI magnitudes between both investigated age groups. These clinically observed data were used to verify DDI simulations of the developed PBPK framework in the elderly and subsequently DDI magnitudes were predicted across the entire adult lifespan. The model indicated that DDI magnitudes were unchanged across adulthood regardless of the involved drugs, the DDI mechanism, or the sex of the investigated individual. This general model-based hypothesis was verified with independent clinically observed data from 17 DDIs.

As DDI magnitudes are not impacted by aging, static methods can be applied to predict DDI magnitudes in elderly patients, who receive two drugs with an uncharacterized DDI magnitude. Predictions are based on the fraction of metabolism by a specific enzyme and the strength of an inhibitor or inducer. In contrast to the PBPK approach, the static method provides a more straightforward supportive tool to rationalize dose adjustments to overcome a given DDI.

In conclusion, this thesis demonstrates marginal pharmacokinetic alterations of antiretroviral drugs and no age-related changes of DDI magnitudes. Therefore, a dose adjustment of antiretroviral drugs or a different management of DDIs in clinical practice are a priori not necessary when treating aging male and female PLWH in the absence of severe comorbidities. These general rules being broadly applicable to antiretroviral and non-HIV drugs support the overall care of elderly PLWH beyond HIV and therapies of future effective drugs.

Chapter 1:

General Introduction

1. General Introduction

1.1	Human immunodeficiency virus	Page 11
1.1.1	Viral structure and replication cycle	Page 11
1.1.2	Antiretroviral therapy	Page 12
1.1.3	The “graying” of the HIV epidemic	Page 14
1.2	Effects of aging on the pharmacokinetics of antiretroviral drugs	Page 16
1.3	Age-related comorbidities, polypharmacy, and drug-drug interactions in aging people living with HIV	Page 17
1.4	Physiologically based pharmacokinetic modelling	Page 19
1.5	Aim of this thesis	Page 21

1.1 *Human immunodeficiency virus*

Globally, 37.9 million people are living with the human immunodeficiency virus (HIV) of whom 1.7 million people got newly infected with HIV in 2018. The incidence of infections decreased by 70% in the past 20 years [1, 2]. When being untreated, the HIV infection leads to the acquired immunodeficiency syndrome (AIDS). AIDS is uniformly fatal, because the human body is no longer able to defend itself against invading pathogens [3]. AIDS-related deaths were reduced by over 70% in the past twenty years [1, 2], which is an achievement of the combined effective antiretroviral therapies that became available in the mid-1990 [4]. In 2019, 24.5 million people living with HIV (PLWH) had access to antiretroviral treatment [1], which needs to be lifelong because no current HIV therapy can eradicate the virus [5]. HIV is efficiently suppressed in PLWH on antiretroviral therapy by the disruption of different phases of the viral replication cycle.

1.1.1 Viral structure and replication cycle

HIV is a lentivirus belonging to the retroviruses. The variability of HIV is enormous, which remains a challenge in HIV care [6]. A key characteristic is that HIV has not the capability to reproduce itself and thus needs a suitable human or human primate host [7]. Two single ribonucleic acids (RNA) form the HIV genome that is contained in a protein capsid (Figure 1.1) [8]. Nine genes encode for three structural, two envelope, six regulatory proteins, and three enzymes [9]. HIV is further surrounded by a lipid bilayer derived from the host plasma membrane [10]. The outer membrane contains the two glycoproteins gp41 and gp120 that are essential to bind to the cluster of differentiation (CD) 4 receptor and the chemokine receptor (CCR) 5 [11]. The binding leads to the fusion of the viral and the host cell membrane and subsequently the viral capsid is released into the cytoplasm of the host cell [12]. The viral RNA is uncoated and the reverse transcriptase rewrites the single-stranded viral RNA into deoxyribonucleic acid (DNA) [13]. The newly synthesized viral DNA enters the nucleus of the host cell with the help of viral proteins [14]. In a next step, the viral integrase integrates the viral DNA into the cellular genome, where the cellular machinery is used for transcription and translation [15]. HIV synthesizes two large precursor proteins, namely the gag-polypolyprotein that contains the structural proteins for the capsid and the gag-pol protein that contains the viral enzymes such as the reverse transcriptase [16]. From the latter, the viral protease is cleaved autocatalytically and hydrolysis the precursor polyproteins [17]. Afterwards, the virus is assembled and leaves the host cell through budding [9].

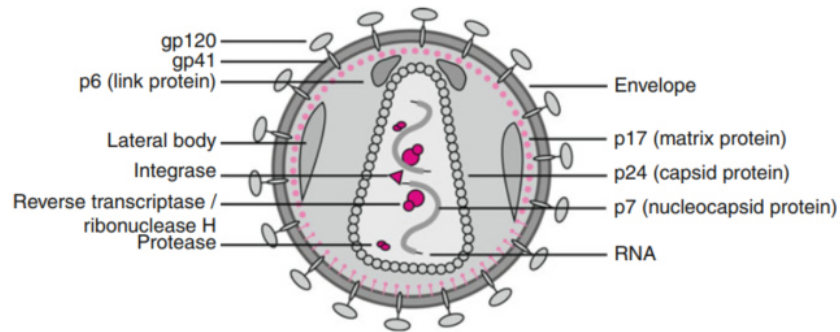


Figure 1.1: Schematic structure of HIV. Reproduced with permission from [18].

Key: gp = glycoprotein, p = protein, RNA = ribonucleic acid.

1.1.2 Antiretroviral therapy

Antiretroviral therapy can effectively control the replication rate of HIV and hence suppress the virus [19]. Six different antiretroviral drug classes (Table 1.1) are currently available, which disrupt different phases of the reproduction cycle of HIV (Figure 1.2) [20]. The first class are the nucleoside/nucleotide reverse transcriptase inhibitors (NRTI) that competitively inhibit the reverse transcriptase and thus disrupt the synthesis of the viral DNA. NRTIs are prodrugs that are phosphorylated to their active form by host kinases [21]. They are called the backbone of the antiretroviral therapy [22]. Currently, tenofovir (derived from the prodrugs tenofovir disoproxil fumarate or tenofovir alafenamide) and emtricitabine are commonly used NRTIs in antiretroviral therapy [20].

Table 1.1: Antiretroviral drugs currently in use, their antiretroviral drug classes, and targets.

Class	Target	Drugs
Nucleoside/nucleotide reverse transcriptase inhibitors (NRTI)	Reverse transcriptase	Abacavir Emtricitabine Lamivudine Tenofovir Zidovudine
Non-nucleoside reverse transcriptase inhibitors (NNRTIs)	Reverse transcriptase	Doravirine Efavirenz Etravirine Nevirapine Rilpivirine
Integrase inhibitors	HIV integrase	Bictegravir Dolutegravir Elvitegravir Raltegravir
Protease inhibitors	HIV protease	Atazanavir Darunavir Lopinavir Ritonavir
Entry inhibitors	Chemokine receptor 5 (CCR5) Glycoprotein (gp) 41 Cluster of differentiation (CD) 4 receptor	Maraviroc Albuvirtide Ibalizumab
Fusion inhibitors	Fusion of viral and host cell membrane	Enfuvirtide
Pharmacokinetic enhancers	Cytochrome P-450 (CYP) 3A inhibition	Ritonavir Cobicistat

In contrast to NRTIs, non-nucleoside reverse transcriptase inhibitors (NNRTIs) bind to the reverse transcriptase non-competitively, therefore blocking the ability to use endogenous nucleosides for the DNA synthesis [23]. Efavirenz and nevirapine are first generation NNRTIs, whereas rilpivirine, etravirine, and doravirine belong to the second and third generation, respectively [24, 25]. Integrase inhibitors such as raltegravir, dolutegravir, elvitegravir, and bictegravir belong to the third class of antiretrovirals. They block the integration of the viral DNA into the cellular host genome [26]. The fourth class are the protease inhibitors, which inhibit the maturation of the immature virions. The viral protease is no longer able to cleave the precursor polypeptides into functional proteins [27]. Atazanavir, darunavir, and lopinavir belong to protease inhibitors that are highly effective against HIV [28].

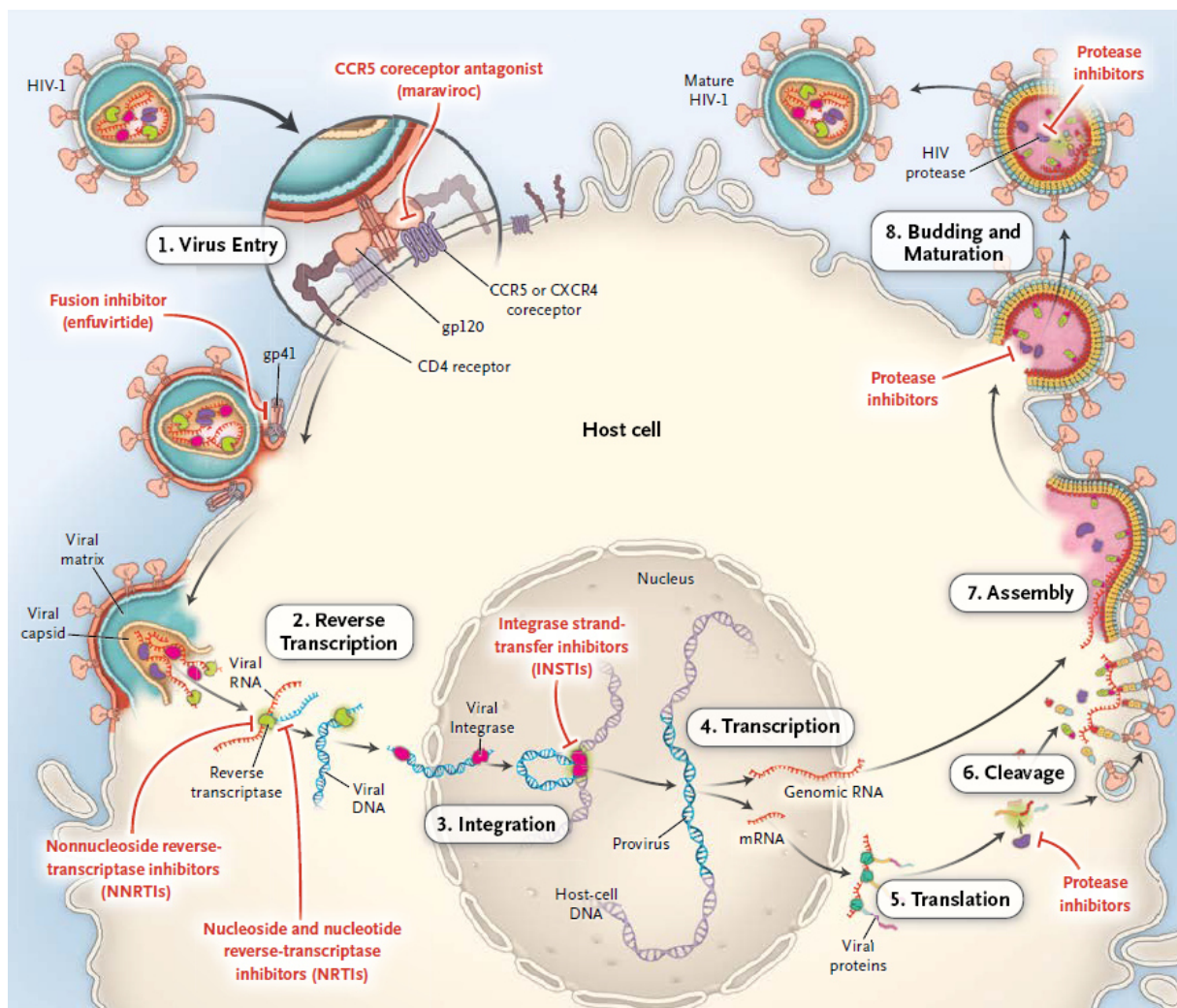


Figure 1.2: Reproductive cycle of HIV and targets for antiretroviral drugs. Explanations can be found in the main text. Reproduced with permission from [29], Copyright Massachusetts Medical Society.

Key: CD4 = cluster of differentiation 4, CCR5 = chemokine receptor 5, CXCR4 = CX-Chemokine receptor 4, DNA = deoxyribonucleic acid, gp = glycoprotein, RNA = ribonucleic acid.

Maraviroc, albuvirtide, and ibalizumab are entry inhibitors, which belong to the fifth class of antiretrovirals. Maraviroc binds reversibly to CCR5 and therefore, inhibits the fusion between the viral and the host cell membrane [30]. Maraviroc does not demonstrate efficacy in every PLWH and is therefore not recommended as first-line therapy [28]. Albuvirtide targets gp41 and the monoclonal antibody ibalizumab binds to the CD4 receptor, therefore blocking the entry of HIV into the host cell [31, 32]. The last class are the entry inhibitors with the therapeutic protein enfuvirtide being the only representative [33]. Enfuvirtide is only used if no other treatment option is available [28].

In addition to the six antiretroviral drug classes, there are two pharmacokinetic enhancers, ritonavir and cobicistat. They inhibit cytochrome P-450 (CYP) 3A leading to an increased drug exposure and consequently to a longer duration of the effect of other antiretrovirals metabolized by CYP3A [34, 35].

The treatment strategy is to combine three antiretroviral drugs that interrupt at least two different points in the replication cycle of HIV. The current recommendation as first-line therapy are two NRTIs combined with an integrase or protease inhibitor [36]. To increase the adherence of PLWH, different antiretroviral drugs are combined in a single tablet. Prevention strategies such as preexposure prophylaxis, which focuses on HIV-negative individuals who are at high risk of acquiring HIV [37], are also implemented.

1.1.3 The “graying” of the HIV epidemic

The highly effective antiretroviral therapy increased the life expectancy of PLWH through the last decades till it reached the life expectancy of the general population [38, 39]. Consequently, the number of aging PLWH is growing as shown by the age distribution of the Swiss HIV Cohort Study over the past 30 years (Figure 1.3) [40]. Worldwide, 6 million PLWH were older than 50 years by the end of 2018 [1]. Every second PLWH belonged to the aged group in the Western Countries [41]. The number of PLWH at least 50 years is projected to increase to over 70% in Europe by 2030 [42]. The general life expectancy in African countries, where the majority of PLWH live, is 55 to 60 years [43], and therefore only a minority of Africans living with HIV reaches the age of 50 years. In the future, the life expectancy of the general African population and Africans living with HIV are projected to increase, especially in Eastern and Southern Africa [43, 44]. Most PLWH aged older than 50 years acquired the disease earlier in life, but 17% of newly infected US-Americans were aged 50 years and older [45].

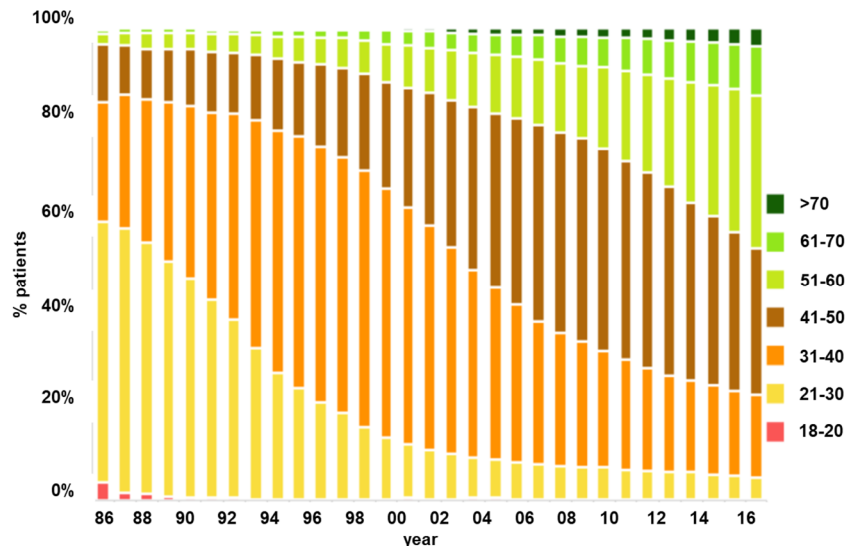


Figure 1.3: Age distribution of active patients by year in the Swiss HIV Cohort Study, 1986-2016 [40].

The age cut-off of 50 years to define an elderly PWLH was chosen historically with the finding that HIV accelerates aging [46-48], which is a matter of discussion given that not all PLWH have a shorter life-expectancy compared with the general population [38, 39]. Aging and HIV infection show similarities at the cellular level regarding inflammation and immunosenescence, which could lead to combined effects and hence accelerate aging [49, 50]. Furthermore, mortality was found to be increased in large cross-sectional studies. However, other studies found the mortality and the risk for comorbidities to be similar at all studied ages between PLWH and non-infected controls [41]. The observed difference of mortality between studies might be explained by different antiretroviral therapies. The first-generation protease inhibitors and NRTIs as well as efavirenz had more severe side effects such as glucose intolerance, hyperlipidemia or an added risk for chronic kidney disease that could contribute to aging [51-53]. In addition, the lifestyle between PLWH and the general population might differ in terms of smoking, alcohol, drug use, and other viral infections such as hepatitis [54].

In the absence of a pharmacological and clinical definition of an “elderly” individual [55], the age of 65 years is used, which is purely based on the age of retirement in Western Countries [56].

The “graying” of HIV brings new challenges to the care of PLWH besides virologic suppression [57]. Effects of aging on the pharmacokinetics and pharmacodynamics of antiretroviral therapy alone, frailty, age-related comorbidities, polypharmacy, and subsequently the risk for drug-drug interactions (DDIs) and inappropriate prescribing need to be considered in geriatric HIV care.

1.2 Effects of aging on the pharmacokinetics of antiretroviral drugs

Aging leads to demographical, physiological, and biological changes in men and women, which all could impact drug pharmacokinetics [58]. The effect of aging on the human body is extensively discussed in chapter 2. In brief, contradictory findings are reported for the effect of aging on drug absorption. Different studies found gastric emptying time to be slower, similar or faster in elderly compared with young individuals [59-64]. Distribution of drugs and consequently the volume of distribution could change with advanced aging, because of altered body composition with increased adipose tissue weight and reduced total body water in the elderly [65]. It is a matter of debate whether hepatic enzyme activity and therefore drug metabolism is altered with advanced aging; however, the small samples size and the general large variability of CYP and uridine diphosphate-glucuronosyltransferase (UGT) activity remains a challenge when investigating the impacted of aging on enzyme activity [66-68]. The hepatic drug clearance is affected by age-related alterations in the liver volume and the hepatic blood flow [69]. The most prominent change with aging is the decline in kidney function leading potentially to a change in renal drug clearance [70]. Despite the known physiological alterations with advanced aging, clinical studies investigating age-related pharmacokinetic changes of antiretroviral drugs are limited [71-75].

In a pilot study, the pharmacokinetics of two common antiretroviral regimens (tenofovir + emtricitabine + efavirenz or atazanavir/ritonavir) were assessed in six PLWH aged 55 to 65 years. The area under the curve (AUC) of tenofovir and boosted atazanavir decreased by 8 to 13% and 12% in aging compared with young PLWH. In contrast, the AUC of emtricitabine and ritonavir was increased by 19 to 78%. Exposure of efavirenz was unchanged in middle-aged PLWH [71]. A second study showed higher protease inhibitor concentrations with aging obtained from regular therapeutic drug monitoring, but no age-related pharmacokinetic changes for NNRTIs [73]. In a third study, the AUC of dolutegravir was unchanged in PLWH aged 60 to 79 years, whilst the peak concentration (C_{max}) increased by 25% compared with young PLWH [72]. A forth study supported the findings of the previous ones with a 40% decrease in boosted darunavir clearance in elderly PLWH and no age-related changes for dolutegravir and lamivudine [74]. In a fifth study, physiologically based pharmacokinetic (PBPK) modelling estimated the exposure of the renally cleared antiretroviral drugs emtricitabine, lamivudine, and tenofovir to be increased by 40%, 42%, and 48% in PLWH aged 65 to 74 years compared with young individuals aged 20 to 50 years [75].

There are substantial limitations to the available studies investigating the impact of aging on antiretroviral drug pharmacokinetics. These include the small number of individuals in each study particularly above the age of 65 years. Additionally, all aforementioned studies including the one which used PBPK modelling compared the pharmacokinetics between two groups (i.e. young subjects aged 20 to 50 years and elderly individuals aged at least 65 years); however, aging is a continuous process [58] and longitudinal data in the same individual are entirely lacking for antiretroviral and non-HIV drugs.

As a consequence of the limited clinical studies, drug labels of antiretrovirals do not give any dose recommendations for elderly PLWH [76-84], except for atazanavir for which no dose adjustment is necessary based on the age of the treated PLWH [85]. Thus, evidence-based prescribing is not possible when treating aging PLWH. Clinicians are faced with the challenge to adjust the dose based on empirical experience.

1.3 Age-related comorbidities, polypharmacy, and drug-drug interactions in aging people living with HIV

Aging PLWH in high income countries face the challenge of age-related comorbidities such as cardiovascular diseases, hypertension, dyslipidemia, diabetes, and depression [86]. The number of comorbidities increases with advanced aging [87]. In the French HIV Cohort, 4% of the enrolled PLWH aged 50 to 74 years had more than four comorbidities. The number increased to 18% in PLWH at least 75 years [88].

Given the high prevalence of age-related comorbidities, polypharmacy being defined as taken more than five concomitant drugs, is common amongst the elderly [86, 89]. Importantly, the antiretroviral regimen, consisting usually of three different antiretroviral drugs, is not considered for the definition of polypharmacy in HIV care to allow the comparison to non-infected individuals [90, 91]. Polypharmacy is more prevalent in middle-aged PLWH compared with the general population, but the difference is less marked with advanced aging [92]. This finding can probably be explained by the occurrence of age-related chronic diseases regardless of the HIV infection. Importantly, polypharmacy appears to increase with the duration of the HIV infection, which is explainable by the side effects of long-term antiretroviral

treatment [93]. The most commonly prescribed comedications in aging PLWH are cardiovascular drugs, antiplatelet/anticoagulant medications, and gastrointestinal agents [92, 94].

One issue of polypharmacy are DDIs, because the risk for a DDI increases exponentially with every drug taken [95]. Clinical management of DDIs is important, because DDIs can lead to unsafe or inefficacious therapies. Therefore, either doses of the victim drug can be adjusted to overcome a given DDI or alternative drugs with less interaction potential could be administered [96]. Antiretroviral drugs have a high DDI potential as they can serve as the victim drug, the inhibitor, or the inducer of a DDI. Examples of victim drugs are the integrase inhibitors raltegravir, dolutegravir, and bictegravir, the NNRTIs rilpivirine and doravirine as well as the entry inhibitor maraviroc, which are all extensively metabolized in the liver but have no inhibitory or inducing potential [78, 79, 84, 97-99]. Conversely, the boosting agent cobicistat inhibits hepatic enzymes [35], whereas the NNRTIs efavirenz and etravirine have inducing properties [100, 101]. Ritonavir, a protease inhibitor used to boost other antiretrovirals, has both inhibitory (e.g. CYP3A) and inducing (e.g. CYP2C9, CYP2C19, UGT1A1) potential, which is different to the second pharmacokinetic enhancer cobicistat, which is more selective towards CYP3A inhibition [102]. Additionally, antiretroviral drugs can lead to transporter mediated DDIs. Atazanavir, darunavir, and ritonavir can competitively inhibit the hepatic organic anion transporting polypeptide (OATP) 1B1 [103]. In addition to enzyme- and transporter-mediated DDIs in the liver, intestine, and kidney, there can be DDIs at the level of drug absorption. Neutralizing agents change the gastric pH and lead consequently to a reduced absorption of atazanavir and rilpivirine [104, 105]. All integrase inhibitors contain an ion-chelating motif that could lead to complex formation with divalent cations such as calcium, when the drug is taken together with mineral supplements or antacids, containing for instance calcium carbonate, which decreases the absorption of integrase inhibitors [106]. When administering two drugs with a similar toxicity profile, a pharmacodynamic interactions might occur with an additive risk for adverse events.

A study conducted in the framework of the Swiss HIV Cohort Study found a higher DDI frequency in PLWH at least 50 years (51%) compared with PLWH aged 20 to 50 years (35%) [94], manifesting that the risk for DDIs increases with advanced aging [48, 86, 107, 108]. Consistent with age-dependent comorbidities occurring in elderly PLWH, DDIs involving antiretrovirals are commonly observed with cardiovascular drugs and psychotropic drugs [48, 92, 94, 107, 108]. Despite the declining DDI potential

of newer antiretroviral drugs, the number of DDIs is similar which is explained by the high prevalence of age-related comorbidities and the consequent use of more medications [109].

Only a limited number of drug combinations are evaluated in clinical studies. The entire variety of prescribed drug combinations in clinical practice cannot feasible or pragmatical be studied. Generally, the effect of one strong inhibitor or inducer is investigated on the victim drug of interest leading to missing guidance of firstly moderate perpetrators and secondly of DDIs between several different administered drugs that might interact mutually. To rationalize the clinical management of DDIs, estimates for DDI magnitudes can be obtained from the fraction metabolized by a certain enzyme and the strength of an inhibitor or inducer to alter the activity of this specific enzyme. Before using a prediction method, appropriate verification would be necessary, which has not been performed for antiretroviral drugs [110].

Additionally, clinical studies investigating the pharmacokinetics and DDI magnitudes are often conducted in healthy volunteers, making it challenging to understand the effect of the disease. Furthermore, the impact of aging on the inhibition and induction of enzymes and transporters is largely unknown, but DDI studies in the elderly are hardly conducted. The DDI magnitude of midazolam administered with clarithromycin was shown to be similar between young individuals aged 20 to 50 years and elderly subjects aged at least 65 years [111, 112], but the effect of advanced aging on other DDI scenarios remains uncertain. However, there are several challenges when designing a clinical DDI study in aging PLWH. HIV therapy cannot be disrupted, because current antiretroviral therapies only suppress the virus, but cannot eradicate it. Therefore, a virologic failure with increasing virions would likely be the result of the treatment interruption [113]. Furthermore, participants should have no chronic disease or medication that could potentially influence the DDI of interest, because otherwise it is not possible to understand the effects mechanistically.

1.4 Physiologically based pharmacokinetic modelling

To overcome the practical and ethical limitations to conduct clinical studies in the elderly, PBPK modelling offers the possibility to perform virtual clinical trials. The development of a PBPK model is extensively discussed in chapter 3. In brief, a PBPK model describes the absorption, distribution, metabolism, and excretion of a drug mathematically in a physiologically relevant compartmental

structure, where each compartment represents an organ or tissue (Figure 1.4) [114]. Dynamic movement of the drug between the model compartments is mediated by the regional blood flows and described by ordinary differential equations. An advantage of the PBPK approach is the prediction of intracellular concentrations that cannot easily be measured in humans. The distribution into a compartment can be either limited by perfusion (well-stirred models) or by the cell membrane (permeability-limited models) [115].

The PBPK model is informed by virtual populations (system data), drug, and trial design data [115]. Virtual populations are generated based on measured organ weights, regional blood flows, and other important physiological parameters to predict drug pharmacokinetics [58]. By incorporating variability for all system parameters, certain subpopulation with high risk for DDIs (e.g. poor metabolizers for CYP2D6) can be identified [116]. A combination of measured in vitro and clinically observed in vivo data are used to correctly simulate the absorption, distribution, metabolism, and elimination of a drug [117]. System and drug data are combined in the trial design component considering dose, dosing regimen, route of administration, and number of virtual individuals to simulate the clinical scenario of interest. Importantly, simulations of the PBPK model need to be verified against clinically observed data before extrapolating to unknown clinical scenarios of interest.

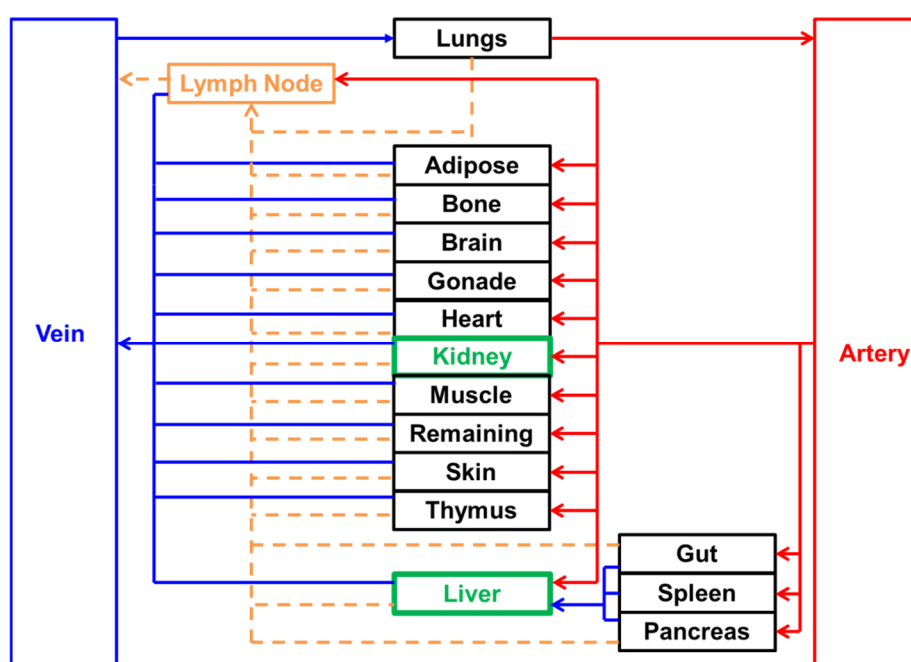


Figure 1.4: Structure of a whole-body PBPK model. Perfusion-limited and permeability-limited compartments are shown in black and green. Venous blood flows, arterial blood flows, and lymphatic flows are displayed in blue, red, and orange, respectively. Adapted from [118].

1.5 Aim of this thesis

The aim of this thesis was to investigate the continuous effect of aging on drug pharmacokinetics and DDI magnitudes by combining clinically observed data with modelling and simulation. The two-research questions of this thesis were:

- 1) Do the pharmacokinetics of antiretrovirals change with aging to a degree that would support a dose adjustment based on the age of the treated PLWH?
- 2) Are DDI magnitudes impacted by aging and is there consequently the need for a different clinical management of DDIs?

To answer the two research questions, firstly, age-related demographical, physiological, and biological changes were analyzed to generate a virtual aging population (Chapter 2). Secondly, a PBPK model framework was coded in the mathematical programming language Matlab® and informed by the developed virtual aging population (Chapter 3). Thirdly, the developed PBPK model and population were verified against published clinical data for ten non-HIV drugs that are commonly used as comedications in aging PLWH. The PBPK model determined the continuous effect of aging on drug pharmacokinetics and the cause for observed age-related changes of drug exposure (Chapter 4). Subsequently, the found rules for non-HIV drugs were applied to antiretroviral drugs after verifying the predictive performance of the developed PBPK model to simulate antiretroviral drug disposition against clinically observed data from PLWH at least 55 years ([74]; Chapter 5). Fourthly, a prospective clinical study was conducted in the framework of the Swiss HIV Cohort Study at the University Hospitals Basel and Lausanne to investigate for the first time DDI magnitudes between antiretroviral drugs and cardiovascular agents in elderly PLWH. Consequently, these clinically observed data were used to verify the predictive potential of the developed PBPK model to simulate DDI magnitudes in the elderly. Afterwards, the age-dependency of 50 DDI magnitudes, developed during all studies contained in this thesis, were analyzed (Chapter 6). Lastly, a predictive, static tool was developed and verified for DDIs involving antiretrovirals to quickly assess magnitudes of uncharacterized DDIs in HIV care (Chapter 7).

Chapter 2:

Development of a Virtual Aging Population

2. Development of a Virtual Aging Population

2.1	Abstract	Page 26
2.2	Key Points	Page 27
2.3	Introduction	Page 27
2.4	Methods	Page 28
2.4.1	Data sources	Page 28
2.4.2	Data analysis	Page 30
2.5	Results	Page 31
2.5.1	Age and sex distribution	Page 32
2.5.2	Body height and body weight	Page 32
2.5.3	Liver	Page 34
2.5.4	Kidney	Page 36
2.5.5	Adipose tissue	Page 38
2.5.6	Muscle	Page 38
2.5.7	Brain	Page 39
2.5.8	Heart	Page 39
2.5.9	Blood	Page 40
2.5.10	Other organs	Page 42
2.5.11	Tissue composition	Page 42
2.5.12	Parameters affecting drug absorption	Page 43
2.6	Discussion	Page 45
2.7	Conclusion	Page 49
2.8	Electronic Supplementary Information	Page 50

This chapter is a pre-printed version of a peer-reviewed original research article published under the following reference:

Repository describing an aging population to inform physiologically based pharmacokinetic models considering anatomical, physiological, and biological age-dependent changes

Felix Stader, Marco Siccardi, Manuel Battegay, Hannah Kinvig, Melissa A Penny, & Catia Marzolini

Clinical Pharmacokinetics 2019; 58(4): 483-501.

DOI: 10.1007/s40262-018-0709-7

2.1 Abstract

Background:

Aging is characterized by anatomical, physiological, and biological changes that can impact drug pharmacokinetics. The elderly are often excluded from clinical trials and knowledge about drug pharmacokinetics and drug-drug interaction magnitudes are sparse. Physiologically based pharmacokinetic modelling can overcome this clinical limitation but detailed descriptions of the population characteristics are essential to adequately inform models.

Objective:

The objective of this study was to develop and verify a population database for aging Caucasians considering anatomical, physiological, and biological system parameters required to inform a physiologically based pharmacokinetic model, which includes population variability.

Methods:

A structured literature search was performed to analyze age-dependent changes of system parameters. All collated data were carefully analyzed, and descriptive, mathematical equations were derived.

Results:

A total of 362 studies were found of which 318 studies were included in the analysis as they reported rich data for anthropometric parameters and specific organs (e.g. liver). Continuous functions could be derived for most system parameters describing a Caucasian population from 20 to 99 years of age with variability. Areas with sparse data were identified such as tissue composition, but knowledge gaps were filled with plausible qualified assumptions. The developed population was implemented in Matlab® and estimated system parameters from 1,000 virtual individuals were in accordance with independent observed data, showing the robustness of the developed population.

Conclusion:

The developed repository for aging subjects provides a singular specific source for key system parameters needed for physiologically based pharmacokinetic modelling and can in turn be used to investigate drug pharmacokinetics and drug-drug interaction magnitudes in the elderly.

2.2 Key Points

The developed repository provides a singular specific source of age-dependent anatomical, physiological, and biological system parameters required to inform physiologically based pharmacokinetic models. The parameters and associated developed equations can be implemented into existing physiologically based pharmacokinetic frameworks and can be used to overcome sparse clinical data in subjects at least 65 years to investigate age-dependent changes in drug pharmacokinetics and drug-drug interaction magnitudes *in silico*. These parameterized and informed physiologically based pharmacokinetic models for the elderly can provide more rational frameworks for dose-adjustments to overcome drug-drug interactions.

2.3 Introduction

Worldwide, the number of elderly people has increased substantially in the recent years [119]. An “elderly” individual is defined as being above the age of 65 years [56], which is in line with the age of retirement in most Western countries. Older individuals are prone to multi-morbidities and hence polypharmacy and consequently drug-drug interactions (DDIs) [86, 120, 121]; however, there is no clear pharmacological or clinical definition of an “elderly” [55]. Often, elderly subjects are excluded from clinical trials, resulting in a general lack of knowledge about the efficacy, safety, and pharmacokinetics of a drug at different ages [122].

There are certain age-dependent anatomical, physiological, and biochemical changes influencing drug pharmacokinetics including decreased kidney weight [123], reduced renal blood flow [124], declined glomerular filtration rate [125], and reductions in liver volume and hepatic blood flow [126-128]. For other parameters such as enzyme and transporter abundance, or the concentration of plasma-binding proteins, data are limited, contradictory, or entirely missing. In addition, it is difficult to investigate aging because other environmental and behavioral factors such as diseases, food, and smoking can have effects themselves or enhance the aging process [129].

Physiologically based pharmacokinetic (PBPK) modelling can help to overcome the lack of clinical data and to understand drug absorption, distribution, metabolism, and elimination at different ages. Furthermore, PBPK models have the ability to predict DDI magnitudes in aging individuals and support

more rational identification of dose adjustments to overcome given DDIs. To develop a PBPK model, system data (where system refers to the population of interest, e.g. elderly) are required to inform the PBPK model. To generate reliable predictions, a comprehensive description of system characteristics is essential to fully represent the population of interest. To date, only two databases have been published to inform PBPK models for the elderly, of which one does not distinguish between ethnicities [130] and the other does not consider population variability and provides no descriptive functions of physiological and anatomical parameters [131].

The objective of this work was to collate and analyze data from the literature with the view to create a new comprehensive description of system characteristics for PBPK modelling and to address shortcomings of previous databases. The work focuses on parameters to inform a PBPK model for aging people that considers population variability, and to develop continuous functions describing physiological parameters of interest between 20 and 99 years of age for a Caucasian population.

2.4 Methods

2.4.1 Data sources

A structured literature search was performed using the MEDLINE database for age-dependency of anatomical, physiological, and biological parameters required to inform a PBPK model for aging subjects. Keywords used were “aging”, “elderly” or “geriatric” plus the parameter of interest (Table 2.1 and Figure 1.4 for the investigated compartments of the developed PBPK model). No restrictions were applied regarding the language or the publication year of the article. Abstracts were screened, and studies included if the study population were Caucasians, at least age has been reported in addition to the parameter of interest, and subjects were healthy or their disease/organ function was deemed unlikely to affect the parameter of interest such as the effect of chronic liver disease on brain blood flow [132]. Studies performed with North Americans and Australians were considered if at least 80% of the study population were of European heritage. Studies including subjects over the age of 65 years should at least report a mean age per age decade. The reference list of chosen articles was manually screened to identify further references.

Table 2.1: System parameters necessary to describe a population of interest.

Demographics	Blood	Tissues	Liver	Kidney	GI tract
age distribution	hematocrit	tissue weight	HPGL / MPPGL	glomerular filtration rate	volumes and blood flows of different segments
proportion of women	albumin	tissue density	hepatic CYP abundance and turnover		gastric pH
body height	alpha-acid glycoprotein	tissue composition	hepatic UGT abundance and turnover		gastric emptying time
body weight		vascular space of a tissue	hepatic transporter abundance and turnover		intestinal CYP abundance and turnover
frequency of enzyme and transporter genotypes and phenotypes		interstitial space of a tissue			intestinal transporter abundance and turnover
		intracellular space of a tissue			
		cardiac output and regional blood flows			
		total lymph flow and regional lymph flows			

Key: CYP = cytochrome-P450, GI = gastrointestinal, HPGL = hepatocytes per gram liver, MPPGL = microsomal protein per gram liver, UGT = uridine diphosphate-glucuronosyltransferase.

2.4.2 Data analysis

Data analysis was performed in Matlab® 2015b. Data were converted to consistent units and a normal distribution was assumed for each parameter to make published data comparable. If a study reported the median, minimum, and maximum, data were converted to the arithmetic mean and standard deviation according to Hozo *et al.* [133] and if the interquartile range was given, the conversion was done according to Wan *et al.* [134].

Collated data were separated into a development and verification dataset. Studies in the development dataset were required to report age, sex, body height, body weight, and ethnicity in addition to the parameter of interest as necessary covariates to describe correlations. Otherwise, studies with less reported covariates were used in the verification dataset. If at least three different studies covering the entire age range with at least one value in each age decade and all required covariates for the development dataset were available for a parameter of interest, the data were randomly separated into a development and a verification dataset. In the case of missing covariates such as anthropometric parameters in the verification dataset or cardiac output for regional blood flow analysis, the covariates have been estimated by the derived equations following the approach by Williams & Leggett [135]. The body surface area was calculated according to DuBois and DuBois [136].

We performed a weighted linear regression to derive descriptive continuous equations for the parameter of interest from 20 to 99 years considering age, sex, anthropometric parameters, location of the study, the publication year, and methods of measurement as independent variables. Location was used as an independent variable to investigate if studies conducted in Europe, North America, and Australia can be combined without bringing a bias into the data. Publication year has been used to investigate differences in key parameters (e.g. body weight) over the last century and if different methods used at different times have an impact. Data obtained by different methods have only been pooled when there was no significant difference between methods.

Linear, polynomial, and exponential functions were investigated during the regression analysis. Covariates with a p-value below 0.01 have been considered as significant. Visual and numerical regression diagnostic were performed. The corrected Akaike's information criterion was used for

numerical diagnostics to select the best fitted function [137]. Variability for each parameter was calculated as the weighted coefficient of variance (CV) of the development dataset for each individual mean and standard deviation (equation 1) and it was visually investigated whether age had an impact on variability. The variability of a parameter of interest was estimated by the variability of the covariates describing the parameter of interest and, if necessary, additional random variability to fully capture the observed variability.

$$CV = \frac{\text{standard deviation}}{\text{mean}} \quad (1)$$

The derived equations for all parameters necessary to describe a white population have been implemented in Matlab® and 1,000 virtual men and women have been created and the estimated system parameters have been compared to the independent verification dataset. Normal distribution with the derived CV (Table 2.2) was used to describe variability of the parameter of interest. Furthermore, it was analyzed if the sum of organ weights and regional blood flows did not exceed body weight and cardiac output.

2.5 Results

A total of 362 studies were found of which 318 studies were included in the analysis. Studies were mostly excluded because the age or ethnicity of the study population was insufficiently defined. Rich data were found for anthropometric parameters (body height and body weight), adipose tissue, brain, heart, kidney, and liver. Data for some regional blood flows, such as to the bone, and in general composition of tissues were difficult to obtain from the literature. Although including data for centenarians, most of the data were found for ages up to the mid-80s identifying a general knowledge gap for very old individuals. Derived equations and the population variability expressed as the CV can be found in Table 2.2. Detailed information on the number of subjects in each age decade used in the development dataset, the number of total studies in the development and verification dataset, the methods used to measure the parameter of interest, the study location, and the references can be found for each investigated parameter in the electronic supplementary material of the published article (<https://link.springer.com/article/10.1007%2Fs40262-018-0709-7#SupplementaryMaterial>).

2.5.1 Age and sex distribution

Data regarding age and sex distribution were taken from Eurostat [138] for all 28 member states of the European Union and the Federal Office for Statistics of Switzerland (Figure 2.1) [139]. The number of subjects in each age decade was found to be uniform between 20 and 59 years. The number of subjects declined from the age of 60 years, with only 2% of the Swiss population being above 90 years of age. A Weibull distribution with $\alpha = 1.55$ and $\beta = 61.73$ best described the age distribution. The proportion of women was found to be 50% of the population in Europe till the age of 69 years and increased to over 80% for very old Swiss subjects above the age of 100 years. In all following equations, age is expressed in years and sex is either 0 for men or 1 for women.

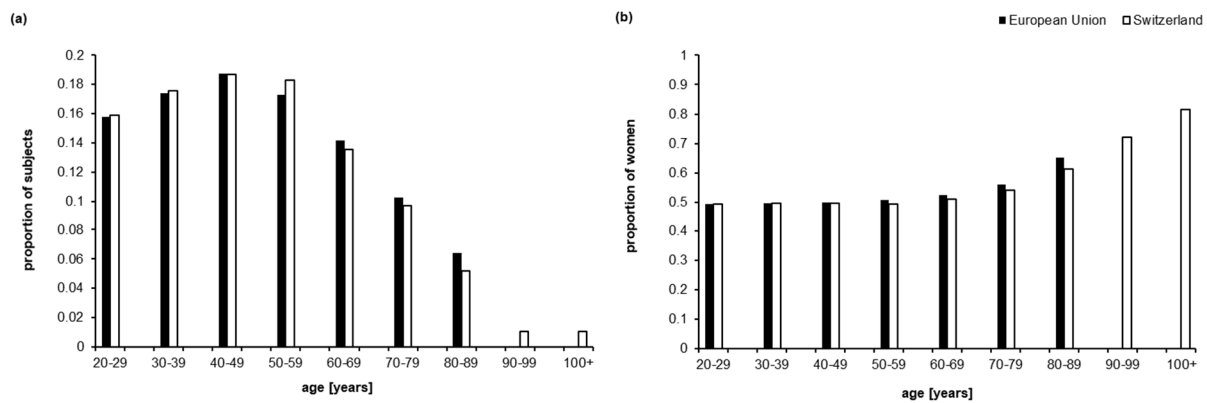


Figure 2.1: Proportion of subjects (a) and proportion of women (b) per age decade. Data are from the 28 member states of the European Union (black bars) and Switzerland (white bars).

2.5.2 Body height and body weight

Anthropometric data of 106,698 Caucasians have been analyzed in the developmental dataset [139-185] and the derived equations have been verified with data from 14,096 subjects [186-201]. The mean body height of Caucasians aged 20 to 59 years was 178 cm for men and 166 cm for women with a sex-independent CV of 3.8%. Body height declined by 2% per age decade from the age of 60 years (Figure 2.2a). The difference between men and women was constant at all age ranges. Location was found to be a significant variable during regression, with lower height observed in Southern Europe, and an exclusion of data reported from Portugal, Spain, and Italy led to a non-significance of location.

The mean body weight of a Caucasian aged 20 to 49 years was 79.9 kg for men and 64.1 kg for women with a CV of 15.7% (Figure 2.2b). Body weight increased in subjects in the fifth and sixth age decade by about 4% and decreased afterwards by about 10% in each age decade. In women, the decline started one age decade later than in men. In contrast to body height, location was not significant for body weight, but publication year was with a significant increase since 2000.

Table 2.2: Descriptive equations and population variability for anatomical, physiological, and biological parameters necessary to inform a PBPK model. Virtual subjects from 20 to 99 years can be generated. Blood flows are relative to cardiac output and the variability is only propagated from cardiac output.

Parameter	Unit	Descriptive equation	CV [%]
Body height	cm	$-0.0039 \times Age^2 + 0.238 \times Age - 12.5 \times Sex + 176$	3.8
Body weight	kg	$-0.0039 \times Age^2 + 1.12 \times Body\ height + 0.611 \times Age - 0.424 \times Sex - 137$	15.2
Lung weight	kg	$e^{(0.028 \times Body\ height + 0.0077 \times Age - 5.6)}$	0
Adipose tissue weight	kg	$0.68 \times Body\ weight - 0.56 \times Body\ height + 6.1 \times Sex + 65$	29.6
Bone weight	kg	$e^{(0.024 \times Body\ height - 1.9)}$	13.2
Brain weight	kg	$e^{-0.0075 \times Age + 0.0078 \times Body\ height - 0.97}$	9.0
Gonad weight	kg	$-0.00034 \times Body\ weight - 0.00022 \times Age - 0.03 \times Sex + 0.072$	34.8
Heart weight	kg	$0.34 \times BSA + 0.0018 \times Age - 0.36$	17.9 (m), 22.7 (f)
Kidney weight	kg	$-0.00038 \times Age - 0.056 \times Sex + 0.33$	19.3 (m), 23.2 (f)
Muscle weight	kg	$17.9 \times BSA - 0.0667 \times Age - 5.68 \times Sex - 1.22$	11.8
Skin weight	kg	$e^{(-0.0058 \times Age - 0.37 \times Sex + 1.13)}$	8.3
Thymus weight	kg	0.0221	44.8
Gut weight	kg	$3E^{-06} \times Body\ height^{2.49}$	7.3
Spleen weight	kg	$e^{1.13 \times BSA - 3.93}$	51.7
Pancreas weight	kg	0.103	27.8
Liver weight	kg	$e^{(0.87 \times BSA - 0.0014 \times Age - 1.0)}$	23.7
Blood weight	kg	$e^{(0.067 \times BSA - 0.0025 \times Age - 0.38 \times Sex + 1.7)}$	10.4
Cardiac output (CO)	L/h	$159 \times BSA - 1.56 \times Age + 114$	21.1
Adipose tissue blood flow	% of CO	$(0.044 + 0.027 \times Sex) \times Age + 2.4 \times Sex + 3.9$	-
Bone blood flow	% of CO	5	-
Brain blood flow	% of CO	$e^{-0.48 \times BSA + 0.04 \times Sex + 3.5}$	-
Gonad blood flow	% of CO	$-0.03 \times Sex + 0.05$	-
Heart blood flow	% of CO	$-0.72 \times Body\ height - 10 \times Sex + 134$	-
Kidney blood flow	% of CO	$-8.7 \times BSA + 0.29 \times Body\ height - 0.081 \times Age - 13$	-
Muscle blood flow	% of CO	$-6.4 \times Sex + 17.5$	-
Skin blood flow	% of CO	5	-
Thymus blood flow	% of CO	1.5	-
Gut blood flow	% of CO	$2 \times Sex + 14$	-
Spleen blood flow	% of CO	3	-
Pancreas blood flow	% of CO	1	-
Liver blood flow	% of CO	$-0.108 \times Age + 1.04 \times Sex + 27.9$	-
Albumin	g/L	$-0.0709 \times Age + 47.7$	7.9
GFR	mL/min	$e^{-0.0079 \times Age + 0.5 \times BSA + 4.2}$	14.7

Key: BSA = body surface area, CV = coefficient of variance, GFR = glomerular filtration rate, m = male, f = female.

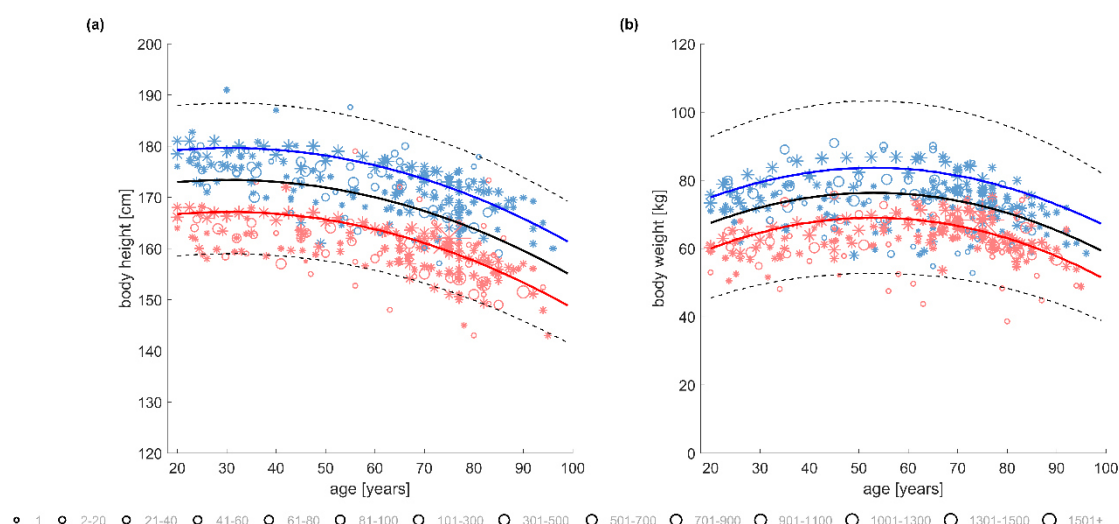


Figure 2.2: Body height (a) and body weight (b) per age decade in an aging population. The blue, red, and black lines represent the predicted mean of virtual men, virtual women, and from all virtual subjects, respectively. The dashed lines represent the 5 and 95% confidence interval of the predictions. Stars show observed data from the development and circles represent overserved data from the independent verification dataset. The size of the stars and circles indicates the size of the studied population.

2.5.3 Liver

Liver weight

The liver is the major organ of drug metabolism. Liver weight was analyzed from over 3,000 subjects [144, 156, 166, 167, 170, 184, 187, 193, 202, 203] and was found to be on average 1.78 kg in men and 1.49 kg in women with a CV of 23.7% till the age of 65 years. Thereafter, liver weight decreased by 10 to 15% in women per age decade reaching 1.03 kg at the age of 100 years. The decrease in men was around 20% per age decade reaching 1.01 kg on average in 90 years old individuals (Figure 2.3a).

Liver blood flow

Absolute total liver blood flow decreased by 60% between 60 and 90 years in men and women, but relative to cardiac output the changes were only significant between 90 and 100 years of age (Figure 2.3b) [128, 204]. The age-dependent changes in total liver blood flow might come from changes of the splanchnic blood flow [192, 204-209], explaining observed differences in the first pass effect between young and old subjects [210-212]. The hepatic arterial blood flow appears to be constant with age [135, 204, 213].

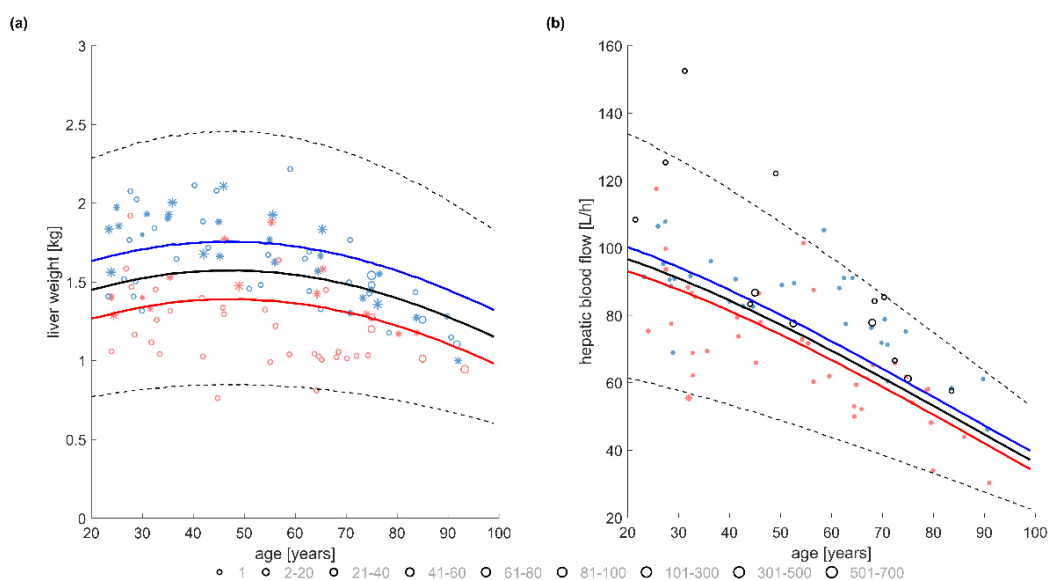


Figure 2.3: Liver weight (a) and hepatic blood flow (b) per age decade in an aging population. The blue, red, and black lines represent the predicted mean of virtual men, virtual women, and from all virtual subjects, respectively. The dashed lines represent the 5 and 95% confidence interval of the predictions. Stars show observed data from the development and circles represent observed data from the independent verification dataset. Black circles represent data from an undefined gender population. The size of the stars and circles indicate the size of the studied population.

In-vitro-to-in-vivo extrapolation factors

PBPK models are informed by in-vitro-to-in-vivo extrapolation, meaning that for instance the in vivo clearance is extrapolated from measured in vitro data. Hepatic scaling factors like the hepatocellularity or microsomal proteins per gram liver are needed [214]. Barter *et al.* reported age-dependent equations for hepatocytes per gram liver [215] and microsomal proteins per gram liver [216] with the oldest individuals in the analysis being between the mid-70s and the early 80s.

Hepatic enzyme activity

Studies concerning the age-dependency of hepatic cytochrome P-450 (CYP) enzyme activity are sparse and contradictory. The biggest challenge is the high variability in hepatic CYP enzyme abundance [217, 218] and the small sample size generally used for analysis [66, 219]. In a recent large meta-analysis investigating hepatic CYP abundance to inform PBPK models, age was only a significant covariate for CYP2C9 [218]. It is worthwhile mentioning, that the different genotypes known for CYP2C9 increase the sample size needed to identify age-dependency even further. A significant age-dependency was detected for CYP1A2, CYP2D6, and CYP2E1 in a different study, but not for CYP2C9 [67]. In a third

study, CYP1A2 activity was reported to be independent of age [68]. CYP3A4 activity is consistently reported to be not affected by aging between different studies [220-222].

Posalek *et al.* investigated drug clearances in the elderly for probe substrates such as caffeine (CYP1A2), warfarin (CYP2C9), phenytoin (CYP2C19), desipramine (CYP2D6), and midazolam (CYP3A) and found a clearance decrease of 30 to 40% in 70 years old subjects compared with young individuals, which can be explained by the decline in liver volume and hepatic blood flow rather than hepatic CYP enzyme activity [223]. In addition inflammation affects CYP enzyme activity [224], making it difficult to analyze data from non-healthy elderly individuals.

Uridine diphosphate-glucuronosyltransferase (UGT) activity is reported to be independent of age in the literature [67, 225-227]. Taken together, this lack of evidence and data to inform age dependency necessitates a more judicious approach assuming no age-dependent hepatic enzyme activity and thus assuming the same values in aging subjects as in young individuals.

Hepatic drug transporter activity

Recently, a compact meta-analysis about hepatic drug transporter abundance to inform a PBPK model was published and age was tested as a covariate in the analysis and was reported to be not significant for any hepatic drug transporter [228]. In a PBPK model, we are interested in activity rather than abundance because the activity of enzymes and drug transporters can explain the clinically observed data. If the abundance of drug transporters does not change, there might still be an age-dependent difference in drug transporter activity; however, these data are currently not available. Comparable to hepatic enzymes, it is therefore recommended to use the same drug transporter activity in elderly as in young subjects.

2.5.4 Kidney

Kidney weight

The literature search yielded nine different studies with a total of 1,620 data points measuring kidney weight after autopsy (Figure 2.4a) [144, 156, 157, 166, 167, 170, 184, 193, 200]. The average kidney weight in young male and female individuals was 0.318 kg with a CV of 19.3% and 0.259 kg with a CV

of 23.2%, respectively. The reduction in kidney weight increased with age starting from 5% at the age of 70 years to 15% at the age of 80 years to 25% up to the age of 100 years in both sexes.

Kidney blood flow

Absolute kidney blood flow decreased by 5 to 10% per age decade till the age of 65 years and thereafter decreased by 25% per age decade (Figure 2.4b) [192, 205, 209, 229-237]. Kidney blood flow relative to cardiac output was 19.7% in young men and decreased to 11.9% at the age of 85 years. The decrease was 5 to 20% per age decade. In women, the average kidney blood flow relative to cardiac output was 16.5% and stayed constant till the age of 70 years. Thereafter, it decreased to 9.2% at the age of 85 years.

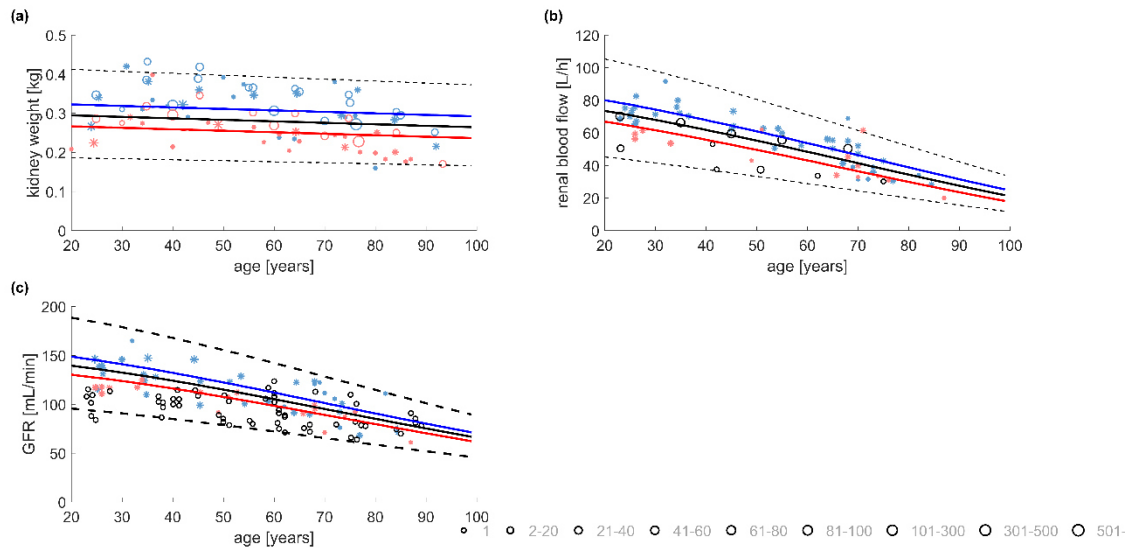


Figure 2.4: Kidney weight (a), renal blood flow (b), and glomerular filtration rate (GFR) (c) per age decade in an aging population. The blue, red, and black lines represent the predicted mean of virtual men, virtual women, and from all virtual subjects, respectively. The dashed lines represent the 5 and 95% confidence interval of the predictions. Stars show observed data from the development and circles represent observed data from the independent verification dataset. Black circles represent data from an undefined gender population. The size of the stars and circles indicates the size of the studied population.

Glomerular filtration rate

Only studies using inulin or ^{51}Cr -EDTA as a biomarker for glomerular filtration rate have been considered in this work [229-235, 237-241]. Equations to estimate the glomerular filtration rate like Cockcroft-Gault [125] and the Modification of Diet in Renal Disease [242] use serum creatinine, which is problematic considering senile sarcopenia in aging subjects [243]. The average glomerular filtration rate was between 130 and 140 mL/min in men aged between 20 and 50 years and around 120 mL/min in women

of the same age. In the fifth age decade, glomerular filtration rate declined in men to 115 mL/min, which was like the value in women (112 mL/min). Afterwards, the decline in glomerular filtration rate was roughly 10% per age decade independent of sex reaching 50% of the value of a young adult at the age of 90 years (Figure 2.4c).

2.5.5 Adipose tissue

Adipose tissue weight

Adipose tissue weight is usually measured via X-ray absorptiometry and bioelectric impedance analysis. Data from 18 different studies from 12,323 subjects were available for the development dataset [140, 141, 151, 152, 156, 157, 160-163, 172, 174, 175, 177, 180, 183, 188, 244]. In young men, adipose tissue weight was on average 17.8 kg with a CV of 24%. It increased by 5 to 10% per age decade to 22.9 kg at the age of 70 years. The CV increased to 28%. In young women, adipose tissue weight was found to be 17.3 kg with a CV of 29%. Between 20 and 70 years, adipose tissue weight increased to 25.2 kg with a CV of 37% in women and decreased again to 21.9 kg with a CV of 37% at the age of 85 years.

Adipose tissue blood flow

Adipose tissue blood flow increased from 5% in young to 9% in aged male individuals and from 8% in young to 10% in aged female individuals [245, 246].

2.5.6 Muscle

Muscle weight

Data from 11 different studies with 5,542 participants were available to analyze muscle weight, which was measured by X-ray absorptiometry and bioelectrical impedance analysis [141, 156, 157, 160, 165, 179, 188, 194, 196, 198, 244]. The average muscle weight was 32.0 kg in men aged 20 to 65 years and 19.8 kg in women of the same age. Muscle weight decreased by 10% per age decade between 65 and 100 years. The CV was 11.8% and was similar for male and female individuals.

Muscle blood flow

Only sparse data concerning muscle blood flow have been found in the literature, which do not cover all age decades but suggest 17.5% of cardiac output in men and 11.1% in women [247-250].

2.5.7 Brain**Brain weight**

Brain weight was analyzed by using data from eight different studies with 2,425 participants [144, 156, 157, 166, 167, 170, 193, 251] and was found to be independent of age. The average brain weight was 1.39 kg in male and 1.28 kg in female individuals with a sex-independent CV of 9%.

Brain blood flow

The literature search yielded 12 different studies with 956 participants for brain blood flow [252-263]. Brain blood flow relative to cardiac output was 11.8% in men and 15.6% in women below the age of 40 years and increased to 15.6% in men and 16.3% in women in the fourth age decade and was constant thereafter.

2.5.8 Heart**Heart weight**

Heart weight was analyzed using data from ten different studies measuring heart weight after autopsy [144, 156, 157, 168, 170, 176, 184, 193, 264, 265] and increased in both, male and female individuals, from 0.325 kg and 0.241 kg at the age of 25 years to 0.390 kg and 0.317 kg in the ninth age decade.

Heart blood flow

Blood flow to the heart relative to cardiac output increased from 5.5% at the age of 25 years to 12% at the age of 85 years in men and from 4.3% at the age of 25 years to 11.3% at the age of 70 years in women [266-271].

Cardiac output

Cardiac output is the volume of blood being ejected by the heart per minute. Data from 12 studies involving 645 subjects were used to analyze cardiac output [154, 178, 185, 189, 192, 199, 205, 209, 247, 250, 272, 273]. Cardiac output decreased from 352 L/h in 30 years old male individuals and 312 L/h in young female individuals between 5 and 10% every age decade to 258 L/h in aged male individuals and 201 L/h in aged female individuals (Figure 2.5). The CV was similar between both sexes with a value of 21.1%.

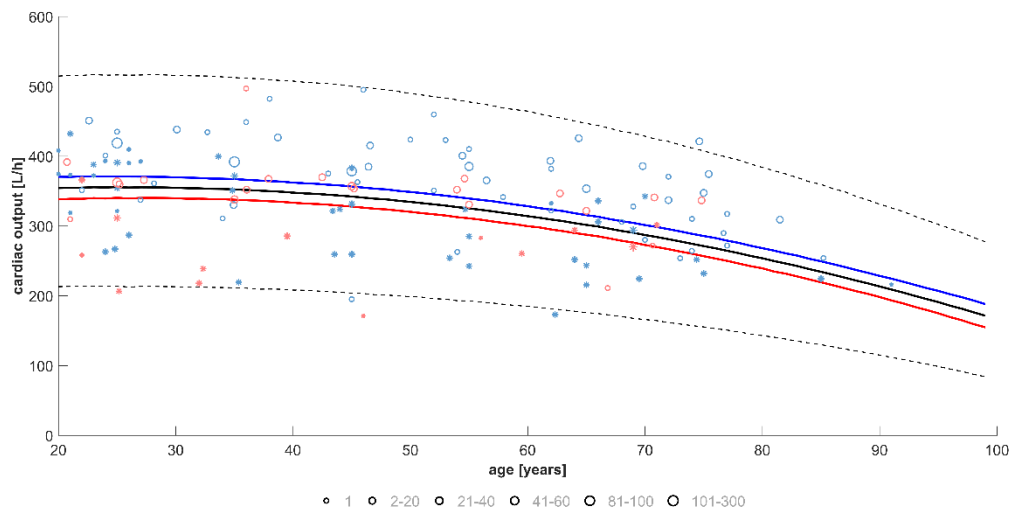


Figure 2.5: Cardiac output per age decade in an aging population. The blue, red, and black lines represent the predicted mean of virtual men, virtual women, and from all virtual subjects, respectively. The dashed lines represent the 5 and 95% confidence interval of the predictions. Stars show observed data from the development and circles represent observed data from the independent verification dataset. The size of the stars and circles indicates the size of the studied population.

2.5.9 Blood

Blood weight

Blood weight was analyzed from seven different studies with 382 male and 179 female participants [142, 145, 146, 159, 181, 190, 274]. In young male individuals, blood weight was 5.8 kg with a CV of 10% and decreased to 5.0 kg at the age of 90 years (Figure 2.6a). In young women, blood weight was lower with 3.8 kg, but stayed constant over different age decades. At the age of 70 years, female blood weight was still 3.7 kg; the CV was the same as in male individuals.

Hematocrit

Hematocrit and the level of albumin and alpha-acid glycoprotein were the blood parameters analyzed (Figure 2.6b). Data of 1,752 subjects aged 21 to 90 years were available to analyze hematocrit [234, 254, 275-280]. Sex was the only significant covariate. Mean values were 0.443 ± 0.064 for men and 0.410 ± 0.063 for women.

Plasma binding protein level

Regression analysis of albumin yielded age as a significant covariate [281-289] with an overall CV of 7.9%. The albumin concentration declined about 1.5% in each age decade (Figure 2.6c). Malnutrition and acute illnesses, both occurring often in the elderly, can have a significant impact on the analysis of age-dependent albumin levels [281, 286, 290]. Therefore, only data from apparently healthy subjects have been used in the analysis.

Alpha-acid glycoprotein showed no significant covariate when analyzing data of 472 subjects aged 24 to 90 years from five different studies (Figure 2.6 d) [288, 290-293]. The mean value was 0.798 g/L with a CV of 24.3%.

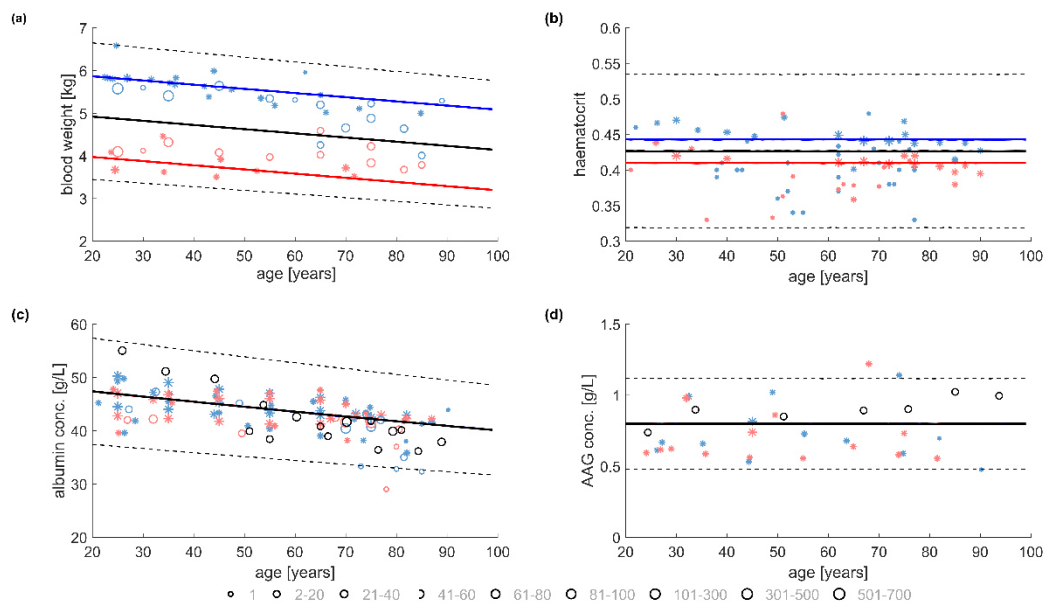


Figure 2.6: Blood weight (a), hematocrit (b), albumin (c), and alpha-acid glycoprotein (AAG) (d) concentration per age decade in an aging population. The blue, red, and black lines represent the predicted mean of virtual men, virtual women, and from all virtual subjects, respectively. The dashed lines represent the 5 and 95% confidence interval of the predictions. Stars show observed data from the development and circles represent overserved data from the independent verification dataset. Black circles represent data from an undefined gender population. The size of the stars and circles indicates the size of the studied population.

2.5.10 Other organs

Other organs such as the spleen and pancreas are not described in detail here, but the descriptive equations to describe an aging Caucasian population can be found in Table 2.2. Organs that have not been considered in the model are lumped in a remaining organ compartment. Its weight and blood flow are calculated as the sum of all organ weights and regional blood flows subtracted from the body weight and cardiac output (Figure 2.7).

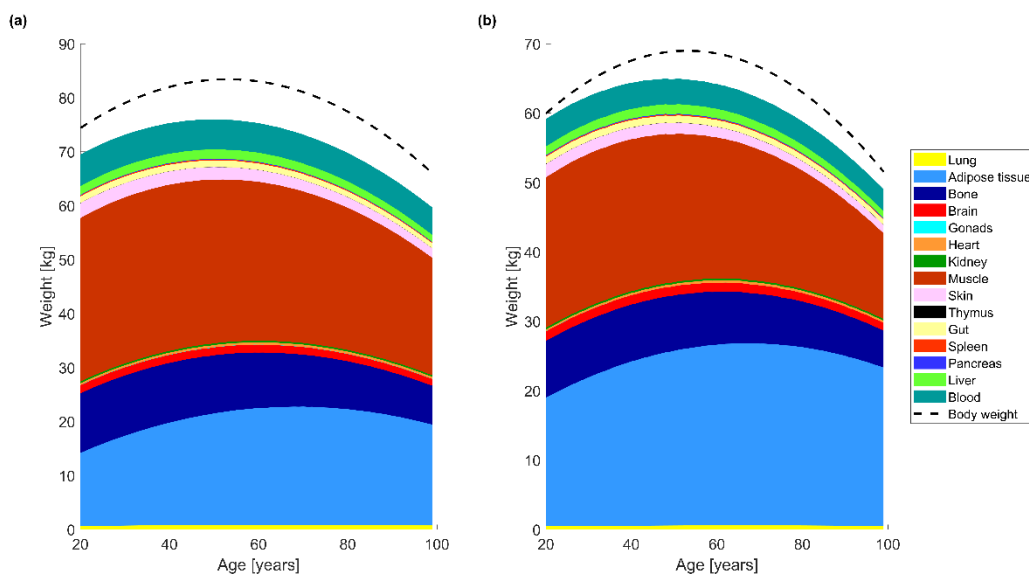


Figure 2.7: Sum of all organ weights (colored areas) in comparison to body weight (dashed line) in male (a) and female (b) subjects.

2.5.11 Tissue composition

Tissue composition is an important parameter to predict the distribution of drugs into tissues in a PBPK model. Data regarding the composition of lipids and proteins of tissues are generally sparse in humans and no age-dependency was found in the literature, but total body water, total extracellular water, and total body cell mass have been reported in aging subjects [65, 141, 152, 180, 294-301]. Age-independent fractions of tissue volumes [302] coupled with age-dynamic tissue volumes have been used to calculate the vascular and interstitial space of tissues (representing the extracellular water) and the intracellular space minus the intracellular water (representing the cell mass). Organ densities to convert organ weights obtained from the derived functions to organ volumes have been used from the International Commission on Radiological Protection database [303, 304]. The weighted mean of the organ density and the fraction of tissue compositions of investigated organs was used for the remaining

organ. The values of all tissues have been summed and compared against the observed data (Figure 2.8). The prediction of total body water and total cell mass was well in agreement with the observed data, leading to the conclusion that the made assumptions were adequate to inform a PBPK model.

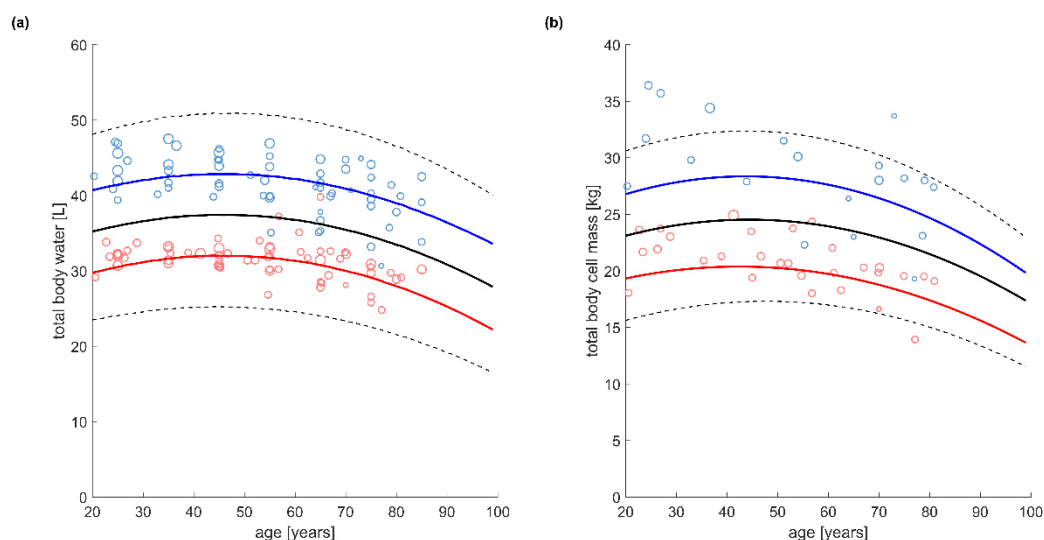


Figure 2.8: Total body water (a) and total body cell mass (b) per age decade in an aging population. The blue, red, and black lines represent the predicted mean of virtual men, virtual women, and from all virtual subjects, respectively. The dashed lines represent the 5 and 95% confidence interval of the predictions. Stars show observed data from the development and circles represent observed data from the independent verification dataset. The size of the stars and circles indicates the size of the studied population.

2.5.12 Parameters affecting drug absorption

Physiological parameters having an impact on drug absorption are gastric pH, gastric emptying, and small intestinal transit time, the surface area available for absorption, and intestinal enzyme and drug transporter abundance.

Gastric pH

One study compared gastric pH in fasted and fed state between 24 young healthy volunteers aged 21 to 35 years [305] and 79 subjects aged 65 to 83 years [306]. The study reported a significant age-dependent difference between the median pH in fasted state (interquartile range) with 1.72 (1.08 – 2.34) in the young group and 1.28 (0.90 – 5.60) in the aged group. The variability appeared to be much greater in older individuals, but the difference in sample size need to be kept in mind. Another study in young

subjects below the age of 65 years found a median fasted pH of 1.45 [307]. To conclude, it is doubtful if there is an age-dependency of gastric pH in the fasted state and more data need to be generated and included in the meta-analysis to judge the age effect properly. Gastric pH in fed state was not significantly different between young and elderly subjects [305, 306], but the decline of gastric pH from fed to fasted state was exponential with a half-life of 1.8 hours (CV: 65%) in young subjects and was linear with a half-life of 3.0 hours (CV: 80%) in aging subjects [306]. Eight percent of Caucasians are achlorhydric, meaning they do not secrete hydrochloric acid in the gastric juice [308] and thus have a gastric pH of 7.1 in fasted state [306]. In Japanese individuals, the number of achlorhydric subjects increases with age [309], but this appears not to be the case in healthy aging Caucasians [306].

Gastric emptying time

Reports in the literature about gastric emptying time are contradictory. Some studies report a slower gastric emptying time [59, 60] in aging subjects, some report no changes [61, 62], and some report a faster rate [63, 64]. Many influencing factors exist for gastric emptying time such as gastric pH [310], particle size [63], and food [62, 63, 311], making it difficult to analyze age-dependency. Furthermore, gastric emptying has a circadian rhythm, making a difference if the study is conducted in the morning or in the evening [312]. Two studies have investigated gastric emptying time after fluid and food intake in young controls and aging subjects [311, 313]. Both studies used the same marker and the same method, and both started in the morning. Gastric emptying time was different between fluids and food but did not show any age-dependency, which was verified by the regression analysis. Therefore, it is recommended to use the same gastric emptying time in aging subjects as in young individuals.

Small intestinal transit time

Small intestinal transit time appears to be independent of age and a fixed value can be used to inform a PBPK model [314, 315].

Passive permeability

The mucosal area is reported to decline with age [316, 317], but enterocytes and villi appear to be unchanged [317]. Malnutrition, disease, and drug intake could alter the mucosa and need to be carefully considered when investigating age-dependency. Passive permeability was reported to be impaired in aging subjects [316], but two studies investigating mannitol and lactulose, two carbohydrates that are

passively absorbed, showed no difference in passive permeability between young controls and aging subjects after correcting the data for the age-dependent decline in the glomerular filtration rate [318, 319]. It is therefore assumed that neither the surface area available for passive diffusion nor the rate of passive diffusion differ in aging subjects compared with young individuals.

Intestinal enzyme and drug transporter abundance

Data regarding intestinal enzyme and drug transporter abundance are generally sparse and therefore age-dependency cannot be analyzed sufficiently.

2.6 Discussion

The described population database for aging subjects summarizes anatomical, physiological, and biological system parameters required to inform PBPK modelling. Descriptive continuous functions for systems parameters from the age of 20 to 99 years have been derived and verified with observed data extracted from the peer-reviewed literature. Population variability was considered for each parameter.

Two previous databases have been described in the literature for aging individuals. Thompson *et al.* gathered extensive data from the literature, but the authors did not consider different ethnic groups and combined data from Caucasians, Latin-Americans, and Asians [130]. However, it is known that ethnicity can have a significant impact on system parameters, for instance hepatic enzyme abundance, and therefore on clearance prediction [320]. Schlender *et al.* recently published a database for elderly individuals further processing the data from Thompson *et al.* for Caucasians only [131]. A limitation of this study is that only values for organ weight and blood flow for each age decade were considered, making it difficult to extrapolate to other ages of interest. Furthermore, population variability of system parameters was not considered by Schlender *et al.*, which is an essential element for reasonable predictions of drug pharmacokinetics using PBPK models [116].

One notable novelty of the presented repository for Caucasian subjects are the derived continuous functions that allow prediction for a population from 20 to 99 years of age. The advantage of continuous functions is the creation of only one population with one distinct value at a certain age. If two separated populations would have been built with one representing young subjects from 20 to 65 years and the

other one representing elderly individuals from 65 to 99 years, there would be two separated equations calculating system parameters at the age of 65 years, which might lead to unphysiological steps. Another advantage for the prediction of monoclonal antibody kinetics or long-term drug therapies could be to introduce time-varying physiology [321], meaning that subjects age during the time of the simulation.

A few limitations need to be acknowledged. Data from individuals over the age of 85 years are sparse, meaning the derived equations could be less robust and extrapolation to older ages might be difficult. However, data for centenarians have been included for some system parameters [193] and were adequately estimated by the derived functions. Clinical studies are usually not performed in very old individuals, making it impossible to verify the described population by analyzing drug pharmacokinetics. It is therefore recommended to use the described repository with caution at older ages. This holds particularly true for regional blood flows to adipose tissue, heart, muscle, and skin because almost no geriatric data are currently available in the literature.

Another area with sparse data is tissue composition, where more research is needed in the future, because it is important to predict the distribution into tissues accurately. It was shown that the assumptions used in this work are plausible for total body water and cell mass (Figure 2.8); however, exception for single tissues cannot be excluded and data for lipid composition in the elderly were generally not found in the literature.

The analysis of system parameters to inform a PBPK model for aging Caucasians was complicated by the fact that some studies combined age groups together, meaning individuals aged 65 to 100 years might have been included, but only one mean age is given. This can lead to a bias in the data and hinders the characterization of age-dependent changes. Reports that insufficiently described age should generally be excluded unless no other data are available. Furthermore, ethnicity, particular in European studies, is not always clearly defined and need to be assumed from the given study location.

Predictions of system parameters become more robust when model parameters are correlated with each other and co-variability can be described [322, 323]. To obtain such descriptive correlations, studies need to report important covariates, which is unfortunately not always the case. Weighted

regression analysis has been used to correlate parameters and to receive a more robust aging population. Linear regression can only describe linear relationships; however, using data transformation such as logarithm might compensate. Using regression, it is easy to overfit and model the noise in the data rather than the relationship between parameters. In this work, the corrected Akaike's information criterion was used to select the best performing function among those tested, which in contrast to the coefficient of determination exhibits no bias to higher parameterized models. Another limitation of regression analysis is its sensitivity towards outliers. Visual inspection of the estimated mean and variability of each parameter compared to observed data in this work, showed an adequate fit for all investigated parameters (Figure 2.2 to 2.8).

The evaluation of variability was further complicated by being unable to set boundaries for publication year and study location. For a few parameters, for instance blood weight, data were only available from specific regions (e.g. USA) and from the 1950s. Both, location and publication year have therefore been used as independent variables during regression and their impact has been quantified when sufficient data were available. Body height and body weight are key parameters to describe a population adequately and data from 106,698 individuals were available. Location was found to have an impact to body height, with a lower height correlated with Southern Europe. Otherwise, location was not a significant covariate for any variable and therefore combining data of studies conducted in Europe, the United States, and Australia appears not to bring a bias into the data. However, the derived equations should not be used to predict aging African or Asian individuals as aging processes might be different. Publication year had a significant impact on body weight, showing a weight increase particularly in the last ten years. Consequently, the developed population will require constant updates to include future potential changes such as body weight.

A challenge when studying older individuals is that the definition of an "elderly" individual is not universal. The World Health Organization specifies "elderly" as being above the age of 65 years [56], which is in accordance with the age of retirement in most Western countries, but a clear pharmacological or clinical age-cut off is missing [55]. For some patient groups, such as people infected with HIV, the age cut-off is even as early as 50 years [324]. We compared organ parameters important for drug disposition for men and women aged 50 and 70 years with subjects aged 30 years (Figure 2.9). There is a progressive decline in relevant system parameters, such as adipose tissue weight, hepatic, and renal blood flow,

with age. However, it is challenging to conclude a “pharmacological” or “clinical” age cut-off for the elderly based on the age-dependent changes in anatomical and physiological parameters because it is unknown when those changes affect drug pharmacokinetics significantly. No study has been undertaken to compare the pharmacokinetics of a drug between different age decades and correlate those data to age-dependent changes of organ parameters. Furthermore, elderly subjects included in clinical trials can have diseases influencing the parameter of interest. It is therefore a challenge to define “healthy” in terms of an aged person.

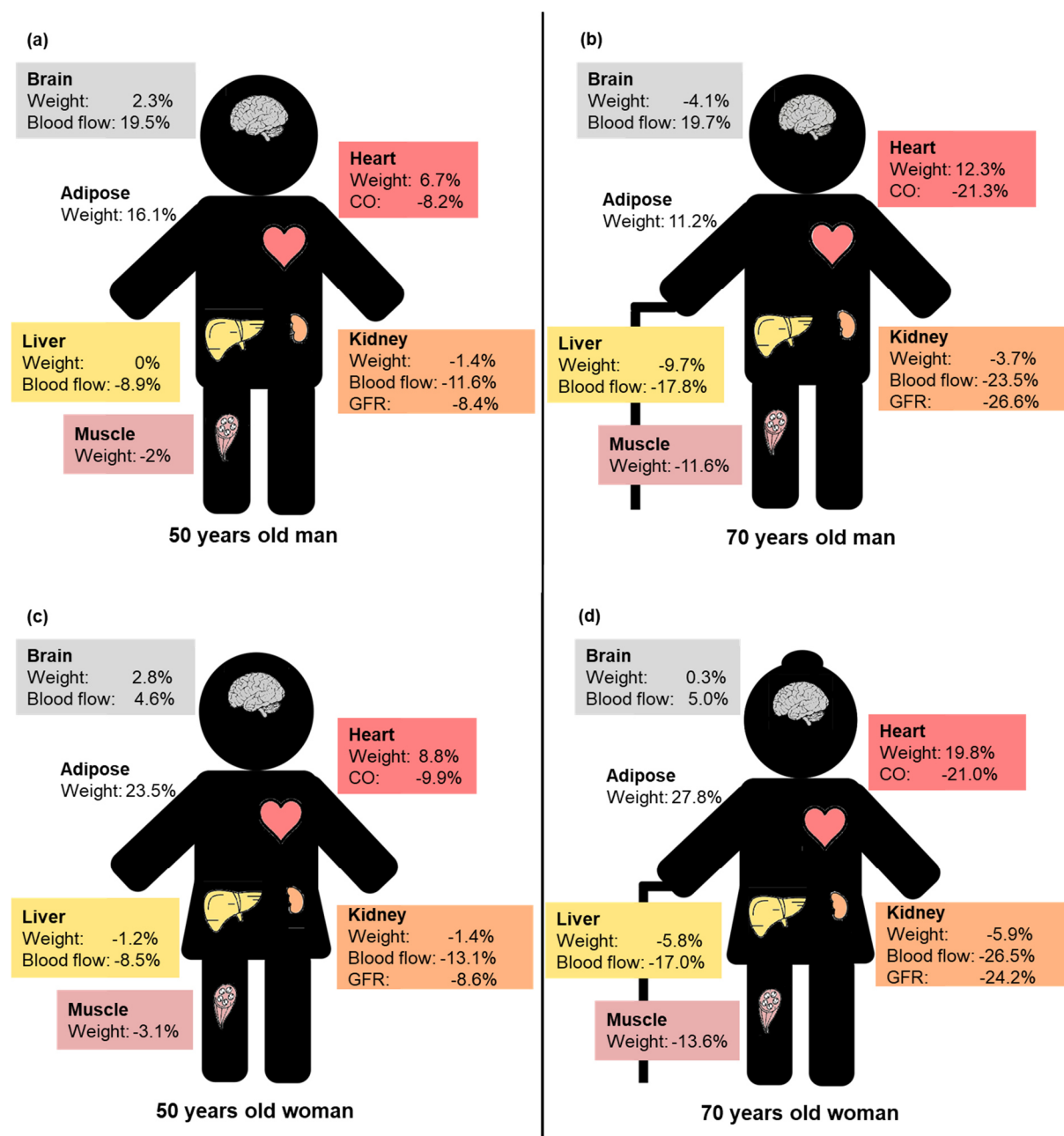


Figure 2.9: Comparison of a 50 and 70 years old man (a and b) and woman (c and d) with a 30 years old subject, who was arbitrarily chosen to represent a young individual. Blood flow is relative to cardiac output and all values are relative to a 30 years old man and woman, respectively.

Despite the limitations, in this work, it was possible to derive descriptive continuous functions to generate a virtual population from 20 to 99 years in accordance with observed independent data. The elderly are a growing vulnerable patient population with a high frequency of comorbidities and in turn polypharmacy. However, aging subjects are often excluded from clinical trials and knowledge concerning drug pharmacokinetics and DDI magnitudes is scarce. The developed population database can be implemented into existing PBPK frameworks and then be used to predict drug pharmacokinetics and DDI magnitudes in aging subjects, thereby overcoming the lack of clinical data and providing a rational framework for dose optimization to overcome DDIs.

2.7 Conclusion

The population database for aging subjects presented in this work can be implemented into existing PBPK frameworks and allows the prediction of drug pharmacokinetics and DDI magnitudes in the elderly. It provides descriptive continuous functions for anatomical and physiological parameters from 20 to 99 years of age necessary to inform PBPK models and provides a view of the current literature concerning metabolizing enzymes and drug transporters in aging individuals. Furthermore, population variability is considered for all system parameters providing a framework for realistic pharmacokinetic predictions.

2.8 *Electronic Supplementary Material*

The online version of this article contains supplementary material:

<https://doi.org/10.1007/s40262-018-0709-7>

Figure S1: Structure of the used PBPK model. See Figure 1.4.

Figure S2: Sum of all organ weights in comparison to body weight. See Figure 2.7.

Table S1: System parameters necessary to describe the population of interest. See Table 2.1.

Table S2: Number of subjects in the development dataset used to derive the equations. Not included in this thesis.

Table S3: Mean value per age decade for all system parameters. Not included in this thesis.

Table S4: Detailed metrics for all system parameters. Not included in this thesis.

Chapter 3:

PBPK Model Development

3. Physiologically based pharmacokinetic Model Development

3.1	Summary	Page 54
3.2	Background	Page 54
3.3	Five steps to build a PBPK model in Matlab	Page 56
3.3.1	Step 1: Define the parameter of the model	Page 57
3.3.2	Step 2: Generation of the population	Page 62
3.3.3	Step 3: Calculation of the required drug parameters	Page 62
3.3.4	Step 4: Bridge system and drug data – the ordinary differential equation solver	Page 74
3.3.5	Step 5: Work with the simulated data – the postprocessing step	Page 79
3.4	Simulation of the DDI between rivaroxaban and darunavir/ritonavir	Page 80
3.5	Conclusion	Page 82
3.6	Appendix	Page 84
3.7	Electronic Supplementary Information	Page 86

This chapter is a pre-printed version of an invited peer-reviewed tutorial article published under the following reference:

A comprehensive framework for physiologically based pharmacokinetic modelling in Matlab

Felix Stader, Melissa A. Penny, Marco Siccardi, & Catia Marzolini

CPT Pharmacometrics & Systems Pharmacology 2019; 8(7): 444-459.

DOI: 10.1002/psp4.12399

3.1 Summary

Physiologically based pharmacokinetic (PBPK) models are useful tools to predict clinical scenarios for special populations for whom there are high hurdles to conduct clinical trials such as children or the elderly. However, the coding of a PBPK model in a mathematical programming language can be challenging. This tutorial illustrates how to build a whole-body PBPK model in Matlab® to answer specific pharmacological questions, involving drug disposition and magnitudes of drug-drug interactions in different patient populations.

3.2 Background

Physiologically based pharmacokinetic (PBPK) models have been applied with significant impact during drug development and post-marketing phases and achieved regulatory acceptance [325] as shown by the recent guidelines of the U.S. Food and Drug Administration [326] and the European Medicines Agency [327]. PBPK models are useful for the prediction of drug-drug interaction (DDI) magnitudes [328] and drug disposition in special populations such as pediatrics [329], pregnant and breastfeeding women [330, 331], and patients with liver cirrhosis [332] or renal impairment [333], for all of whom there are high hurdles to design and conduct clinical trials. In addition, PBPK models have been successfully applied to simulate different routes of administration [334] and for the design of novel formulations.

A PBPK model describes the absorption, distribution, metabolism, and elimination of a drug in a physiologically relevant compartmental structure, where each compartment represents an organ or tissue [114]. The organs and tissues are connected via arteries and veins, which themselves merge in the lung. Dynamic drug movement through regional blood flows to the different organs and tissues is described by ordinary differential equations (ODEs). Tissue distribution can be predicted by a PBPK model that is of high relevance to most drugs because the drug targets are usually in specific populations of cells in an organ or tissue. The distribution into a compartment can either be limited by perfusion (well-stirred models) or by the cell membrane (permeability-limited models) [115].

An important characteristic of the PBPK modelling approach is the separation of system data (where system refers to the population of interest) from drug metabolism and pharmacokinetic data and the trial design [115]. System data contain all relevant information to build a population of virtual individuals such

as demographics, organ weights, and regional blood flows. It is of tremendous importance that the system data used to parameterize the PBPK system components reflects the “true” (meaning observed) population to produce reliable predictions [58]. The incorporated physiological, biochemical, and genetic variability of system parameters allows the identification of certain subpopulations with high risks for DDIs (e.g. poor metabolizers for the enzyme cytochrome P-450 (CYP) 2D6), where clinical data are often lacking [116]. However, variability is often underestimated in PBPK models because of missing parameters or processes involved with physiological changes caused by diseases or specific patient characteristics, all of which add uncertainty and variability [335].

Drug metabolism and pharmacokinetic data describe the information related to physicochemical properties (e.g. molecular weight), absorption (e.g. intestinal permeability), distribution (e.g. binding to plasma proteins), metabolism (e.g. kinetic parameters for an enzyme), and excretion (e.g. renal clearance) [117]. Usually drug characteristics, such as the intrinsic clearance of an enzyme, are quantified through laboratory based experiments that are then scaled to the in vivo clearance under the consideration of system parameters such as the enzyme abundance in the liver per gram protein, the protein content per gram liver, the liver weight, and the hepatic blood flow [214]. By considering variability in these system parameters, it is possible to obtain reliable population predictions of drug clearance [116]. System and drug data can be combined in the trial design component, considering parameters such as dose, dosing regimen, route of administration, number of individuals, and duration of administration to simulate clinical scenarios of interest.

Several commercial PBPK software platforms, such as SimCYP® (Certara UK, Sheffield, UK) [336], PK-Sim® (Bayer Technology Services, Leverkusen, Germany) [337], and GastroPlus® (SimulationPlus, Lancaster, CA) [338] simplify the model management for unexperienced modelers and are based on structural PBPK models. However, they are limited in flexibility to simulate specific pharmacological questions. In this tutorial, a general framework on how to build a whole-body PBPK model in Matlab® (MathWorks, Natick, MA) is described for scientists and users with interest in mathematical modelling and its application in pharmacology. The general development can also be adapted in other programming languages such as R® or other Matlab® packages like Simbiology®.

3.3 Five steps to build a PBPK model in Matlab®

Matlab® offers a powerful mathematical programming language with matrix-based operations (<https://uk.mathworks.com/products/matlab.html>). The basic principles of Matlab® are extensively described in the documentation by MathWorks® (<https://uk.mathworks.com/help/matlab/index.html>). This tutorial illustrates the different steps necessary to build a PBPK model to simulate specific clinical scenarios with examples of pseudo code separated by lines from the main text. The entire code is published open access (<https://doi.org/10.1002/psp4.12399>) and tables listing the abbreviation and units for all used parameters can be found in the appendix of Chapter 3 (Section 3.7; Table A3.1 and A3.2). The Statistic and Machine Learning Toolbox is a required Add-On to the Matlab® suite to execute the code.

A “building block” system is used for separating system, drug, and trial design data to inform the PBPK model [115]. Advantages are that each block can be used for a different purpose (e.g. the generated population could be used in a different model) and each block can be exchanged (e.g. aging white population vs. pediatric population [339]). Each building block described in this tutorial is a Matlab® function. Matlab® requires one script indicating the order in which the functions should be executed, which in this tutorial is called the main function.

%Main function: Calls each function of a PBPK model

Define the model structure and the model parameters

Generation of the virtual population

Load the drug files and perform the in vitro to in vivo extrapolation

Solve the ordinary differential equations (ODEs)

Process the data from the ODE solution and output the results

The variables used in different functions in Matlab® need either to be passed onto the next function or to be defined as globals using the “global” command. However, it is good practice to scope variables as local if they are only used within a specific script.

3.3.1 Step 1: Define the parameters of the model

The modelling process is started by defining the objective and the purpose of the model, identifying the pharmacological scenario to be simulated [340]. The model structure proposed can vary based on the overall purpose of the simulations, and a representative compartmental model is shown in Figure 3.1. As an example, it would be of scientific interest to simulate clinical scenarios in aging HIV-infected patients, because clinical data of antiretroviral drug disposition and DDI magnitudes between antiretroviral agents and comedications are currently lacking. When simulating anti-HIV therapy, drug penetration into viral reservoirs, such as the testis and the brain [341], and into the lymphatic system being the target site for antiretroviral drugs can represent a relevant pharmacokinetic factor. The flexible computational structure supports the inclusion of the lymphatic system, dividing each compartment into the vascular, the interstitial, and the intracellular space (Figure 3.2) with lymph fluid flowing from the interstitial space of each organ to a central lymph-node compartment and further to the venous blood pool. Organs not being simulated are lumped in a remaining organ compartment [58]. In our example, the model is used to simulate the effect of the CYP3A4 inhibitor ritonavir, used as pharmacokinetic enhancer to boost the concentrations of co-administered HIV protease inhibitors like darunavir, on the disposition of the anticoagulant rivaroxaban being metabolized by CYP3A4 in aging white subjects.

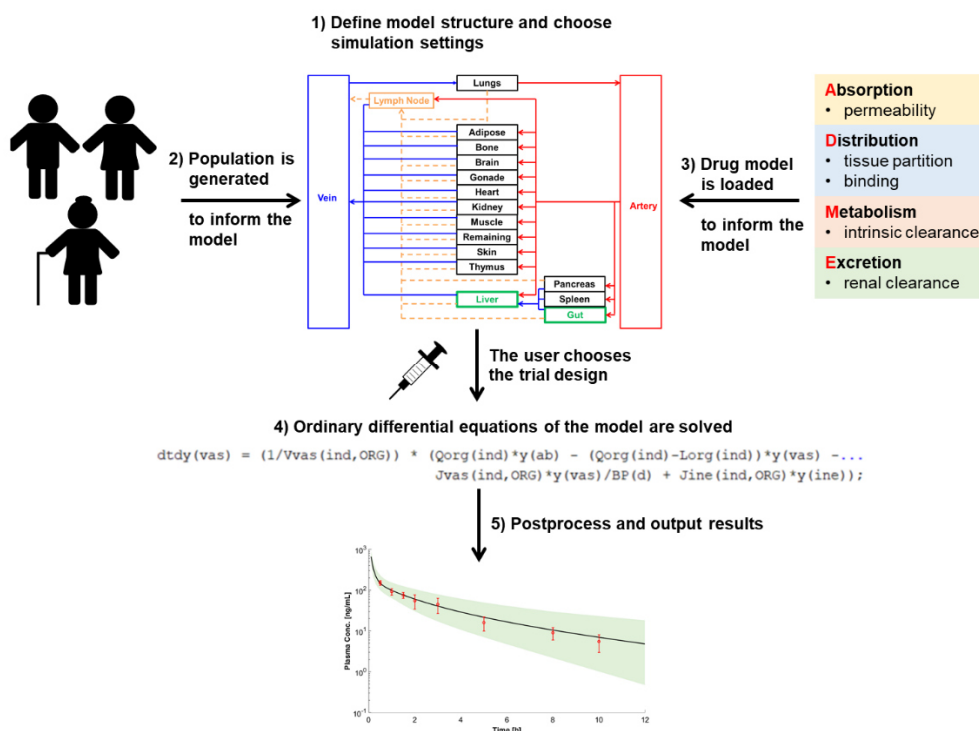


Figure 3.1: Schematic illustration of the five steps to build a PBPK model.

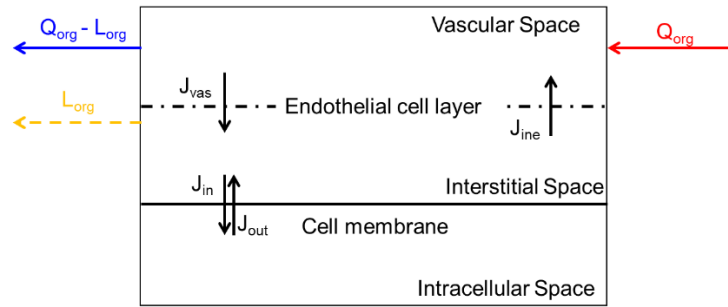


Figure 3.2: Structure of an organ in the PBPK model.

Key: J_{in} = flux into the cell, J_{ine} = flux from the interstitial to the vascular space, J_{out} = flux out of the cell, J_{vas} = flux from the vascular to the interstitial space, L_{org} = regional lymph flow, Q_{org} = regional blood flow.

First, the model structure and model variables including populations, compartments, drugs, and route of administration are defined by a number because Matlab® is a numerical software tool. The number assigned to each variable (e.g. drugs) refers to the column in each matrix containing specific data (e.g. if darunavir is defined by a one, data of darunavir would be in the first column; Figure 3.3). Each variable is also defined by a string defining its name for the outputs.

DrugParameter = zeros(IndNo, DrugNo);

Number of virtual subjects referring to the row

Number of drugs simulated in parallel referring to the column

	Drug 1 Darunavir	Drug 2 Ritonavir	Drug 3 Rivaroxaban
Individual 1	0.95	0.55	0.70
Individual 2	0.90	0.65	0.70
Individual 3	1.00	0.60	0.75
Individual 4	1.00	0.55	0.80
Individual 5	0.95	0.55	0.75

Figure 3.3: Example of the organization of drug parameters with variability. Each row contains data for a drug. Parameter clues are illustrative only.

Key: DrugNo = number of drugs, IndNo = number of virtual individuals.

After defining all necessary variables of the model, the target population and the drugs to be used in a specific simulation need to be entered. The virtual trial design can be described by firstly indicating the number of virtual individuals in the simulation. The appropriate number of individuals depends on the

variability of system data involved to describe the pharmacokinetics of the simulated drug (e.g. enzymatic vs. total clearance) and the number of patients included in clinical trials to verify the model. To come to the “true” population mean for most anatomical, physiological, and biological parameters, a sample size of at least 100 individuals is recommended. Therefore, if observed clinical data are available for six patients, it is recommended to run 20 trials times six patients resulting in 120 virtual individuals. The split into different trials allows the comparison of the mean predicted concentration of each trial with the mean observed data. The mean observed is used because often observed concentration from individuals are not published or available. Observed data from six individuals may not be representative of the whole patient population taking the drug of interest; thus, it is important to recognize that the mean prediction obtained might be different and far from the mean of the six observed subjects, but it might be close to the “true” population of patients. Therefore, if the observed data from six subjects fit the prediction of one trial, even when its prediction should be on the upper or lower end of all simulations, this is still considered to be a “successful” outcome.

Next the proportion of men and women in the simulated population and the age range of the virtual individuals can be specified. In addition, the resolution of each simulated time unit needs to be given for the outputs.

Once the individual characteristics are described, the dosing regimen for each drug can be defined, indicating the route of administration, the number of doses (1 for a single dose and n for multiple doses), the dose, and the dosing interval. After entering the trial design, a dose event matrix can be set up to allow the simultaneous simulations of darunavir, ritonavir, and rivaroxaban alone and in combination to investigate DDIs. The matrix contains five columns with the start and the end time of each dose, the dose, the route of administration, and the resolution for each dosing event. Only unique start and end times for each dosing event are needed, which need to be extracted.

The code to define the model parameters and choose the simulation settings is given by:

```
function[] = DefineParameters()  
  
%This function defines the population, and model structure (PBPK compartments),  
%the drugs, the virtual trial design, and the simulation settings to be used
```

%=====

Define the populations saved on the hard drive by a number and a string

Define the compartments of the model by a number and a string

Define enzymes for the dynamic abundance calculation in case of DDIs by a number and a string

Define the number of subcompartments

Define the drugs saved on the hard drive by a number and a string

Define plasma-binding proteins by a number and a string

Define the route of administration by a number and a string

%=====

User sets the population to be simulated (if more than one is saved on the hard drive)

User sets the number of drugs to be simulated

Initialize drug name

Define a case for each simulated drug

 Define a drug name for each drug to be simulated

end

Define the number of trials

Define the number of virtual individuals per trial

Calculate the number of all virtual individuals to be simulated

Ask the user for the proportion of women in the virtual population

Ask the user for the minimal and maximal age of the virtual population to be simulated

Ask the user for the resolution of each time step

Initialize the route of administration, the number of doses, the dose, the dosing interval,...

The start time point for the dose, and the prolongation of the terminal elimination phase

Define a case for each drug to be simulated

 Define the route of administration to be an intravenous bolus or oral

 Define the number of doses and dose given in mg

 Define the dose interval in h

 Set a start time for the drug to be administered in h

 Set the prolongation for the terminal elimination phase in h

end

%=====

Define the name of the columns for the dose event matrix

Calculate the number of columns of the dose event matrix

Initialize a matrix containing the regimen for each drug

Define a case for each drug

 Define a case for each dose being administered

 Calculate the start and end time for the first dosing event

 Calculate the start and end time for all dosing events

 Consider the prolongation of the terminal elimination phase

 end

end

Define a case for each drug

 Sort the regimen matrix based on the start time of each drug

 Delete zero values

end

%Combine the dosing regimen for each drug to be simulated simultaneously

Define a case for each drug

 Combine the dosing regimens for different drugs

 Use a function to find unique dosing events for each drug

 Set dose, route of administration, and resolution for the other drugs to be zero

 Sort the matrix according to the start time

 Find unique start times

 Output the dose event matrix for each drug based on the unique start times

 end

end

Calculate the number of events

Combine the dose event matrix

end

3.3.2 Step 2: Generation of the population

A repository summarizing anatomical, physiological, and biological system parameters required to inform a PBPK model has been recently published [58]. The described continuous, age-dependent equations and the variability for each system parameter can be directly entered in Matlab®:

```
function[] = Population()
```

```
%This function generates the virtual population based on the user settings
```

```
%Attention: the normrnd command needs the Statistics and Machine Learning Toolbox
```

```
Calculate age from a Weibull distribution for each virtual individual
```

```
    while age of an individual is smaller or larger than the minimal or maximal user-defined age
```

```
        Resample age from the Weibull distribution
```

```
    end
```

```
end
```

```
Calculate number of virtual female individuals
```

```
Assign randomly a zero (defined as "male") or one (defined as "female") to each virtual subject
```

```
Calculate system parameters as described in reference [58]
```

```
Add random variability to the system parameters by using a normal distribution
```

```
end
```

3.3.3 Step 3: Calculation of the required drug parameters

In the next step, the user-defined drug file is loaded from the library containing all developed drug files. The string defining the drug (e.g. "darunavir") is converted to the function in the drug library to load the drug-dependent data to inform the PBPK model (Figure 3.4):

```

1) Define the drug as a variable
Darunavir = 1; name{darunavir} = ,darunavir';

2) Convert the string ,darunavir' to the function
„darunavir“ to load drug data for darunavir
Drug1 = str2func(name{darunavir});
Drug1();

3) Data from the drug model darunavir saved
in the function „darunavir“ are used
function[] = darunavir

%_PhysChem_____
%molecular weight (MW) in g/mol
MW(darunavir) = 547.7; %Molto et al. (2016)

%octanol-water partition coefficient (logP)
logP(darunavir) = 1.8;% %Molto et al. (2016)

```

Figure 3.4: Steps from the user-defined drug to be simulated to the drug parameter that are loaded to inform the PBPK model.

```
function[] = Drug()
```

```
%This function loads the relevant drug files from the drug library and...
```

```
%performs the in vitro-to-in vivo extrapolation
```

```
Prepare empty vectors/matrices for all drug parameters (Table 3.1)
```

```
Define a case for each drug
```

```
Load the Matlab® file containing the drug parameter by converting the string defining the...
```

```
Drug to the function in the drug library
```

```
end
```

```
Delete all zero values and extract all drug files chosen by the user
```

```
end
```

Drug parameters incorporated in a drug file are shown in Table 3.1. The measured drug properties included in the drug file can be derived through experimental in vitro methods, and are integrated into specific equations for drug absorption, distribution, and elimination as described in the following sections.

Table 3.1: Parameters required for a drug file to inform the PBPK model.

Parameter	Typical unit	Explanation
<i>Physicochemical properties</i>		
MW	g/mol	molecular weight
logP	-	octanol-water partition coefficient
drug type	-	important property to predict tissue distribution according to Rodgers & Rowland
pKa	-	acid dissociation constant
BP	-	blood-to-plasma ratio
f _{uPL}	-	fraction unbound in plasma
<i>Absorption</i>		
P _{app}	10 ⁻⁶ cm/sec	apparent permeability
<i>Distribution</i>		
K _p scalar	-	scalar to alter predicted tissue partition coefficients
<i>Metabolism & Elimination</i>		
V _{max} /K _m or CL _{int}	pmol/min/pmol enzyme / μ M or μ L/min/pmol enzyme	kinetic parameters per enzyme and metabolic pathway
CL _{int,hep}	μ L/min/mg protein	unspecified intrinsic clearance
CL _r	L/h	renal clearance
CL _{ad}	L/h	additional plasma clearance
<i>Transporter</i>		
CL _{pd}	μ L/min/Mio cells	passive diffusion flux
V _{max} /K _m or CL _{int}	pmol/min/pmol transporter / μ M or μ L/min/pmol transporter	kinetic parameters for transporters
<i>Interactions</i>		
K _i	μ M	inhibition constant for competitive inhibition
K _{app}	μ M	apparent enzyme inhibition constant for mechanism-based inhibition
k _{inact}	1/h	maximum inactivation rate constant
IndMax	-	maximum fold of induction
IC ₅₀	μ M	half maximum inhibitory concentration

Key: V_{max} = maximal velocity, K_m = Michaelis-Menten constant, CL_{int} = intrinsic clearance.

Absorption

The compartmental absorption and transit model proposed by Yu & Amidon about 20 years ago is used as a basis [342]. Assumptions of the original compartmental absorption and transit model are:

- 1) the drug is immediately dissolved,
- 2) absorption occurs primarily in the small intestine and not in the stomach or the colon,
- 3) transit time and radii are similar for each compartment,
- 4) intestinal metabolism is negligible, and
- 5) only passive diffusion occurs through the gut wall.

It can be assumed that assumption 1 holds true for antiretroviral drugs because they are often given as an immediate-release tablet. Formulation and dissolution play a crucial role when simulating capsules or delayed-release tablets, and more complex absorption models can be built into the model as previously described [308, 343]. The compartmental absorption and transit model consists of five different compartments, namely, the stomach, duodenum, jejunum, ileum, and colon. The stomach serves as an entry compartment for the orally administered drug. It is assumed that the drug can only move further to the duodenum and no absorption or other processes occur in the stomach. Movement between different compartments representing the intestine can be described by first order rate constants calculated from the gastric emptying and the intestinal transit time [342].

Permeability into enterocytes and further into the systemic circulation can be mediated by passive or active processes. Drug transporters are present on the apical and basolateral site of the small intestine [344]. An established experimental model, such as human epithelial colorectal adenocarcinoma cells seeded as a monolayer can be used to measure the apparent permeability (P_{app}) in vitro and depending on the experimental conditions, the measured flux into the cell can be the sum of passive and active. The measured P_{app} can be converted to the effective permeability in man ($P_{eff,man}$) describing the flux of the drug from the lumen into the enterocytes in humans [345] as follows:

$$P_{eff,man} = 10^{0.6795 \cdot \log(P_{app}) - 0.3355}, \quad (1)$$

where P_{app} is in 10^{-6} cm/s and $P_{eff,man}$ is in 10^{-4} cm/s. $P_{eff,man}$ needs to be multiplied by the available enterocyte surface for drug absorption (permeability surface area: PSA) to arrive at the absorption clearance (CL_{ab} ; please note that the flux between two compartments can be written as a clearance), namely:

$$CL_{ab} = P_{eff,man} * PSA * 0.001 * 3600, \quad (2)$$

where CL_{ab} is in L/h. The PSA can be calculated by assuming that the gut has a cylindric shape, namely:

$$PSA = 2 * \pi * r * Le * F_{villi}, \quad (3)$$

where r is the radius of each intestinal segment in cm, Le is the length of each intestinal segment in cm, and F_{villi} is a fold expansion factor for the villi surface area. The length and the expansion factors for the

different gastrointestinal segments has been extensively described previously [304, 346]. Drugs penetrate through the intestinal wall mainly by the transcellular pathway because of tight junctions between enterocytes. Paracellular transport is only possible for drugs with a molecular weight less than 300 Da, being positively charged and with an octanol-water partition coefficient (logP) greater than 0 [347].

To estimate the concentration in the enterocyte, the volume of the enterocytic cell layer needs to be determined. A jejunal biopsy was undertaken in 11 healthy controls (five women) aged younger than 30 years and 3,040 enterocytes were found in the sample. The volume of one enterocyte is $770 \mu\text{m}^3$, calculated as a cylinder from the measured height and radius [348]. The surface of the small intestine can be calculated by assuming a cylindric shape and the radius and length of 2.25 cm and 280/260 cm for an average male/female subject, respectively [304]. The resulting surface area of the small intestine is $3,958/3,676 \text{ cm}^2$. Scaling the number of enterocytes from the biopsy sample to the entire small intestine leads to $1.20 \cdot 10^{11}/1.12 \cdot 10^{11}$ cells. The total volume of all enterocytes in the small intestine is therefore 0.093/0.086 L.

The drug distributes further from the enterocytes to the interstitial space and could move further either via the systemic or the lymphatic circulation. The potential strategies for antiretroviral drugs include manipulating the formulation in such a way so that more drug gains access into the lymphatic system, because (a) it is the relevant target site, (b) there will be no first pass metabolism, and (c) the drugs stay longer in the body because intestinal lymph flow is about 600-fold slower than intestinal blood flow [302, 304]. To move preferentially into the lymphatic circulation rather than into the systemic circulation, a drug needs to be highly lipophilic, positively charged, and it should have a high molecular weight [349]. However, there are no quantitative relationships in the literature. A manual restriction factor can be implemented into the model defining a proportion of the drug going via the lymphatic system to test new formulations. The rest of the drug will distribute via the systemic circulation.

Distribution – passive and active pathways

The prediction of tissue distribution is important in a PBPK model. Intracellular concentration cannot be easily obtained, particularly in humans, but most drug targets are in cells. In addition, metabolism occurs in hepatocytes and enterocytes, and therefore, the intracellular concentration is important to predict

metabolism and DDI magnitudes adequately. Several models are described in the literature to predict distribution into tissues [350-355]. Poulin and Theil assume homogenous distribution in a tissue [350, 351], which does not hold true if the cell membrane is a tight barrier. Therefore, the approach of Rodgers and Rowland is used in this model [352-354]. In contrast to Poulin and Theil, Rodgers and Rowland consider binding to different constituents of the cell, such as lipids and proteins.

Calculation of partition coefficients

Monoprotic and diprotic basic drugs with an acid dissociation constant >7 interact preferentially with acidic phospholipids in the tissue through electrostatic interactions. Binding to extracellular proteins may not play an important role because basic drugs preferentially bind to alpha-acid glycoprotein, which is mostly restricted to plasma. Therefore, an affinity constant for acidic phospholipids ($KaAP$) is calculated for red blood cells. The partition coefficient for the unbound drug into red blood cells can be calculated from the blood-to-plasma (BP) ratio, which itself can be measured in vitro. It is assumed that $KaAP$ is similar for all tissues. Generally, the tissue partition coefficient of the unbound drug (Kpu) for muscle should be preferred as there is a good correlation between the distribution into muscle and the distribution into other tissues. The unbound drug partition coefficient for erythrocytes is given by [352]:

$$Kpu_{RBC} = \frac{C_{RBC}}{C_{PL} \cdot fu_{PL}} = \frac{BP \cdot HCT + (1 - HCT)}{fu_{PL}}, \quad (4)$$

where C = concentration, fu = fraction unbound in plasma, HCT = hematocrit, PL = plasma, and RBC = red blood cells. The affinity constant for acidic phospholipids is given by [352]:

$$KaAP_{RBC} = \left[Kpu_{RBC} - \left(\left(\frac{K_{io,RBC}}{K_{io,PL}} \right) * f_{IW,RBC} \right) - \left(\frac{\log P * f_{NL,RBC} + (0.3 * \log P + 0.7) * f_{NP,RBC}}{K_{io,PL}} \right) \right] * \left[\frac{K_{io,PL}}{[AP]_{RBC} * (K_{io,RBC} - 1)} \right], \quad (5)$$

$$Kpu_{org} = \left(\frac{K_{io,IW} * f_{IW,org}}{K_{io,PL}} \right) + f_{EW,org} + \left(\frac{KaAP_{RBC} * [AP]_{org} * (K_{io,IW} - 1)}{K_{io,PL}} \right) + \left(\frac{\log P * f_{NL,org} + (0.3 * \log P + 0.7) * f_{NP,org}}{K_{io,PL}} \right), \quad (6)$$

where, K_{io} = ionized form according to Henderson-Hasselbalch [353], f_{IW} = fraction of intracellular water, f_{EW} = fraction of extracellular water, f_{NL} = fraction of neutral lipids, f_{NP} = fraction of neutral phospholipids,

and AP = acidic phospholipids. The subscript *org* represents organ. For the partitioning into the adipose tissue, it is more accurate to use the vegetable oil:water partition coefficient ($\log D_{vo:w}$) rather than $\log P$, namely [350]:

$$\log D_{vo:w} = (1.115 * \log P - 1.35) - \log(K_{io,PL}). \quad (7)$$

Binding to extracellular albumin should be considered for drugs that are not moderate to strong bases thus requiring the determination of the affinity constant for binding proteins ($KaPR$). The calculation is done for plasma because albumin concentration in plasma is known, and the unbound fraction in plasma can be determined in in vitro experiments. It is assumed that $KaPR_{PL}$ holds true for all tissues [353], namely:

$$KaPR_{PL} = \left[\frac{1}{fu_{PL}} - 1 - \left(\frac{\log P * f_{NL,PL} + (0.3 * \log P + 0.7) * f_{NP,PL}}{K_{io,PL}} \right) \right] * \frac{1}{PR_{PL}}, \quad (8)$$

where PR_{PL} is the binding protein concentration in plasma in g/L. The unbound drug partition coefficient is given by [353]:

$$Kpu_{org} = \left(\frac{K_{io,IW} * f_{IW,org}}{K_{io,PL}} \right) + f_{EW,org} + (KaPR_{PL} * KpPR_{org} * PR_{PL}) + \left(\frac{\log P * f_{NL,org} + (0.3 * \log P + 0.7) * f_{NP,org}}{K_{io,PL}} \right), \quad (9)$$

where $KpPR_{org}$ is the partition coefficient of plasma binding proteins in different organs.

The apparent volume of distribution in steady state (V_{ss}) can be calculated as follows [354]:

$$V_{ss} = \frac{V_{PL}}{fu_{PL}} + \sum V_{org} * Kp_{org}, \quad (10)$$

where V is the volume and Kp is the total tissue partition coefficient, which is defined as [352]:

$$Kp = \frac{C_{org}}{C_{PL}} = fu * Kpu. \quad (11)$$

A Kp scalar can be introduced to the model, which multiplies the predicted Kp

$$Kp_{used} = Kp * Kp \text{ scalar}, \quad (12)$$

and can be used to correct for insufficient tissue partition prediction. One such example is the extensive lysosomal trapping or binding to intracellular constituents such as DNA (e.g. doxorubicin) [352].

When splitting every compartment of the PBPK model into the subcompartments vascular, interstitial, and intracellular spaces, the distribution through the endothelial cell layer and through the cell membrane are required to inform the PBPK model. The endothelial cell layer is not a tight barrier for small molecule drugs; thus, it can be assumed that the extracellular water is almost instantaneously in equilibrium. Under physiological conditions, blood comes with high pressure into the capillaries and its content is pushed against the endothelial cell layer and through the small and large pores into the interstitial space [356]. There is a partial fluid loss, the lymph, which is recycled back to the venous blood pool via the lymph nodes. Erythrocytes cannot cross the endothelial cell layer and hence the lymph is colorless.

The calculated Kp is used to estimate the flux through the cell membrane between the interstitial and the intracellular spaces, when experimental data about cell membrane permeability are not available. It holds true that the concentration in plasma equals the concentration in the vascular space, which is considered to belong to the blood, namely:

$$Kp = \frac{C_{org}}{C_{PL}} = \frac{C_{ine} + C_{cel}}{C_{vas}} = \frac{C_{ine}}{C_{vas}} + \frac{C_{cel}}{C_{vas}}, \quad (13)$$

where the subscripts *vas*, *ine*, and *cel* represent vascular, interstitial, and intracellular, respectively. Kp is determined in steady state and under steady-state conditions, the vascular and interstitial space concentration differ by the drug concentration in erythrocytes, and the interstitial and intracellular drug concentration differ by the fraction unbound and the flux through the membrane, namely:

$$Kp = \frac{1}{BP} + \frac{J_{in} * fu_{ine}}{J_{out} * fu_{cel}}. \quad (14)$$

Kp can only be described by the ratio of influx (J_{in}) and efflux (J_{out}) of the cell.

Fraction unbound in the interstitial and intracellular space

A critical parameter for the distribution of a drug is fu in each compartment. Usually, fu is only measured in plasma samples, but the site of metabolism or efflux transporters is intracellular, making it necessary

to know $f_{u_{cel}}$. In a first step, the age-dependency of f_u is calculated for each virtual individual based on the measured f_u in vitro and the main binding protein. *Ref* refers to a 30 years old adult, who is arbitrarily used to represent a “young” subject. It is assumed that the binding affinity does not change with age, and therefore f_u for plasma is given by [333]:

$$f_{u_{PL}} = \frac{1}{1 + PR_{PL} * \left(\frac{1}{\frac{f_{u_{Ref}}}{PR_{PL,Ref}} - 1} \right)}. \quad (15)$$

In a second step, f_u in the interstitial space of each organ is estimated based on the known partition coefficient for plasma binding proteins in each tissue [352]. It is assumed that the binding affinity is the same as in plasma. Thus, $f_{u_{ine}}$ is calculated as follows:

$$f_{u_{ine,org}} = \frac{1}{\frac{KpPR_{org}}{f_{EW,org}} * \left(\frac{1}{f_{u_{PL}} - 1} \right) + 1}. \quad (16)$$

$f_{u_{cel}}$ is calculated according to Rodgers & Rowland [353], namely:

$$f_{u_{cel,org}} = \frac{1}{1 + \left[\frac{(\log P * f_{NL,org} + (0.3 * \log P + 0.7) * f_{NP,org})}{K_{io,PL}} + KpPR_{org} * PR_{PL} \right]}. \quad (17)$$

Active drug transporters

Drug transporters can theoretically be implemented into any compartment of the model to represent active distribution into cells, but absolute transporter abundance values to inform the PBPK model are only available for the liver [228]. There are some important points to consider before implementing a transporter into a PBPK model. Each transporter has a direction, and its impact will depend on whether the transporter is expressed on the apical or basolateral site. Passive permeability can occur besides active transport for given compounds, and therefore it is important to define the contribution of each of these transport processes. The overall contribution of uptake transporters is likely to be negligible for compounds characterized by a high passive permeability. Conversely, efflux transporters will have a pronounced impact for compounds characterized by a slow passive diffusion. Importantly, uptake and efflux transporters are exposed to different drug concentrations and thus the unbound drug concentrations in the interstitial and intracellular spaces should be used for uptake and efflux transporters, respectively [357]. Transporter functionality can be described by Michaelis-Menten

kinetics; however, $V_{max,T}/K_{m,T} = CL_{u,int,T}$ [358], where $V_{max,T}$ is the maximum transport rate, $K_{m,T}$ is the Michaelis-Menten constant for a transporter, and $CL_{u,int,T}$ is the intrinsic transport clearance of the unbound drug, only holds true if the unbound concentration is much smaller than K_m ($fu * C \ll K_m$). This is the case under physiological conditions in the cell but might not hold true for uptake transporters being exposed to the interstitial concentration. In addition, Michaelis-Menten assume one binding site per transporter, which is questionable for instance for the organic anion transporting polypeptide 1B1 [359]. Active hepatic drug transporters can be described by [358]:

$$CL_{int,T,tot,hep} = \left[\sum_{u=1}^m \left(\left(\frac{V_{max,up,hep,u}}{K_{m,up,hep,u} + C_{ine} * fu_{ine}} + CL_{int,up,hep,u} \right) * AB_{up,hep,u} \right) - \sum_{e=1}^m \left(\left(\frac{V_{max,ef,hep,e}}{K_{m,ef,hep,e} + C_{cel} * fu_{cel}} + CL_{int,ef,hep,e} \right) * AB_{ef,hep,e} \right) \right] * HPGL * liver\ weight, \quad (18)$$

where $HPGL$ is the hepatocellularity and AB is the abundance. The subscripts T , tot , hep , up , ef , u , and e stand for transporter, total, hepatic, uptake, efflux, uptake, and efflux transporter isoform, respectively.

Metabolism and elimination

The following four different options are described to represent drug clearance in the model:

- 1) enzymatic intrinsic clearance,
- 2) intrinsic hepatic clearance not assigned to a specific enzyme,
- 3) renal clearance, and
- 4) additional plasma clearance.

Enzymatic intrinsic clearance can be either represented as $CL_{int,E}$ or through $V_{max,E}$ and $K_{m,E}$, where $CL_{int,E}$ is the intrinsic clearance, $V_{max,E}$ is the maximum metabolism rate for each enzyme, and $K_{m,E}$ is the Michaelis-Menten constant for each enzyme. Different pathways can be implemented, considering active metabolic pathways [360], namely:

$$CL_{int,E,tot,hep} = \sum_{j=1}^J \left(\sum_{i=1}^I \left(\left(\frac{V_{max,E,hep,j,i}}{K_{m,E,hep,j,i}} + CL_{int,E,hep,j,i} \right) * AB_{E,hep,j} \right) \right) * MPPGL * liver\ weight, \quad (19)$$

$$CL_{int,E,tot,gut} = \left[\sum_{j=1}^J \left(\sum_{i=1}^I \left(\left(\frac{V_{max,E,gut,j,i}}{K_{m,E,gut,j,i}} \right) + CL_{int,E,gut,j,i} * AB_{E,gut,j} \right) \right) \right], \quad (20)$$

where $MPPGL$ is the microsomal protein per gram liver. The subscript E stands for enzyme, i stands for the metabolic pathway, and j represents the enzyme isoform.

The intrinsic hepatic clearance not assigned to a specific enzyme has the units $\mu\text{mol}/\text{min}/\text{mg}$ and is scaled via $MPPGL$ and liver weight but not CYP abundance, namely:

$$CL_{int,tot,hep} = CL_{int,E,tot,hep} + CL_{int,hep} * MPPGL * liver\ weight. \quad (21)$$

The well-stirred liver model is used to calculate the hepatic clearance from the intrinsic clearance [361] and is given by:

$$CL_{hep} = \frac{Q_{LI} * fu_{BL} * CL_{int,tot,LI}}{Q_{LI} + fu_{BL} * CL_{int,tot,LI}}, \quad (22)$$

where CL_{hep} is the total hepatic clearance in L/h, Q_{LI} is the hepatic blood flow, and fu_{BL} is the fraction unbound in blood.

The renal clearance is scaled via the glomerular filtration rate (GFR) and ignores tubular secretion and active transport processes, which would require a more mechanistic PBPK model [362], and is given by [363]:

$$CL_R = CL_{R,Ref} * \frac{GFR}{GFR_{Ref}} * \frac{fu}{fu_{Ref}}, \quad (23)$$

where CL_R is the renal clearance in L/h.

The fourth clearance option in the PBPK model is the additional plasma clearance (CL_{ad}). This parameter is always used as a fixed value, not scaled to any population, but it offers the possibility to enter an in vivo clearance value if clearance mechanism pathways are completely unknown. In cases when there are no measured in vitro values for enzymatic kinetic parameters or $CL_{int,tot,hep}$ but the in vivo clearance and the different contributions of metabolism and elimination pathways are known, a retrograde calculation can be performed to inform the PBPK model [364].

The total clearance can be written as follows:

$$CL_{tot} = \frac{Q_{LI} * fu_{BL} * CL_{int,tot,LI}}{Q_{LI} + fu_{BL} * CL_{int,tot,LI}} + CL_R + CL_{ad}. \quad (24)$$

Drug-drug interactions

The PBPK framework allows simulation of competitive inhibition (whereby the inhibitor binds to the active site of the enzymes and blocks its activity), mechanism-based inhibition (whereby the inhibitor represses the transcription or translation of the metabolizing enzyme leading to a loss of enzyme concentration), and induction. The enzymatic intrinsic clearance (equation 19 for the liver and equation 20 for the gut) needs to be modified accordingly [365]:

$$\sum_{j=1}^J \left(\sum_{i=1}^I \left(\left(\frac{Vmax_{E,x,j,i} * [Sub]}{Km_{E,x,j,i} * \left(1 + \sum_{c=1}^C \frac{[Inh]_c}{Ki_c} \right) + [Sub]} \right) \right) * ABt_{E,x,j} \right), \quad (25)$$

where $[Sub]$ represents the substrate concentration, $[Inh]$ is the concentration of the c^{th} competitive inhibitor, Ki stands for the inhibition constant, ABt is the time-dependent enzyme abundance, and the subscript x represents either the liver or the gut. In the case of mechanism-based inhibition or induction, the enzyme concentration changes with time. The basal state can be described by [365]:

$$\frac{dABt_E}{dt} = k_{deg,E} * AB_E - k_{deg,E} * ABt_E = k_{deg,E} * (AB_{cyp} - ABt_{cyp}), \quad (26)$$

where k_{deg} represent the degradation rate. It holds that $ABt(0) = AB$. In the case of mechanism-based inhibition, equation 26 changes as follows [365]:

$$\frac{dABt_E}{dt} = k_{deg,E} * AB_E - \left(k_{deg,E} + \sum_{m=1}^M \frac{k_{inact,E,m} * [Inh]_m}{K_{app,E,m} + [Inh]_m} \right) * ABt_E, \quad (27)$$

where k_{inact} and K_{app} are the inactivation rate of an enzyme and the apparent enzyme inhibition constant of the m^{th} mechanism-based inhibitor. The syntheses rate changes as followed for induction [365]:

$$\frac{dABt_E}{dt} = k_{deg,E} * AB_E * \left(1 + \sum_{i=1}^I \frac{IndMax_{E,i} * [Inh]_i}{IC_{50,E,i} + [Inh]_i} \right) - k_{deg,E} * ABt_E, \quad (28)$$

where $IndMax$ and IC_{50} are the maximum fold of induction and the half maximal inducer concentration of the i^{th} inducer. All DDI mechanisms are accounted for in Equation 25.

3.3.4 Step 4: Bridge system and drug data – the ordinary differential equation solver

After generating the population and drugs to inform the PBPK model, the ODEs are set up. ODEs are solved for each individual (*ind*) and each dose event (*n*) by the build-in stiff ODE solver ode15s [366] to ensure efficient running times of the code.

```
function[] = Solve ODE()
```

```
%This function solves the ordinary differential equations (ODEs)
```

```
Convert variables from global to local
```

```
Calculate the number of ODE equations
```

```
Get the number of simulated time points for each dosing event and the entire simulation
```

```
Initialize a vector for the simulated time points
```

```
Initialize a matrix for the simulated concentrations
```

```
Run the ODE system for each virtual individual separately
```

```
Set the initial concentrations for the first / single dose
```

```
Run the ODE system for each dosing event separately
```

```
Set the initial concentrations for multiple dosing events
```

```
Solve the ODEs
```

```
Generate time steps for each dosing event with the user-defined resolution
```

```
Evaluate the solution from the ODE system for each given time point
```

```
Combine time points for each dosing event in the time vector
```

```
Combine concentrations for each dosing event
```

```
end
```

```
end
```

```
end
```

The function defining the initial concentration C_0 for single doses and M_0 for multiple dosing events needs to consider the drug concentration in a compartment at the timepoint of the n^{th} multiple dose and is given by:

```
function C0 = Initialize();
```

```
    Set the initial concentration of each compartment to zero
```

```
    Set the initial CYP abundance in the liver and intestine according to [66, 367]
```

```
    Define a case for each drug
```

```
        switch the route of administration for each drug
```

```
            iv bolus: venous blood concentration is the dose divided by the venous volume
```

```
            oral: stomach concentration is the dose divided by the stomach volume
```

```
        end
```

```
    end
```

```
end
```

```
function M0 = Initialize_M(C0)
```

```
    if the first dose is administered
```

```
        then M0 has been defined by C0
```

```
    else
```

```
        M0 is defined by the calculated concentration of the last dosing event
```

```
    Define a case for each drug
```

```
        switch the route of administration for each drug
```

```
            iv bolus: add dose divided by venous volume to the venous concentration
```

```
            oral: add dose divided by the stomach volume to the stomach concentration
```

```
        end
```

```
    end
```

```
end
```

```
end
```

A relevant element is to define the right-hand side of the ODEs to describe the dynamic drug movement from and to each compartment. The ODEs can be written as follows for the vascular, interstitial, and intracellular space of a generic compartment:

$$\frac{dC_{vas,org}}{dt} = \frac{1}{V_{vas,org}} * \left[Q_{org} * C_{ab} - (Q_{org} - L_{org}) * C_{vas,org} - J_{vas,org} * \left(\frac{C_{vas,org}}{BP} \right) + J_{ine,org} * C_{ine,org} \right], \quad (29)$$

$$\frac{dC_{ine,org}}{dt} = \frac{1}{V_{ine,org}} * \left[J_{vas,org} * \left(\frac{C_{vas,org}}{BP} \right) - J_{ine,org} * C_{ine,org} - L_{org} * C_{ine,org} - J_{in,org} * C_{ine,org} * fu_{ine,org} + J_{out,org} * C_{cel,org} * fu_{cel,org} \right], \quad (30)$$

$$\frac{dC_{cel,org}}{dt} = \frac{1}{V_{cel,org}} * \left[J_{in,org} * C_{ine,org} * fu_{ine,org} - J_{out,org} * C_{cel,org} * fu_{cel,org} \right], \quad (31)$$

where Q is the blood flow, L is the lymph flow, J is a flux, and the subscript ab represents the arterial blood pool. The Matlab® function defining the right-hand side of the ODEs 29 to 31 is written in the following way:

```
function dtdy = rhs(~, y)
```

```
    Initialize the output as a column vector containing only zeros
```

```
    Write the differential equations
```

```
end
```

Some organs require a more detailed ODE than the generic ODEs described in equations 29 to 31. Blood flows from the venous blood pool into the lungs and after being loaded with oxygen, blood returns to the arterial blood pool. Therefore, the ODE of the vascular space of the lungs is given by:

$$\frac{dC_{vas,LU}}{dt} = \frac{1}{V_{vas,LU}} * \left[CO * C_{vb} - (CO - L_{LU}) * C_{vas,LU} - J_{vas,LU} * \left(\frac{C_{vas,LU}}{BP} \right) + J_{ine,LU} * C_{ine,LU} \right], \quad (32)$$

where CO is the cardiac output, and the subscripts LU and vb represents the lung and the venous blood pool, respectively.

In the kidney, the renal clearance should be considered. A mechanistic kidney model including renal transporters is not described in this tutorial.

$$\begin{aligned} \frac{dC_{vas,KI}}{dt} = \frac{1}{V_{vas,KI}} * \left[Q_{KI} * C_{ab} - (Q_{KI} - L_{KI}) * C_{vas,KI} - J_{vas,KI} * \left(\frac{C_{vas,KI}}{BP} \right) + J_{ine,KI} * \right. \\ \left. C_{ine,KI} - CL_R * C_{vas,KI} * \frac{fu_{PL}}{BP} \right], \end{aligned} \quad (33)$$

where the subscript *KI* stands for the kidney.

In the liver, active drug transporters and hepatic metabolism by enzymes are included and given by:

$$\begin{aligned} \frac{dC_{vas,LI}}{dt} = \frac{1}{V_{vas,LI}} * \left[Q_{ha} * C_{ab} + Q_{PVBV} * C_{ab} + (Q_{GU} - L_{GU}) * C_{vas,GU} + Q_{SP} * \right. \\ \left. C_{vas,SP} + (Q_{PA} - L_{PA}) * C_{vas,PA} - (Q_{LI} - L_{LI}) * C_{vas,LI} - J_{vas,LI} * \right. \\ \left. \left(\frac{C_{vas,LI}}{BP} \right) + J_{ine,LI} * C_{ine,LI} \right], \end{aligned} \quad (34)$$

$$\begin{aligned} \frac{dC_{ine,LI}}{dt} = \frac{1}{V_{ine,LI}} * \left[J_{vas,LI} * \left(\frac{C_{vas,LI}}{BP} \right) - J_{ine,LI} * C_{ine,LI} - L_{LI} * C_{ine,LI} - J_{in,LI} * C_{ine,LI} * \right. \\ \left. fu_{ine,LI} + J_{out,LI} * C_{cel,LI} * fu_{cel,LI} - \sum_{u=1}^m \left(\frac{V_{max,up,hep,u} * C_{ine,LI} * fu_{ine,LI}}{K_{m,up,hep,u} + C_{ine,LI} * fu_{ine,LI}} + \right. \right. \\ \left. \left. CL_{int,up,hep,u} * C_{ine,LI} * fu_{ine,LI} \right) * AB_{up,hep,u} * HPGL * W_{LI} + \right. \\ \left. \sum_{e=1}^m \left(\frac{V_{max,eff,hep,e} * C_{cel,LI} * fu_{cel,LI}}{K_{m,eff,hep,e} + C_{cel,LI} * fu_{cel,LI}} + CL_{int,eff,hep,e} * C_{ine,LI} * fu_{ine,LI} \right) * \right. \\ \left. AB_{eff,hep,e} * HPGL * W_{LI} \right], \end{aligned} \quad (35)$$

$$\begin{aligned} \frac{dC_{cel,org}}{dt} = \frac{1}{V_{cel,org}} * \left[J_{in,LI} * C_{ine,LI} * fu_{ine,LI} - J_{out,LI} * C_{cel,LI} * fu_{cel,LI} + \right. \\ \left. \sum_{u=1}^m \left(\frac{V_{max,up,hep,u} * C_{int,LI} * fu_{int,LI}}{K_{m,up,hep,u} + C_{int,LI} * fu_{int,LI}} + CL_{int,up,hep,u} * C_{ine,LI} * fu_{ine,LI} \right) * \right. \\ \left. AB_{up,hep,u} * HPGL * W_{LI} - \sum_{e=1}^m \left(\frac{V_{max,eff,hep,e} * C_{cel,LI} * fu_{cel,LI}}{K_{m,eff,hep,e} + C_{cel,LI} * fu_{cel,LI}} + \right. \right. \\ \left. \left. CL_{int,eff,hep,e} * C_{ine,LI} * fu_{ine,LI} \right) * AB_{eff,hep,e} * HPGL * W_{LI} - \right. \\ \left. \left[\sum_{j=1}^J \left(\sum_{i=1}^I \left(\frac{V_{max,E,hep,j,i}}{K_{m,E,hep,i,j} * (1 + \sum [Inh]) / Ki} + C_{cel,LI} * fu_{cel,LI} \right) + CL_{int,E,hep,j,i} \right) * \right. \right. \\ \left. \left. AB_{t,E,hep,j} \right) + CL_{int,hep} \right] * MPPGL * W_{LI} * C_{cel,LI} \right], \end{aligned} \quad (36)$$

where the subscripts *LI*, *ha*, *PVBY*, *GU*, *SP*, *PA*, *up*, and *eff* represents liver, hepatic arterial, portal vein bypass, gut, spleen, pancreas, uptake, and efflux, respectively.

Lymph fluid flows through afferent lymph vessels from the interstitial space of organs to the central lymph-node compartment and further to the venous blood pool, given by:

$$\frac{dC_{vas, LN}}{dt} = \frac{1}{V_{vas, LN}} * [Q_{LN} * (C_{ab} - C_{vas, LN}) + L_{tot} * (C_{ine, LN} - C_{vas, LN})], \quad (37)$$

$$\begin{aligned} \frac{dC_{ine, LN}}{dt} = \frac{1}{V_{ine, LN}} * [\sum_{org=1}^O (L_{org} * C_{ine, org}) - L_{tot} * C_{ine, LN} - J_{in, LN} * C_{ine, LN} * \\ fu_{ine, LN} + J_{out, LN} * C_{cel, LN} * fu_{cel, LN}], \end{aligned} \quad (38)$$

where L_{tot} is the total lymph flow and the subscript *LN* represents the central lymph-node compartment.

The ODEs for the venous and arterial blood compartments are given by:

$$\begin{aligned} \frac{dC_{vb}}{dt} = \frac{1}{V_{vb}} * [C_{vas, AD} * (Q_{AD} - L_{AD}) + C_{vas, BO} * Q_{BO} + C_{vas, BR} * (Q_{BR} - L_{BR}) + \\ C_{vas, GO} * (Q_{GO} - L_{GO}) + C_{vas, HE} * (Q_{HE} - L_{HE}) + C_{vas, KI} * (Q_{KI} - L_{KI}) + \\ C_{vas, MU} * (Q_{MU} - L_{MU}) + C_{vas, SK} * (Q_{SK} - L_{SK}) + C_{vas, TH} * (Q_{TH} - L_{TH}) + \\ C_{vas, LI} * (Q_{LI} - L_{LI}) + C_{vas, LN} * (Q_{LN} + L_{tot}) + C_{vas, RE} * (Q_{RE} - L_{RE}) - \\ CO * C_{vb}], \end{aligned} \quad (39)$$

$$\frac{dC_{ab}}{dt} = \frac{1}{V_{ab}} * [(CO - L_{LU}) * C_{vas, LU} - \sum_{o=1}^O (Q_{org, o} * C_{ab}) - CL_{ad} * C_{ab} * \frac{fu_{PL}}{BP}], \quad (40)$$

where the subscripts *AD*, *BO*, *BR*, *GO*, *HE*, *MU*, *SK*, *TH*, and *RE* represent adipose tissue, bone, brain, gonads, heart, muscle, skin, thymus, and remaining organ, respectively.

The solution of the different equation needs to be evaluated in Matlab® using the implemented *deval* function over a predefined number of time points (*NumPoints*). The solution for the drug concentration of each compartment is saved in the matrix *Conc*, and the corresponding time point to the concentration is saved in the vector *Time* as described previously.

3.3.5 Step 5: Work with the simulated data – the postprocessing step

The solution of the ODE solver has been saved into a single matrix. The first step of postprocessing is therefore to extract the concentration for each compartment of the model from the solution matrix of the ODE solver. Different statistics can now be calculated with the extracted concentrations such as the mean and the 5% and 95% confidence interval with predefined Matlab® commands, which require the Statistics and Machine Learning Toolbox as an Add-On to the Matlab® suite.

One important aspect of postprocessing is to ensure mass balance of the model. The concentration of each compartment is multiplied by the compartmental volume, and the drug amount cleared by a specific pathway as well as the amount not being absorbed are integrated and added together. The product should be equivalent to the dose entered in the study design.

Pharmacokinetic parameters, such as the peak concentration (C_{max}), the time to reach peak concentration (t_{max}), the area under the curve (AUC), the apparent clearance (CLF), the apparent volume of distribution (VdF), and the elimination half-life ($t_{1/2}$) can be calculated for each compartment. The elimination rate is used to extrapolate the AUC to infinity and to calculate the clearance and the volume of distribution.

```
function[] = PostProcessing()

%This function processes the data from the ODE solution and outputs the results
%Attention: Some statistical calculations (geomean , prctile) require...
%the Statistical and Machine Learning Toolbox

Initialize Cmax
Initialize tmax
Initialize AUCt          %area under the curve for one dosing interval

Calculate PK parameters for each simulated drug
    Calculate PK parameters for each virtual individual
        if the venous concentration at timepoint t is greater than Cmax
            than the venous concentration at timepoint t is the new Cmax
            than the timepoint t is the new tmax
        end
```

```

        Calculate the AUCt according to the linear trapezoidal rule
    end
end

Take the logarithm of the concentration for extrapolation to infinity

Initialize the slope and beta

Calculate the slope and beta for each simulated drug
    Calculate the slope and beta for each virtual individual
        Linear regression of the last four time points
        Beta is the slope of the regression
    end
end

LogVenousConc = log10(VenousConc);

Half-life is the natural logarithm of two divided by beta
AUC extrapolated to infinity is the AUCt plus the venous concentration at the last simulated...
time point divided by beta
Clearance is the dose divided by the AUC extrapolated to infinity
Volume of distribution is the clearance divided by beta

end

```

As shown above for the concentration, the mean and the confidence interval or other statistics can be calculated for pharmacokinetic parameters.

The results can be either output graphically using the build-in *plot* function or can be exported to Excel® (Microsoft, Redmond, WA) using the *xlswrite* command.

3.4 Simulation of the DDI magnitude between rivaroxaban and darunavir/ritonavir

To illustrate the steps of PBPK model development, the DDI magnitude between a single dose of rivaroxaban and darunavir boosted with ritonavir under steady state conditions will be simulated (Figure 3.5). The rivaroxaban PBPK model was developed combining published in vitro data (bottom-up approach) with clinical clearance data (top-down approach). Verified PBPK models for darunavir and ritonavir were used [368]. Ritonavir has an impact on the renal clearance of rivaroxaban [369], which

was considered in the model. The parameters of the drug models can be found in the code (<https://ascpt.onlinelibrary.wiley.com/doi/full/10.1002/psp4.12399>). A clinical DDI study investigating the effect of 600 mg ritonavir twice daily on a single 10 mg dose of oral rivaroxaban in 12 healthy men aged 18 to 44 years was used to verify the rivaroxaban model [369]. A total of 10 virtual trials with 12 men (proportion of women is set to zero) aged 20 to 44 years were simulated. Afterwards, the effect of 800/100 mg darunavir/ritonavir once daily on a single oral dose of 10 mg rivaroxaban was simulated because the boosted protease inhibitor is given in clinical practice.

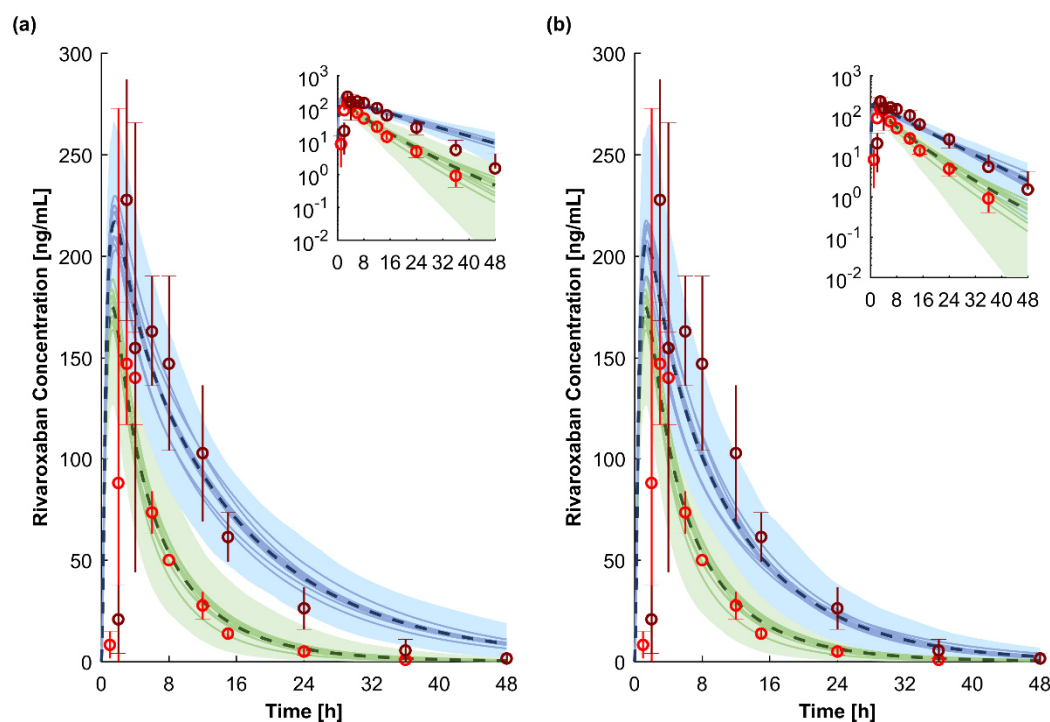


Figure 3.5: PBPK simulations for a single dose of 10 mg rivaroxaban administered with 600 mg ritonavir twice daily (a) and 800/100 mg darunavir/ritonavir once daily in steady state (b). Green and blue represent rivaroxaban in the absence and presence of the perpetrators. The dashed line and the shaded area are the mean and the 95% confidence interval for the prediction of all virtual individuals, respectively. The solid lines show the mean of each virtual trial (10 trials with 12 virtual subjects per trial have been simulated). The red and the dark red circles show observed clinical data of 10 mg rivaroxaban alone and co-administered with 600 mg ritonavir twice daily [369].

The simulation of 10 mg rivaroxaban with and without 600 mg of oral ritonavir were in good agreement with the observed clinical data (Figure 3.5a). The t_{\max} of rivaroxaban was underpredicted by twofold because t_{\max} was achieved 1.5 h later in the clinical study compared to the simulation. However, the predicted t_{\max} ratio of rivaroxaban administered with 600 mg ritonavir twice daily and rivaroxaban given without a perpetrator was within 1.25-fold of the observed data. The elimination half-life of rivaroxaban was overpredicted by twofold, but C_{\max} and AUC were predicted within 1.25-fold (bioequivalence

criterion; Table 3.2) of clinically observed data. The effect of 100 mg ritonavir once daily used to boost darunavir in clinical practice is predicted to be similar to 600 mg of ritonavir twice daily (Figure 3.5b), because full inhibition of CYP3A4 and CYP2J2 is already achieved at lower ritonavir concentrations.

The predicted concentrations of the two perpetrators darunavir (800 mg once daily) and ritonavir (100 mg once daily) are in accordance to observed clinical data from various studies (Figure 3.6). The t_{\max} of ritonavir was underpredicted by twofold, but all other pharmacokinetic parameter of boosted darunavir and ritonavir were within the 1.25-fold interval of the clinically observed data (Table 3.2).

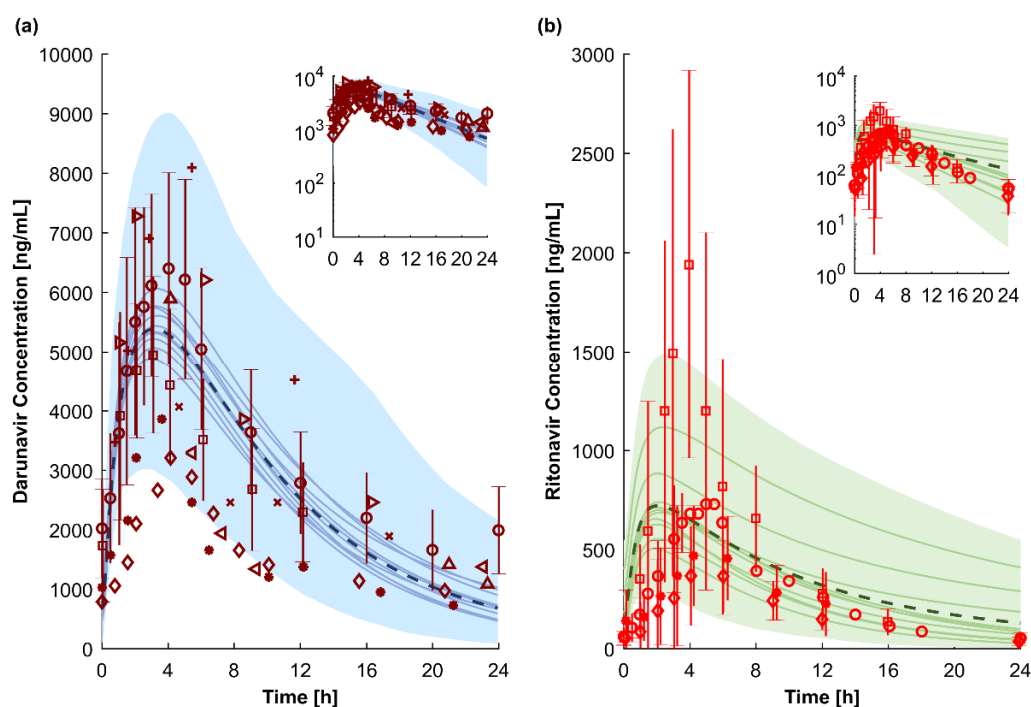


Figure 3.6: PBPK simulations for 800 mg darunavir once daily boosted with 100 mg ritonavir once daily (a) and 100 mg ritonavir once daily (b). The dashed line and the shaded area are the mean and the 95% confidence interval for the prediction of all virtual individuals, respectively. The solid lines how the mean of each virtual trial (10 trials with 12 virtual subjects per trial have been simulated). The red markers show observed clinical data (a: [370-372] and b: [371, 373, 374]).

3.5 Conclusion

We have described a comprehensive strategy to develop and code a PBPK model in Matlab® with potential applications in other pharmacological scenarios. Of interest, PBPK models are increasingly accepted for the prediction of DDIs and drug disposition in special populations such as pediatrics and the elderly. Furthermore, this type of computational framework can be integrated with pharmacodynamic models, which can be easily added to custom build PBPK models in Matlab®.

Table 3.2: Observed vs. predicted pharmacokinetic parameters for rivaroxaban (10 mg; single) in combination with ritonavir (600 mg once daily) and boosted darunavir (800/100 mg once daily), darunavir (800 mg once daily) boosted with ritonavir (100mg once daily).

Pharmacokinetic parameter	C_{max} [ng/mL]		t_{max} [h]		AUC [ng·h/mL]		$t_{1/2}$ [h]	
	observed	predicted	observed	predicted	observed	predicted	observed	predicted
Rivaroxaban 10 mg	153.7 ± 23.7	162.7 ± 26.9	3.0 ± 0.5	1.5 ± 0.1	1,000 ± 161	1,208 ± 268	5.7 ± 1.8	12.5 ± 3.3
Rivaroxaban 10 mg + Ritonavir 600 mg twice daily	238.0 ± 55.7	197.4 ± 32.6	4.0 ± 2.2	1.6 ± 0.2	2,529 ± 425	2,761 ± 875	6.9 ± 2.2	20.2 ± 4.7
Ratio	1.55 ± 0.43	1.21 ± 0.28	1.33 ± 0.77	1.09 ± 0.14	2.53 ± 0.59	2.29 ± 0.88	1.21 ± 0.53	1.62 ± 0.57
Rivaroxaban 10 mg + Darunavir/r 800/100 mg once daily	-	190.0 ± 31.2	-	1.7 ± 0.2	-	2,510 ± 685	-	19.9 ± 5.2
Ratio	-	1.17 ± 0.27	-	1.16 ± 0.15	-	2.08 ± 0.73	-	1.60 ± 0.60
Darunavir/r 800/100 mg once daily	6,803 ± 1,618	5,432 ± 1,929	3.6 ± 1.6	3.1 ± 0.5	75,780 ± 22,102	75,002 ± 56,887	14.4 ± 5.2	10.9 ± 5.7
Ritonavir 100 mg once daily	606 ± 281	531 ± 280	3.1 ± 2.0	1.8 ± 0.5	5,296 ± 4,664	5,470 ± 3,132	6.3 ± 1.5	5.4 ± 1.4

Data are presented as mean +/- standard deviation. Published clinically observed data were used for model verification for rivaroxaban [369], darunavir [370-372], and ritonavir [371, 373].

Key: AUC = area under the curve, C_{max} = peak concentration, t_{max} = time to C_{max} , $t_{1/2}$ = elimination half-life.

3.6 Appendix

Table A3.1: Parameters with their abbreviation and units used to build the PBPK model.

Parameter	Abbreviation	Unit
concentration of acidic phospholipids	[AP]	-
inhibitor concentration	[Inh]	mg/L
substrate concentration	[Sub]	mg/L
abundance	AB	hepatic enzymes pmol/mg hepatic transporters pmol/Mio cells intestinal enzymes nmol/intestine intestinal transporter fmol/cm ²
time-dependent abundance	ABt	units see abundance
blood-to-plasma ratio	BP	-
concentration	C	mg/L
clearance	CL	L/h
absorption clearance	CL _{ab}	L/h
intrinsic clearance of an enzyme / transporter isoform	CL _{int}	μL/min/pmol enzyme / transporter
intrinsic clearance not assigned to a specific enzyme	CL _{int,hep}	μL/min/mg protein
cardiac output	CO	L/h
fraction of extracellular water	f _{EW}	-
fraction of intracellular water	f _{IW}	-
fraction of neutral lipids	f _{NL}	-
fraction of neutral phospholipids	f _{NP}	-
fraction unbound	f _u	-
fold expansion factor for the villi of the surface area	F _{villi}	-
glomerular filtration rate	GFR	mL/min
hematocrit	HCT	-
hepatocytes per gram liver	HPGL	Mio cells / g liver
half maximal inducer concentration	IC ₅₀	μM
maximum fold induction	IndMax	-
flux	J	L/h
affinity constant for acidic phospholipids	KaAP	-
apparent inhibition constant	K _{app}	μM
affinity constant for binding proteins	KaPR	-
degradation rate	k _{deg}	1/h
inhibition constant	K _i	μM
inactivation rate	k _{inact}	1/h
ionized form	K _{io}	-
Michaelis-Menten constant	K _m	μM
partition coefficient of plasma binding proteins	KpPR	-
unbound drug partition coefficient	Kpu	-
length	Le	cm
lymph flow	L	L/h
vegetable oil-water partition coefficient	logD	-
octanol-water partition coefficient	logP	-
total lymph flow	L _{tot}	L/h
microsomal proteins per gram liver	MPPGL	mg / g liver
apparent permeability	P _{app}	10 ⁻⁶ cm/sec
effective permeability in man	P _{eff,man}	10 ⁻⁴ cm/sec
binding protein concentration	PR	g/L

Table A3.1: cont.

Parameter	Abbreviation	Unit
permeability surface area	PSA	cm ²
blood flow	Q	L/h
radius	R	cm
volume	V	L/h
maximum velocity	V _{max}	pmol/min/pmol enzyme / transporter
volume of distribution at steady state	V _{ss}	L

Table A3.2: Subscripts and their abbreviation used to build the PBPK model.

Parameter	Abbreviation
arterial blood	ab
additional	ad
adipose tissue	AD
bone	BO
brain	BR
intracellular space	cel
enzyme	E
efflux	ef
gonads	GO
gut	GU
hepatic arterial	ha, hep
heart	hep
interstitial space	ine
intracellular water	IW
kidney	KI
liver	LI
lymph-node	LY
lung	LU
muscle	MU
organ	org
pancreas	PA
plasma	PL
portal vein bypass	PVBY
renal	R
red blood cells	RBC
remaining organ	RE
refers to a 30 years old subject arbitrarily chosen to represent a "young" subject	Ref
skin	SK
spleen	SP
transporter	T
thymus	TH
total	tot
uptake	up
vascular space	vas
venous blood	vb

3.7 *Electronic Supplementary Material*

The online version of this article contains supplementary material:

<https://doi.org/10.1002/psp4.12399>

Table S1: Parameters and their abbreviation and units used to build the PBPK model. See Table A3.1.

Table S2: Subscripts and their abbreviation used to build the PBPK model. See Table A3.2.

Material S1: The PBPK model code is published open access. Not included in this thesis.

Chapter 4:

Pharmacokinetic Changes in the Elderly

4. Pharmacokinetic Changes in the Elderly

4.1	Abstract	Page 90
4.2	Key Points	Page 91
4.3	Introduction	Page 91
4.4	Methods	Page 93
4.4.1	Physiologically based pharmacokinetic model	Page 93
4.4.2	Parameters of simulated drugs	Page 93
4.4.3	Workflow for simulations	Page 95
4.4.4	Verification of the PBPK drug models	Page 96
4.4.5	Extrapolation to aged individuals	Page 96
4.4.6	Sensitivity analysis	Page 98
4.4.7	Verification of the extrapolation to aged individuals	Page 98
4.5	Results	Page 99
4.5.1	Predicting drug pharmacokinetics in the elderly	Page 99
4.5.2	Pharmacokinetic parameters driving age-related changes in drug exposure	Page 108
4.6	Discussion	Page 114
4.7	Conclusion	Page 118
4.8	Electronic Supplementary Information	Page 119

This chapter is a pre-printed version of a peer-reviewed original research article published under the following reference:

Physiologically based pharmacokinetic modelling to identify pharmacokinetic parameters driving drug exposure changes in the elderly

Felix Stader, Hannah Kinvig, Melissa A. Penny, Manuel Battegay, Marco Siccardi, & Catia Marzolini

Clinical Pharmacokinetics 2020; 59(3): 383-401.

DOI: 10.1007/s40262-019-00822-9

4.1 Abstract

Background:

Medication use is highly prevalent with advanced aging, but clinical studies are rarely conducted in the elderly, leading to limited knowledge regarding age-related pharmacokinetic changes.

Objective:

The objective of this study was to investigate which pharmacokinetic parameters determine drug exposure changes in the elderly by conducting virtual clinical trials for ten drugs (midazolam, metoprolol, lisinopril, amlodipine, rivaroxaban, repaglinide, atorvastatin, rosuvastatin, clarithromycin, and rifampicin) using our physiologically based pharmacokinetic (PBPK) framework.

Methods:

PBPK models for all ten drugs were developed in young adults (20 to 50 years) following the best practice approach, before predicting pharmacokinetics in the elderly (at least 65 years) without any modification of drug parameters. A descriptive relationship between age and each investigated pharmacokinetic parameter (peak concentration: C_{\max} , time to C_{\max} : t_{\max} , area under the curve: AUC, clearance, apparent volume of distribution, elimination-half-life: $t_{1/2}$) was derived using the final PBPK models, and verified with independent clinically observed data from 52 drugs.

Results:

The age-related changes in drug exposure were successfully simulated for all ten drugs. Pharmacokinetic parameters were predicted within 1.25-fold (70%), 1.5-fold (86%), and 2.0-fold (100%) of clinical data. AUC increased progressively by 0.9% per year throughout adulthood from the age of 20 years, which was explained by decreased clearance, while C_{\max} , t_{\max} , and the apparent volume of distribution were not affected by aging. Additional clinical data of 52 drugs were contained within the estimated variability of the established age-dependent correlations for each pharmacokinetic parameter.

Conclusion:

The progressive decrease in hepatic and renal blood flow, as well as in the glomerular filtration rate led to a reduced clearance driving exposure changes in the healthy elderly, independent of the drug.

4.2 Key Points

Drug pharmacokinetics in the elderly (at least 65 years) were accurately predicted by our developed physiologically based pharmacokinetic framework. The model suggested an average 0.9% increase in the area under the curve per year from the age of 20 years, which was explained by a decrease in clearance rather than an effect of altered drug absorption and distribution, because the peak concentration (C_{\max}), time to C_{\max} , and apparent volume of distribution were not affected by advanced aging. Sensitivity analysis and statistical analysis of clinical pharmacokinetic data collected for 52 drugs showed that the progressive decrease of hepatic and renal blood flow and the glomerular filtration rate led to the reduced clearance, and thus drove drug exposure changes in the elderly, independent of the drug.

4.3 Introduction

The number of people older than 65 years is predicted to double in the United States and Europe by 2050 [375, 376]. The burden of age-related comorbidities, such as cardiovascular diseases, hypertension, diabetes mellitus, and renal impairment, increases in the elderly [377], resulting in twice as high medication use compared with middle-aged adults [378]. Despite the growing population of elderly individuals, clinical trials are generally not conducted in this special population, leading to a knowledge gap regarding the effect of adult age on drug pharmacokinetics [379]. However, advanced aging is characterized by anatomical, physiological, and biological changes [58], which have the potential to affect the absorption, distribution, metabolism, and elimination processes of a drug, resulting in altered pharmacokinetics.

The impact of advanced aging on drug absorption processes remains inconclusive due to contradictory findings in the literature. For instance, gastric emptying time is reported to be slower, similar or faster in elderly compared with young adults. The distribution of drugs is affected by a progressive increase of adipose tissue weight, while total body water declines in the elderly. Hepatic drug metabolism is potentially affected by age-related changes in liver weight and hepatic blood flow, which are decreased by 10% and 18%, respectively, in 70 years old individuals compared with 30 years old individuals. Reports regarding hepatic enzyme activity in the elderly are sparse and contradictory. The only well-studied hepatic enzyme is cytochrome P-450 (CYP) 3A, which shows age-independent activity [58].

Polasek *et al.* investigated five different probe substrates for hepatic metabolism, namely caffeine (CYP1A2), warfarin (CYP2C9), phenytoin (CYP2C19), desipramine (CYP2D6), and midazolam (CYP3A), and found a clearance decrease of 30 to 40% in 70 years old subjects compared with younger individuals, which was explained by the changes in liver volume and hepatic blood flow rather than enzyme activity [223]. Data regarding drug transporter activity are generally sparse, but in a compact meta-analysis, age was tested as a covariate for hepatic drug transporter activity and was found to be non-significant [228]. Lastly, the most significant change with adult aging is the reduction in renal drug clearance, namely because of a reduction in kidney weight caused by a loss of nephrons, decreased renal blood flow, and consequently, a decline in the glomerular filtration rate during the entire adulthood [58].

Age-dependent anatomical, physiological, and biological changes can be incorporated into a physiologically based pharmacokinetic (PBPK) model, which is used to overcome sparse clinical data offering the possibility to run virtual clinical trials for special populations such as the elderly [58, 131, 380]. A PBPK model describes the absorption, distribution, metabolism, and elimination of a drug in a physiologically relevant compartmental structure, where each compartment represents an organ or tissue. Dynamic movement of the drug between compartments is mediated by regional blood flows and described by ordinary differential equations. The PBPK model is informed by a combination of in vitro and in vivo data regarding drug characteristics that are separated from physiological data describing the population of interest [118].

The first aim of the present study was to evaluate the prediction of drug disposition in the elderly of our previously developed and parameterized PBPK framework [118]. The second aim was to determine pharmacokinetic parameters driving clinically observed drug exposure changes in the elderly through sensitivity analysis on age. We investigated which physiological and drug-specific parameters determined the degree of age-dependent changes of pharmacokinetic parameters in the model by sensitivity analysis and with clinically observed data for 52 drugs additionally collected. Lastly, we analyzed the age at which pharmacokinetic parameters changed more than expected with respect to interindividual variability in comparison to the youngest studied age group (20 to 24 years).

4.4 Methods

4.4.1 Physiologically based pharmacokinetic model

A whole-body PBPK model constructed in Matlab® 2017a was used. The model structure and code have been published previously [118]. Virtual individuals aged 20 to 99 years were generated according to our published repository describing age-dependent changes in anatomical, physiological, and biological system parameters. Variability was considered for all population parameters by using a normal distribution [58].

4.4.2 Parameters of simulated drugs

A structured literature search was performed to identify drugs with available pharmacokinetic data in elderly individuals in order to clinically verify the PBPK model simulations. Ten drugs were selected including midazolam, metoprolol, lisinopril, amlodipine, rivaroxaban, repaglinide, atorvastatin, rosuvastatin, clarithromycin, and rifampicin. Input drug parameters were obtained from verified, published PBPK models [101, 118, 328, 358, 381-385], except for lisinopril. The lisinopril PBPK model was developed combining published in vitro data (bottom-up approach) with available clinical clearance data (top-down approach). PBPK models were modified to adequately predict the pharmacokinetics in young adults before scaling the PBPK models to the elderly. Simulations of metoprolol were carried out in extensive metabolizers of CYP2D6 only. Tissue distribution of the amlodipine model has been modified to be used in a whole-body PBPK model based on the observed volume of distribution [386]. Metabolic CYP3A4 clearance of amlodipine was calculated from the fraction of CYP3A4 mediated clearance [387] and clinically obtained intravenous clearance [386]. The in vitro ratio between CYP3A4- and CYP3A5-mediated clearance for amlodipine was implemented [388]. The rest of the missing, observed amlodipine clearance was assigned to the unspecified hepatic intrinsic clearance. Active hepatic drug transport was included in the repaglinide PBPK model based on published in vitro data [385]. The rifampicin clearance after intravenous administration was retrogradely calculated to an unspecified intrinsic hepatic clearance under the consideration of the renal clearance of rifampicin [365, 389]. The parameters of the ten simulated drugs can be found in Table 4.1.

Table 4.1: Parameter of the simulated non-HIV drugs.

Parameter	Unit	MID	MET	LIS	AML	RIV	REP	ATO	ROS	CLA	RIF
<i>Physicochemical properties</i>											
MW	g/mol	325.8 [384]	267.4 [381]	405.5 [390]	408.9 [382]	435.9 [391]	452.6 [101]	558.7 [383]	481.5 [358]	748.0 [384]	823.0 [389]
logP		3.89 [392]	1.88 [381]	-1.10 [393]	2.96 [382]	1.50 [391]	3.95 [101]	5.70 [383]	2.40 [358]	3.16 [394]	3.28 [389]
drug type		mb [395]	mb [381]	am [396]	mb [382]	mb [397]	am [398]	ma [383]	ma [358]	mb [399]	am [389]
pKa 1		6.2 [395]	9.8 [381]	7.2 [396]	9.1 [382]	-1.6 [397]	6.2 [398]	4.5 [383]	4.3 [358]	9.0 [394]	1.7 [389]
pKa 2				3.1 [396]			4.0 [398]				7.9 [389]
BP		0.60 [384]	1.15 [381]	0.60 pre [401]	0.60 [382]	0.71 [400]	0.62 [101]	0.61 [383]	0.63 [358]	0.64 [384]	0.90 [389]
fup		0.03 [384]	0.88 [381]	1.00 [401]	0.03 [382]	0.07 [400]	0.03 [101]	0.05 [383]	0.11 [358]	0.43 [384]	0.15 [389]
binding protein		HSA [402]	HSA [381]	-	HSA [403]	HSA [391]	HSA [404]	HSA [405]	HSA [358]	HSA [406]	HSA [407]
<i>Absorption</i>											
P _{app}	10 ⁻⁶ cm/sec	210 [384]	27.0 [408]	0.33 [343]	22.3 [409]	8.00 [391]	26.1 [101]	17.6 [383]	0.55 [358]	1.23 [384]	1.47 [389]
Lag Rate			0.2 op	0.2 op	0.04 op	1.25 op	3.0 op	3.0 op	1.0 op	0.3 op	3.0 op
<i>Distribution</i>											
Tissue Scalar					2.3 op			3.0 op		0.7 op	
Adipose tissue Scalar					15.0 op						
Muscle Scalar					10.0 op						
Liver Scalar					3.0 op						
<i>Metabolism & Elimination</i>											
CYP2D6 CL _{int}	μL/min/pmol		3.81 [381]								
CYP3A4 CL _{int}	μL/min/pmol	2.58 [384]	0.038 [381]		0.942 ret	0.06 [400]	0.50 [410]	2.15 [383]			
CYP3A5 CL _{int}	μL/min/pmol	4.86 [384]			0.104 ret		8.03 [410]				
CYP2C8 CL _{int}	μL/min/pmol					3.62 [400]		0.010 [383]			
CYP2J2 CL _{int}	μL/min/pmol							0.16 [383]			
UGT1A1 CL _{int}	μL/min/pmol							0.21 [383]			
UGT1A3 CL _{int}	μL/min/pmol										
UGT1A4 CL _{int}	μL/min/pmol	0.470 [384]									
Unspecified	μL/min/mg		5.23 [381]	5.00 [412]	7.03 ret	5.09 [400]			1.83 [411]	11.8 [384]	9.05 ret
CL _{renal}	L/h	0.085 [384]			1.80 [382]	4.70 [400]		0.47 [383]	17.0 [358]	7.80 [384]	1.20 [365]
CL _{bile}	L/h				12.0 [382]						
<i>Active transport</i>											
CL _{pd}	L/h/Mio cells						0.001 [385]	0.001 [383]	0.0002 [358]		
OATP1B1 CL _{int}	μL/min/pmol						16.3 [385]	14.4 [383]	41.2 [358]		
OATP1B3 CL _{int}	μL/min/pmol								5.3 [358]		
NTCP CL _{int}	μL/min/pmol								63.8 [358]		
BCRP CL _{int}	μL/min/pmol								42.5 [358]		

Key for Table 4.1: am = ampholyte, AML = amlodipine, ATO = atorvastatin, BP = blood-plasma-ratio, CLA = clarithromycin, CL_{int} = intrinsic clearance, CL_{pd} = passive diffusion clearance, f_{up} = fraction unbound in plasma, HSA = human serum albumin, LIS = lisinopril, logP = octanol-water partition coefficient, ma = monoprotic acid, mb = monoprotic base, MET = metoprolol, MID = midazolam, MW = molecular weight, op = optimized to match profile in young adults (20 to 50 years) – values unchanged in simulation in the elderly, P_{app} = apparent permeability, pKa = acid dissociation constant, pre = predicted by SimCYP, REP = repaglinide, ret = retrograde calculation (see text for more information), RIV = rivaroxaban, RIF = rifampicin, ROS = rosuvastatin.

4.4.3 Workflow for simulations

The strategy for building and verifying the PBPK models and subsequently extrapolating the pharmacokinetics to elderly adults is described in Figure 4.1. All PBPK models were verified in young adults (20 to 50 years), following the best practice approach [413], before scaling to elderly adults (at least 65 years) without any modification of drug parameters. Published clinical study results (Table 4.2) were used to assess the accuracy of the predictions. Observed data were extracted from the literature using GetData Graph digitizer V. 2.26. Pharmacokinetic parameters were not given in six publications [412, 414-418] and thus the area under the curve for one dosing interval (AUC_i) was calculated by the linear trapezoidal method, the area under the curve extrapolated to infinity (AUC_{inf}) was extrapolated from the last three given concentration-time points, and the clearance was calculated as dose / AUC_{inf} . If more than one published study was available, the weighted mean and standard deviation of reported pharmacokinetic parameters were calculated. Observed data were published in different formats and were converted into arithmetic mean and standard deviation [133, 134].

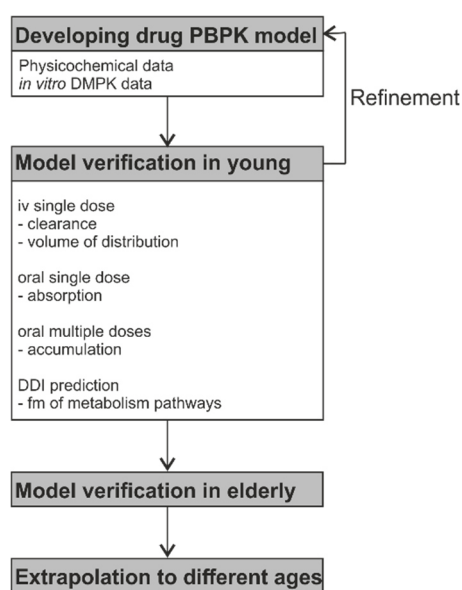


Figure 4.1: Workflow for the verification of the used physiologically based pharmacokinetic framework.

Key: DDI = drug-drug interaction, DMPK = drug metabolism and pharmacokinetics, fm = fraction metabolized.

The simulations were matched as closely as possible to the published observed studies in terms of demographics, dose, dosing regimen, and number of subjects (n) with 10 trials x n virtual subjects being simulated in each case. If more than one published study was available for a drug, the dosing regimen was the same, the study participants were summed up, and the weighted mean of demographic parameters was used. No adjustment of the drug parameters was carried out when scaling drug pharmacokinetics to the elderly.

4.4.4 Verification of the PBPK drug models

Predicted concentration-time profiles were visually compared with observed clinically data for young and elderly adults (Table 4.2). Furthermore, published pharmacokinetic parameters (peak concentration: C_{max} , time to C_{max} : t_{max} , AUC, and elimination half-life: $t_{1/2}$) were compared against our simulation results. Simulations were defined as being successful in young adults if the predicted pharmacokinetic parameters were within the twofold interval of the clinically observed data, which is considered best practice for modelling and simulation by the regulatory authorities [326, 327].

4.4.5 Extrapolation to aged individuals

The final PBPK models were utilized to predict age-related changes in pharmacokinetic parameters from 20 to 99 years in 500 virtual individuals split into 10 different trials (proportion of women: 0.5) in five-year steps. The analyzed pharmacokinetic parameters (C_{max} , t_{max} , AUC, clearance, apparent volume of distribution, and $t_{1/2}$) were normalized to the youngest investigated age group (20 to 24 years). We examined when age-related differences of investigated pharmacokinetic parameters changed more than expected from interindividual variability defined as the 1.25-fold interval (bioequivalence criterion). Additionally, the normalized pharmacokinetic parameters were fitted to descriptive linear, exponential, and monotonic functions containing age as an independent variable. The corrected Akaike's information criterion was used to select the best performing function amongst those tested, which, in contrast to the coefficient of determination, exhibits no bias to higher parameterized models. The analysis was performed for men, women, and all virtual subjects to investigate whether sex has an impact on age-related changes of pharmacokinetic parameters.

Table 4.2: Published clinical studies for non-HIV drugs used to verify the developed PBPK models.

Drug	Dosing regimen	Health status	Young adults				Elderly adults					
			reference	n	age [years]	prop female	weight [kg]	reference	n	age [years]	prop female	weight [kg]
Midazolam	4 mg single oral (young)	healthy	[111]	16	31.5	0.5	71.5	[112]	16	71.0	0.5	84.0
	3–4 mg single oral (elderly)											
Metoprolol	100 mg single oral	healthy	[419]	8	21.0	1	63.0	[419]	8	69.0	1	58.0
			[414]	8	22.6	0.25	64.7	[414]	8	67.4	0.25	63.3
Lisinopril	20 mg single oral	healthy	[415]	6	28.7	-	-	[415]	6	76.3	-	-
			[416]	8	-	0	69.4	[416]	8	-	0.5	-
			[417]	12	27.5	0	69.4					
			[412]	1	33.0	0	-					
Amlodipine	2.5 mg oral once daily	hypertension	[420]	13	35.0	0.23	87.0	[420]	15	68.0	0.2	83.0
Rivaroxaban	10 mg single oral	healthy	[421]	9	30.3	0	81.3	[421]	8	76.8	0	80.1
			9	33.9	1	70.0		8	77.8	1	67.4	
Repaglinide	2 mg single oral	healthy	[422]	8	33.0	0	81.2					
			[423]	12	32.7	0.5	79.9	[423]	12	67.1	0.5	75.9
Atorvastatin	40 mg single oral	healthy	[424]	16	28.0	0.5	67.9	[424]	16	75.0	0.5	66.7
			[425]	10	25.0	0.4	68.0					
			[426]	10	28.0	0.5	66.3					
			[427]	12	36.0	0.5	67.0					
			[428]	23	32.0	0.52	72.0					
			[429]	16	24.4	0.5	66.7	[429]	16	67.7	0.5	71.8
Rosuvastatin	40 mg single oral	healthy	[430]	18	41.2	0	81.6					
			[431]	10	35.7	0	77.6					
			[432]	36	30.2	0.14	75.1					
			[433]	12	24.0	0	76.0	[433]	12	74.5	0.92	66.5
Clarithromycin	500 mg oral twice daily	healthy						[112]	16	71.0	0.5	84.0
Rifampicin	300 mg oral twice daily	healthy	[418]	6	30.0	0.5	-	[434]	6	76.0	0	62.1

4.4.6 Sensitivity analysis

Sensitivity analysis was performed to investigate which population- and drug-specific parameter drive the age-related pharmacokinetic parameter changes in the used PBPK model. A fictive drug was generated, informed by the median input parameters of the ten investigated drugs, and it was ensured that age-related pharmacokinetic changes fell within the average predicted range (data not shown). Sensitivity analysis was run in a single male individual representative of the entire population at ages 20 to 99 years, in five years steps, looking at the:

- (a) octanol-water partition coefficient (logP) between -5 and +5, and its impact on age-related changes in the apparent volume of distribution;
- (b) fraction unbound in plasma (f_{up}) between 0.01 and 1, and its impact on age-related changes in clearance;
- (c) hepatic blood flow between 8 and 30% of cardiac output, and its impact on age-related changes in clearance of a fictive drug being exclusively cleared hepatically;
- (d) renal blood flow between 5 and 25% of cardiac output, and its impact on age-related changes in clearance of a fictive drug being exclusively cleared renally;
- (e) glomerular filtration rate between 60 and 150 mL/min and its impact on age-related changes in clearance of a fictive drug being exclusively cleared renally.

Additionally, the total clearance of the fictive drug was either assigned completely to CYP3A4, CYP2D6, CYP2C9, CYP1A2, CYP2C8, to an unspecified hepatic intrinsic clearance, or to the renal clearance to investigate the impact of different clearance pathways on the age-related changes of total drug clearance.

4.4.7 Verification of the extrapolation to aged individuals

To verify the derived correlations between age and the investigated pharmacokinetic parameters, a literature search was performed using the MEDLINE database to screen for clinical studies comparing the pharmacokinetics in young and elderly individuals. Keywords used were “pharmacokinetic” plus “aging”, “young vs. elderly” or “young vs. geriatric”. Inclusion criteria were a direct comparison of the pharmacokinetics between young adults with a mean age up to 35 years and adults aged at least

40 years. The age bands were chosen to allow inclusion of middle-aged adults. The subject should apparently be healthy, with no disease conditions or medication use that could possibly alter the pharmacokinetics of the drug of interest (the included drugs and references are detailed in Table 4.3). Included pharmacokinetic parameters were normalized to young adults and the observed data were visually compared against the prediction of the derived age-dependent functions.

To check the performed sensitivity analysis against clinically observed data, logP, fup, and the main metabolizing enzyme were collected for each of the investigated drug in the additional dataset (Table 4.3). Physiological parameters, such as the hepatic and renal blood flow and the glomerular filtration rate, important in determining drug clearance, were not usually measured in the published clinical studies and were thus calculated assuming random variability to adequately describe the general aging population [58]. Between-group comparisons of the main route of elimination (hepatic vs. renal) and route of administration (intravenous vs. oral) were performed using the Wilcoxon test after checking normal distribution, by the Shapiro-Wilk test. Analysis of variance was performed for the impact of the main metabolizing enzyme on age-related changes in clearance. Pearson's correlation was done for continuous variables (i.e. logP, fup, age, hepatic and renal blood flow, and glomerular filtration rate).

4.5 Results

4.5.1 Predicting drug pharmacokinetics in the elderly

PBPK models for all drugs were developed and adjusted in young adults (20 to 50 years) until simulations captured the clinically observed concentrations (used clinical studies are listed in Table 4.2) visually and the observed pharmacokinetic parameters were predicted within twofold. Afterwards, drug pharmacokinetics were simulated in elderly adults aged at least 65 years, without any modification of drug parameters, and the predictions were compared with clinically observed data (Table 4.4). Ten drugs commonly used in the elderly and for which clinical pharmacokinetic data have been published in study participants older than 65 years, were investigated. The enzymes and transporters involved in the disposition of the ten investigated drugs, as well as references to clinical studies used to verify the simulations, can be found Tables 4.1 and 4.2.

Table 4.3: Studies used to verify the derived age-related relationships of pharmacokinetic parameters.

Drug	Dosing regimen	logP	fup	Elimination route	n (young)	Age (young)	n (elderly)	Age (elderly)	QLI / QKI	GFR	References
Allopurinol	200 mg oral single	-1.8	1	renal	9	30.3	10	76.5	0.60	0.71	[435]
Alprazolam	1 mg oral single	2.37*	0.2	CYP3A4	8	29.8	8	68.4	0.65	-	[436]
Amantadine	200 mg oral single	2.44	0.33	renal	6	27.0	10	65.0	0.60	0.70	[437]
Amiloride	2.5 mg oral single / once daily	-0.3	0.6	renal	6	24.0	6	73.7	0.57	0.67	[438]
Ampicillin	1,000 mg iv single	1.35	1	renal	12	27.0	12	81.0	0.54	0.61	[439]
	2,000 mg iv single				8	30.0	8, 8	51.0, 73.9	0.77, 0.63	0.83, 0.71	[440]
Atenolol	50 mg oral single / once daily	0.16	0.9	CYP2D6, renal	6	24.0	6	73.7	0.57	0.67	[438]
	50 mg oral once daily				6	28.0	6	69.0	0.59	0.71	[441]
Avibactam	500 mg iv single	-2.7*	0.93	renal	17	29.7	16	69.0	0.68	0.76	[442]
Azithromycin	500 mg loading + 250mg oral once daily	3.03	0.49	biliary	13	29.0	12	72.0	0.58	0.70	[443]
Caffeine	5 mg/kg iv/oral single	-0.07	0.7	CYP1A2	8	20.5	8	71.2	0.58	-	[444]
Cefixime	400 mg oral single / once daily	-0.4	0.35	hepatic, renal	12	22.8	12	68.9	0.60	0.71	[445]
Cefpodoxime	100 mg oral single	-0.03*	0.75	renal	12	33.0	12	72.0	0.60	0.72	[446]
Cilazapril	1 mg oral single	0.8	0.76	renal	12	22.2	12	69.1	0.60	0.72	[447]
Ciprofloxacin	400 mg iv single / once daily	0.28	0.7	CYP1A2, renal	12	25.8	12	68.3	0.67	-	[448]
Citalopram	10 mg oral once daily	3.76	0.2	CYP3A4	8	28.0	24	69.0	0.63	-	[449]
Desipramine	50 mg oral single	4.9	0.18	CYP2D6	22	30.9	24	70.0	0.67	-	[450]
Diazepam	0.1 mg/kg iv single	2.82	0.02	CYP3A4	28	26.5	27, 15	51.8, 68.8	0.82, 0.67	-	[451]
Diphenhydramine	25 mg oral single	3.72	0.2	CYP2D6	20	29.9	17	67.2	0.70	-	[452]
	1.25 mg/kg oral single				7	31.5	7	69.4	0.68	-	[453]
Enalapril	10 mg iv/oral single	0.07	0.5	CYP3A4, renal	9	25.0	9	69.0	0.60	0.72	[454]
Escitalopram	600 mg oral single / once daily	8.8	0.6	UGT1A1	12	29.8	12	69.9	0.70	-	[455]
Fluxetine	40 mg oral once daily	4.05	0.06	CYP2C19	14	28.8	17	70.0	0.68	-	[456]
Hydrochlorothiazide	250 mg oral single / once daily	-0.07	0.32	renal	6	24.0	6	73.7	0.57	0.67	[438]
Imipramine	12.5 mg iv / 50 mg oral single	4.8	0.22	CYP2D6	22	30.9	24	70.0	0.67	-	[450]
Lidocaine	25 mg iv single	2.44	0.3	CYP3A4	24	28.6	13	71.0	0.72	-	[457]
Lorazepam	2 mg iv single	2.39	0.15	UGT2B15	15	27.3	15	69.8	0.69	-	[458]
Meropenem	500 mg iv single	-0.6	0.98	renal	8	28.0	12	73.0	0.55	0.68	[459]
Metformin	850 mg oral single	-2.6	1	renal	6	27.5	3, 12	42.7, 71.4	0.87, 0.58	0.91, 0.70	[460]
Methylprednisolone	10 mg iv single	1.5	0.22	CYP3A4	5	31.0	7	75.0	0.70	-	[461]
Montelukast	7 mg / 10 mg iv/oral single / once daily	7.9	0.01	CYP2C8	12	31.4	12	69.4	0.70	-	[462]
Morphine	10 mg iv/oral single	0.87	0.65	UGT2B7	8	27.4	9	74.0	0.62	-	[463]
Nalbuphine	10 mg iv single	1.4	1	UGTs	9	26.0	9	80.0	0.51	-	[464]
Naproxen	375 mg oral single / twice daily	3.18	0.01	CYP2C9	10	29.0	10	71.0	0.64	-	[465]
Nifedipine	2.5 mg iv / 10mg oral single	2.2	0.05	CYP3A4	11	27.1	6	77.8	0.56	-	[210]
	60 mg oral once daily				23	21.4	24	72.7	0.56	-	[466]
Omeprazole	40 mg oral single	2.23	0.05	CYP2C19	18	23.0	14	76.0	0.56	-	[467]

Table 4.3: cont.

Drug	Dosing regimen	logP	fup	Elimination route	n (young)	Age (young)	n (elderly)	Age (elderly)	QLI / QKI	GFR	References
Oxprenolol	80 mg oral once daily	2.1	0.19	CYP2D6	6	28.0	6	69.0	0.66	-	[441]
Oxycodone	10 mg oral single	0.7	0.55	CYP3A4	10	26.5	10, 10, 10	66.9, 74.0, 82.0	0.71, 0.64, 0.60	-	[468]
Pentopril	125 mg oral single	4.09 [469]	-	renal	6	23.3	6	72.2	0.57	0.68	[470]
Pravastatin	20 mg oral single	0.59	0.55	CYP3A4, biliary	40	25.6	30	69.9	0.69	-	[471]
Prazosin	1 (y) / 0.5 (e) mg single iv	1.3	0.03	CYP3A4, biliary	7	27.0	7	72.0	0.64	-	[472]
	1 mg oral single				10	25.9	10	69.6	0.64	-	[473]
Propanolol	0.15 mg/kg iv / 40mg oral single	3.48	0.1	CYP1A2	7	29.0	8	78.0	0.59	-	[474]
	80 mg oral once daily				6	28.0	6	69.0	0.66	-	[441]
Rimantadine	200 mg oral single	3.6	0.6	renal	6	27.0	10	65.0	0.60	0.70	[437]
Risperidone	1 mg oral single	2.95*	0.12	CYP2D6	8	30.0	12	69.0	0.69	-	[475]
Sertraline	200 mg oral once daily	5.1	0.02	CYP2B6	26	32.6	27	70.9	0.70	-	[476]
Sibutramine\$	15 mg oral single	5.2	0.03	CYP3A4	12	24.0	12	70.3	0.65	-	[477]
Sulbactam	500 mg iv single	-0.89*	0.62	renal	12	27.0	12	81.0	0.54	0.61	[439]
	100 mg iv single				8	30.0	8, 8	51.0, 73.9	0.77, 0.63	0.86, .71	[440]
Telithromycin	400 (y) / 480 (e) mg iv/oral single	3	0.35	CYP3A4	12	20.5	12	75.0	0.59	-	[478]
Theophylline	6 (y) / 5 (e) mg/kg iv single	-0.02	0.6	CYP1A2	6	25.0	6	72.0	0.68	-	[479]
	200 mg oral single				14	23.1	14	76.2	0.66	-	[480]
Ticlopidine	250 mg oral once daily	2.9	0.02	CYP2B6	12	28.9	13	69.5	0.61	-	[481]
Triazolam	0.25 mg oral single	2.42	0.18	CYP3A4	23	29.0	21	67.5	0.66	-	[482]
	0.5 mg oral single				17	25.5	17	71.0	0.67	-	[483]
Valproic Acid	400 mg iv single	2.75	0.82	CYP3A4	7	27.5	6	81.0	0.54	-	[484]
Verapamil	180 mg oral once daily	3.79	0.1	CYP3A4	30	31.0	30	72.5	0.67	-	[485]
Ziprasidone	20 mg oral twice daily	3.8	0.01	CYP3A4	19	28.1	16	70.0	0.69	-	[486]
Zolpidem	5 mg oral single	3.02	0.08	CYP3A4	24	26.3	16	73.7	0.62	-	[487]

Data for logP, fup, main route of elimination, and main metabolizing enzyme are either taken from DrugBank [488] unless otherwise mentioned.

* no experimentally measured logP value was found and therefore, a predicted logP was taken.

\$Sibutramine is rapidly metabolized and therefore data of its metabolite was taken for analysis.

Key: AUC = area under the curve, C_{max} = peak concentration, CL_E = apparent clearance, CYP = cytochrome-P-450, fup = fraction unbound in plasma, GFR = glomerular filtration rate, iv = intravenous, logP = octanol-water partition coefficient, QKI = renal blood flow, QLI = hepatic blood flow, t_{max} = time to C_{max}, t_{1/2} = half-life, UGT = uridine diphosphate-glucuronosyltransferase, VdF = apparent volume of distribution.

Midazolam

The benzodiazepine midazolam is predominantly metabolized by CYP3A (95.2%) and to a lesser extent by UGT1A4 (4.7%). The remaining 0.1% of midazolam is excreted via glomerular filtration [384]. Clinically observed data of a single oral dose of midazolam (4 mg in young and 3-4 mg in the elderly) were contained in the 95% prediction interval for the PBPK simulations in both age groups (Figure 4.2 a/b). Pharmacokinetic parameters were normalized to 4 mg for comparison between young and elderly subjects. The predicted AUC was in close agreement to the observed clinical data in young (44.1 ± 23.2 ng*h/mL vs. 50.9 ± 19.1 ng*h/mL) and elderly adults (42.9 ± 17.2 ng*h/mL vs. 54.8 ± 22.5 ng*h/mL), including the observed variability [111, 112]. The ratio of elderly/young for C_{\max} and t_{\max} was predicted to be within the 1.25-fold interval (predicted:observed ratio: 0.98 and 0.87, respectively), while $t_{1/2}$ of midazolam was overpredicted in both age groups (predicted:observed ratio: 1.30 and 1.89) [111, 112].

Metoprolol

Metoprolol is predominantly metabolized by CYP2D6 (79.2%). Other routes of metoprolol elimination involve CYP3A (13.7%) and renal clearance (7.1%) [381]. The beta-blocker metoprolol was studied as a single oral dose of 100 mg. The variability of metoprolol was covered by the PBPK model in young and elderly individuals (Figure 4.2 c/d). C_{\max} , AUC, and $t_{1/2}$ were accurately scaled to elderly individuals by the PBPK model (predicted:observed ratio of the ratio elderly/young: 1.10, 1.06, and 0.97, respectively). The t_{\max} of metoprolol was overpredicted in the elderly by twofold as the model suggested only a slight increase in the elderly compared with young adults, whereas t_{\max} was half in the observed study [414, 419].

Lisinopril

The angiotensin-converting enzyme (ACE) inhibitor lisinopril is filtered by the glomerulus and is not bound to any plasma-binding protein [401]. The predictions of a single oral dose of lisinopril (20 mg) were in close agreement to clinically observed data in young and elderly adults (Figure 4.2 e/f). The C_{\max} of lisinopril was well-predicted in young adults (predicted:observed ratio: 0.95), but C_{\max} was simulated to increase in the elderly by 9% and was increased in the clinical study by 51% [415, 416]. The ratio elderly/young for t_{\max} and the AUC were accurately predicted by the model (predicted:observed ratio: 1.10 and 0.95).

Table 4.4: Observed vs. predicted pharmacokinetic parameters for non-HIV drugs in young and elderly individuals.

	Young adults		Elderly adults		Ratio elderly/young	
	observed	predicted	observed	predicted	observed	predicted
Midazolam						
C_{max} [ng/mL]	16.2 ± 7.7	15.9 ± 6.4	15.3 ± 7.3	14.8 ± 6.3	0.94	0.93
t_{max} [h]	0.7 ± 0.2	0.5 ± 0.1	0.8 ± 0.6	0.5 ± 0.2	1.10	0.96
AUC [ng*h/mL]	44.1 ± 23.2	50.9 ± 19.1	42.9 ± 17.2	54.8 ± 22.5	0.97	1.08
$t_{1/2}$ [h]	3.4 ± 1.6	4.4 ± 1.4	3.2 ± 2.2	6.1 ± 2.0	0.94	1.37
Metoprolol						
C_{max} [ng/mL]	115 ± 24	124 ± 69	106 ± 24	126 ± 79	0.92	1.02
t_{max} [h]	2.4 ± 0.4	2.3 ± 0.4	1.2 ± 0.1	2.3 ± 0.4	0.50	1.00
AUC [ng*h/mL]	1,048 ± 196	878 ± 559	1,021 ± 105	910 ± 754	0.97	1.04
$t_{1/2}$ [h]	9.9 ± 0.3	8.8 ± 2.9	9.6 ± 0.4	8.3 ± 2.1	0.97	0.94
Lisinopril						
C_{max} [ng/mL]	87.4	83.3 ± 23.3	132.1	90.4 ± 34.9	1.51	1.09
t_{max} [h]	7.0	6.2 ± 0.4	7.3	7.1 ± 0.6	1.04	1.15
AUC [ng*h/mL]	1,399	1,339 ± 359	1,736	1,577 ± 566	1.24	1.18
$t_{1/2}$ [h]	24.4	17.0 ± 2.4	-	23.2 ± 5.0	-	1.36
Amlodipine						
C_{max} [ng/mL]	4.2 ± 1.1	4.1 ± 1.0	5.8 ± 1.7	5.3 ± 1.2	1.38	1.30
t_{max} [h]	7.0 ± 2.0	3.5 ± 0.5	8.0 ± 2.0	4.0 ± 0.6	1.14	1.14
AUC [ng*h/mL]	81 ± 22	86 ± 22	112 ± 40	113 ± 26	1.38	1.31
$t_{1/2}$ [h]	53 ± 14	66 ± 6	69 ± 20	79 ± 6	1.30	1.19
Rivaroxaban						
C_{max} [ng/mL]	190 ± 54	191 ± 33	237 ± 50	213 ± 40	1.25	1.12
t_{max} [h]	2.3 ± 0.6	1.2 ± 0.2	2.6 ± 0.1	1.3 ± 0.2	1.12	1.12
AUC [ng*h/mL]	1,245 ± 417	1,262 ± 348	1,890 ± 432	1,604 ± 347	1.52	1.27
$t_{1/2}$ [h]	9.0 ± 6.4	10.5 ± 2.9	11.6 ± 3.7	13.2 ± 2.8	1.29	1.26
Repaglinide						
C_{max} [ng/mL]	38.0 ± 20.7	31.9 ± 8.0	47.5 ± 29.3	38.2 ± 8.9	1.25	1.20
t_{max} [h]	0.7 ± 0.4	0.6 ± 0.1	0.7 ± 0.2	0.7 ± 0.1	1.00	1.17
AUC [ng*h/mL]	43.9 ± 36.7	51.7 ± 19.7	78.7 ± 48.7	83.5 ± 23.4	1.79	1.62
$t_{1/2}$ [h]	1.3 ± 0.3	2.3 ± 0.6	1.9 ± 0.4	3.0 ± 0.6	1.46	1.30
Atorvastatin						
C_{max} [ng/mL]	14.8 ± 7.6	16.2 ± 8.0	18.1	15.2 ± 8.9	1.22	0.94
t_{max} [h]	1.0 ± 0.3	1.4 ± 0.4	1.8	1.5 ± 0.5	1.8	1.07
AUC [ng*h/mL]	77.9 ± 30.9	86.3 ± 50.3	107.8	114.1 ± 68.7	1.38	1.32
$t_{1/2}$ [h]	9.2 ± 3.6	13.1 ± 3.7	18.8	16.1 ± 4.5	2.04	1.23
Rosuvastatin						
C_{max} [ng/mL]	20.9 ± 10.6	16.2 ± 5.7	19.9 ± 7.4	14.8 ± 5.0	0.95	0.91
t_{max} [h]	5.0 ± 1.6	2.5 ± 0.5	4.0 ± 1.2	3.0 ± 0.7	0.8	1.2
AUC [ng*h/mL]	188 ± 78	188 ± 59	194 ± 28	233 ± 92	1.03	1.24
$t_{1/2}$ [h]	18.6 ± 4.8	14.8 ± 4.9	24.4 ± 12.5	16.8 ± 6.4	1.31	1.14
Clarithromycin						
C_{max} [ng/mL]	2,410 ± 670	2,570 ± 497	3,217 ± 927	3,672 ± 764	1.33	1.43
t_{max} [h]	2.1	2.3	3.1	2.5	1.45	1.07
AUC [ng*h/mL]	18,870 ± 5,550	20,227 ± 4,116	28,840 ± 9,549	29,940 ± 5,260	1.53	1.48
$t_{1/2}$ [h]	11.7 ± 3.4	13.8 ± 2.2	21.3 ± 8.0	17.7 ± 2.9	1.82	1.28
Rifampicin						
C_{max} [ng/mL]	5,570 ± 2,200	7,841 ± 2,230	7,300 ± 2,300	8,310 ± 1,977	1.31	1.06
t_{max} [h]	1	1.4 ± 0.3	1.5 ± 1.1	1.5 ± 0.3	1.46	1.07
AUC [ng*h/mL]	21,428 ± 7,648	23,608 ± 15,742	37,342 ± 16,485	36,793 ± 20,424	1.74	1.56
$t_{1/2}$ [h]	4.9 ± 1.7	4.3 ± 1.5	7.9 ± 3.5	6.0 ± 2.0	1.62	1.40

Key: AUC = area under the curve, C_{max} = peak concentration, t_{max} = time to C_{max} , $t_{1/2}$ = elimination half-life.

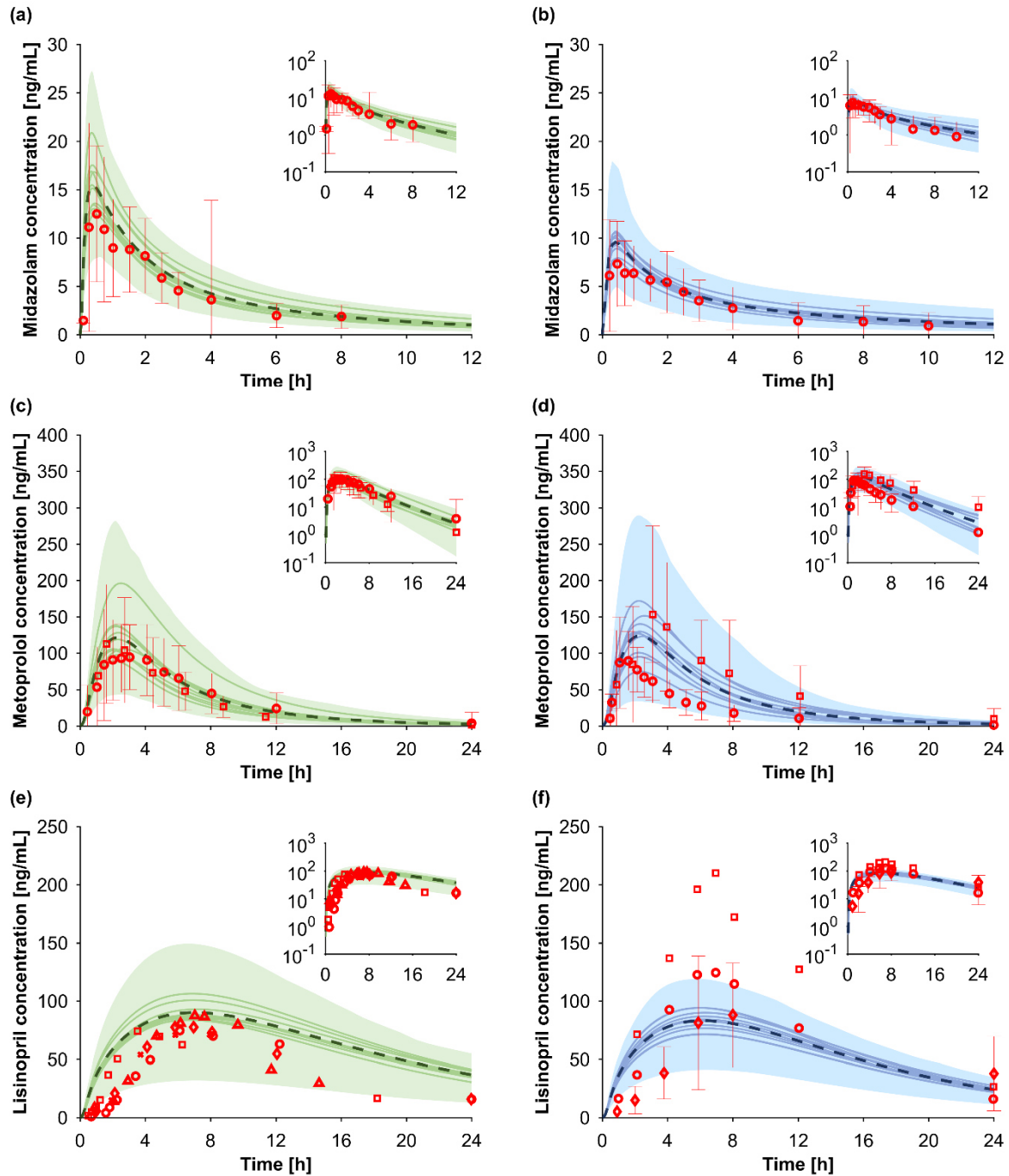


Figure 4.2: Predicted vs. observed concentration-time profiles for midazolam (a: young and b: elderly), metoprolol (c: young and d: elderly), and lisinopril (e: young and f: elderly). The red markers show the observed clinical data (mean \pm standard deviation), the solid lines, the dashed line, and the shaded area represent the mean of each virtual trial, the mean, and the 95% confidence interval of all virtual individuals. Green and blue show simulations in young and elderly adults, respectively. Used clinical studies for model verification can be found in Table 4.2.

Amlodipine

Amlodipine is metabolized by CYP3A (49.4%), an unspecified enzymatic pathway (4.0%), and eliminated unchanged by glomerular filtration (6.1%). Additionally, biliary clearance (40.5%) was implemented in the model, representing clearance of amlodipine metabolites [382]. The observed elimination phase of amlodipine (2.5 mg once daily) was well captured by the PBPK model for young and elderly individuals, including variability (Figure 4.3 a/b). C_{\max} was well predicted in both age groups (predicted:observed ratio: 0.98 and 0.92), but t_{\max} was reached too early in the simulation (predicted:observed ratio: 0.5 in both age groups). However, the age-related increase in t_{\max} of 14% observed in the clinical study in elderly compared with young study participants [489] was correctly captured by the model (predicted:observed ratio: 1.0). Simulated AUC and $t_{1/2}$ were both in close agreement with the observed clinical data (predicted:observed ratio: 1.06 and 1.25 in the young and 1.01 and 1.14 in the elderly, respectively).

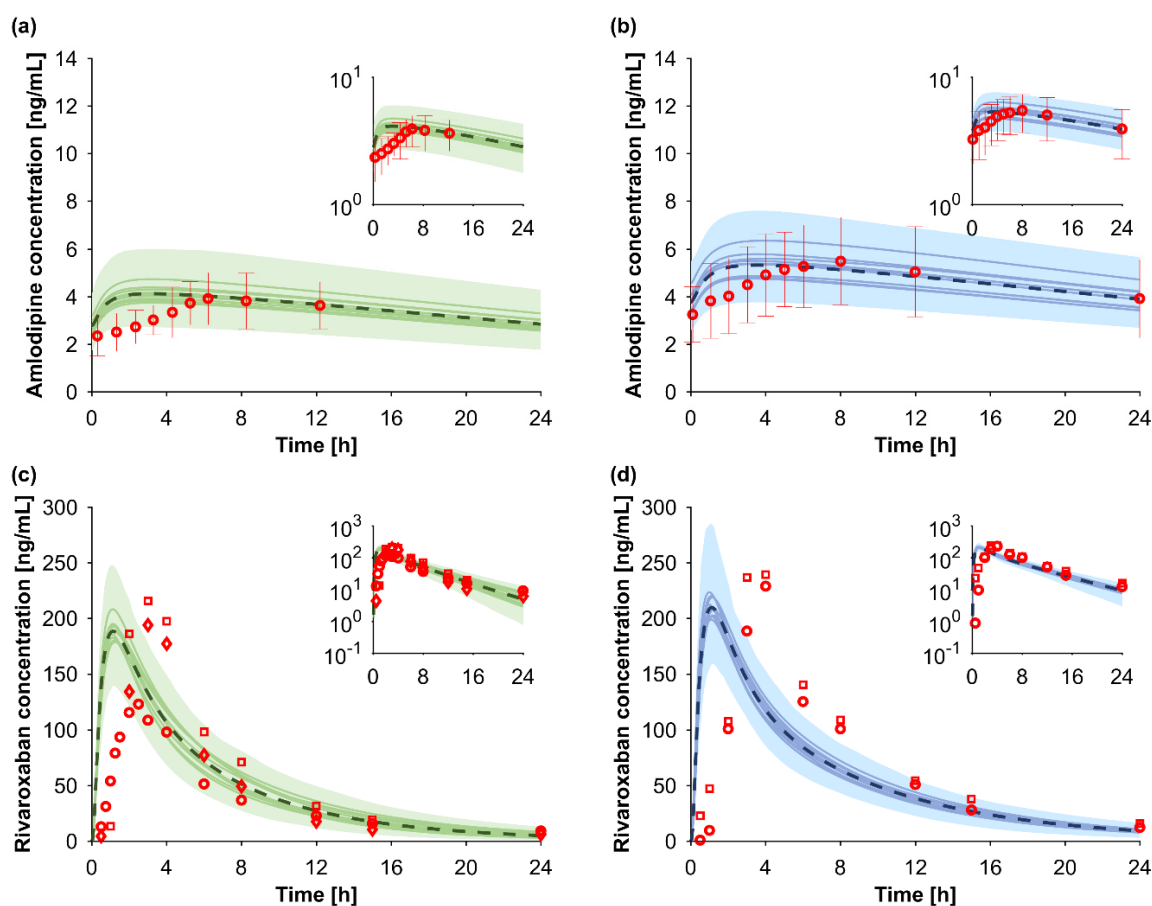


Figure 4.3: Predicted vs. observed concentration time profiles for amlodipine (a: young and b: elderly) and rivaroxaban (c: young and d: elderly). The red markers show the observed clinical data (mean \pm standard deviation), the solid lines, the dashed line, and the shaded area represent the mean of each virtual trial, the mean, and the 95% confidence interval of all virtual individuals. Green and blue show simulations in young and elderly adults, respectively. Used clinical studies for model verification can be found in Table 4.2.

Rivaroxaban

Rivaroxaban is metabolized by CYP3A4 (20.0%), CYP2J2 (15.7%), an unspecified enzymatic pathway (18.3%), and is cleared unchanged by the kidney (46.0%) [118]. A 10 mg single oral dose of the anticoagulant rivaroxaban was studied. The observed terminal elimination phase of rivaroxaban was contained within the 95% confidence interval of the PBPK model simulations for young and elderly adults (Figure 4.3 c/d) as were the observed ratios elderly/young adults of C_{max} , AUC, and $t_{1/2}$ (predicted:observed ratio: 0.89, 0.84, and 0.98, respectively).

Repaglinide

Repaglinide is mainly metabolized by CYP2C8 (75.5%) and to a minor extent by CYP3A4 (24.5%) [410]. The uptake of the antidiabetic drug repaglinide into hepatocytes is mediated by the organic anion transporting polypeptide (OATP) 1B1 [385]. A single oral 2 mg dose of repaglinide was simulated. The mean prediction of repaglinide was close to the mean observed, but the observed variability of repaglinide pharmacokinetics was not completely captured by the model (Figure 4.4 a/b). C_{max} , t_{max} , and AUC were predicted with good accuracy in young (predicted:observed ratio: 0.84, 0.86, and 1.18, respectively) and elderly adults (predicted:observed ratio: 0.80, 1.00, and 1.06, respectively). The $t_{1/2}$ was overpredicted in both age groups (predicted:observed ratio: 1.77 and 1.58), but the predicted ratio elderly/young was in agreement to clinically observed data (predicted:observed ratio: 0.89) [423].

Atorvastatin

Atorvastatin is mainly metabolized by CYP3A (88.9%). Other minor excretion routes for atorvastatin are CYP2C8 (0.2%), UGT1A1 and 1A3 (4.9% each), and renal elimination (1.1%). Atorvastatin uptake into hepatocytes is mediated by OATP1B1 [383]. The concentration-time profile of atorvastatin (40 mg single dose) was in good agreement with the observed data of young volunteers, also capturing the variability adequately (Figure 4.4 c). In the elderly, only one clinical pharmacokinetic study was identified, and the terminal elimination phase was underpredicted in adults aged older than 65 years (Figure 4.4 d). C_{max} was shown to increase by 22% in the clinical study [424], but was predicted to be 6% lower by the PBPK model. The AUC was accurately predicted in young and elderly adults (predicted:observed ratio: 1.11 and 1.06). The $t_{1/2}$ was overpredicted by 42% in the young (observed: 9.2 ± 3.6 h vs. predicted: 13.1 ± 3.7 h) but was predicted adequately by the PBPK model in the elderly (predicted:observed ratio: 0.86).

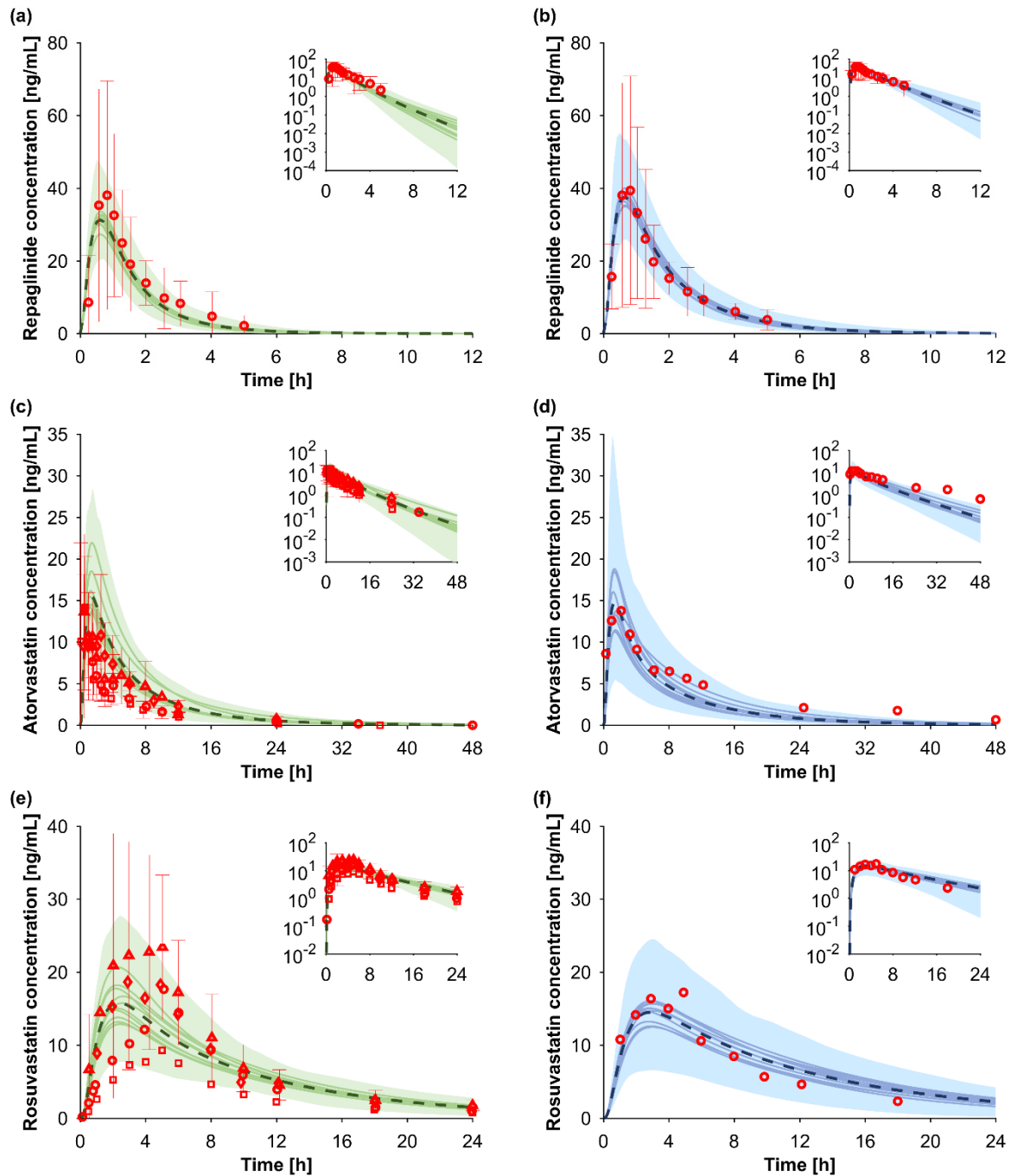


Figure 4.4: Predicted vs. observed concentration time profiles for repaglinide (a: young and b: elderly), atorvastatin (c: young and d: elderly), and rosuvastatin (e: young and f: elderly). The red markers show the observed clinical data (mean \pm standard deviation), the solid lines, the dashed line, and the green shaded area represent the mean of each virtual trial, the mean, and the 95% confidence interval of all virtual individuals. Green and blue show simulations in young and elderly adults, respectively. Used clinical studies for model verification can be found in Table 4.2.

Rosuvastatin

The uptake of rosuvastatin into hepatocytes is mediated by different uptake transporters. Rosuvastatin is cleared via enzymatic metabolism (1.8%), biliary (74.6%), and renal clearance (23.6%) [358]. A single

oral dose of rosuvastatin (40 mg) was captured by the model (Figure 4.4 e/f). C_{\max} of rosuvastatin was underpredicted in young and elderly adults (predicted:observed ratio: 0.78 and 0.74), but the decrease in C_{\max} with age was accurately predicted for rosuvastatin (predicted:observed ratio for the elderly/young ratio of C_{\max} : 0.96). The predicted increase of AUC and $t_{1/2}$ with adult age was in accordance to the observed clinical data (predicted:observed ratio: 1.20 and 0.87).

Clarithromycin

The antibiotic clarithromycin is mainly metabolized in the liver (75.6%), predominately by CYP3A and to a lesser extent by the kidney (24.4%) [490]. Clinically observed data of 500 mg oral clarithromycin twice daily were contained in the 95% prediction interval for the PBPK simulations of young and elderly adults (Figure 4.5 a/b). All pharmacokinetic parameters were predicted within 1.25-fold of clinically observed data.

Rifampicin

Rifampicin, a potent inducer of CYP3A, is mainly metabolized in the liver (92.6%) and only a small fraction is excreted by the kidney (7.4%) [491]. Predictions of 300 mg rifampicin twice daily were comparable with clinically observed data for young and elderly individuals (Figure 4.5 c/d). The AUC was accurately predicted in young ($21,428 \pm 7,648$ ng*h/mL vs. $23,608 \pm 15,742$ ng*h/mL) and elderly adults ($37,342 \pm 16,485$ ng*h/mL vs. $36,793 \pm 20,424$ ng*h/mL). The simulated increase of C_{\max} , t_{\max} , and $t_{1/2}$ was in accordance to clinically observed data (predicted:observed ratio: 0.81, 0.73, and 0.87, respectively).

4.5.2 Pharmacokinetic parameters driving age-related changes in drug exposure

After the successful prediction of drug pharmacokinetics in adults older than 65 years, the developed PBPK models of all ten drugs have been used to simulate C_{\max} , t_{\max} , AUC, clearance, apparent volume of distribution, and $t_{1/2}$ for individuals 20 to 99 years of age. The impact of adult age on C_{\max} was not consistent for the different drugs investigated (Figure 4.6). The predicted C_{\max} of atorvastatin declined with age by 0.42%, whereas C_{\max} of amlodipine and clarithromycin increased by 1.1% per year. C_{\max} of midazolam, metoprolol, and rosuvastatin did not change with advanced age. T_{\max} showed a tendency to increase with age, but it was only outside the bioequivalence criterion for lisinopril and rosuvastatin

with a maximum change of 43%. The predicted AUC showed a linear increase of 0.9% per year from the age of 20 years. Atorvastatin showed no changes of the AUC with age, whereas repaglinide and lisinopril showed the highest change with up to a 2.5-fold difference compared with young adults. Clearance decreased with age with more than a 1.25-fold change at the age of 55 years. Atorvastatin showed the least change with age (0.06% per year), while lisinopril showed the highest change with a 0.84% decrease in drug clearance per year, matching the decline in the glomerular filtration rate. The apparent volume of distribution was independent of adult age for all investigated drugs. $T_{1/2}$ increased with an average rate of 0.8% per year. The lowest and highest age-related change of $t_{1/2}$ was estimated for clarithromycin (0.32% per year) and lisinopril (1.4% per year). The age-dependent changes for all investigated pharmacokinetic parameters were independent of sex.

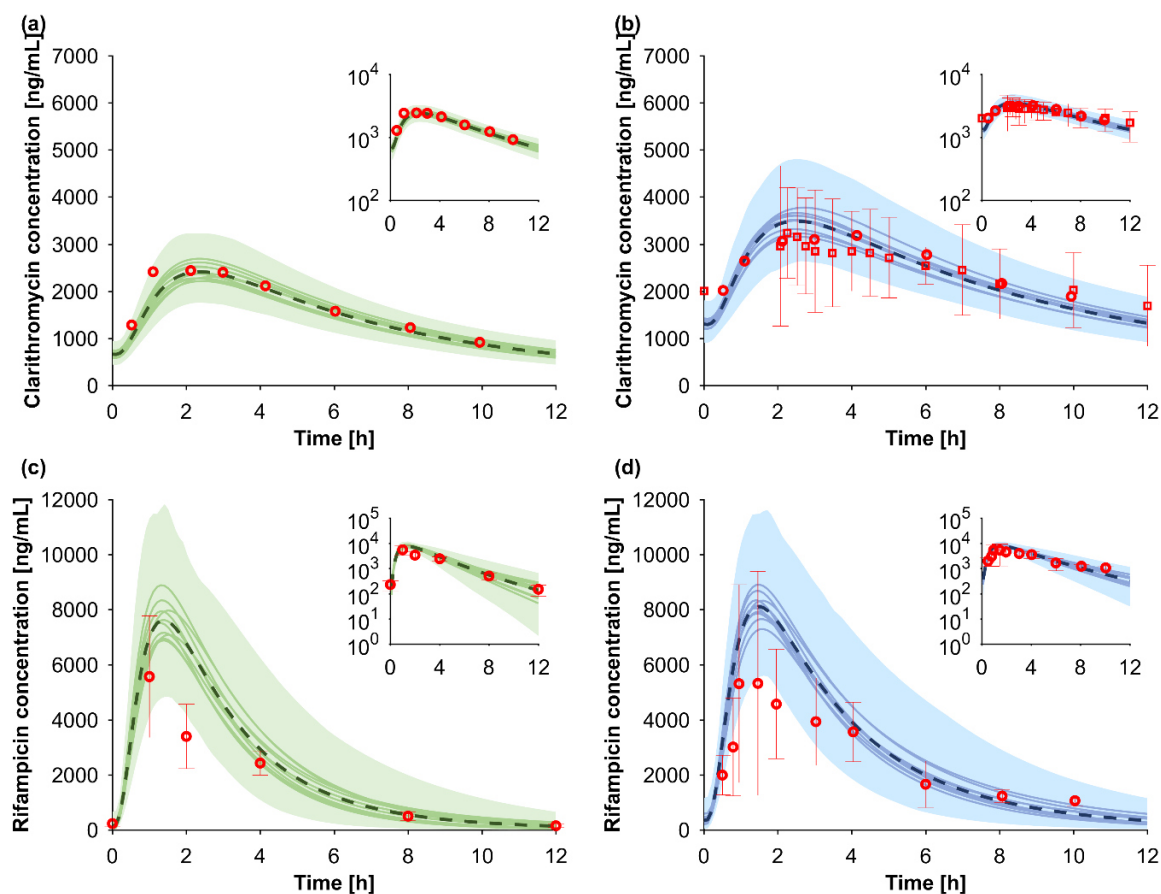


Figure 4.5: Predicted vs. observed concentration time profiles for clarithromycin (a: young and b: elderly) and rifampicin (c: young and d: elderly). The red markers show the observed clinical data (mean \pm standard deviation), the solid lines, the dashed line, and the shaded area represent the mean of each virtual trial, the mean, and the 95% confidence interval of all virtual individuals. Green and blue show simulations in young and elderly adults, respectively. Used clinical studies for model verification can be found in Table 4.2.

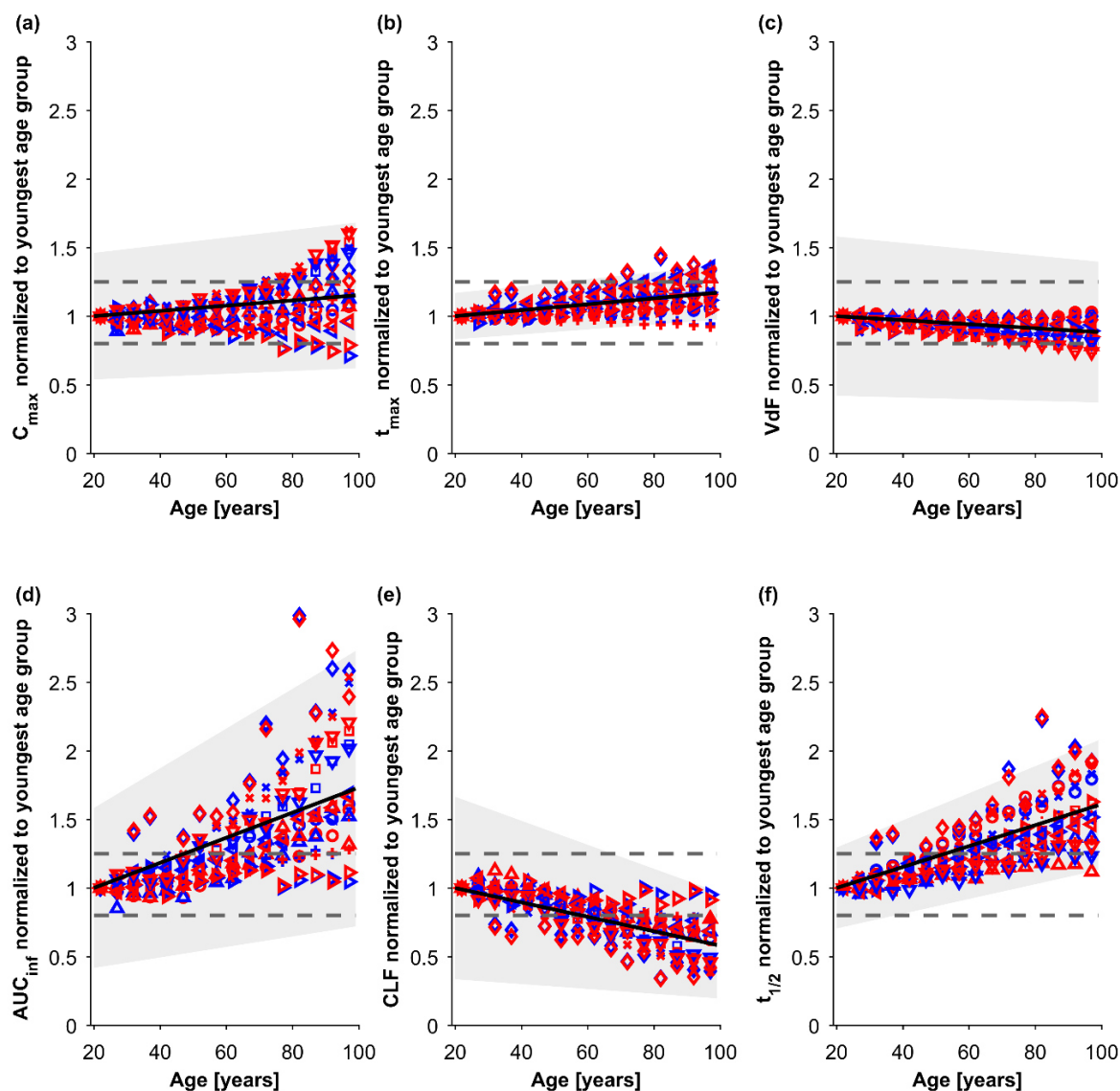


Figure 4.6: Age-related changes of pharmacokinetic parameters for non-HIV drugs normalized to the youngest investigated age group (20 to 24 years). Circles, triangles, diamonds, squares, plus, cross, left-, right-, and downward-pointing triangles, and dots represent midazolam, metoprolol, lisinopril, amlodipine, rivaroxaban, repaglinide, atorvastatin, rosuvastatin, clarithromycin, and rifampicin, respectively. Blue and red markers show data for men and women. The solid line and the grey shaded area display the fitted mean relationship with estimated variability between age and the pharmacokinetic parameter of interest. The grey dashed lines represent the 1.25-fold interval (bioequivalence criterion).

Key: AUC = area under the curve, C_{max} = peak concentration, CLF = clearance, t_{max} = time to C_{max} , $t_{1/2}$ = elimination half-life, VdF = apparent volume of distribution.

Sensitivity analysis demonstrated that predicted age-related changes of the apparent volume of distribution and drug clearance did not depend on investigated drug characteristics (logP, f_{up} , route of elimination), but did depend on physiological changes of hepatic and renal blood flow and glomerular filtration rate (Figure 4.7).

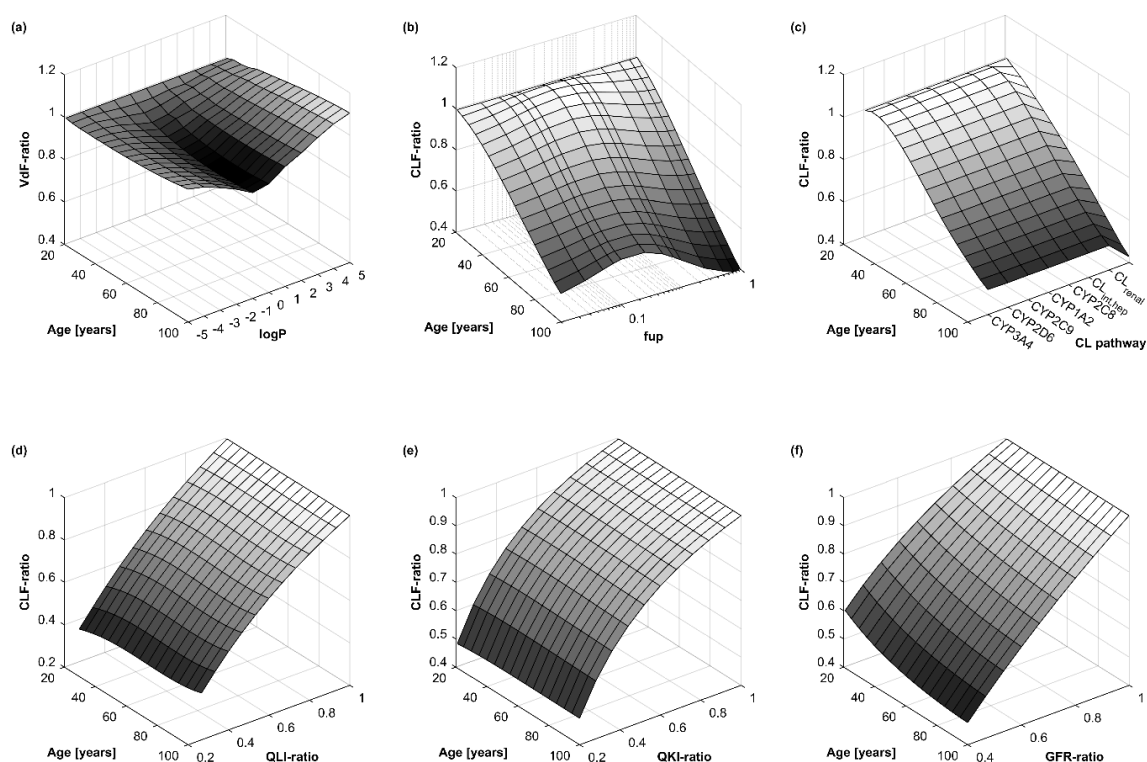


Figure 4.7: Sensitivity analysis to analyze the impact of drug (a-c) and physiological (d-f) parameters on age-related pharmacokinetic changes. Physiological and pharmacokinetic parameters are both normalized to the youngest investigated age group.

Key: CYP = cytochrome P-450, CLF = clearance, CL_{int,hep} = intrinsic, hepatic clearance, fup = fraction unbound in plasma, GFR = glomerular filtration rate, logP = octanol-water partition coefficient, QKI = renal blood flow, QLI = hepatic blood flow, VdF = apparent volume of distribution.

Our derived correlations between altered pharmacokinetics and age (Figure 4.6) should hold true for any drug, if age-related pharmacokinetic changes are drug independent as demonstrated by the conducted sensitivity analysis. In order to verify this hypothesis, a literature search was conducted to seek for studies having a direct pharmacokinetic comparison between young and elderly adults. Clinically observed data for 52 additional drugs (Table 4.3) were gathered. The observed age-dependent pharmacokinetic alterations of this additional dataset could be appropriately described by our derived relationship (Figure 4.8). Variability was underestimated for C_{max} and t_{max} , but clinically observed data for the apparent volume of distribution, AUC, clearance, and $t_{1/2}$ were mostly contained within the estimated variability of derived age-related changes. There were no significant differences between main route of elimination (hepatic vs. renal) and route of administration (intravenous vs. oral) for any of the investigated pharmacokinetic parameters. Aging was significantly correlated with changes in AUC, clearance, and volume of distribution, but not with C_{max} , t_{max} and $t_{1/2}$ (Table 4.5).

Table 4.5: Results of the Pearson correlation for continuous variables to explain age-related pharmacokinetic changes of the clinical data for 52 drugs additionally collected.

Variable	C _{max}	t _{max}	AUC	CLF	VdF	t _{1/2}
Age						
Correlation coefficient	0.21 [0, 0.40]	0.18 [-0.05, 0.39]	0.35 [0.17, 0.51]	-0.31 [-0.47, -0.12]	-0.22 [-0.40, -0.02]	0.09 [-0.11, 0.28]
p value	0.05	0.12	0.0003	0.002	0.03	0.39
logP						
Correlation coefficient	0.04 [-0.17, 0.25]	-0.04 [-0.27, 0.19]	-0.10 [-0.28, 0.10]	0.13 [-0.08, 0.31]	0.12 [-0.08, 0.31]	-0.05 [-0.24, 0.15]
p value	0.71	0.74	0.33	0.19	0.22	0.64
fu						
Correlation coefficient	-0.14 [-0.34, 0.07]	0 [-0.23, 0.24]	-0.07 [-0.26, 0.12]	0.06 [-0.14, 0.25]	-0.15 [-0.34, 0.05]	-0.08 [-0.27, 0.12]
p value	0.18	0.97	0.46	0.58	0.15	0.46
QLI						
Correlation coefficient	-0.32 [-0.53, -0.06]	-0.08 [-0.35, 0.19]	-0.30 [-0.49, -0.07]	0.27 [0.05, 0.47]	0.07 [-0.17, 0.30]	-0.09 [-0.32, 0.14]
p value	0.01	0.56	0.01	0.02	0.56	0.44
QKI						
Correlation coefficient	-0.40 [-0.67, -0.03]	0.20 [-0.28, 0.60]	-0.56 [-0.77, -0.24]	0.60 [0.30, 0.79]	0.54 [0.21, 0.76]	0.05 [-0.33, 0.41]
p value	0.03	0.41	0.002	0.01	0.003	0.81
GFR						
Correlation coefficient	-0.38 [-0.66, -0.01]	0.23 [-0.25, 0.62]	-0.64 [-0.81, -0.35]	0.65 [0.38, 0.82]	0.52 [0.19, 0.75]	-0.04 [-0.41, 0.34]
p value	0.04	0.35	0.0002	0.001	0.004	0.83

Key: AUC = area under the curve, C_{max} = peak concentration, CLF = clearance, fu = fraction unbound, GFR = glomerular filtration rate, logP = octanol-water partition coefficient, QKI = renal blood flow, QLI = hepatic blood flow, t_{max} = time to C_{max}, t_{1/2} = elimination half-life, VdF = apparent volume of distribution.

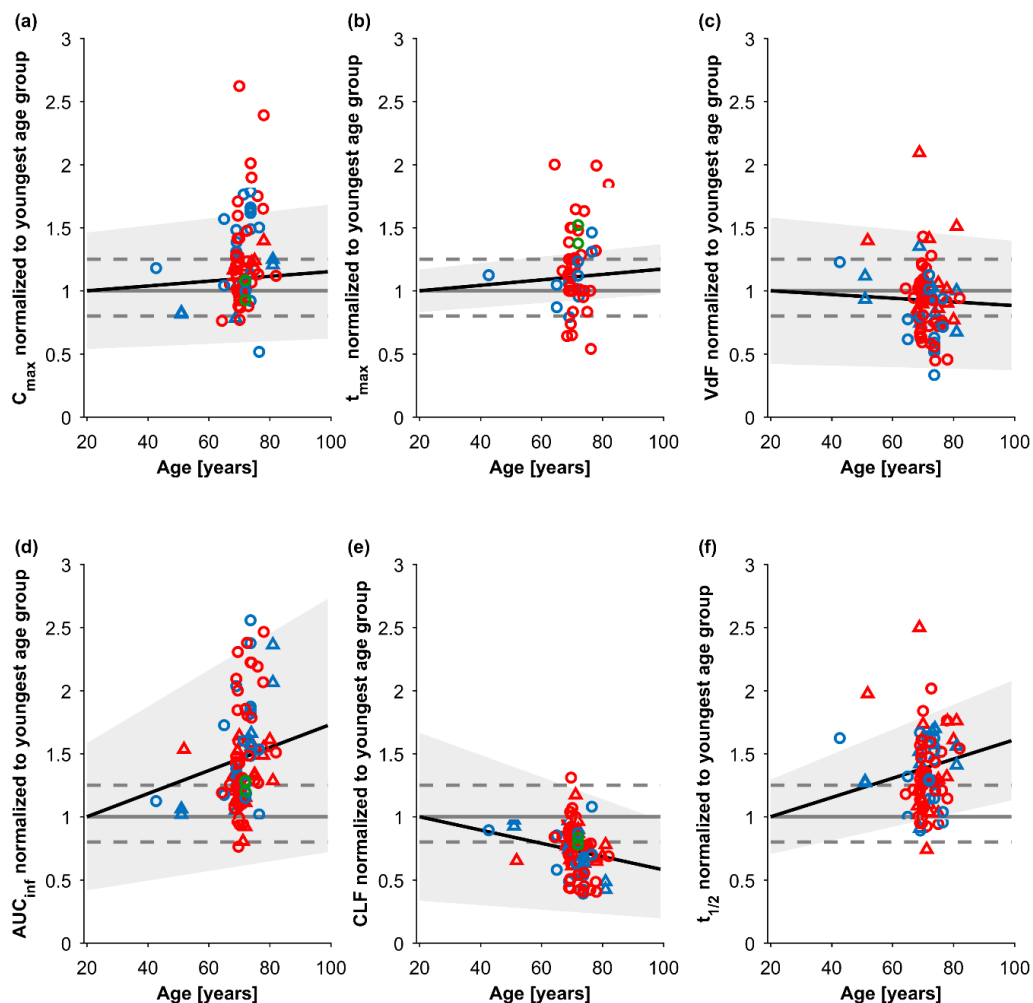


Figure 4.8: Verification of derived pharmacokinetic parameter changes with age against 52 additional drugs. The solid black line, the shaded grey area, and the dashed grey lines represent the fitted mean relationship, the estimated variability, and the 1.25-fold interval (bioequivalence criterion). Red, blue, and green marker show drugs primarily undergoing hepatic, renal, and biliary eliminations. Triangle and circles represent intravenous and oral drug administration. References of the studied drugs can be found in Table 4.3.

Key: AUC = area under the curve, C_{max} = peak concentration, CLF = clearance, t_{max} = time to C_{max} , $t_{1/2}$ = elimination half-life, VdF = apparent volume of distribution.

Surprisingly, there was no correlation between the lipophilicity of a drug and the clinically observed changes in the volume of distribution with aging (Figure 4.7 and 4.9). Age-related changes of drug clearance were neither impacted by the extend of protein binding (p-value: 0.58) nor the main enzyme responsible for drug metabolism (p-value: 0.31). In contrast, there was a linear correlation between the clearance of mainly hepatically cleared drugs and the hepatic blood flow (correlation coefficient [95% confidence interval]: 0.27 [0.05, 0.48], p-value = 0.02) as well as a correlation between the clearance of mainly renally cleared drugs and the renal blood flow (correlation coefficient [95% confidence interval]:

0.60 [0.30, 0.79], p-value = 0.006) and the glomerular filtration rate (correlation coefficient [95% confidence interval]: 0.65 [0.38, 0.82], p-value = 0.001) (Figure 4.9).

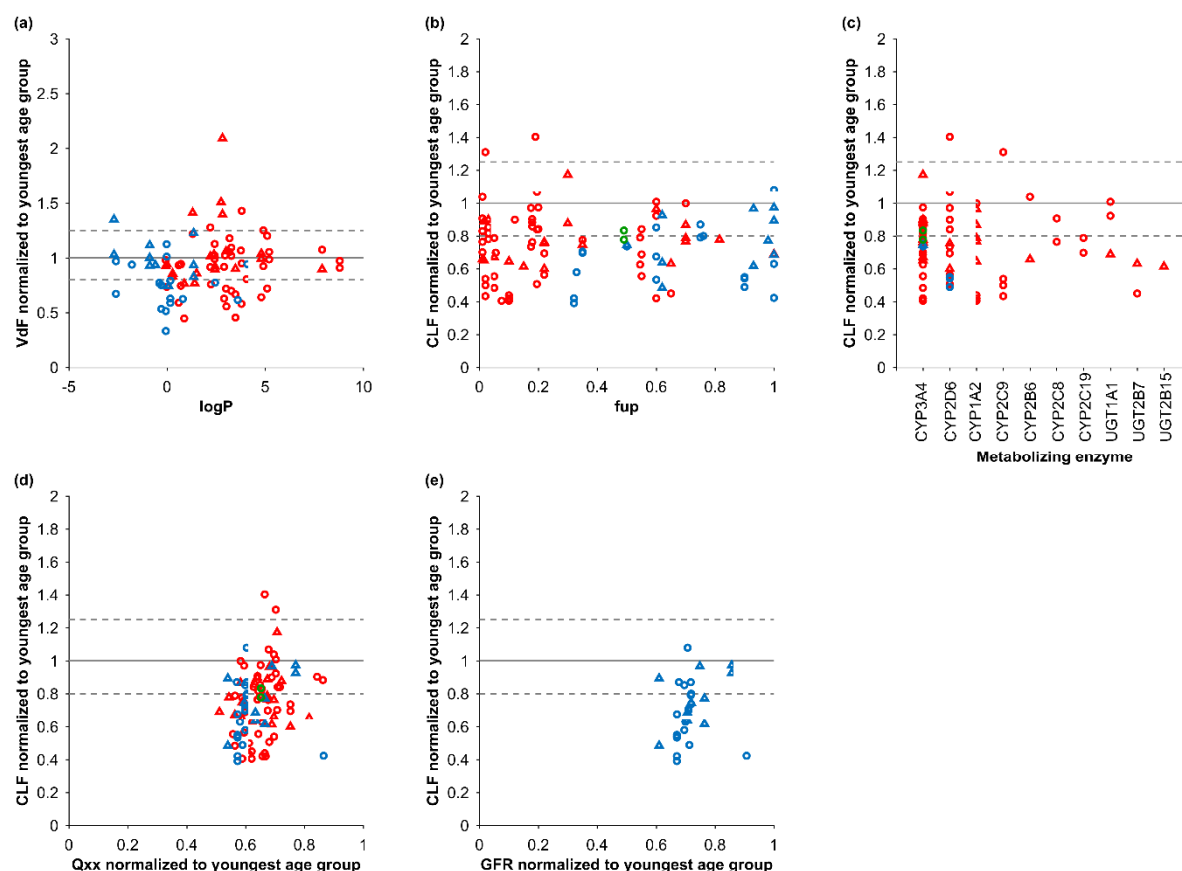


Figure 4.9: Correlation between drug (octanol-water partition coefficient: logP, fraction unbound in plasma: fup, metabolizing enzymes) and physiological parameters (blood flow to respective organ: Qxx, glomerular filtration rate: GFR) against age-related changes in apparent volume of distribution (VdF) and clearance (CLF). Red, blue, and green marker show drugs primarily undergoing hepatic, renal, and biliary eliminations. Triangle and circles represent intravenous and oral drug administration. References of the studied drugs can be found in Table 4.3.

Key: CYP = cytochrome P-450, UGT = uridine diphosphate-glucuronosyltransferase.

4.6 Discussion

The elderly population is usually excluded from clinical trials resulting in a knowledge gap regarding the effect of adult age on drug pharmacokinetics. In this study, the pharmacokinetics of ten drugs that are metabolized and excreted through different pathways were successfully predicted in the elderly using a whole-body PBPK model, demonstrating the predictive power of the PBPK approach to investigate and predict drug disposition in special populations. The conducted virtual trials across adulthood elucidated that an increase in the AUC of 0.9% per year from the age of 20 years is mainly determined by decreased

drug clearance, which itself is caused by a progressive decrease of hepatic and renal blood flow, as well as of the glomerular filtration rate. Those physiological changes drive age-dependent drug exposure changes in the elderly, independent of the drug, as shown by sensitivity analysis and clinically observed data of 52 drugs additionally collected.

Predictions from our developed PBPK models for all investigated drugs compared well with observed clinical data based on visual inspection. In all cases, clinical data in the elderly were quite sparse. The predicted decline in midazolam clearance with age (i.e. -21% by the age of 85 years when clearance is corrected by body weight) is in agreement with the result reported by Polasek *et al.* [223], who investigated the influence of adult age on drugs being metabolized by a dominant hepatic CYP enzyme. The age-dependent pharmacokinetics of metoprolol have previously been investigated in three different studies with contradictory findings. Kendall *et al.* found a decline in clearance by 60% [414], which could be explained through the age-dependent changes in liver weight and hepatic blood flow [58], but two other studies reported a higher clearance in the elderly compared with young study participants [419, 492]. Metoprolol is mainly metabolized by CYP2D6, an enzyme with known genotypes, leading to distinct drug metabolizing phenotypes, which could explain the observed variability [381]. It would be of interest to conduct a clinical pharmacokinetic study for metoprolol in the elderly, using CYP2D6 genotyping, to adequately analyze the impact of aging on metoprolol clearance. We found lisinopril had the highest age-dependent impact on drug clearance, due to the pronounced age-dependent decline in the glomerular filtration rate [58]. Tubular secretion was not modelled and it is worthwhile mentioning that tubular secretion cannot be excluded for lisinopril although its renal clearance matches the glomerular filtration rate [493]. The rate of absorption was predicted too rapidly for amlodipine and rivaroxaban; however, the observed C_{max} were well predicted and the observed terminal elimination phases were contained in the 95% prediction interval of the PBPK model simulations for both drugs. The reason for the slower absorption rate observed in clinical studies could be formulation and more sophisticated absorption models [308, 338] might improve the prediction of t_{max} . Nevertheless, the t_{max} -ratio elderly/young were exactly predicted by the PBPK model (predicted:observed ratio: 1.0 for both drugs) and were thus judged to be sufficient for age-dependent analysis. Across the ten drugs studied, the drug clearance of atorvastatin was least impacted by age and is likely explained by the fact that metabolism in the intestine is least impacted by adult age and extensive intestinal metabolism is a key characteristic of atorvastatin [494].

Overall the pharmacokinetics of the ten selected drugs for model qualification were adequately predicted in the elderly, confirming the predictive power of the PBPK approach in special populations, which was previously shown for seven model drugs of CYP enzymes [380], as well as for morphine and furosemide administered intravenously [131]. The AUC was generally predicted to increase progressively with an average rate of 0.9% per year from the age of 20 years. Despite the higher drug exposure in the elderly, dose adjustment based on age alone is not recommended in the label of any of the ten studied drugs. The age-related changes of the AUC can be explained by the linear decrease of drug clearance as a result of reduced hepatic and renal blood flow and glomerular filtration rate [58], rather than drug characteristics (i.e. logP, fup, main metabolizing enzyme, main route of elimination) as shown by our conducted sensitivity analysis (Figure 4.7) and statistical analysis of clinically observed age-dependent pharmacokinetic alterations of 52 drugs additionally collected (Figure 4.9). These findings are contrary to conventional thinking. It is believed that volume of distribution changes with advanced aging, because of altered body composition [65], which would suggest a higher volume of distribution for lipophilic drugs and a lower volume of distribution for hydrophilic drugs. Indeed, there are contradictory findings in the literature regarding altered [450, 495, 496] and unaltered volume of distributions [211, 439, 464] with advanced age. Cusack *et al.* investigated digoxin pharmacokinetics in the elderly and found that the volume of distribution was not different when corrected for body weight [497], which was used in our study. Contradictory findings were also found for the main metabolizing enzyme of a drug. Age was found to be a significant covariate for CYP2C9 only in a compact meta-analysis looking at hepatic CYP abundance [66]. However, in a study investigating probe substrates, age-dependency was detected for CYP1A2, CYP2D6, and CYP2E1, but not CYP2C9 [67]. In contrast, in a third study CYP1A2 activity was reported to be independent of aging [68]. Taken together, the small samples size generally used for analysis and the high biological variability (e.g. for hepatic CYP abundance) prevented a meaningful investigation regarding the impact of drug characteristics on age-related changes of drug pharmacokinetics. In our compact analysis, we combined clinically observed data and PBPK modelling to demonstrate the described drug characteristics do not significantly impact age-related pharmacokinetic changes.

Blood flows were usually not measured in the clinical studies of the 52 drugs additionally collected and hence were estimated based on observed data of reduced hepatic and renal blood flow with advanced aging [58], and thus was a limitation of this study. However, Vestal *et al.* measured age-related changes

of propranolol clearance, a purely passively distributed drug, and determined hepatic blood flow alterations in the same subjects, showing a linear correlation and supporting therefore the results of our study [498]. The glomerular filtration rate is often determined by measuring creatinine clearance, which is not an ideal marker in the elderly due to senile sarcopenia in aging subjects [243], but linear correlations between the rate of glomerular filtration alterations and age-related changes of clearance of mainly renally excreted drugs were shown in numerous different studies [439, 445, 454] supporting the findings of the present work.

Importantly, the impact of age was independent of sex for all investigated drugs, which is line with clinically observed data [421, 424, 499]. However, the pharmacokinetics can differ between women and men [500] and therefore, more research is needed to investigate the impact of sex in combination with aging.

A clear limitation of our study is that clinical pharmacokinetic data for individuals aged older than 85 years are sparse and thus the simulation results in this age group need to be interpreted with caution. Furthermore, clinical data, as well as the virtual population used in this study, represent healthy elderly individuals. It is known that certain comorbidities, for instance renal impairment [333], liver cirrhosis [332] or heart disease [501] can change physiology and thus impact drug pharmacokinetics. Whether these physiological changes are more pronounced in elderly adults needs to be determined.

It should be emphasized that age-related changes in physiology and biology do not just impact pharmacokinetics but also modify the pharmacodynamic of drugs, resulting in altered drug effects. Differences in the effects of drugs in the elderly can be explained by changes in the number of receptors, the affinity of the drugs to its receptor, and changes in physiological and homeostatic processes with aging [502]. Elderly adults are more sensitive to the sedative effect of benzodiazepines such as midazolam. The dose of midazolam required to reach comparable sedation like in young adults below the age of 50 years was shown to be halved in the elderly [503]. Conversely, the sensitivity to the beta-adrenergic receptor and therefore the pharmacodynamic effect of beta blockers, such as metoprolol, is reduced in the elderly caused by receptor downregulation or alterations in binding affinity [502]. Age-related differences in the antihypertensive effect of lisinopril appear not to be clinically relevant [504]. Conversely, the decrease in systolic blood pressure after amlodipine administration was shown to be

greater in the elderly compared with young patients, while the decrease in diastolic blood pressure was similar in both age groups [489, 505]. Rivaroxaban has a well-established correlation between plasma concentration and FXa activity and prothrombin time prolongation [506]. Thus, the higher plasma concentration in the elderly may lead to a more pronounced pharmacodynamic effect compared with young adults [507]. Statins appear to have the same pharmacodynamic effect in the elderly compared with young adults [508]. Taken together, clinical management of elderly individuals should consider not only age-related pharmacokinetic changes but also age-related pharmacodynamic changes and the presence of comorbidities, all of which predispose elderly individuals to inappropriate prescribing .

4.7 Conclusion

Conducting virtual clinical trials across the entire adulthood in combination with clinically observed data in young and elderly individuals elucidated that drug elimination rather than absorption or distribution is likely responsible for age-related drug exposure changes in the elderly. Our PBPK model in combination with statistical analysis of the clinically observed pharmacokinetic data of 52 drugs additionally collected, showed that the age-related physiological decrease in hepatic and renal blood flow, and glomerular filtration rate, rather than drug characteristics, are responsible for drug exposure changes in the elderly. The empirical rule of reducing the doses by 25 to 50% independent of the drug [509] was justified through the PBPK simulations with an average predicted increase in the AUC of 1.7-fold. Furthermore, age-related differences in drug exposure were outside of the expected interindividual variability (defined as the 1.25-fold interval) at 55 years of age compared with the youngest studied age group. Importantly, this finding can inform future clinical trials aiming to understand the pharmacokinetic differences in older versus younger adults. Additionally, pharmacodynamic alterations and the presence of comorbidities should be considered when prescribing treatments in the elderly.

4.8 *Electronic Supplementary Material*

The online version of this article contains supplementary material:

<https://doi.org/10.1007/s40262-019-00822-9>

Table S1: Parameters of the simulated drugs. See Table 4.1.

Table S2: Published clinical studies used to verify the developed PBPK model. See Table 4.2.

Table S3: Studies used to verify the derived age-related relationships of pharmacokinetic parameters.

Partly contained in Table 4.3

Chapter 5:
Antiretroviral Pharmacokinetics with Aging

5. Antiretroviral Pharmacokinetics with Aging

5.1 Abstract	Page 124
5.2 Introduction	Page 125
5.3 Methods	Page 126
5.3.1 Clinical data for model verification	Page 126
5.3.2 Physiologically based pharmacokinetic modelling	Page 127
5.3.3 Impact of aging on antiretroviral pharmacokinetics across adulthood	Page 130
5.3.4 Impact of ethnicity on age-related pharmacokinetic changes	Page 131
5.4 Results	Page 131
5.4.1 Verification of plasma concentration predictions in the elderly	Page 131
5.4.2 Impact of aging on antiretroviral pharmacokinetics	Page 136
5.4.3 Impact of ethnicity on age-related pharmacokinetic changes	Page 138
5.5 Discussion	Page 140
5.6 Study Highlights	Page 147
5.7 Supplementary Material	Page 148

This chapter is a pre-printed version of a peer-reviewed original research article published under the following reference:

Clinical data combined with modelling and simulation demonstrate a limited effect of aging on the pharmacokinetics of antiretroviral drugs

Felix Stader, Perrine Courlet, Hannah Kinvig, Manuel Battegay, Laurent A. Decosterd, Melissa A. Penny, Marco Siccardi, & Catia Marzolini

British Journal of Clinical Pharmacology 2020; [Epub ahead of print].

DOI: 10.1111/bcp.14402

5.1 Abstract

Background:

The impact of aging on antiretroviral pharmacokinetics remains uncertain, leading to missing dosing recommendations for elderly people living with the human immunodeficiency virus (HIV: PLWH).

Methods:

Plasma concentrations for 10 first line antiretrovirals were obtained in PLWH at least 55 years, participating in the Swiss HIV Cohort Study, and used to proof the predictive performance of our physiologically based pharmacokinetic (PBPK) model. The verified PBPK model predicted the continuous effect of aging on HIV drug pharmacokinetics across adulthood (20 to 99 years). The impact of ethnicity on age-related pharmacokinetic changes between whites and other races was statistically analyzed.

Results:

Clinically observed concentration-time-profiles of all investigated antiretrovirals were generally within the 95% confidence interval of the PBPK simulations, demonstrating the predictive power of the modelling approach used. The predicted decline in drug clearance drove age-related pharmacokinetic changes of antiretrovirals, resulting in a maximal 70% [95% confidence interval: 40%, 120%] increase in antiretrovirals exposure across adulthood. Peak concentration, time to peak concentration, and apparent volume of distribution were predicted to be unaltered by aging. There was no statistically significant difference of age-related pharmacokinetic changes between studied ethnicities.

Conclusion:

Dose adjustment for antiretrovirals based on age of male and female PLWH is a priori not necessary in the absence severe comorbidities considering the large safety margin of the current first-line HIV treatments.

5.2 Introduction

Potent antiretroviral therapy increased the life-expectancy of people living with the human immunodeficiency virus (HIV: PLWH) close to the general population [510]. It is estimated that by 2030 over 70% of PLWH will be aged at least 50 years in the western countries [42]. Nevertheless, clinical studies are rarely conducted in elderly PLWH, resulting in limited knowledge concerning the effect of aging on HIV drug pharmacokinetics and consequently if dose adjustment is necessary in clinical practice.

Advanced aging is characterized by demographical, physiological, and biological changes with the potential to alter drug absorption, distribution, metabolism, and elimination. The most significant change with age is the decrease in renal blood flow and glomerular filtration rate affecting renal drug clearance [58]. Drug excretion is further reduced by the hepatic component, because of decreased liver mass and hepatic blood flow whilst hepatic enzyme and transporter activity appear to remain unchanged with aging [58, 228]. Additionally, drug distribution can be altered as a result of increased adipose tissue weight and reduced total body water [58].

Physiologically based pharmacokinetic (PBPK) modelling, an approach accepted by the regulatory authorities [325, 511], offers the possibility to conduct virtual clinical trials for clinical scenarios that cannot easily or ethically be studied [118]. Virtual populations informing the PBPK model are generated based on measured organ weights, regional blood flows, glomerular filtration rate, and other physiological parameters important to predict drug pharmacokinetics [58]. A combination of measured in vitro and clinically observed in vivo data are used to correctly simulate drug disposition in the human body [118]. Simulations are compared against clinically observed data to verify the model before extrapolating to unknown scenarios of interest.

The aim of the present study was to investigate age-related pharmacokinetic changes of HIV drugs by using our previously developed and verified PBPK framework in combination with clinically observed data sampled as part of the Swiss HIV Cohort Study in aging PLWH [74]. We analyzed if our findings in Europeans can be extrapolated globally by comparing published age-related pharmacokinetic changes between ethnicities.

5.3 Methods

We took three steps to analyze the impact of aging on antiretroviral pharmacokinetics. Firstly, we used clinically observed data for antiretroviral drug plasma concentrations obtained in aging PLWH at least 55 years to verify the predictive performance of our PBPK framework [118]. Secondly, the verified PBPK model predicted antiretroviral drug pharmacokinetics across adulthood (20 to 99 years) to investigate the continuous effect of aging. Results were compared to our study for non-HIV drugs to support the overall care beyond HIV [512]. Thirdly, the general impact of ethnicity on age-related changes of drug pharmacokinetics was analyzed.

5.3.1 Clinical data for model verification

Ritonavir, darunavir boosted with ritonavir (darunavir/r), atazanavir/r, dolutegravir, raltegravir, rilpivirine, efavirenz, etravirine, tenofovir (administered as tenofovir disoproxil fumarate) and emtricitabine were analyzed in PLWH at least 55 years in the framework of two clinical studies within the Swiss HIV Cohort Study. Both studies were conducted in accordance with the Declaration of Helsinki and are registered at clinicaltrials.gov (NCT 03515772). The Ethics Committee of Vaud and Northwest/Central Switzerland approved the study protocol (CER-VD 2018-00369). Written informed consent was collected from each participant.

Intensive plasma concentration sampling was used from the first study and sparse sampling collected at the biannual visit of PLWH was used from the second study for the verification of the predictive performance of the used modelling approach to simulate HIV drug pharmacokinetics in the elderly. Details on study design and analytical methods were published previously [74]. Pharmacokinetic parameters were only calculated non-compartmentally from the first study. Pharmacokinetic parameters were not available for raltegravir and rilpivirine in the elderly.

We identified additional published clinical data in aging PLWH for ritonavir, atazanavir/r, dolutegravir, tenofovir, emtricitabine, and efavirenz, which were used for model verification [71, 72, 513]. Observed data were extracted from the literature using GetData Graph digitizer V. 2.26. Exposure of etravirine was measured in PLWH aged 20 to 77 years with a mean age of 35 years and we thus used this estimate for verification of the young [371]. Clinical studies used for model verification are detailed in Table 5.1.

5.3.2 Physiologically based pharmacokinetic modelling

A whole-body PBPK model constructed in Matlab® 2017a was used [118]. Virtual individuals aged 20 to 99 years were generated considering age-related changes of demographical (e.g. body weight), physiological (e.g. organ weight), and biological (e.g. enzyme abundance) parameters. Variability was considered for all population parameters by using normal distribution [58].

Table 5.1: Published clinical studies for antiretroviral drugs used to verify the developed PBPK models. Clinically observed data of etravirine were obtained in PLWH aged 20 to 77 years with a mean age of 35 years and have therefore been defined as young adults for the purpose of this study [371].

Drug	Dosing regimen	Young adults (20-50 years)	Elderly adults (55-85 years)
Ritonavir	100 mg once daily	[371, 373, 374, 514, 515], #	[71], #
Darunavir/r	800/100 mg once daily	[370-372], #	[74], #
Atazanavir/r	300/100 mg once daily	[374, 514, 515], #	[71], #
Atazanavir	400 mg once daily	[374, 514, 515]	
Dolutegravir	50 mg once daily	[72, 516, 517], #	[72, 74], #
Raltegravir	400 mg twice daily	[518-521], #	#
Rilpivirine	25 mg once daily	[516, 522], #	#
Efavirenz	600 mg once daily	[513, 523], #	[71, 513], #
Etravirine	400 mg once daily	[371], #	#
Tenofovir	300 mg once daily	[524, 525], #	[71], #
Emtricitabine	200 mg once daily	[522, 524-526], #	[71], #

Key: # = own clinical data obtained from PLWH, who participated in the Swiss HIV Cohort Study, r = boosted with ritonavir.

Input parameters (Table 5.2) of the ten studied antiretroviral drugs, which belong to the current first-line therapy for HIV as described by the US, European, and WHO guidelines, were obtained from published models, modified, and verified for our PBPK framework [118]. If not available, the apparent permeability used to predict drug absorption after oral administration was calculated from the published fraction absorbed and the rate of absorption or from physicochemical values [342, 527]. Tissue distribution was optimized to match clinically observed data in young adults and verified with at least one independent clinical study. Clearance for darunavir was split between the cytochrome P-450 enzymes (CYP) 3A4 and an unspecified enzymatic pathway based on direct glucuronidation of darunavir [528]. The intrinsic clearance for dolutegravir and rilpivirine were retrogradely calculated from clinical data considering the

in vitro measured fraction metabolized for each enzymatic pathway [529, 530]. Prediction for efavirenz were performed in extensive (EM) and poor metabolizer (PM) of CYP2B6. Our developed PBPK framework does not include renal transporters and therefore tubular secretion of tenofovir and emtricitabine was modelled as an additional clearance, which does not change with aging. The metabolism of emtricitabine was accounted for by an unspecified enzymatic pathway [531].

Our workflow for predicting and extrapolating drug pharmacokinetics was described previously [512]. In brief, drug disposition was firstly simulated in young adults aged 20 to 50 years before scaling drug pharmacokinetics to the elderly (55 to 85 years) without modifying drug parameters. Successful prediction was judged by overlaying clinically observed data with the simulation results and pharmacokinetic parameters (peak concentration: C_{max} , area under the curve to τ : AUC_t , and elimination half-life: $t_{1/2}$) had to be predicted within twofold of clinically observed data, which is considered best practice for modelling by the regulatory agencies [326]. Model verification of pharmacokinetic parameters is reported as mean \pm standard deviation. Simulations were matched as closely as possible to the published clinical trials regarding dose and dosing regimen. We simulated ten trials containing ten virtual individuals in each case. The ratio predicted/observed was calculated for each virtual trial and are given as mean and the 95% confidence interval.

5.3.3 Impact of aging on antiretroviral pharmacokinetics across adulthood

Age-related changes of analyzed pharmacokinetic parameters (C_{max} , time to C_{max} : t_{max} , AUC_t , oral clearance: CLF, apparent volume of distribution: V_dF , and $t_{1/2}$) were predicted across adulthood (20 to 99 years) in 500 virtual individuals (50% women) per five years using the verified PBPK model. Investigated pharmacokinetic parameters were normalized to the youngest investigated age group (20 to 24 years). We examined the age at which pharmacokinetic parameters changed more than expected from interindividual variability defined as the 1.25-fold interval (bioequivalence criterion). This analysis was undertaken for men, women, and across all virtual subjects to investigate whether sex has an impact on age-related changes of pharmacokinetic parameters. The slopes of the age-related pharmacokinetic changes between men and women were statistically compared by a t-test for each investigated drug and pharmacokinetic parameter. All results were compared to our previous analysis for non-HIV drugs [512]. Results are given as mean and the 95% confidence interval.

Table 5.2: Parameters of the simulated antiretroviral drugs.

Parameter	Unit	RTV	DRV	ATV	DTG	RAL	RPV	EFV	ETV	TFV	FTC
<i>Physicochemical properties</i>											
MW	g/mol	721 [368]	548 [368]	705 [413]	419 [334]	445 [532]	366 [334]	316 [368]	435 [368]	287 [334]	247 [334]
logP		4.3 [368]	1.8 [368]	4.5 [413]	2.2 [334]	0.6 [532]	4.3 [334]	4.6 [368]	5.2 [368]	1.3 [334]	-0.4 [334]
drug type		mb [368]	mb [368]	mb [413]	ma [533]	ma [534]	mb [530]	ma [413]	mb [535]	mb [536]	mb [537]
pKa		2.0 [368]	2.4 [368]	5.6 [413]	8.3 [334]	6.67 [532]	3.3 [334]	10.2 [368]	3.8 [368]	3.8 [334]	2.7 [334]
BP		0.59 [368]	0.60 [368]	0.75 [413]	0.55 [334]	0.60 [532]	0.67 [334]	0.74 [368]	0.70 [368]	0.58 [538]	1.00 [334]
fup		0.02 [368]	0.06 [368]	0.14 [413]	0.07 [334]	0.17 [532]	0.03 [334]	0.02 [368]	0.02 [368]	0.99 [538]	0.96 [334]
binding protein		AAG [539]	AAG [539]	AAG [413]	HSA [540]	HSA [541]	[532]	HSA [542]	HSA [100]	HSA [538]	HSA [538]
<i>Absorption</i>											
P_{app}	10^{-6} cm/sec	2.1 [368]	5.5 [368]	19.2 [413]	0.9 [368]	6.6 [532]	12.0 [334]	2.5 [368]	0.2 [368]	3.9 [334]	3.7 [334]
Lag Rate		3.0 op	0.3 op	1.0 op		1.2 op		0.3 op	0.1 op	1.0 op	1.0 op
<i>Distribution</i>											
Tissue Scalar			0.4 op		0.01 op	0.25 op	0.7 op	3 op	15 op	0.8 op	0.2 op
Adipose tissue Scalar			0.1 op		0.1 op	5 op	10 op	5 op			10 op
Muscle Scalar			0.1 op		0.1 op	5 op	10 op	5 op			10 op
<i>Metabolism & Elimination</i>											
CYP2D6 CL_{int}	$\mu\text{L}/\text{min}/\text{pmol}$	0.93 [368]	3.36 ret	6.57 [413]	0.004 ret		0.573 ret	0.007 [368]	0.013 [368]		
CYP3A4 CL_{int}	$\mu\text{L}/\text{min}/\text{pmol}$	20.1 [368]		6.57 [413]				0.03 [368]			
CYP3A5 CL_{int}	$\mu\text{L}/\text{min}/\text{pmol}$							0.07 [368]			
CYP1A2 CL_{int}	$\mu\text{L}/\text{min}/\text{pmol}$							0.08 [368]			
CYP2A6 CL_{int}	$\mu\text{L}/\text{min}/\text{pmol}$							0.55 [368]			
CYP2B6 CL_{int}	$\mu\text{L}/\text{min}/\text{pmol}$										
CYP2C19 CL_{int}	$\mu\text{L}/\text{min}/\text{pmol}$								0.75 [368]		
UGT1A1 CL_{int}	$\mu\text{L}/\text{min}/\text{pmol}$		4.89 ret	1.94 [413]	0.022 ret	1.0 [532]	16.63 ret				0.17 ret
Unspecified	$\mu\text{L}/\text{min}/\text{mg}$				0.15 ret					7.5 ret	7.47 ret
CL_{renal}	L/h				0.18 ret	3.6 [532]				6.7 ret	10.96 ret
$CL_{additional}$	L/h										

Table 5.2: cont.

Parameter	Unit	RTV	DRV	ATV	DTG	RAL	RPV	EFV	ETV	TFV	FTC
Interactions											
CYP2D6 K_i	μM	2.9 [539]		2.35 [413]							
CYP3A4 K_i	μM	0.029 [539]	0.44 [368]	3 [413]			0.7 [368]	20.6 [368]			
CYP3A4 K_{inact}	1/h	17.47 [543]		0.84 [413]							
CYP3A5 K_{inact}	1/h	4.37 [543]		3 [413]							
CYP3A4 K_{app}	μM	0.091 [543]		0.84 [413]							
CYP3A5 K_{app}	μM	0.109 [543]									
CYP3A4 IndMax		13.4 [368]	2.2 [368]					6.5 [368]	2.5 [368]		
CYP2B6 IndMax								5.7 [368]			
CYP3A4 IC_{50}	μM	0.44 [368]	0.18 [368]					3.9 [368]	5.2 [368]		
CYP2B6 IC_{50}	μM							0.8 [368]			

Key: AAG = alpha-acid glycoprotein, ATV = atazanavir, BP = blood-plasma-ratio, CL_{int} = intrinsic clearance, CYP = cytochrome P-450, DRV = darunavir, DIG = dolutegravir, EFV = efavirenz, ETV = etravirine, FTC = emtricitabine, fup = fraction unbound in plasma, HSA = human serum albumin, IC₅₀ = half maximal inhibitory concentration, IndMax = maximum fold of induction, K_{app} = concentration of mechanism-based inhibitor associated with half maximal inactivation rate, K_i = inhibition constant, K_{inact} = inactivation rate of an enzyme suppressed by mechanism-based inhibition, logP = octanol-water partition coefficient, ma = monoprotonic acid, mb = monoprotonic base, MW = molecular weight, op = optimized, P_{app} = apparent permeability, pKa = acid dissociation constant, RAL = rilpivirine, RTV = raltegravir, RPV = rilpivirine, st = see text, TFV = tenofovir, UGT = uridine diphosphate-glucuronosyltransferase.

5.3.4 Impact of ethnicity on age-related pharmacokinetic changes

A literature search yielded clinical studies comparing age-related pharmacokinetic alterations in other ethnicities than whites for any drug (Table 5.3). Keywords used were “pharmacokinetic” plus “aging”, “young vs. elderly” or “young vs. geriatric” plus different ethnicities. Inclusion criteria were a direct pharmacokinetic comparison between young adults with a mean age up to 35 years and aging adults with a mean age at least 55 years to match our own clinical study, at least 80% of the studied population had to belong to a different ethnic group than whites, and subjects had no severe disease and chronic medication that could potentially impact the pharmacokinetic of the drug of interest. Pharmacokinetic parameters were normalized to the youngest age group investigated. Group-wise comparison of age-related pharmacokinetic changes between whites [512] and other ethnic groups were performed by a t-test.

5.4 Results

5.4.1 Verification of plasma concentration predictions in the elderly

Protease inhibitors

Clinically observed data for ritonavir (100 mg once daily), darunavir/r (800/100 mg once daily), and atazanavir/r (300/100 mg once daily) were generally contained within the 95% confidence interval of the model predictions in young and elderly subjects (Figure 5.1). Pharmacokinetic parameters were simulated within 2.0-fold, 1.25-fold, and 1.6-fold of clinically observed data for ritonavir, darunavir/r, and atazanavir/r, respectively (Table 5.4). Clinical data for unboosted atazanavir (400 mg once daily) were only available for young adults (data not shown). The observed AUC_t of atazanavir was correctly predicted with $27,452 \pm 4,158$ ng*h/mL vs. $28,007 \pm 25,043$ ng*h/mL. The predicted increase in drug exposure between the young and the elderly group was 51% for ritonavir (predicted:observed ratio: 1.67 [1.07; 2.67]), 33% for darunavir/r (predicted:observed ratio: 1.04 [0.83; 1.28]), and 28% for atazanavir/r (predicted:observed ratio: 1.76 [1.28; 2.63]).

Table 5.3: Studies used to investigate the impact of ethnicity on age-related pharmacokinetic changes.

Drug	Dosing regimen	Elimination route	Ethnicity	Health status	n (young)	Age (young)	n (elderly)	Age (elderly)	References
Balofloxacin	200 mg iv single	renal	Japanese	healthy	6	30.0	10	71.8	[544]
Biapenem	300 mg iv single 600 mg iv single	renal	Japanese	healthy	5	23	5	71.6 77.6	[545]
Donepezil	2 mg oral single	CYP2D6	Japanese	young: healthy elderly: hospitalized	12	23	6	74	[546]
Famotidine	20 mg oral single	renal	Japanese	young: healthy elderly: hospitalized	6	23	10	66	[547]
Grepafloxacin	200 mg oral single / once daily	CYP1A2	Japanese	healthy	6	30	7	71.1	[544]
Lamivudine	100 mg oral single	renal	Japanese	healthy	6	20.8	6	67.5	[548]
Metformin	750 mg oral single (fed) 500 mg oral single (fasted)	renal	Korean	healthy	20	23	12	68	[549]
Midazolam	15 mg oral single	CYP3A	Chinese	healthy	10	23	10	57 72 77	[550]
Oseltamivir	1 mg oral single	hepatic / renal	Japanese	healthy	7	23	5	84	[551]
Rivaroxaban	5 mg oral single 10 mg oral single 20 mg oral single 40 mg oral single	CYP3A / renal	Chinese	healthy	8 8 8 8	34.4 34.8 34.1 34.8	12 10 11 12	61.7 62.9 63.5 64.7	[552, 553]
Verapamil	80 mg oral single	CYP3A	Japanese	healthy	12	20.5	12	70.5	[554]

Key: CYP = cytochrome P-450, iv = intravenous.

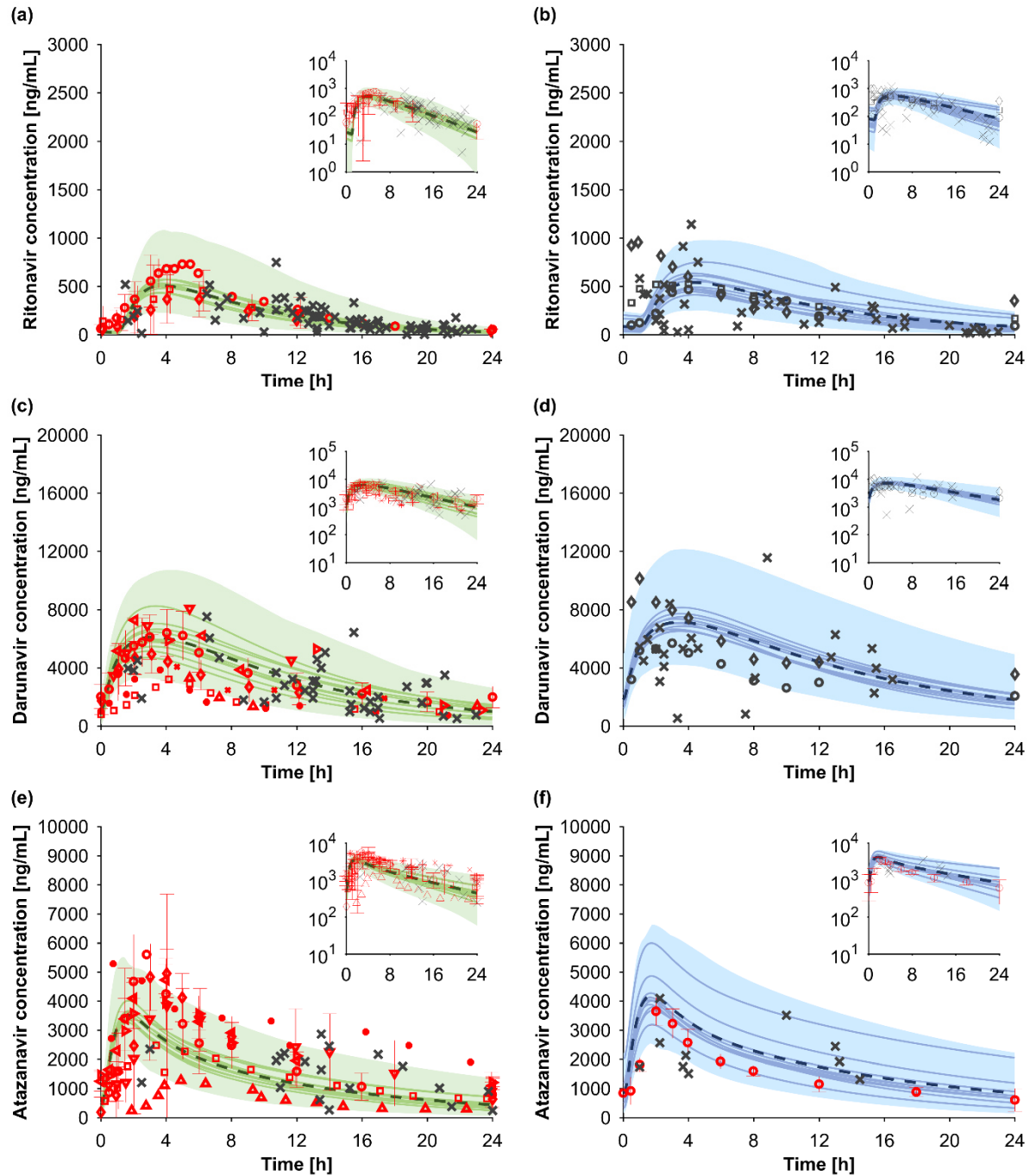


Figure 5.1: Predicted vs. observed concentration time profiles for ritonavir (100 mg once daily; a: young and b: elderly), darunavir/r (800/100 mg once daily; c: young and d: elderly), and atazanavir/r (300/100 mg once daily; e: young and f: elderly). Red markers show published clinical data with different markers indicating different clinical studies (mean \pm standard deviation). Dark grey markers represent clinical data from the Swiss HIV Cohort Study. Different markers indicate different individuals from intensive pharmacokinetic sampling (study 1) and crosses show sparse plasma concentration sampling from PLWH that came for their biannual visit to the HIV clinics (study 2). The solid lines, the dashed line, and the shaded area represent the mean of each virtual trial, the mean, and the 95% confidence interval of all virtual individuals. Used clinical studies for model verification can be found in Table 5.1.

Table 5.4: Observed vs. predicted pharmacokinetic parameters (mean \pm standard deviation) of antiretroviral drugs for young (20 to 50 years) and elderly adults (55 to 85 years). The ratios predicted/observed are given as mean [95% confidence interval] calculated for the entire virtual population and each virtual trial.

	Young adults (20-50 years)			Elderly adults (55-85 years)		Ratio elderly/young		Ratio predicted/observed		
	observed	predicted		observed	predicted	observed	predicted	young	elderly	elderly/young
ritonavir	C_{max} [ng/mL]	524 \pm 268		479 \pm 252	555 \pm 307	1.00 \pm 0.79	1.06 \pm 0.80	1.10 [0.93; 1.23]	1.16 [0.85; 1.42]	1.06 [0.74; 1.32]
	AUC_t [ng*h/mL]	5,025 \pm 3,681		5,336 \pm 3,303	7,580 \pm 6,804	0.90 \pm 0.90	1.51 \pm 1.75	0.85 [0.67; 0.97]	1.42 [0.93; 2.42]	1.67 [1.07; 2.67]
	$t_{1/2}$ [h]	3.9 \pm 1.1		8.0 \pm 3.1	5.6 \pm 2.4	1.20 \pm 1.08	1.44 \pm 0.80	0.59 [0.48; 0.68]	0.70 [0.54; 0.97]	1.20 [0.99; 1.46]
darunavir/r	C_{max} [ng/mL]	6,359 \pm 2,325		7,969 \pm 2,372	7,186 \pm 2,533	1.25 \pm 0.59	1.16 \pm 0.61	0.97 [0.82; 1.09]	0.90 [0.75; 1.03]	0.93 [0.79; 1.08]
	AUC_t [ng*h/mL]	75,780 \pm 22,102		96,447 \pm 23,315	105,478 \pm 48,191	1.27 \pm 0.48	1.33 \pm 0.95	1.05 [0.81; 1.24]	1.09 [0.86; 1.31]	1.04 [0.83; 1.28]
	$t_{1/2}$ [h]	14.4 \pm 5.2		20.9 \pm 13.7	20.3 \pm 7.6	1.45 \pm 1.08	1.42 \pm 0.87	0.99 [0.87; 1.16]	0.97 [0.89; 1.08]	0.98 [0.80; 1.18]
atazanavir/r	C_{max} [ng/mL]	4,757 \pm 954		3,493 \pm 1,844	4,056 \pm 1,547	0.73 \pm 0.41	1.13 \pm 0.54	0.75 [0.64; 0.87]	1.16 [1.05; 1.26]	1.54 [1.35; 1.91]
	AUC_t [ng*h/mL]	45,285 \pm 11,571		32,900 \pm 9,630	52,238 \pm 40,674	0.73 \pm 0.28	1.28 \pm 1.34	0.90 [0.68; 1.31]	1.59 [1.33; 1.88]	1.76 [1.28; 2.63]
	$t_{1/2}$ [h]	9.1 \pm 2.2		7.3 \pm 6.1	9.3 \pm 5.5	0.80 \pm 0.70	1.28 \pm 0.98	0.79 [0.62; 1.01]	1.28 [1.16; 1.41]	1.61 [1.23; 2.02]
dolutegravir	C_{max} [ng/mL]	3,532 \pm 909		4,391 \pm 1,139	4,717 \pm 1,693	1.24 \pm 0.45	1.18 \pm 0.56	1.13 [0.94; 1.28]	1.07 [0.94; 1.21]	0.95 [0.79; 1.20]
	AUC_t [ng*h/mL]	53,291 \pm 15,810		61,629 \pm 29,902	71,393 \pm 36,677	1.16 \pm 0.66	1.31 \pm 0.92	1.02 [0.73; 1.25]	1.16 [0.95; 1.36]	1.14 [0.86; 1.63]
	$t_{1/2}$ [h]	12.8 \pm 4.3		13.6 \pm 5.1	13.9 \pm 5.9	1.07 \pm 0.53	1.28 \pm 0.78	0.85 [0.58; 1.03]	1.02 [0.88; 1.15]	1.20 [0.91; 1.71]
raltegravir	C_{max} [ng/mL]	3,125 \pm 1,327			3,437 \pm 923		1.14 \pm 0.46	1.04 [0.88; 1.29]		
	AUC_t [ng*h/mL]	15,315 \pm 6,779			18,833 \pm 9,131		1.44 \pm 0.99	1.01 [0.78; 1.45]		
	$t_{1/2}$ [h]	7.4 \pm 4.0			5.7 \pm 2.1		1.24 \pm 0.66	0.60 [0.52; 0.69]		
rilpivirine	C_{max} [ng/mL]	144 \pm 68			244 \pm 83		1.16 \pm 0.59	1.45 [1.21; 1.72]		
	AUC_t [ng*h/mL]	2,132 \pm 930			2,711 \pm 1,319		1.29 \pm 1.04	0.99 [0.78; 1.30]		
	$t_{1/2}$ [h]	47.2 \pm 12.1			35.9 \pm 15.7		1.34 \pm 0.88	0.57 [0.49; 0.67]		
efavirenz	C_{max} [ng/mL]	4,035 \pm 1,190		4,121 \pm 2,430	4,260 \pm 1,503	1.02 \pm 0.67	1.17 \pm 0.62	0.90 [0.75; 1.04]	1.03 [0.92; 1.16]	1.15 [0.93; 1.40]
	AUC_t [ng*h/mL]	57,572 \pm 23,067		67,600 \pm 37,037	62,463 \pm 27,387	1.17 \pm 0.80	1.21 \pm 0.82	0.90 [0.71; 1.11]	0.92 [0.80; 1.06]	1.03 [0.79; 1.32]
	$t_{1/2}$ [h]	47.5 \pm 4.3		46.6 \pm 20.2	58.2 \pm 16.6	0.98 \pm 0.65	1.25 \pm 0.65	0.98 [0.84; 1.19]	1.25 [1.17; 1.34]	1.27 [1.01; 1.48]
etravirine	C_{max} [ng/mL]	790 \pm 287		1242 \pm 437	1,004 \pm 664	1.57 \pm 0.80	1.49 \pm 1.54	0.85 [0.82; 0.92]	0.81 [0.64; 1.19]	0.95 [0.74; 1.40]
	AUC_t [ng*h/mL]	10,410 \pm 4,186		17,984 \pm 7,087	18,007 \pm 14,438	1.73 \pm 0.97	1.63 \pm 2.08	1.06 [0.91; 1.16]	1.00 [0.75; 1.59]	0.95 [0.71; 1.50]
	$t_{1/2}$ [h]	35		33.3 \pm 14.8	41.1 \pm 14.6	0.95 \pm 0.42	1.34 \pm 0.80	0.75 [0.70; 0.81]	1.23 [1.11; 1.54]	1.65 [1.26; 1.82]
tenofovir	C_{max} [ng/mL]	278 \pm 72		313 \pm 147	290 \pm 47	1.13 \pm 0.60	1.21 \pm 0.26	0.86 [0.82; 0.92]	0.93 [0.89; 0.97]	1.07 [0.99; 1.15]
	AUC_t [ng*h/mL]	2,774 \pm 474		3,510 \pm 741	3,351 \pm 325	1.27 \pm 0.34	1.25 \pm 0.18	0.96 [0.92; 1.01]	0.95 [0.91; 0.98]	0.99 [0.93; 1.06]
	$t_{1/2}$ [h]	20.3 \pm 8.4		19.2 \pm 14.2	21.3 \pm 4.5	0.95 \pm 0.80	1.20 \pm 0.32	0.88 [0.79; 0.97]	1.11 [1.02; 1.18]	1.27 [1.10; 1.41]
emtricitabine	C_{max} [ng/mL]	1,647 \pm 565		1,790 \pm 480	2,027 \pm 325	1.09 \pm 0.47	1.07 \pm 0.25	1.15 [1.09; 1.21]	1.13 [1.05; 1.18]	0.99 [0.92; 1.08]
	AUC_t [ng*h/mL]	9,715 \pm 2,225		14,929 \pm 6,436	13,680 \pm 1,033	1.54 \pm 0.75	1.16 \pm 0.12	1.21 [1.19; 1.23]	0.92 [0.89; 0.94]	0.75 [0.73; 0.78]
	$t_{1/2}$ [h]	15.4 \pm 13.9		6.1 \pm 1.2	12.0 \pm 2.3	0.40 \pm 0.36	1.08 \pm 0.28	0.72 [0.67; 0.77]	1.96 [1.78; 2.15]	2.73 [2.47; 2.98]

Key: AUC_t = area under the curve to tau, C_{max} = peak concentration, $t_{1/2}$ = elimination half-life.

Integrase inhibitors

The pharmacokinetics of dolutegravir (50 mg once daily) and raltegravir (400 mg twice daily) were accurately predicted in young individuals (Figure 5.2). Clinically observed data of dolutegravir were contained within the 95% confidence interval of predictions; however, the observed variability of raltegravir plasma concentration was not captured by the model. Pharmacokinetic parameters were predicted within 1.25-fold of clinically observed data for both investigated integrase inhibitors, except $t_{1/2}$ of raltegravir, which was underpredicted in young adults (predicted:observed ratio: 0.60 [0.52; 0.69]). The AUC_t was estimated to increase by 31% for dolutegravir (predicted:observed ratio: 1.14 [0.86; 1.63]) and 44% for raltegravir.

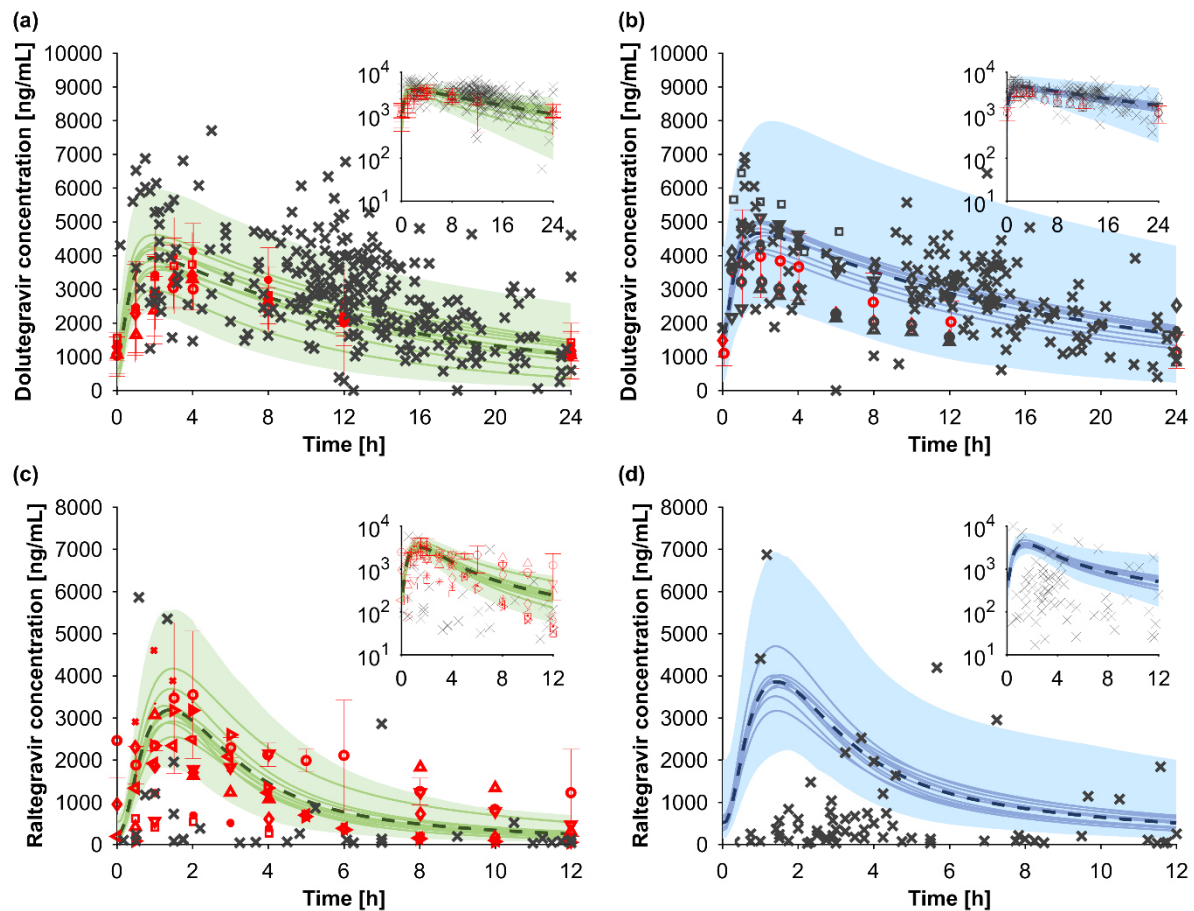


Figure 5.2: Predicted vs. observed concentration time profiles for dolutegravir (50 mg once daily; a: young and b: elderly) and raltegravir (400 mg twice daily; c: young and d: elderly). Red markers show published clinical data with different markers indicating different clinical studies (mean \pm standard deviation). Dark grey markers represent clinical data from the Swiss HIV Cohort Study. Different markers indicate different individuals from intensive pharmacokinetic sampling (study 1) and crosses show sparse plasma concentration sampling from PLWH that came for their biannual visit to the HIV clinics (study 2). The solid lines, the dashed line, and the shaded area represent the mean of each virtual trial, the mean, and the 95% confidence interval of all virtual individuals. Used clinical studies for model verification can be found in Table 5.1.

Non-nucleoside reverse transcriptase inhibitors

Clinically observed data for non-nucleoside reverse transcriptase inhibitors (NNRTIs; rilpivirine: 25 mg once daily, efavirenz: 600 mg once daily, and etravirine: 400 mg once daily) were contained within the 95% confidence interval of the PBPK predictions of both investigated age groups (Figure 5.3). Pharmacokinetic parameters were generally predicted within 1.5-fold of clinically observed data for rilpivirine and etravirine and within 1.25-fold for efavirenz. Drug exposure of rilpivirine, efavirenz, and etravirine was predicted to increase by 29%, 21% (predicted:observed ratio: 1.03 [0.79; 1.32]), and 63% (predicted:observed ratio: 0.95 [0.71; 1.50]), respectively. Efavirenz exposure in PM of CYP2B6 felt generally within the 95% confidence interval of the model predictions (data not shown).

Nucleoside/nucleotide reverse transcriptase inhibitors

The mainly renally excreted nucleoside/nucleotide reverse transcriptase inhibitors (NRTIs) tenofovir (300 mg once daily administered as tenofovir disoproxil fumarate) and emtricitabine (200 mg once daily) were predicted in close agreement to the clinically observed data in young and elderly subjects (Figure 5.4). Pharmacokinetic parameters were predicted within 1.25-fold of clinically observed data, except for $t_{1/2}$ of emtricitabine in the elderly, which was 6.1 ± 1.2 h observed and 12.0 ± 2.3 h predicted (predicted:observed ratio: 1.96 [1.78; 2.15]). The AUC_t of tenofovir and emtricitabine was predicted to increase by 25% (predicted:observed ratio: 0.99 [0.93; 1.06]) and 16% (predicted:observed ratio: 0.75 [0.73; 0.78]) in the elderly compared with the young group.

5.4.2 Impact of aging on antiretroviral pharmacokinetics

All developed drug models were used to investigate the impact of aging on C_{max} , t_{max} , AUC_t , CLF, VdF, and $t_{1/2}$ across adulthood (20 to 99 years). C_{max} increased for all investigated HIV drugs by 34% [18%; 51%] in the oldest compared with the youngest studied age group (Figure 5.5). In contrast, t_{max} and VdF were predicted to be similar across adulthood. Simulated AUC_t and $t_{1/2}$ progressively increased by 0.58% [0.54%; 0.63%] per year of age, respectively. Correspondingly, CLF decreased by maximal 70% [40%; 180%] across adulthood. Overall, there were more changes in HIV drug pharmacokinetics at the age 57 years than expected from interindividual variability. The age-dependent changes for all investigated pharmacokinetic parameters were independent of sex (Table 5.5). Predicted age-related pharmacokinetic changes of antiretroviral drugs were comparable to non-HIV drugs (Table 5.6) [512].

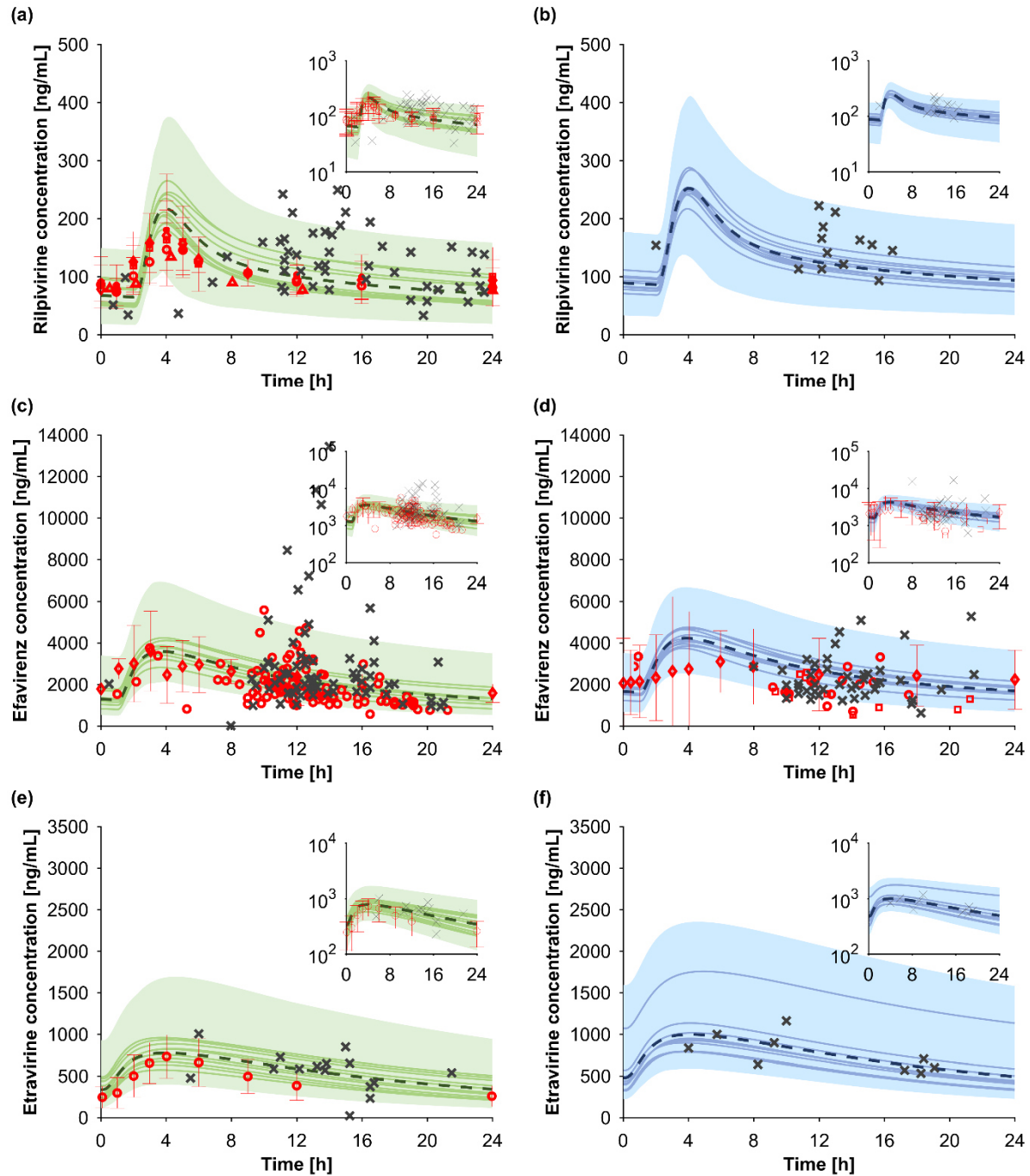


Figure 5.3: Predicted vs. observed concentration time profiles for rilpivirine (25 mg once daily; a: young and b: elderly), efavirenz (600 mg once daily; c: young and d: elderly), and etravirine (400 mg once daily; e: young and f: elderly). Red markers show published clinical data with different markers indicating different clinical studies (mean \pm standard deviation). Dark grey markers represent clinical data from the Swiss HIV Cohort Study. Different markers indicate different individuals from intensive pharmacokinetic sampling (study 1) and crosses show sparse plasma concentration sampling from PLWH that came for their biannual visit to the HIV clinics (study 2). The solid lines, the dashed line, and the shaded area represent the mean of each virtual trial, the mean, and the 95% confidence interval of all virtual individuals. Used clinical studies for model verification can be found in Table 5.1.

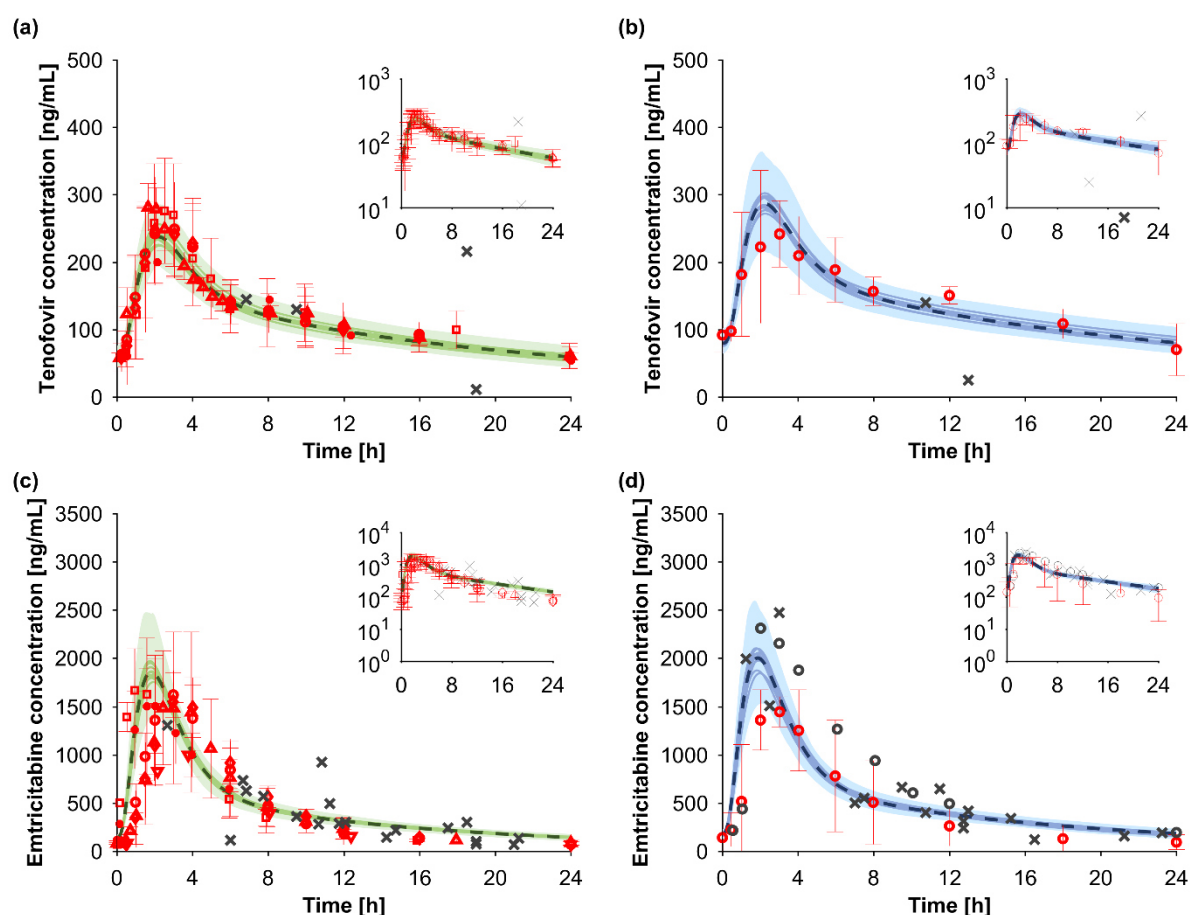


Figure 5.4: Predicted vs. observed concentration time profiles for tenofovir (300 mg once daily; a: young and b: elderly) and emtricitabine (200 mg once daily; c: young and d: elderly). Red markers show published clinical data with different markers indicating different clinical studies (mean \pm standard deviation). Dark grey markers represent clinical data from the Swiss HIV Cohort Study. Crosses show sparse plasma concentration sampling from PLWH that came for their biannual visit to the HIV clinics (study 2). The solid lines, the dashed line, and the shaded area represent the mean of each virtual trial, the mean, and the 95% confidence interval of all virtual individuals. Used clinical studies for model verification can be found in Table 5.1.

5.4.3 Impact of ethnicity on age-related pharmacokinetic changes

Our used clinical data and the virtual population represent PLWH of white ethnicity only. Recognizing that on a global scale, there is large ethnic diversity of HIV-infected individuals, we investigated the impact of ethnicity on age-related pharmacokinetic alterations. A literature search yielded 21 studies analyzing drug pharmacokinetics in young and elderly adults of different ethnicity than white. Following the inclusion criteria, six studies were excluded because more than 20% of the studied population were white, four studies were excluded because the mean age of the young age group was over 35 years, and one study was excluded because age was not given. The remaining ten studies included populations that were all Asians. Lamivudine was the only antiretroviral drug amongst the studied 11

drugs. The increase of C_{\max} was significantly higher in Asians compared with whites (p-value: 0.01 [-0.69, -0.11]). However, age-related changes of all other pharmacokinetic parameters for renally excreted and hepatically metabolized drugs were not different amongst the investigated ethnicities (Figure 5.6).

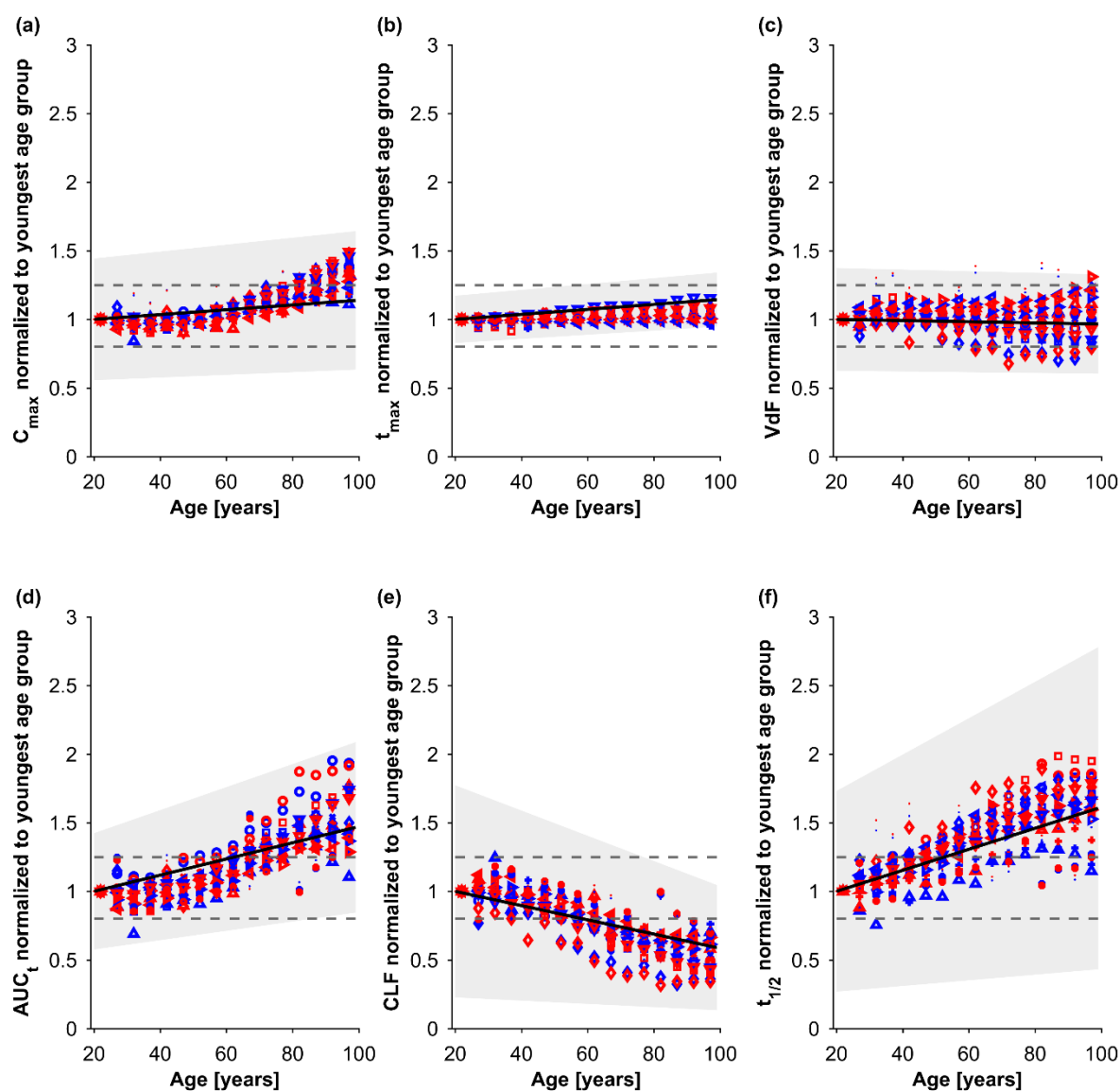


Figure 5.5: Pharmacokinetic parameters of antiretroviral drugs (Ritonavir (circles), boosted darunavir (triangles), boosted atazanavir (diamonds), atazanavir (squares), dolutegravir (plus), raltegravir (cross), rilpivirine (left-pointed triangles), efavirenz (right-pointed triangles), etravirine (down-pointed triangles), tenofovir (asterixis), and emtricitabine (dots) normalised to the youngest investigated age group (20 to 24 years). Blue and red markers show data for men and women. The solid line and the grey shaded area display the fitted mean and the estimated variability of age-related pharmacokinetic changes obtained from non-HIV drugs [512]. The grey dashed lines represent the 1.25-fold interval (bioequivalence criterion).

Key: AUC_t = area under the curve to tau, C_{\max} = peak concentration, CLF = oral clearance, t_{\max} = time to C_{\max} , $t_{1/2}$ = elimination half-life, VdF = apparent volume of distribution.

Table 5.5: P-values to analyse the difference in regression slopes of relative-age-related pharmacokinetic changes for men and women by a t-test.

	C_{\max}	t_{\max}	AUC_t	CLF	VdF	$t_{1/2}$
RTV	0.99	1.00	0.96	0.96	0.85	0.84
DRV/r	1.00	1.00	0.81	0.99	0.99	0.09
ATV/r	0.95	1.00	0.89	0.96	0.99	0.47
DTG	1.00	0.97	0.92	0.64	1.00	0.63
RAL	0.95	0.99	0.95	0.96	0.96	0.91
RPV	0.89	1.00	0.53	0.74	0.90	0.49
EFV	0.99	0.96	0.42	0.93	0.96	0.80
ETV	1.00	0.96	0.81	0.97	0.88	0.91
TFV	1.00	0.99	1.00	1.00	0.97	0.99
FTC	1.00	0.99	1.00	1.00	1.00	0.99

Key: ATV/r = atazanavir boosted with ritonavir, AUC_t = area under the curve to tau, CLF = clearance, C_{max} = peak concentration, DRV/r = darunavir boosted with ritonavir, DTG = dolutegravir, EFV = efavirenz, ETV = etravirine, FTC = emtricitabine, RAL = raltegravir, RPV = rilpivirine, RTV = ritonavir, t_{1/2} = elimination half-life, t_{max} = time to C_{max}, TFV = tenofovir (administered as tenofovir disoproxil fumarate), VdF = volume of distribution.

5.5 Discussion

Clinical data in aging PLWH are limited, leading to missing guidance whether the dose of antiretroviral drugs needs to be adjusted based on the age of the treated PLWH. Limited clinical data combined with modelling and simulation elucidated a 70% [40%; 120%] increase in antiretroviral drug exposure with advanced aging being in the same range as observed for non-HIV drugs (Table 5.6) [512]. Considering the wide therapeutic window of antiretroviral drugs belonging to the first line treatment, the age-related pharmacokinetic changes are a priori not clinically relevant and thus, the same antiretroviral drug dose can be administered to elderly compared with young PLWH.

Most antiretroviral drug labels provide no dose recommendations for elderly PLWH [76-83], except for atazanavir for which doses do not need to be adjusted based on the age of the treated individual [85]. Because it is not feasible, pragmatical or ethical possible to study every antiretroviral drug across adulthood, we used a cutting-edge modelling approach to investigate the continuous effect of aging on HIV drug pharmacokinetics. PBPK modelling has demonstrated its predictive power to simulate plasma concentrations in special populations such as children [329], pregnant women [555], and renally

impaired individuals [333]. Drug labels are more and more informed by PBPK models to give a dosing recommendation for special populations for whom there are high hurdles to conduct clinical trials [325, 556].

Clinically observed data for all investigated antiretroviral drugs were generally within the 95% confidence interval of the PBPK model predictions (Figure 5.1-5.4), demonstrating the predictive power of the used approach to simulate antiretroviral drug pharmacokinetics in aging subjects. Raltegravir was the only studied antiretroviral drugs for which data obtained from PLWH in our clinical study were mostly underpredicted by the model in contrast to published studies. This could possibly be explained by the known large variability of raltegravir plasma concentrations observed in clinical practice [557]. However, in the case of large variability, the model should over- and underpredict raltegravir plasma concentrations. Another possibility is a difference between healthy volunteers and PLWH. A population pharmacokinetic analysis found marked differences of around 40% in the absorption rate, clearance, and volume of distribution in PLWH compared with healthy volunteers [558]. The physiological causes of these pharmacokinetic differences are unknown. The raltegravir model was developed with clinically observed data from healthy volunteers, and thus, the underprediction in elderly PLWH (Figure 5.2d) might be caused by the impact of the HIV infection on raltegravir pharmacokinetics. This underprediction is similar between young and elderly subjects and therefore, the relative age-related pharmacokinetic changes of raltegravir might still hold true. The low raltegravir concentrations in aging PLWH appear to have no clinical consequences, because viral loads were undetectable in all subjects on raltegravir. Importantly, the sampled antiretroviral drug pharmacokinetics represent real-life data from aging PLWH, having a declined kidney function (i.e. glomerular filtration rate was 65.6 ± 19.2 mL/min/1.73m²), common age-related comorbidities (i.e. hypertension), and receiving combined antiretroviral therapy [74].

Age-related pharmacokinetics changes of antiretroviral drugs are driven by a reduction in drug clearance, which is supported by findings for non-HIV drugs. The reduction in drug clearance is caused by physiological alterations with advanced aging such as the decline in hepatic and renal blood flow and in the glomerular filtration rate, but is independent of drug characteristics [512]. The relative decreases of hepatic and renal blood flow are in a similar range [58], which might be an explanation for why age-related changes in drug clearance are similar between mostly hepatically and renally cleared drugs.

Another explanation is that the activity of metabolizing enzymes and active drug transporters do not depend on age [58, 228]. Being broadly applicable to antiretroviral drugs and non-HIV drugs, this works supports the overall care beyond HIV in elderly PLWH. Furthermore, as age-related pharmacokinetic alterations are independent of drug characteristics, the results are applicable to antiretroviral therapy of future effective drugs entering the market before clinical data have been obtained in the elderly.

Table 5.6: Fold change [95% confidence interval] between the age of 85 years and 20 years for non-HIV [512] and antiretroviral drugs.

	non-HIV drugs [512]	antiretroviral drugs
C_{\max}	1.15 [0.80; 1.42]	1.24 [1.08; 1.36]
t_{\max}	1.12 [0.90; 1.32]	1.02 [0.96; 1.10]
AUC_t	1.43 [0.99; 2.02]	1.43 [1.18; 1.75]
CLF	0.65 [0.45; 0.92]	0.61 [0.35; 0.84]
VdF	0.98 [0.69; 1.27]	1.02 [0.76; 1.31]
$t_{1/2}$	1.51 [1.24; 1.86]	1.55 [1.19; 1.79]

Key: AUC_t = area under the curve to tau, C_{\max} = peak concentration, CLF = oral clearance, t_{\max} = time to C_{\max} , $t_{1/2}$ = elimination half-life, VdF = apparent volume of distribution.

The relative age-related pharmacokinetic changes appear to be independent of the dosing regimen. Our study for non-HIV drugs was mostly done for single doses [512], whereas the current analysis for antiretroviral drugs was done in steady state and results were not different (Table 5.6). Furthermore, we had two patients on darunavir boosted with ritonavir twice daily (600/100 mg) and the relative age-related changes in AUC_t and clearance were not different to the analyzed once daily dosing regimen. However, more clinically observed data are warranted in the future to judge the effect of dosing regimens on age-related pharmacokinetic changes appropriately.

The impact of aging on age-related pharmacokinetic changes was similar for men and women. Sex-related differences were only seen for antiretroviral drugs with high pharmacokinetic variability (e.g. atazanavir/r), but the differences were neither statistically significant (Table 5.6) nor judged to be of clinical relevance. Importantly, the pharmacokinetics can depend on sex [500], but the relative age-related physiological [58] and resulting pharmacokinetic changes are similar between men and women.

A dose adjustment to compensate the increasing drug exposure with advanced aging depends on the therapeutic index of the drug of interest. The safety margin of the current first-line antiretroviral treatment is large enough that doses can be similar across adulthood. For comedications, the “start low go slow” strategy is recommended with a possible dose reduction of 25% at the age of 60 years and of 50% at the age of 75 years [509, 512]. Importantly, dose adaption in patients with renal diseases are necessary regardless of their age [559].

Globally, 16% of the 37.9 million PLWH are above the age of 50 years [1]. This numbers is expected to increase in the future, particularly in Eastern and Southern Africa [44], making it necessary to understand the impact of ethnicity on age-related antiretroviral drug exposure changes. Due to the lower life expectancy in African countries of 55 to 60 years [43], our literature search did not yield any clinical data in Africans, but Asians. Like Africans, Asians have distinct physiological (e.g. organ weights, regional blood flows) and biological (e.g. CYP genotypes) differences compared with Europeans [320]. However, clinical studies indicated that age-dependent physiological alterations such as the decline in hepatic blood flow and in the glomerular filtration rate are similar between Asians and Europeans despite having different values at younger ages [58, 560, 561]. Therefore, the age-related decrease in drug clearance was not statistically significant different between whites and Asians (Figure 5.6). This research provides evidence that age-related pharmacokinetic changes of renally and hepatically eliminated drugs, including those metabolized by CYP enzymes with distinct genotype differences between ethnicities, are comparable and thus, results of this study can possibly be interpreted globally. However, more data are warranted in the future for Africans and antiretroviral drugs in all ethnic groups.

Pharmacogenomics need careful consideration, especially when interpreting the result of the present study globally. CYP2B6 phenotypes contribute to the pharmacokinetic variability of efavirenz. PMs of CYP2B6 have higher efavirenz concentrations than EMs [513]. The PM frequency for CYP2B6 is higher in Africans compared with Europeans [562] and differs in Asians compared with whites [563]. As physiological alterations with advanced aging cause age-related pharmacokinetic changes [512], the relative increase in drug exposure is similar between PM and EM despite having a different absolute drug exposure (data not shown).

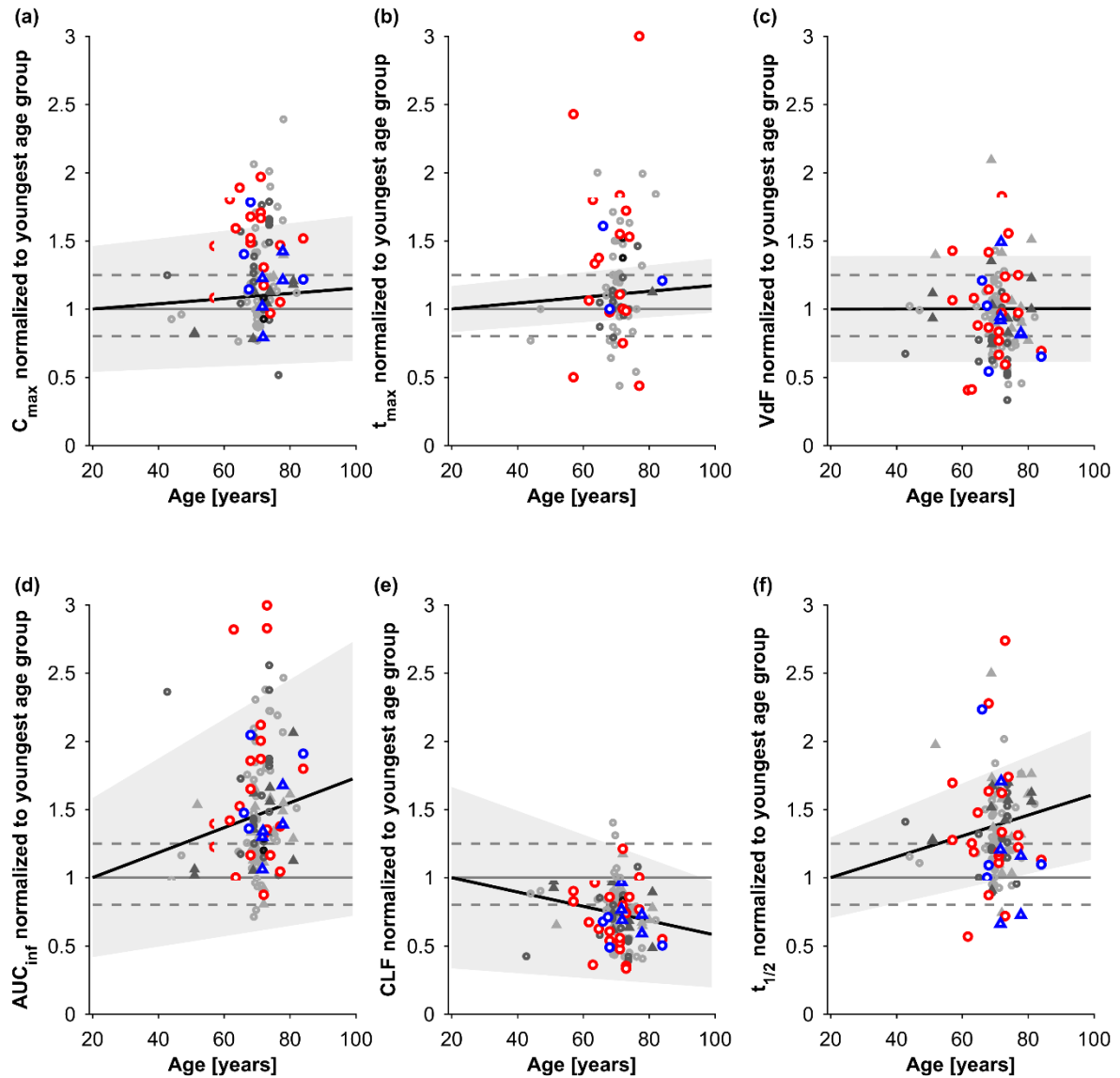


Figure 5.6: Impact of ethnicities on age-related pharmacokinetic changes. The dashed grey lines, solid black line, and the shaded grey area represent the 1.25-fold interval (bioequivalence criterion), the fitted mean, and the estimated variability of age-related pharmacokinetic changes obtained from non-HIV drugs [512]. Light grey, grey, and dark grey markers show historic data of drugs primarily undergoing hepatic, renal, and biliary elimination for whites [512]. Red and blue markers represent drugs primarily undergoing hepatic and renal elimination in other ethnic groups. Triangles and circles stand for intravenous and oral drug administrations. References for the studied drugs can be found in the Table 5.3.

Key: AUC = area under the curve, C_{max} = peak concentration, CLF = oral clearance, t_{max} = time to C_{max}, t_{1/2} = elimination half-life, VdF = apparent volume of distribution.

Intracellular concentrations are important to assess the concentration at the target site but are usually difficult to obtain in humans. The pilot study of Dumond *et al.* measured the intracellular concentration of tenofovir diphosphate (after administering tenofovir disoproxil fumarate) and emtricitabine diphosphate in peripheral blood mononuclear cells of 12 PLWH aged 55 to 65 years. The authors found the intracellular tenofovir diphosphate concentration to be increased by 57.7% and the intracellular emtricitabine diphosphate concentration to be decreased by 22.4% [71]. The results between both drugs are contradictory, but the small sample size and the age of the participants must be considered. Additional clinical data regarding intracellular antiretroviral drug concentration in elderly PLWH are missing. A whole-body PBPK model used in our study could help to understand age-related changes in intracellular drug exposure (i.e. between tenofovir disoproxil fumarate and tenofovir alafenamide) but needs to be carefully verified with existing clinical data which are not available.

Several limitations of our study should be acknowledged. Firstly, clinical data in individuals over the age of 85 years were limited and therefore, simulation results in this age group need to be interpreted with caution.

Secondly, our clinically observed data were obtained in aging PLWH at least 55 years, having a declined kidney function (i.e. glomerular filtration rate up to 65.6 ± 19.2 mL/min/1.73m²) and common comorbidities (e.g. hypertension), but had no severe conditions such as advanced renal impairment stage 4 to 5 or heart failure classified as New York Heart Association 3 to 4. Therefore, results might not be applicable to elderly PLWH with severe diseases. A French study found that 75% of PLWH at least 75 years were non-frail, 22% had a risk for frailty, and 4% were complex patients [564], demonstrating that our findings support the clinical care of the majority of aging PLWH. Clinical studies investigating the combined effects of aging and frailty as well as severe comorbidities are warranted in the future.

Thirdly, HIV infection per se affects physiology [565, 566]; however, these changes translate only to marginal pharmacokinetic differences of around 20% for some antiretroviral drugs [567]. Even so, our model was verified with clinically observed data from healthy volunteers and PLWH and all were contained within the 95% confidence interval of the model predictions.

Fourthly, our PBPK framework does not include a mechanistic kidney model and therefore, tubular secretion of tenofovir and emtricitabine was implemented as an additional clearance that was assumed not to change with age. Age-dependent activity of renal transporters has not been studied, and even though hepatic drug transporter activity is unaltered with age [228], it remains uncertain if age-dependency of hepatic transporters can be linked to renal transporters. Exposure of digoxin, a drug mainly cleared by the kidney through glomerular filtration and tubular secretion, had a 56% higher exposure in individuals aged 72 to 91 years compared with subjects aged 34 to 64 years [497], which is in line with the decrease in glomerular filtration rate, indicating that tubular secretion might be unaltered in the elderly.

Age-related changes in physiology and biology do not only affect pharmacokinetics but can also modify drug pharmacodynamics. Resulting altered drug effects can be explained by changes in the number of receptors, the affinity of the drug to its receptor as well as changes in physiological and homeostatic processes with aging [568]. Limited data regarding antiretroviral pharmacodynamics in aging PLWH suggest efficient viral suppression [88]. Both, age related pharmacodynamic changes, as well as the presence of comorbidities predispose elderly individuals to inappropriate prescribing.

In conclusion, the impact of advanced aging on antiretroviral drug pharmacokinetics is not clinically relevant considering the large therapeutic index of the current first-line treatment. In our study, neither sex nor ethnicity appear to impact age-related pharmacokinetic changes. Overall, antiretroviral drug dose adjustment is a priori not necessary in aging male and female PLWH in the absence of severe comorbidities.

5.6 Study Highlights

What is already known about this subject?

- Age-related changes in physiology might impact the pharmacokinetics of antiretroviral drugs to a clinically relevant extent.
- Clinically observed pharmacokinetic data in elderly people living with the human immunodeficiency virus (HIV) are limited.
- Labels of the current first-line HIV treatments provide no dosing recommendations based on the age of treated individuals.

What this study adds?

- Clinical data for 10 antiretrovirals were obtained in aging people living with HIV and used to verify a predictive physiologically based pharmacokinetic model.
- Predicted antiretroviral drug exposures increased by maximal 70% across adulthood, which is not clinically relevant for antiretrovirals given the wide safety margins and, thus, dose adjustments are not necessary.

5.7 *Supplementary Material*

The online version of this article contains supplementary material:

<https://doi.org/10.1111/bcp.14402>

Table S1: References for clinical studies used for model verification. See Table 5.1.

Table S2: Input parameters for drug models. See Table 5.2.

Table S3: Studies to investigate the impact of ethnicity on age-related pharmacokinetic changes. See Table 5.3.

Table S4: Relative age-related changes of the peak concentration for men and women. Not included in this thesis.

Table S5: Relative age-related changes of the time to peak concentration for men and women. Not included in this thesis.

Table S6: Relative age-related changes of the area under the curve to tau for men and women. Not included in this thesis.

Table S7: Relative age-related pharmacokinetic changes of clearance for men and women. Not included in this thesis.

Table S8: Relative age-related pharmacokinetic changes of the volume of distribution for men and women. Not included in this thesis.

Table S9: Relative age-related pharmacokinetic changes of the elimination half-life for men and women. Not included in this thesis.

Table S10: Statistical analysis of relative age-related pharmacokinetic changes between men and women. See Table 5.5.

Figure S1: Impact of phenotypes on age-related pharmacokinetic changes of efavirenz. Not included in this thesis.

Chapter 6:
Drug-Drug Interaction Magnitudes with Aging

6. Drug-Drug-Interaction Magnitudes with Aging

6.1 Clinical study in aging PLWH to investigate drug-drug interaction

magnitudes between cardiovascular agents and antiretrovirals **Page 152**

6.1.1 Summary **Page 152**

6.1.2 Introduction **Page 152**

6.1.3 Material and Methods **Page 153**

6.1.4 Results **Page 154**

6.1.5 Discussion **Page 155**

6.2 Physiologically based pharmacokinetic modelling of drug-drug

interaction magnitudes with advanced aging **Page 156**

6.2.1 Abstract **Page 156**

6.2.2 Introduction **Page 157**

6.2.3 Methods **Page 158**

6.2.4 Results **Page 164**

6.2.5 Discussion **Page 174**

6.2.6 Study Highlights **Page 181**

6.2.7 Appendix **Page 182**

6.2.8 Supplementary Material **Page 198**

This chapter contains two pre-printed manuscripts: one research letter describing the outcome of the conducted clinical study and one original research article describing the continuous effect of aging on DDI magnitudes.

Aging does not impact drug-drug interaction magnitudes with antiretrovirals: a Swiss HIV Cohort Study

Felix Stader, Laurent A. Decosterd, Marcel Stoeckle, Matthias Cavassini, Manuel Battegay, Susana Alves Saldanha, Catia Marzolini, Perrine Courlet, & the Swiss HIV Cohort Study

AIDS 2020; 34(6): 949-952.

DOI: 10.1097/QAD. 0000000000002489

Clinical data combined with modelling indicate unchanged drug-drug interaction magnitudes in the elderly

Felix Stader, Perrine Courlet, Hannah Kinvig, Melissa A. Penny, Laurent A. Decosterd, Manuel Battegay, Marco Siccardi, & Catia Marzolini

Clinical Pharmacology & Therapeutics 2020; [Epub ahead of print].

DOI: 10.1002/cpt.2017

6.1 Clinical study in aging PLWH to investigate drug-drug interaction magnitudes between cardiovascular agents and antiretrovirals

6.1.1 Summary

The risk of drug-drug interactions (DDIs) is elevated in aging people living with HIV (PLWH) because of highly prevalent age-related comorbidities leading to more comedications. To investigate the impact of aging on DDI magnitudes between comedications (amlodipine, atorvastatin, rosuvastatin) and boosted darunavir, we conducted a clinical trial in aging PLWH at least 55 years. DDI magnitudes were comparable to those reported in young individuals, supporting that the clinical management of DDIs in aging PLWH can be similar.

6.1.2 Introduction

Combined antiretroviral treatments have increased the life expectancy of people living with HIV (PLWH) close to the general population [510]. Consequently, PLWH have an identical high prevalence for age-related comorbidities, such as cardiovascular conditions, leading to complex drug associations with a higher risk for drug-drug interactions (DDIs) [93]. One current issue is the lack of knowledge concerning the magnitude and clinical management of DDIs in aging PLWH. However, despite the high DDI potential of antiretroviral drugs, it is neither feasible nor ethically possible to conduct clinical studies for every single drug combination. Additionally, elderly PLWH are underrepresented in clinical studies. The decline in hepatic and renal blood flow and in the glomerular filtration rate drives age-related pharmacokinetic changes of non-HIV drugs and likely impacts antiretroviral drug pharmacokinetics [512]. The impact of aging on metabolizing enzymes and drug transporters activity is either controversially discussed or lacking in the literature [58], which in addition to pharmacokinetic alterations could both affect the magnitude of DDIs in the elderly.

The aim of this study was to quantify the DDI magnitudes between cardiovascular drugs (i.e. amlodipine, atorvastatin, rosuvastatin) and antiretroviral agents in aging PLWH to provide guidance on DDI management in this fragile population.

6.1.3 Material and Methods

This was a prospective clinical study including PLWH at least 55 years in Lausanne and Basel that are enrolled in the Swiss HIV Cohort Study [74]. Included PLWH received amlodipine, atorvastatin and/or rosuvastatin with a dolutegravir (no drug interaction expected) or a boosted darunavir containing regimen (high interaction potential). PLWH were excluded if they had severe comorbidities such as advanced renal impairment (stage 4 to 5), heart failure (New York Heart Association 3 to 4) or liver cirrhosis (Child-Pugh score C) or if they were receiving comedications with inhibitory or inducing properties. Consenting PLWH came to the HIV clinic in the morning for the collection of serial blood samples over 24 hours. The Ethics Committee of Vaud and Northwest/Central Switzerland approved the study protocol (CER-VD 2018-00369), which is registered at ClinicalTrials.gov (NCT03515772). Written informed consent was collected for each participant.

Plasma samples were isolated by centrifugation and stored at -80°C until batch analysis. Plasma levels determination was performed in the Laboratory of Clinical Pharmacology in Lausanne, using liquid chromatography coupled with tandem mass spectrometry [569].

All doses were normalized as amlodipine, atorvastatin, and rosuvastatin exhibit dose-proportional pharmacokinetics. Pharmacokinetic parameters were calculated noncompartmentally from the measured concentration-time profiles in Matlab® 2017a. The mean and standard deviation of the area under the curve (AUC) were calculated for the comedication received with either dolutegravir or boosted darunavir. The DDI magnitudes were calculated as the AUC of the comedication in the presence of boosted darunavir (inhibitory effects on cytochrome P-450 3A4 (CYP3A4) and/or hepatic/intestinal transporters) divided by the AUC of the comedication in the presence of dolutegravir (no inhibitory effects).

A structured literature search was performed using the MEDLINE database to screen for studies investigating the same DDI magnitudes in young adults to evaluate the impact of aging.

6.1.4 Results

A total of 21 white PLWH (four women) aged 56 to 80 years were included in the study. Amlodipine was taken by eight PLWH (dolutegravir: $n = 6$; boosted darunavir: $n = 2$) aged 64.8 ± 7.0 years. The AUC of amlodipine (dose-normalized to 5 mg) was $1,155 \pm 414$ ng*h/mL and $2,425 \pm 739$ ng*h/mL in combination with dolutegravir and boosted darunavir, resulting in an AUC-ratio of 2.10 ± 0.99 (Table 6.1). In young adults aged 20 to 50 years, the increase in amlodipine exposure in the presence of boosted indinavir was 1.89 [570] and in the presence of ritonavir was 2.11 [382].

Atorvastatin was investigated in nine aging PLWH (dolutegravir: $n = 4$; boosted darunavir: $n = 5$) aged 64.1 ± 8.0 years at a dose of 10 mg. The AUC of atorvastatin in the presence of dolutegravir was 31.4 ± 4.7 ng*h/mL and increased to 193 ± 133 ng*h/mL in PLWH receiving boosted darunavir. The resulting AUC-ratio was 6.16 ± 4.35 . No study could be identified in young individuals for atorvastatin in the presence of boosted darunavir, but for boosted saquinavir (AUC-ratio: 3.93) [571] and boosted tipranavir (AUC-ratio: 9.36) [428].

Rosuvastatin was administered to six PLWH (dolutegravir: $n = 2$ boosted darunavir: $n = 4$) aged 67.7 ± 5.3 years and concentrations were dose-normalized to 10 mg. The rosuvastatin AUC in the presence of dolutegravir and boosted darunavir was 104.2 ± 32.6 ng*h/mL and 166.9 ± 75.5 ng*h/mL, respectively. The resulting AUC-ratio was 1.60 ± 0.88 . One clinical study investigated rosuvastatin exposure in the presence of boosted darunavir in young adults aged 20 to 50 years and reported an AUC-ratio of 1.57 ± 0.54 [572].

Table 6.1: Comparison of DDI magnitudes of amlodipine, atorvastatin, and rosuvastatin combined with boosted darunavir in young (20 to 50 years) and aging individuals (55 to 80 years).

	n	Age [years]	AUC-ratio of aging individuals (55-80 years)	AUC-ratio of young individuals (20-50 years)	Ratio aging/young
amlodipine + boosted darunavir	8	64.8 ± 7.0	2.10 ± 0.99	2.11 (ritonavir alone) [382] 1.89 (boosted indinavir) [570]	1.00 1.11
atorvastatin + boosted darunavir	9	64.1 ± 8.0	6.16 ± 4.35	3.93 (boosted saquinavir) [571] 9.36 (boosted tipranavir) [428]	-
rosuvastatin + boosted darunavir	6	67.7 ± 5.3	1.60 ± 0.88	1.57 ± 0.54 [572]	1.02

Key: AUC = area under the curve.

6.1.5 Discussion

Clinical studies concerning the impact of aging on DDI magnitudes involving antiretroviral drugs do not exist, leading to uncertainty concerning the clinical management of DDIs in aging PLWH. To our knowledge, our study is the first to investigate DDIs of commonly used comedications (amlodipine, atorvastatin, rosuvastatin) and boosted darunavir in PLWH aged at least 55 years. The obtained AUC-ratios in aging PLWH were in the same range as DDI magnitudes reported in young individuals aged 20 to 50 years, thus, demonstrating that aging has a marginal impact on DDI magnitudes.

Two clinical studies with midazolam and clarithromycin (inhibition) or rifampicin (induction) elucidated no age-related changes of the DDI magnitudes, which support our study results [111, 112, 573].

Several limitations should be acknowledged. Firstly, the small number of patients led to an observational study design. Nevertheless, the obtained clinical data show the real-life scenario of amlodipine, atorvastatin, and rosuvastatin in aging PLWH receiving boosted darunavir. Secondly, concentration-time profiles for the comedications in the presence of dolutegravir and boosted darunavir came from two different groups of patients because of medical and ethical reasons. Thirdly, clinical data for our investigated DDIs in young individuals were not obtained in the same study but gathered from published clinical trials that did not administer the same protease inhibitors as in our study. In the case of amlodipine, ritonavir itself is enough to inhibit CYP3A4 completely and thus, the second protease inhibitor can be neglected [373]. In the case of atorvastatin, the inhibition of the organic anion transporting polypeptide (OATP) 1B1 and P-glycoprotein (P-gp) adds to the CYP3A4 inhibition. Saquinavir and ritonavir show the least impact on OATP1B1 followed by darunavir and tipranavir with the latter one being a strong P-gp inhibitor [103, 574]. Therefore, our results for atorvastatin and boosted darunavir are in line with published studies using either saquinavir or tipranavir.

In conclusion, our clinically observed data demonstrated that DDI magnitudes between antiretroviral drugs and comedications appear to be similar in aging PLWH compared with young individuals and thus, the clinical management of DDIs can be similar. Further research is warranted in the future to investigate more DDI scenarios with a larger study population including more women to further support the clinical management of DDIs in aging PLWH.

6.2 *Physiologically based pharmacokinetic modelling of drug-drug interaction magnitudes with advanced aging*

6.2.1 Abstract

Age-related comorbidities and consequently polypharmacy are highly prevalent in the elderly, resulting in an increased risk for drug-drug interactions (DDIs). The effect of aging on DDI magnitudes is mostly uncertain, leading to missing guidance regarding the clinical DDI management in the elderly. Clinical data obtained in aging people living with HIV at least 55 years, who participated in the Swiss HIV Cohort Study, demonstrated unchanged DDI magnitudes with advanced aging for four studied DDI scenarios. These data plus published data for midazolam in the presence of clarithromycin and rifampicin in elderly individuals assessed the predictive potential of the used physiologically based pharmacokinetic (PBPK) model to simulate DDIs in the elderly. All clinically observed data were generally predicted within the 95% confidence interval of the PBPK simulations. The verified model predicted subsequently the magnitude of 50 DDIs across adulthood (20 to 99 years) with 42 scenarios being only verified in adults aged 20 to 50 years in the absence of clinically observed data in the elderly. DDI magnitudes were not impacted by aging regardless of the involved drugs, DDI mechanism, mediators of DDIs, or the sex of the investigated individuals. The prediction of unchanged DDI magnitudes with advanced aging were proofed by 17 published, independent DDIs that were investigated in young and elderly subjects. In conclusion, this study demonstrated by combining clinically observed data with modelling and simulation that aging does not impact DDI magnitudes and thus, clinical management of DDIs can a priori be similar in aging men and women in the absence of severe comorbidities.

6.2.2 Introduction

The number of elderly individuals at least 65 years is estimated to double in the USA and Europe by 2050 [375, 376]. The prevalence of age-related comorbidities increases with advanced aging [377, 575], leading to more comedications [378] and consequently, to a higher risk for drug-drug interactions (DDIs) [95]. However, clinical studies investigating DDI magnitudes in the elderly are generally not conducted, resulting in a knowledge gap about how to manage DDIs in aging individuals in clinical practice.

Organ functions decline with advanced aging with the potential to alter drug pharmacokinetics and thereby the magnitude of DDIs [380, 512]. Significant changes are the reduction in the hepatic and renal blood flows as well as in the glomerular filtration rate affecting drug clearance. Additionally, the age-related reduction in total body water and the increase in adipose tissue weight can affect drug distribution in the elderly [58].

The incorporation of age-related physiological changes into physiologically based pharmacokinetic (PBPK) models allows to conduct virtual clinical trials in the elderly to investigate scenarios that cannot easily or ethically be studied [118]. The model performance is verified against clinically observed data before extrapolating to unknown scenarios of interest.

There is a particular need to investigate DDI magnitudes in aging people living with HIV (PLWH), because their life expectancy is close to the general population [510], and they have a high prevalence for age-related comorbidities [93] and polypharmacy [92]. Furthermore, antiretroviral drugs have a high DDI potential [576]. We previously conducted a clinical study in aging PLWH at least 55 years in the framework of the Swiss HIV Cohort Study to analyze DDI magnitudes between antiretroviral drugs and comedications in the elderly and found similar DDI magnitudes compared to historical data in young adults aged 20 to 50 years [577]. However, the conducted study had limitations regarding the number of studied scenarios and investigated individuals.

The objectives of the present study were to firstly assess the predictive potential of the PBPK approach to simulate DDIs in the elderly and secondly, to investigate comprehensively the impact of aging on DDI magnitudes, involving different drugs and DDI mechanisms, by the verified PBPK model.

6.2.3 Methods

We took three different steps to investigate whether aging impacts the magnitudes of DDIs. Firstly, we used the clinically observed data obtained in aging PLWH at least 55 years for four different DDI scenarios [577] to verify the predictive performance of our previously developed PBPK framework [118] to simulate DDI magnitudes in the elderly. Secondly, the verified PBPK model predicted DDI magnitudes across adulthood for 50 different DDIs with different involved drugs and DDI mechanisms. The simulation results were statistically analyzed to determine the general impact of aging on DDI magnitudes. Thirdly, a meta-analysis was undertaken to seek for clinical data investigating DDI magnitudes in young adults aged up to 40 years and elderly adults at least 55 years to proof the general model-based hypothesis of the present study.

Clinical data to investigate drug-drug interaction magnitudes in aging individuals to verify the physiologically based pharmacokinetic model

In a prospective clinical study, which was conducted at the HIV clinics Lausanne and Basel, PLWH at least 55 years, who participated in the Swiss HIV Cohort Study, were included if they received amlodipine, atorvastatin and/or rosuvastatin with a dolutegravir (no interaction expected) or a boosted darunavir (high interaction potential) containing antiretroviral regimen. The Ethics Committee of Vaud and Northwest/Central Switzerland approved the study protocol (CER-VD 2018-00369), which is registered at ClinicalTrials.gov (NCT03515772). Written informed consent was collected for each participant. Plasma concentrations were collected over 24 hours. Pharmacokinetic parameters were calculated noncompartmentally. Details on the study design were published previously [577]. Historical data from young adults aged 20 to 50 years, receiving the same drug combination as the elderly PLWH in our conducted study, were gathered from the literature for model verification.

To verify analyzed DDI scenarios, for which clinically observed data exist only in the young, a structured literature search was performed to seek for clinical studies investigating DDIs with drugs, we previously used to analyze the impact of aging on drug pharmacokinetics [512, 578]. Observed data were extracted from the literature using GetData Graph digitizer V. 2.26, which has an excellent accuracy [579]. Clinical studies used for model verification are detailed in Table 6.2.

Table 6.2: Published clinical studies used to verify drug-drug interaction predictions of our developed PBPK model.

Victim		Perpetrator		Health status	n	Prop female	Age [years]	Weight [kg]	Reference
drug	dosing regimen	drug	dosing regimen						
midazolam	10 mg oral single	ketoconazole	200 mg oral once daily	healthy	10	0.58	34.2	72.1	[580]
midazolam	4 mg oral single	niotinib	600 mg oral single	healthy	18	0.17	39.9	79.9	[581]
midazolam	0.05 mg/kg iv single	clarithromycin	500 mg oral twice daily	healthy	16	0.50	31.5	71.5	[111]
midazolam	4 mg (v) / 3 mg (e) oral single			healthy	16	0.50	71.0	84.0	[112]
midazolam	1 mg iv single	ritonavir	100 mg oral once daily	healthy	11	0.38	29.0	77.2	[373]
midazolam	0.05 mg/kg iv single	rifampicin	600 mg oral once daily	healthy	28	0.50	26.5		[573]
midazolam	4 mg oral single			chronic diseases	24	0.58	71.0		
midazolam	0.025 mg/kg iv single	etravirine	200 mg oral twice daily	healthy	14				[100]
metoprolol	100 mg oral single			healthy EM	13	0	28.0	77.0	[582]
				healthy PM	4	0	37.5	90.0	
				healthy UM	12	0.08	28.0	76.0	
amlodipine	5 mg oral single	ritonavir	100 mg oral once daily	healthy	14	0.33	34.3	75.7	[583]
	10 mg oral once daily	darunavir/ritonavir	800/100 mg oral once daily	HIV +	8	0.13	64.8		[577]
rivaroxaban	10 mg oral once daily	ketoconazole	400 mg oral once daily	healthy	20	0	34.2	82.9	[369]
rivaroxaban	10 mg oral single	clarithromycin	500 mg oral twice daily	healthy	15	0	37.6	81.1	[369]
rivaroxaban	10 mg oral single	ritonavir	600 mg oral twice daily	healthy	12	0	33.2	84.3	[369]
repaglinide	2 mg oral single			healthy EM	12				[584]
				healthy UM	4				
repaglinide	0.25 mg oral single			healthy ET	12	0.25	24.0	75.0	[585]
				healthy PT	6	0.17	23.0	75.0	
repaglinide	0.25 mg oral single	gemfibrozil	600 mg oral twice daily	healthy	34	0.24	25.9	72.9	[585-587]
repaglinide	0.25 mg oral single	gemfibrozil	600 mg oral twice daily	healthy ET	12	0.25	24.0	75.0	[585]
				healthy PT	6	0.17	23.0	75.0	
atorvastatin	20mg oral single	clarithromycin	500 mg twice daily	healthy	23	0.39	24.4	69.5	[588]
atorvastatin	40 mg oral single	rifampicin	600 mg oral once daily	healthy	10	0.40	25.0	68.0	[425]
atorvastatin	40 mg oral once daily	efavirenz	600 mg oral once daily	healthy	14	0.07	32.0		[589]
atorvastatin	40 mg oral once daily	etravirine	200 mg oral twice daily	healthy	16	0.13	40.0	77.0	[590]
atorvastatin	20 mg oral single			healthy ET	16	0.50	23.0	68.0	[591]
				healthy IT	12	0.42	24.0	69.0	
				healthy PT	4	0.25	23.0	84.0	
atorvastatin	20 mg oral single	gemfibrozil	600 mg oral twice daily	healthy	10	0.40	23.0	73.0	[425]
atorvastatin	10 mg oral once daily	darunavir/ritonavir	800/100 mg oral once daily	HIV +	9	0.11	64.1		[577]
rosuvastatin	10 mg oral single			healthy ET	16	0.50	23.0	68.0	[591]
				healthy IT	12	0.42	24.0	69.0	
				healthy PT	4	0.25	23.0	84.0	
rosuvastatin	80 mg oral single	gemfibrozil	600 mg oral twice daily	healthy	20	0.15	41.2	76.0	[592]
rosuvastatin	10 mg oral single	darunavir/ritonavir	600/100 mg oral twice daily	healthy	12	0.50	25.0		[572]
rosuvastatin	10 mg oral once daily	800/100 mg oral once daily		HIV +	6	0.33	67.7		[577]
rosuvastatin	10 mg oral single	atazanavir/ritonavir	300/100 mg oral once daily	healthy	6	0.50	28.0	73.5	[593]

Table 6.2: con't.

Victim		Perpetrator		Health status	n	Prop female	Age [years]	Weight [kg]	Reference
drug	dosing regimen	drug	dosing regimen						
nilotinib	200 mg oral single	ketoconazole	400 mg oral once daily	healthy	26	0.15	39.1	76.8	[594]
nilotinib	400 mg oral single	rifampicin	600 mg oral once daily	healthy	15	0.20	32.1	79.9	[594]
darunavir	800 mg oral single	ritonavir	100 mg oral once daily	healthy	43	0.30	37.3		[370-372]
	600-1200 mg oral once daily		100 mg oral once daily	HIV+	6	0	68.6		[74]
atazanavir	300 mg oral once daily	ritonavir	100 mg oral once daily	healthy + HIV+	141	0.31	35.0	78.8	[374, 514, 515, 595, 596]
dolutegravir	30 mg oral once daily	atazanavir	400 mg oral once daily	healthy	24	0.12	37.2		[597]
dolutegravir	30 mg oral once daily	atazanavir/ritonavir	300/100 mg oral once daily	healthy	24	0.12	37.2		[597]
dolutegravir	30 mg oral once daily	darunavir/ritonavir	800/100 mg oral once daily	healthy	30	0	28.0	82.1	[598]
	50 mg oral once daily		800/100 mg oral once daily	HIV+	14	0	57.6		[74, 577]
dolutegravir	50 mg oral once daily	rifampicin	600 mg oral once daily	healthy	16	0.44	32.0		[599]
dolutegravir	50 mg oral once daily	etravirine	200 mg oral twice daily	healthy	16	0	41.5	84.8	[517]
rilpivirine	150 mg oral once daily	darunavir/ritonavir	800/100 mg oral once daily	healthy	14				[105]
rilpivirine	150 mg oral once daily	rifampicin	600 mg oral once daily	healthy	16				[105]
rilpivirine	25 mg oral once daily	efavirenz	600 mg oral once daily	healthy	20	0.10	34.5		[600]
raltegravir	400 mg oral single	ritonavir	100 mg oral twice daily	healthy	14	0	28.0	79.6	[521]
raltegravir	400 mg oral single	rifampicin	600 mg oral once daily	healthy	10	0.70	38.4	79.1	[601]
raltegravir	400 mg oral single	efavirenz	600 mg oral once daily	healthy	14	0	34.0	76.6	[521]
raltegravir	400 mg oral once daily	etravirine	200 mg oral twice daily	healthy	20	0.35	29.8	78.5	[518]
efavirenz	600 mg oral once daily	EM CYP2B6		HIV+	61	0.23	44.4	70.4	[513]
		PM CYP2B6		HIV+	8	0.25	38.9	65.8	
		EM CYP2B6		HIV+	23	0.04	61.2	75.1	
		PM CYP2B6		HIV+	2	0	57.0	73.5	
efavirenz	600 mg oral once daily	rifampicin	600 mg oral once daily	healthy	11	0.55	42.6	76.9	[602]
etravirine	200 mg oral twice daily	clarithromycin	500 mg oral twice daily	healthy	16	0	29.0		[603]

Key: e = elderly, EM = enhanced metabolizers, ET = enhanced transporter phenotype, IT = intermediate transporter phenotype, iv = intravenous, PM = poor metabolizers, PT = poor transporter phenotype, UM = ultrarapid metabolizers, y = young.

Physiologically based pharmacokinetic modelling

A whole-body PBPK model was constructed in Matlab® 2017a. The model structure, code, and assumptions were published previously [118]. The model was informed by an aging virtual population considering age-related changes of demographical (e.g. body weight), physiological (e.g. organ weight), and biological (e.g. enzyme abundance) parameters with variability [58].

Used drug models for antiretroviral drugs (i.e. dolutegravir and boosted darunavir) and non-HIV drugs (i.e. amlodipine, atorvastatin, and rosuvastatin) were developed and verified previously [512, 578]. To simulate the combination of dolutegravir with boosted darunavir, the possibility to induce uridine diphosphate-glucuronosyltransferase (UGT) 1A1 was implemented into the existing PBPK model [118]. The turnover rate of UGT1A1 was found to be 0.0693 1/h [604]. In vitro studies investigating the UGT1A1 induction potential of antiretroviral drugs are generally missing. It is suggested that cytochrome P-450 (CYP) 3A and UGT1A1 are both modulated by the pregnane X receptor (PXR) and thus, have a similar half-maximal inducing concentration [605]. The maximal inducing potential was also assumed to be similar in the absence of data. The prediction of clinically observed DDIs for raltegravir, a drug purely metabolized by UGT1A1, in the presence of ritonavir, rifampicin, etravirine, and efavirenz served as the verification of the used assumptions regarding UGT1A1 induction.

PBPK models were developed for ketoconazole and nilotinib to analyze the impact of aging on competitive CYP3A inhibition and gemfibrozil and its glucuronide metabolite as inhibitors of the organic anion transporting polypeptide (OATP) 1B1. Their input parameters (Table 6.3) were obtained from published models [385, 606, 607], tissue scalars were modified to capture the clinically observed data in young adults (Table 6.4), and verified with at least one independent clinical study for our PBPK framework [118]. The generation of the gemfibrozil metabolite was implemented in the liver by the UGT2B7 clearance pathway. If compound characteristics of the gemfibrozil metabolite were not available in the literature, the same value as for gemfibrozil was assumed. The intrinsic clearance for gemfibrozil and nilotinib were retrogradely calculated from clinically observed data considering the in vitro measured fraction metabolized for each enzymatic pathway [385, 607].

Table 6.3: Parameters of ketoconazole (KTZ), nilotinib (NIL), gemfibrozil (GEM), and its glucuronide metabolite (GEU).

Parameter	Unit	KTZ		NIL		GEM		GEU	
Physicochemical properties									
MW	g/mol	531.4	[608]	529.5	[609]	250.3	[385]	426.5	[385]
logP		4.0	[606]	5.0	[609]	4.3	[385]	3.3	[385]
drug type		db	[606]	db	[609]	ma	[385]	ma	[385]
pKa 1		2.94	[606]	5.35	[609]	4.75	[385]	2.68	[385]
pKa 2		6.51	[606]	3.9	[609]				
BP		0.62	[606]	0.68	[610]	0.825	[385]	0.825	[385]
fup		0.029	[606]	0.016	[610]	0.03	[385]	0.115	[385]
binding protein		HSA	[606]	AAG	[611]	HSA	[612]	HSA	[613]
Absorption									
P _{app}	10 ⁻⁶ cm/sec	495	[606]	5.99	[610]	160.9	[385]	-	
Lag Rate				0.27	op			-	
Distribution									
Tissue Scalar		0.5	op	2	op	0.12	op	0.12	op
Adipose tissue Scalar		2	op	0.5	op				
Liver Scalar				0.08	op	8.3	op	8.3	op
Metabolism & Elimination									
CYP2D6 CL _{int}	μL/min/pmol	0.4296	[606]						
CYP3A4 CL _{int}	μL/min/pmol	0.5238	[606]	0.157	st	0.117	st		
CYP1A2 CL _{int}	μL/min/pmol			0.018	st				
CYP2C8 CL _{int}	μL/min/pmol			0.127	st				
UGT1A1 CL _{int}	μL/min/pmol								
UGT2B7 CL _{int}	μL/min/pmol					0.470	st		
Unspecified	μL/min/mg								
CL _{renal}	L/h								
CL _{bile}	L/h							51.9	[385]
Interaction									
CYP3A4 K _i	μM	0.015	[606]	0.448	[614]	68.08	[385]	103.74	[385]
CYP3A5 K _i	μM	0.11	[606]	0.448	[614]				
CYP2C8 K _i	μM			0.236	[614]	6.882	[385]		
UGT1A1 K _i	μM			0.19	[614]	75	[615]		
UGT1A3 K _i	μM					36	[615]		
OATP1B1 K _i	μM					1.8648	[385]	6.162	[385]
OATP1B3 K _i	μM								
CYP2C8 k _{inact}	1/h							9.828	[385]
CYP2C8 K _{app}	μM							7.878	[385]

Key: AAG = alpha-acid glycoprotein, BP = blood-plasma-ratio, CL_{int} = intrinsic clearance, CYP = cytochrome P-450, db = diprotic base, fup = fraction unbound in plasma, HSA = human serum albumin, K_{app} = concentration of mechanism-based inhibitor associated with half maximal inactivation rate, K_i = inhibition constant, k_{inact} = inactivation rate of an enzyme suppressed by mechanism-based inhibition, logP = octanol-water partition coefficient, ma = monoprotic acid, MW = molecular weight, OATP = organic anion transporting polypeptide, op = optimized, P_{app} = apparent permeability, pKa = acid dissociation constant, st = see text, UGT = uridine diphosphate-glucuronosyltransferase.

Table 6.4: Published clinical studies used to verify the developed PBPK models for ketoconazole, nilotinib, and gemfibrozil.

Drug	Dosing regimen	Health status	n	Prop female	Age [years]	Reference
Ketoconazole	200 mg oral; single	healthy	3	0	34.3	[616]
		healthy	8	0.63	23.0	[617]
		healthy	8	0.63	23.0	[617]
		healthy	12	0.50	30.0	[618]
		healthy	5	0	30.0	[618]
		chronic medical conditions	18	0.50	76.0	[619]
Nilotinib	400 mg oral; single	healthy	44	0.50	30.0	[620]
		healthy	44	0.50	30.0	[620]
		healthy	20	0.50	30.0	[620]
		healthy	24	0.50	30.0	[620]
		healthy	15	0.20	32.1	[594]
		healthy	18	0.17	39.9	[581]
Gemfibrozil	600 mg oral; twice daily	healthy	10	0.10	32.7	[587]
		healthy	6	0	30.0	[621]

DDIs were firstly simulated in young adults aged 20 to 50 years. Successful predictions were judged by overlaying clinically observed data with the simulation results. We analyzed if pharmacokinetic parameters were predicted within 1.25-fold (bioequivalence criterion), 1.5-fold, and 2.0-fold of clinically observed data, which is considered best practice for modelling by the regulatory agencies [326]. Simulations were performed in ten trials containing ten virtual individuals each and were otherwise matched as closely as possible to the conducted and published clinical trials regarding dose and dosing regimen. Drug parameters were not modified when performing simulations in the elderly.

Analyzing the impact of aging across adulthood by the developed PBPK model

Age-related changes in DDI ratios (in the presence of the perpetrator divided by the absence of the perpetrator) of analyzed pharmacokinetic parameters (Peak concentration: C_{max} , time to C_{max} : t_{max} , area under the curve: AUC, clearance: CLF, apparent volume of distribution: VdF , and elimination half-life: $t_{1/2}$) were estimated across adulthood (20 to 99 years) in 100 virtual individuals (50% women) per five years using the verified PBPK model. DDI ratios were normalized to the youngest investigated age group (20 to 24 years). The normalized DDI ratios were fitted to descriptive linear functions containing age as an independent variable. The analysis was done for men, women, and all virtual subjects to investigate whether sex has an impact on age-related changes of DDI magnitudes. The correlation between age and normalized DDI ratios were compared between non-HIV drugs and antiretroviral drugs as well as between men and women by a t-test. An analysis of variance (ANOVA) was performed to investigate whether the impact of aging on DDI magnitudes depends on the mediator of DDIs (CYP enzymes, UGT enzymes, or hepatic transporters) or the DDI mechanism (competitive inhibition –

binding of drugs is blocked by the inhibitor binding itself to the active site of the enzyme, mechanism-based inhibition – the inhibitor leads to an altered transcription or translation and therefore to a loss of enzyme, and induction), and an analysis of covariance (ANCOVA) was performed to investigate the combined effects. The statistical analysis was done in R 3.5.

Proofing the predicted age-related effect on DDI magnitudes by independent clinically observed data

A literature search was performed using the MEDLINE database to screen for clinical studies reporting an AUC-ratio in young and elderly individuals for any DDI. Keywords used were “drug-drug interaction” plus “aging”, “young vs. elderly”, or “young vs. geriatric”. Inclusion criteria were a direct comparison of the AUC-ratio between young adults with a mean age up to 40 years and aging adults with a mean age at least 55 years to match our own clinical study [577], and subjects had to be apparently healthy or having no severe disease and comedication that could potentially affect the DDI of interest. AUC-ratios were normalized to the youngest age group investigated. All included clinical studies are detailed in Table 6.5.

6.2.4 Results

Results of our conducted clinical study in aging PLWH at least 55 years and the comparison of the obtained DDI magnitudes between amlodipine, atorvastatin, or rosuvastatin and either dolutegravir (no interaction expected) or boosted darunavir (high interaction potential) and historical data in young individuals aged 20 to 50 years were published previously [577].

Predictive performance of the PBPK model to simulate DDI magnitudes in the elderly

Firstly, published data in the elderly for midazolam in the presence of clarithromycin and rifampicin [111, 112, 573] and clinically observed data from our own clinical study conducted within the framework of the Swiss HIV Cohort Study [577] were used to proof the predictive performance of our PBPK framework [118] to simulate DDI magnitudes in aging individuals. In all cases, the clinically observed data were generally within the 95% confidence interval of the PBPK model predictions (Figure 6.1-6.3) in young (20 to 50 years) and aging individuals (at least 55 years). The AUC-ratio of intravenous midazolam in the presence of rifampicin was overpredicted in young and elderly adults (predicted:observed ratio: 1.69

and 1.64), and the AUC-ratio of midazolam in the presence of clarithromycin and rifampicin was underpredicted in the elderly (predicted:observed ratio: 0.73 and 0.70). All other AUC-ratios were simulated within 1.25-fold of the clinically observed data (Table 6.6). In both investigated age groups, 73%, 81%, and 100% of C_{max} and $t_{1/2}$ values in the absence and presence of the perpetrator were predicted within 1.25-fold, 1.5-fold, and 2.0-fold of the clinically observed data, respectively.

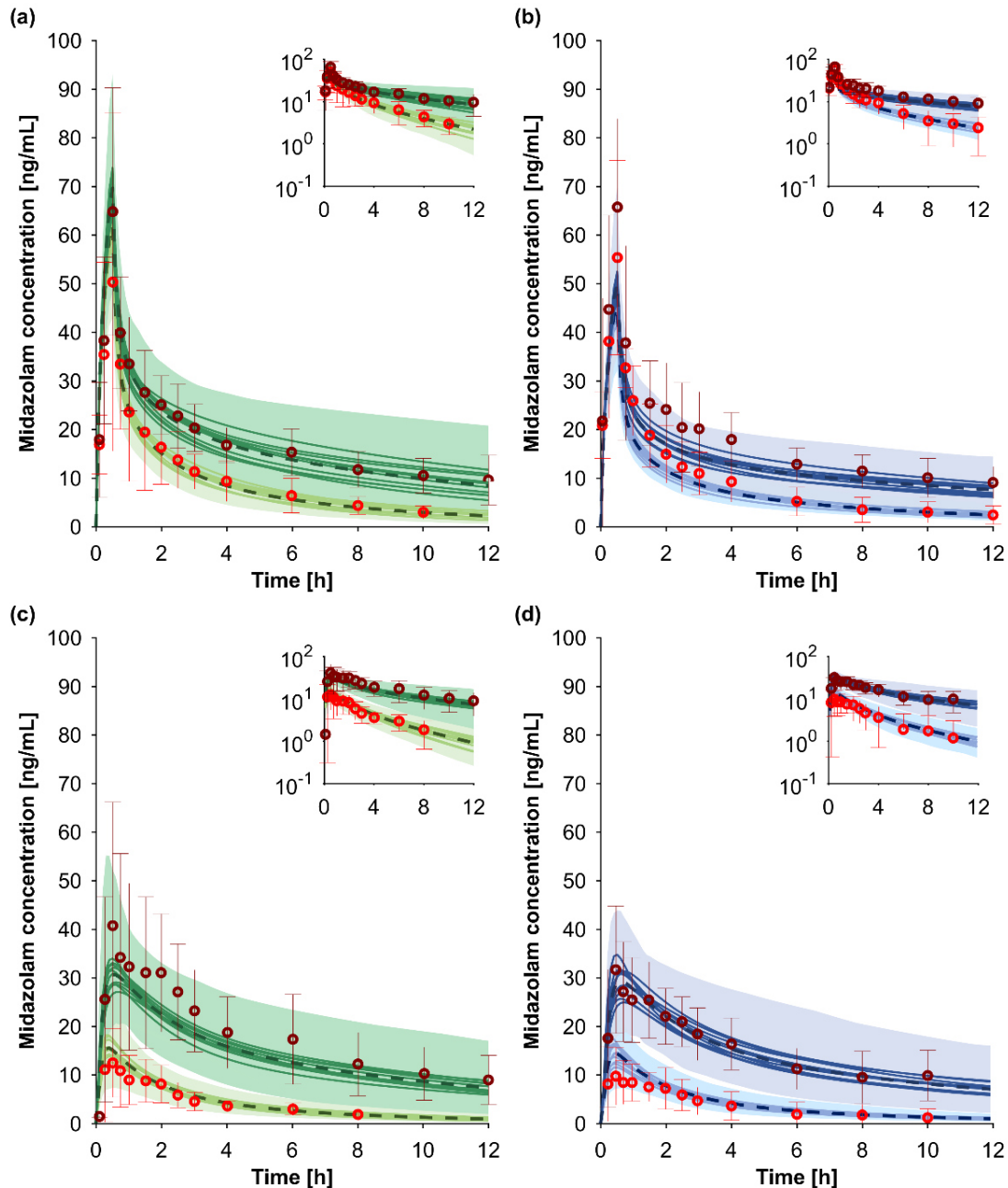


Figure 6.1: Predicted vs. observed concentration time profiles for midazolam in the absence (brighter color) and the presence (darker color) of clarithromycin after intravenous administration (a: young; b: elderly) and oral administration (c: young; d: elderly). The design of the simulated DDI scenarios is detailed in Table 6.2. Red markers show published clinical data. The solid lines, the dashed line, and the shaded area represent the mean of each virtual trial, the mean, and the 95% confidence interval of all virtual individuals, respectively.

Table 6.5: Published studies comparing DDI magnitudes between young and elderly study participants.

Victim	Perpetrator	Mechanism	Mediator	Health status	Young			Elderly			Ratio e/y	Reference
					n	age [years]	weight [kg]	n	age [years]	weight [kg]	AUC-ratio	
Theophylline	Cimetidine	competitive	CYP1A2	healthy	8 (♂)	31.5	77.4	8 (♂)	70.5	84.5	1.02 ± 0.35	0.78 ± 0.36 [622]
				healthy	8 (♀)	27.5	70.4	8 (♀)	71.5	67.5	1.33 ± 0.50	0.94 ± 0.40 [622]
				healthy	12 (♂)	23.6		5 (♂)	61.4		1.28 ± 0.57	0.70 ± 0.57 [623]
				healthy	10 (♂)	26.9	79.9	10 (♂)	72.5	80.1	1.40 ± 0.52	0.99 ± 0.53 [624]
Theophylline	Ciprofloxacin	competitive	CYP1A2	healthy	8 (♂)	31.5	77.4	8 (♂)	70.5	84.5	1.42 ± 0.53	0.95 ± 0.45 [622]
				healthy	8 (♀)	27.5	70.4	8 (♀)	71.5	67.5	1.40 ± 0.37	0.93 ± 0.40 [622]
Theophylline	Cimetidine + Ciprofloxacin	competitive	CYP1A2	healthy	8 (♂)	31.5	77.4	8 (♂)	70.5	84.5	1.64 ± 0.50	1.00 ± 0.51 [622]
				healthy	8 (♀)	27.5	70.4	8 (♀)	71.5	67.5	1.60 ± 0.39	0.89 ± 0.35 [622]
Antipyrine	Cimetidine	competitive	hepatic met.	healthy	6 (♂)	23.5		6 (♂)	71.5		1.37 ± 0.27	0.97 ± 0.28 [625]
				healthy	10 (♂) / 10 (♂)	26.9 / 27.6	79.9 / 73.5	10 (♂) / 10 (♂)	72.5 / 70.1	80.1 / 75.4	0.56 ± 0.23	0.84 ± 0.48 [624]
Theophylline	Smoking	induction	CYP1A2	healthy	10 (♂) / 10 (♂)	26.5 / 26.0	77.0 / 91.3	10 (♂) / 10 (♂)	78.0 / 71.5	76.4 / 76.8	0.47 ± 0.20	0.83 ± 0.45 [626]
				healthy	5 (NA) / 8 (NA)	26.0 / 21.0	70.0 / 66.0	6 (NA) / 6 (NA)	75.0 / 75.0	58.0 / 56.0	0.73 ± 0.29	1.14 ± 0.58 [627]
				healthy	7 (♂) / 10 (♂)	39.6 / 36.1		2 (♂) / 1 (♂)	64.9 / 63.8		0.79 ± 0.18	1.02 ± 0.61 [628]
				healthy	10 (♂)	27.6	73.5	10 (♂)	70.1	75.4	1.44 ± 0.47	1.02 ± 0.50 [624]
Theophylline	Cimetidine + smoking	competitive + induction	CYP1A2	healthy	10 (♂) / 10 (♂)	26.9 / 27.6	79.9 / 73.5	10 (♂) / 10 (♂)	72.5 / 70.1	80.1 / 75.4	0.81 ± 0.28	0.86 ± 0.43 [624]
				healthy	10 (♂)	26.5	77.0	10 (♂)	78.0	76.4	0.69 ± 0.25	1.09 ± 0.54 [626]
Theophylline	Phenylethanol in smokers	induction	CYP1A2	healthy	10 (♂)	26.0	91.3	10 (♂)	71.5	76.8	0.68 ± 0.33	0.95 ± 0.61 [626]
				healthy	10 (♂) / 10 (♂)	26.5 / 26.0	77.0 / 91.3	10 (♂) / 10 (♂)	78.0 / 71.5	76.4 / 76.8	0.32 ± 0.13	0.79 ± 0.41 [626]
Oxycodone	Clarithromycin	MBI	CYP3A	healthy	10 (4♀)	22.0		10 (3♀)	73.5		2.09 ± 1.34	1.14 ± 0.95 [629]
				hypertensive	12 (2♀)	34.5	90.0	12 (2♀)	74.0	86.0	1.91	0.90 [630]
Erythromycin	Rifampicin	MBI / induction	CYP3A	healthy	8 (4♀)	30.0	66.5	8 (4♀)	73.5	64.0	1.29 ± 0.72	1.50 ± 1.35 [631]
				healthy	8 (♂)	32.0	70.9	8 (♂)	67.1	83.5	0.77 ± 0.14	0.99 ± 0.30 [632]
R-Verapamil (iv)	Rifampicin	MBI / induction	CYP3A	healthy	8 (♂)	32.0	70.9	8 (♂)	67.1	83.5	0.03 ± 0.02	1.00 ± 0.97 [632]
				healthy	8 (♂)	32.0	70.9	8 (♂)	67.1	83.5	0.54 ± 0.10	1.09 ± 0.37 [632]
S-Hexobarbitone	Rifampicin	induction	hepatic met.	healthy	6 (♂)	28.8	80.3	6 (♂)	71.3	83.2	0.16 ± 0.03	0.97 ± 0.36 [633]
				healthy	6 (♂)	28.8	80.3	6 (♂)	71.3	83.2	0.05 ± 0.03	1.86 ± 3.40 [633]
Antipyrine	Phenazone	induction	hepatic met.	healthy	8 (3♀)	29.0		6 (3♀)	77.0		0.97 ± 0.64	1.27 ± 1.00 [634]

Key: AUC = area under the curve, CYP = cytochrome P-450, e = elderly, MBI = mechanism-based inhibition, met = metabolism, y = young.

Table 6.6: Observed vs. predicted pharmacokinetics in the absence and presence of the perpetrator in young (20 to 50 years) and aging individuals (at least 55 years).

	Young adults				Elderly adults			
	Victim in the absence of the perpetrator		Victim in the presence of the perpetrator		Victim in the absence of the perpetrator		Victim in the presence of the perpetrator	
	observed	predicted	observed	predicted	observed	predicted	observed	predicted
Midazolam (iv) + Clarithromycin								
C_{max} [ng/mL]	50.3 ± 34.7	61.9 ± 13.0	64.8 ± 25.4	69.7 ± 14.5	1.29 ± 1.02	1.12 ± 0.33	63.2 ± 22.9	67.8 ± 14.7
AUC [ng*h/mL]	125 ± 61	134 ± 64	337 ± 117	379 ± 354	2.69 ± 1.60	2.83 ± 2.98	152 ± 68	176 ± 75
$t_{1/2}$ [h]	3.6 ± 1.8	4.5 ± 1.9	9.2 ± 3.2	9.7 ± 8.4	2.56 ± 1.56	2.15 ± 2.06	5.6 ± 2.5	6.2 ± 2.1
Midazolam (po) + Clarithromycin								
C_{max} [ng/mL]	12.5 ± 7.0	16.1 ± 7.4	40.7 ± 25.4	32.0 ± 10.3	3.26 ± 2.73	1.99 ± 1.12	13.0 ± 5.9	14.9 ± 5.5
AUC [ng*h/mL]	49.4 ± 25.3	56.7 ± 23.9	304 ± 151	289 ± 194	6.16 ± 4.39	5.10 ± 4.03	49.6 ± 39.8	56.4 ± 20.1
$t_{1/2}$ [h]	3.7 ± 1.9	4.2 ± 1.3	6.9 ± 3.4	8.3 ± 4.6	1.87 ± 1.33	1.99 ± 1.28	3.7 ± 2.9	5.1 ± 1.7
Midazolam (iv) + Rifampicin								
C_{max} [ng/mL]	57.5 ± 12.0		52.9 ± 11.4		0.92 ± 0.28		64.1 ± 14.0	
AUC [ng*h/mL]	110 ± 34	93.9 ± 28.3	48.6 ± 11.8	70.0 ± 19.4	0.44 ± 0.17	0.75 ± 0.31	127 ± 50	136 ± 48
$t_{1/2}$ [h]	4.0 ± 1.8	3.5 ± 1.3	1.9 ± 0.6	3.1 ± 1.2	0.46 ± 0.25	0.87 ± 0.47	4.3 ± 1.6	5.2 ± 1.7
Midazolam (po) + Rifampicin								
C_{max} [ng/mL]	18.3 ± 7.1	15.8 ± 7.7	1.8 ± 0.9	1.8 ± 1.7	0.10 ± 0.06	0.12 ± 0.12	23.3 ± 11.4	21.3 ± 9.9
AUC [ng*h/mL]	41.9 ± 23.4	43.1 ± 18.7	4.1 ± 3.2	3.7 ± 2.4	0.10 ± 0.09	0.09 ± 0.07	40.0 ± 20.6	74.2 ± 36.5
$t_{1/2}$ [h]		3.7 ± 1.2	3.2 ± 1.1		0.86 ± 0.42		5.1 ± 1.6	
Amlodipine + Darunavir/Ritonavir								
C_{max} [ng/mL]	11	12.6 ± 3.4	19.9	21.6 ± 5.8	1.80	1.71 ± 0.65	19.3 ± 4.7	15.0 ± 3.5
AUC [ng*h/mL]	777.0	667 ± 233	1,640	1,423 ± 554	2.11	2.13 ± 1.12	1,155 ± 414	884 ± 265
$t_{1/2}$ [h]	38.0	30.0 ± 2.7	48.4	37.4 ± 5.6	1.27	1.25 ± 0.22	48.1 ± 8.0	34.0 ± 2.8
Atorvastatin + Darunavir/Ritonavir								
C_{max} [ng/mL]							4.9 ± 3.6	4.2 ± 2.1
AUC [ng*h/mL]							31.4 ± 4.7	25.3 ± 12.9
$t_{1/2}$ [h]							15.3 ± 3.5	9.9 ± 2.4
Rosuvastatin + Darunavir/Ritonavir								
C_{max} [ng/mL]	7.3 ± 3.1	7.3 ± 2.5	20.1 ± 16.6	17.4 ± 6.3	2.75 ± 2.56	2.38 ± 1.18	9.9 ± 4.3	7.9 ± 2.5
AUC [ng*h/mL]	121 ± 52	97 ± 41	181 ± 97	146 ± 53	1.50 ± 1.03	1.50 ± 0.83	104 ± 33	105 ± 49
$t_{1/2}$ [h]	15.5 ± 6.5	15.4 ± 4.9	18.5 ± 7.6	14.9 ± 4.5	1.19 ± 0.71	0.97 ± 0.42	13.1 ± 3.7	16.5 ± 6.4
Dolutegravir + Darunavir/Ritonavir								
C_{max} [μg/mL]	4.7 ± 0.7	3.9 ± 1.3	4.0 ± 0.8	3.6 ± 1.1	0.85 ± 0.21	0.93 ± 0.42	5.1 ± 1.5	4.2 ± 1.3
AUC [μg*h/mL]	75.6 ± 14.4	74.6 ± 63.2	52.1 ± 8.3	58.8 ± 48.4	0.69 ± 0.17	0.79 ± 0.93	88.2 ± 34.8	109.3 ± 95.0
$t_{1/2}$ [h]	12.1 ± 1.8	10.7 ± 5.6	9.8 ± 1.7	9.7 ± 4.9	0.81 ± 0.18	0.91 ± 0.66	10.4 ± 4.1	14.8 ± 8.3

Key: AUC = area under the curve, C_{max} = peak concentration, DDJ = drug-drug interaction, iv = intravenous, po = oral, $t_{1/2}$ = elimination half-life.

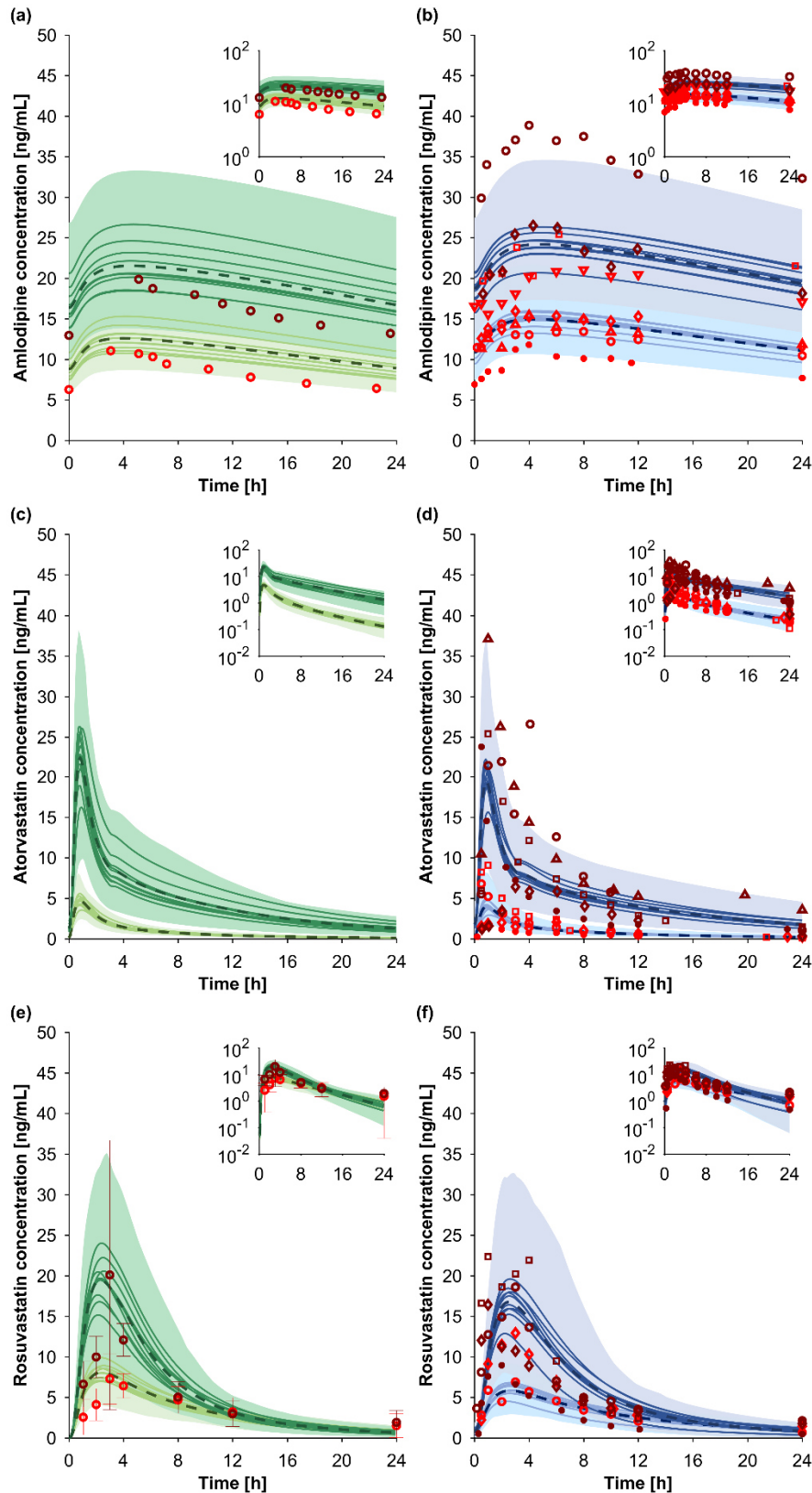


Figure 6.2: Predicted vs. observed concentration time profiles for amlodipine (a: young; b: elderly), atorvastatin (c: young, d: elderly), and rosuvastatin (e: young, f: elderly) in the absence (brighter color) and the presence (darker color) of boosted darunavir. The design of the simulated DDI scenarios is detailed in Table 6.2. Red markers show published clinical data with different markers indicating different individuals. The solid lines, the dashed line, and the shaded area represent the mean of each virtual trial, the mean, and the 95% confidence interval of all virtual individuals, respectively.

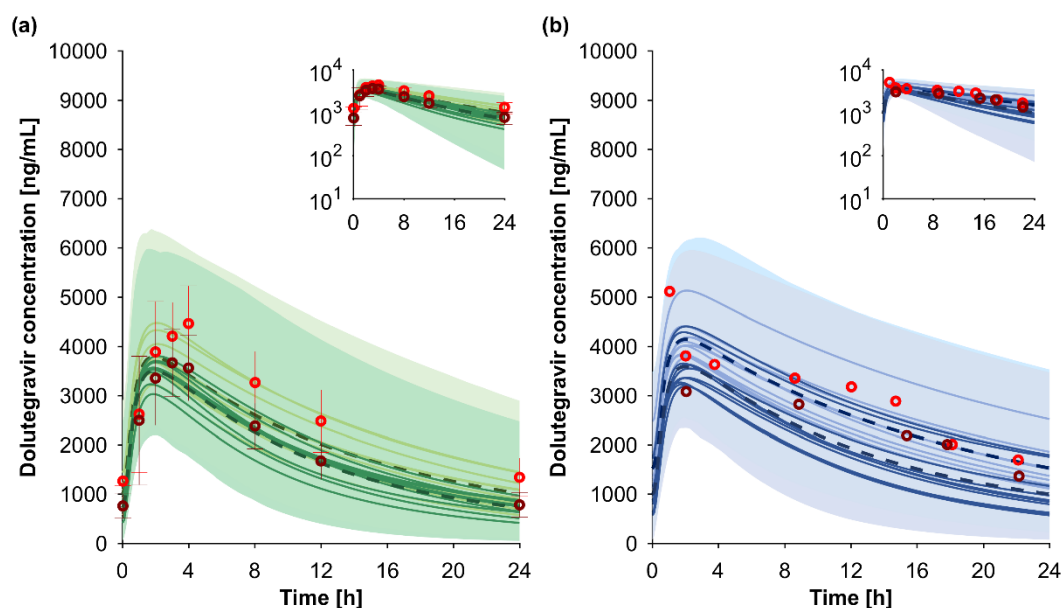


Figure 6.3: Predicted vs. observed concentration time profiles for dolutegravir (a: young; b: elderly) in the absence (brighter color) and in the presence (darker color) of boosted darunavir. The design of the simulated DDI scenario is detailed in Table 6.2. Data for young individuals were normalized to 50 mg for comparison with elderly subjects. Red markers show published clinical data. The solid lines, the dashed line, and the shaded area represent the mean of each virtual trial, the mean, and the 95% confidence interval of all virtual individuals, respectively.

Secondly, additional drug models were developed for ketoconazole and nilotinib to analyze the impact of aging on competitive CYP3A inhibition and gemfibrozil and its glucuronide metabolite to investigate the age-dependency of DDIs mediated by OATP1B1. Clinically observed data for all drugs were always contained within the 95% confidence interval of the PBPK simulations (Figure 6.4-6.5).

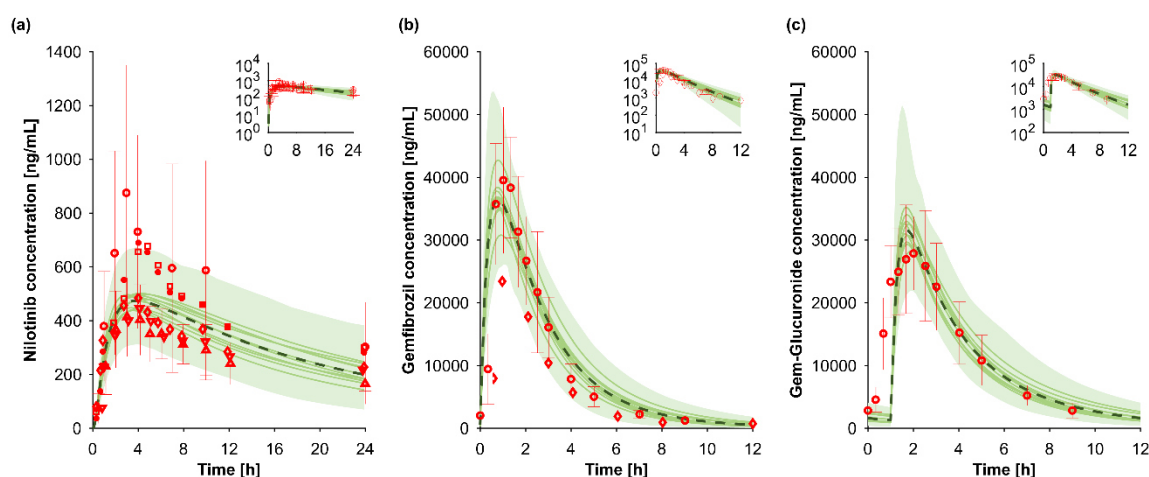


Figure 6.4: Predicted vs. observed concentration time profiles for nilotinib (a; 400 mg single dose), gemfibrozil (b; 600 mg twice daily), and gemfibrozil glucuronide (c) in young individuals aged 20 to 50 years. Red markers show published clinical data (Table 6.4) with different markers representing different clinical studies. The solid lines, the dashed line, and the shaded area represent the mean of each virtual trial, the mean, and the 95% confidence interval of all virtual individuals.

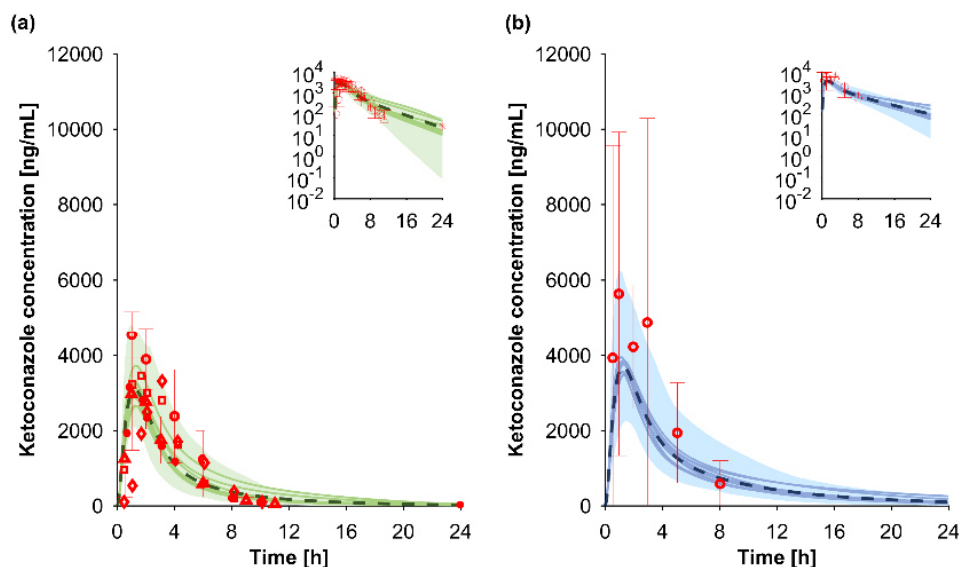


Figure 6.5: Predicted vs. observed concentration time profiles for ketoconazole (200 mg once daily; a: young, b: elderly). Red markers show published clinical data with different markers representing different clinical studies (Table 6.4). The solid lines, the dashed line, and the shaded area represent the mean of each virtual trial, the mean, and the 95% confidence interval of all virtual individuals.

Pharmacokinetic parameters in young adults were predicted within 1.25-fold of clinically observed data (Table 6.7) except for the half-life of ketoconazole, which was overpredicted (predicted:observed ratio: 1.30) and the peak concentration of nilotinib, which was underpredicted (predicted:observed ratio: 0.75). Ketoconazole was the only drug for which clinically observed data in elderly adults with a mean age of 76 years were available (Figure 6.5) [619]. C_{max} for ketoconazole in the elderly was underpredicted with $5,627 \pm 4,297$ ng/mL being observed and $3,827 \pm 1,277$ ng/mL being predicted (predicted:observed ratio: 0.68), but all other pharmacokinetic parameters were simulated within 1.25-fold of the clinically observed data in the elderly.

Thirdly, DDIs with drugs we previously used to analyze the impact of aging on drug pharmacokinetics were verified against clinically observed data in young adults aged 20 to 50 years before extrapolating to elderly individuals using the verified PBPK model. The design of the used clinical studies is detailed in Table 6.2. The predictions captured the clinically observed data adequately in individuals aged 20 to 50 years (Figure A6.1-A6.12). The AUC-ratios were predicted within 1.25-fold, 1.5-fold, and 2.0-fold of clinically observed data in 74%, 95%, and 100% of all investigated DDIs (Table 6.8). C_{max} and $t_{1/2}$ are detailed in Table A6.1.

Table 6.7: Observed vs. predicted parameters for ketoconazole, nilotinib, gemfibrozil, and its glucuronide metabolite in young (20 to 50 years) and elderly (at least 65 years) adults.

	Young adults		Elderly adults		Ratio elderly/young	
	observed	predicted	observed	predicted	observed	predicted
Ketoconazole						
C_{max} [ng/mL]	3,343 ± 704	3,186 ± 940	5,627 ± 4,297	3,827 ± 1,277	1.68	1.20
AUC [ng*h/mL]	13,416 ± 5,376	12,944 ± 8,371	26,178 ± 23,725	22,067 ± 17,648	1.95	1.70
$t_{1/2}$ [h]	2.63 ± 1.61	3.41 ± 1.33	4.51 ± 4.09	5.11 ± 1.94	1.72	1.50
Nilotinib						
C_{max} [ng/mL]	647 ± 247	484 ± 111				
AUC [ng*h/mL]	17,700 ± 6,745	14,807 ± 11,687				
$t_{1/2}$ [h]	14.6 ± 8.5	15.4 ± 6.9				
Gemfibrozil						
C_{max} [ng/mL]	42,400 ± 10,800	37,631 ± 8,693				
AUC [ng*h/mL]	109,544 ± 55,796	124,937 ± 37,865				
$t_{1/2}$ [h]	1.50 ± 0.20	1.59 ± 0.48				
Gemfibrozil-Glucuronide						
C_{max} [ng/mL]	29,900 ± 7,900	32,696 ± 8,414				
AUC [ng*h/mL]	124,368 ± 47,804	123,384 ± 36,196				
$t_{1/2}$ [h]	2.00 ± 0.30	2.44 ± 0.67				

Key: AUC = area under the curve, C_{max} = peak concentration, $t_{1/2}$ = elimination half-life.

Analyzing the impact of aging on DDI magnitudes across adulthood

After the successful verification of the PBPK model, all developed DDIs were used to investigate the impact of aging on the C_{max} -, t_{max} -, AUC-, CLF-, VdF-, and $t_{1/2}$ -ratio (pharmacokinetic parameter of the victim drug in the presence divided by the scenario in the absence of the perpetrator) across adulthood (20 to 99 years). The most common metric to assess a DDI is the AUC-ratio, which was not affected by advanced aging (Figure 6.6). The slope [95% confidence interval] fitted to the mean of the AUC-ratio of all investigated DDI scenarios was close to zero with -9.6E-05 [-2.0E-04; 7.4E-06] (Table 6.9). The drug class (non-HIV drugs vs. antiretroviral drugs) involved in the DDI (p-value: 0.08), the DDI mechanism (p-value: 0.57), the mediator of the DDI (p-value: 0.77), the combination of DDI mechanism and mediator (p-value: 0.58), and the sex of the studied individual (p-value: 0.61) did not affect the negligible impact of advanced aging on AUC-ratios (Table 6.9). The findings for the AUC-ratio were similar for all investigated DDI ratios (Figure A6.13-A6.17), except for t_{max} , which was statistically significant different between DDIs involving antiretroviral drugs or non-HIV drugs (p-value: 0.03), but the difference in the slope was not judged to be clinically relevant (antiretroviral drugs: -6.15E-06 [-6.48E-06; -5.83E-06] and non-HIV drugs: -2.90E-04 [-3.09E-04; 2.70E-04]).

Table 6.8: Predicted vs. observed AUC of the control and DDI scenario and the AUC-ratio (DDI scenario / control scenario).

	AUC [ng*h/mL] – control scenario		AUC [ng*h/mL] – DDI scenario		AUC ratio	
	observed	predicted	observed	predicted	observed	predicted
Midazolam + Ketoconazole	123 ± 76	121 ± 73	1,344 ± 648	1,354 ± 1,490	10.89 ± 8.54	11.18 ± 14.01
Rivaroxaban + Ketoconazole	892 ± 241	1,071 ± 314	2,298 ± 597	2,341 ± 894	2.58 ± 0.97	2.19 ± 1.05
Nilotinib + Ketoconazole	9,682 ± 5,686	13,283 ± 13,260	39,314 ± 18,708	56,183 ± 67,376	4.06 ± 3.07	4.23 ± 6.60
Midazolam + Nilotinib	121 ± 73	149 ± 99	157 ± 71	165 ± 119	1.30 ± 0.98	1.10 ± 1.08
Repaglinide + Gemfibrozil in PT of OATP1B1	7.8 ± 1.7	7.6 ± 3.5	50.1 ± 13.4	38.0 ± 19.7	6.42 ± 2.22	5.00 ± 3.45
Rivaroxaban + Clarithromycin	992 ± 249	1,006 ± 289	1,469 ± 360	1,476 ± 456	1.52 ± 0.50	1.47 ± 0.62
Atorvastatin + Clarithromycin	41.9 ± 19.0	32.7 ± 12.6	108 ± 28	84.4 ± 34.0	2.59 ± 1.36	2.58 ± 1.44
Etravirine + Clarithromycin	16,344 ± 4,757	14,161 ± 4,984	27,664 ± 8,156	21,409 ± 12,908	1.69 ± 0.70	1.51 ± 1.06
Midazolam + Ritonavir	30.8	37.8 ± 12.0	169	154 ± 124	5.47	4.07 ± 3.53
Rilpivirine + Darunavir/Ritonavir					2.30	2.27 ± 1.59
Atorvastatin + Rifampicin	64.0 ± 21.3	68.2 ± 28.1	12.6 ± 3.2	17.3 ± 7.7	0.20 ± 0.08	0.25 ± 0.15
Nilotinib + Rifampicin	11,123 ± 4,819	13,411 ± 10,797	2,227 ± 1,122	2,221 ± 615	0.20 ± 0.13	0.17 ± 0.14
Rilpivirine + Rifampicin					0.20 ± 0.11	0.15 ± 0.10
Rilpivirine + Efavirenz	3,012 ± 1,871	3,250 ± 1,760	2,218 ± 1,546	2,369 ± 1,223	0.74 ± 0.69	0.73 ± 0.55
Efavirenz + Rifampicin	200,335 ± 150,433	202,830 ± 127,928	209,062 ± 149,263	166,651 ± 89,725	1.04 ± 1.08	0.82 ± 0.68
Midazolam + Etravirine					0.69 ± 0.21	0.66 ± 0.11
Atorvastatin + Efavirenz					0.65 ± 0.31	0.85 ± 0.48
Atorvastatin + Etravirine	89.1 ± 48.3	59.0 ± 28.8	51.8 ± 31.2	52.7 ± 25.5	0.58 ± 0.47	0.89 ± 0.61
Dolutegravir + Atazanavir	64,559 ± 12,266	80,393 ± 100,190	177,645 ± 30,200	160,250 ± 187,474	2.75 ± 0.70	1.99 ± 3.41
Dolutegravir + Atazanavir/Ritonavir	64,559 ± 12,266	76,471 ± 68,411	149,820 ± 23,971	112,081 ± 125,322	2.32 ± 0.58	1.47 ± 2.10
Dolutegravir + Rifampicin	65,616 ± 46,285	102,641 ± 130,276	32,924 ± 21,428	41,986 ± 53,973	0.50 ± 0.48	0.41 ± 0.74
Dolutegravir + Etravirine	84,151 ± 18,513	105,295 ± 150,624	19,716 ± 43	27,632 ± 34,591	0.23 ± 0.05	0.26 ± 0.50
Raltegravir + Ritonavir	11,139	13,632 ± 6,964	8,905	9,356 ± 3,038	0.80	0.69 ± 0.42
Raltegravir + Rifampicin	12,273	16,349 ± 10,442	7,350	10,007 ± 3,680	0.60	0.61 ± 0.45
Raltegravir + Efavirenz	12,535	13,556 ± 7,627	7,942	10,635 ± 4,240	0.63	0.78 ± 0.54
Raltegravir + Etravirine	10,804 ± 12,153	7,479 ± 4,297	8,201 ± 7,622	5,813 ± 2,568	0.76 ± 1.11	0.78 ± 0.56
Repaglinide + Gemfibrozil	5.8 ± 3.8	4.8 ± 1.5	44.1 ± 24.9	45.5 ± 30.1	7.58 ± 6.57	9.48 ± 6.91
Atorvastatin + Gemfibrozil	35.2 ± 11.8	36.7 ± 14.7	43.6 ± 15.8	50.2 ± 20.3	1.24 ± 0.61	1.37 ± 0.77
Rosuvastatin + Gemfibrozil	464 ± 223	363 ± 134	897 ± 466	674 ± 303	1.93 ± 1.37	1.86 ± 1.08
Rosuvastatin + Atazanavir/Ritonavir	18.8 ± 16.1	20.3 ± 6.2	48.9 ± 34.3	65.7 ± 29.5	2.60 ± 2.88	3.24 ± 1.76
Metoprolol in PM of CYP2D6	668 ± 303	585 ± 472	3,222 ± 137	2,590 ± 2,227	4.82 ± 2.20	4.43 ± 5.28
Metoprolol in UM of CYP2D6	668 ± 303	585 ± 472	311 ± 117	243 ± 207	0.47 ± 0.27	0.41 ± 0.49
Repaglinide in UM of CYP2C8	106 ± 30.9	72.1 ± 27.1	72.4 ± 37.9	65.2 ± 22.7	0.68 ± 0.41	0.90 ± 0.46
Repaglinide in PT of OATP1B1	4.5 ± 1.6	4.5 ± 1.4	7.8 ± 1.7	7.8 ± 3.1	1.73 ± 0.72	1.74 ± 0.88
Atorvastatin in IT of OATP1B1	24.2 ± 8.6	25.8 ± 11.2	36.2 ± 20.3	33.5 ± 14.9	1.50 ± 0.99	1.30 ± 0.80
Atorvastatin in PT of OATP1B1	24.2 ± 8.6	25.8 ± 11.2	59.3 ± 17.4	60.2 ± 27.3	2.45 ± 1.13	2.33 ± 1.46
Rosuvastatin in IT of OATP1B1	35.0 ± 18.1	42.4 ± 14.1	55.0 ± 22.7	45.4 ± 16.3	1.57 ± 1.04	1.07 ± 0.52
Rosuvastatin in PT of OATP1B1	35.0 ± 18.1	42.4 ± 14.1	56.7 ± 5.1	60.4 ± 27.4	1.62 ± 0.85	1.42 ± 0.80

Key: IT = intermediate transporter phenotype, PM = poor metabolizer, PT = poor transporter phenotype, UM = ultrarapid metabolizer.

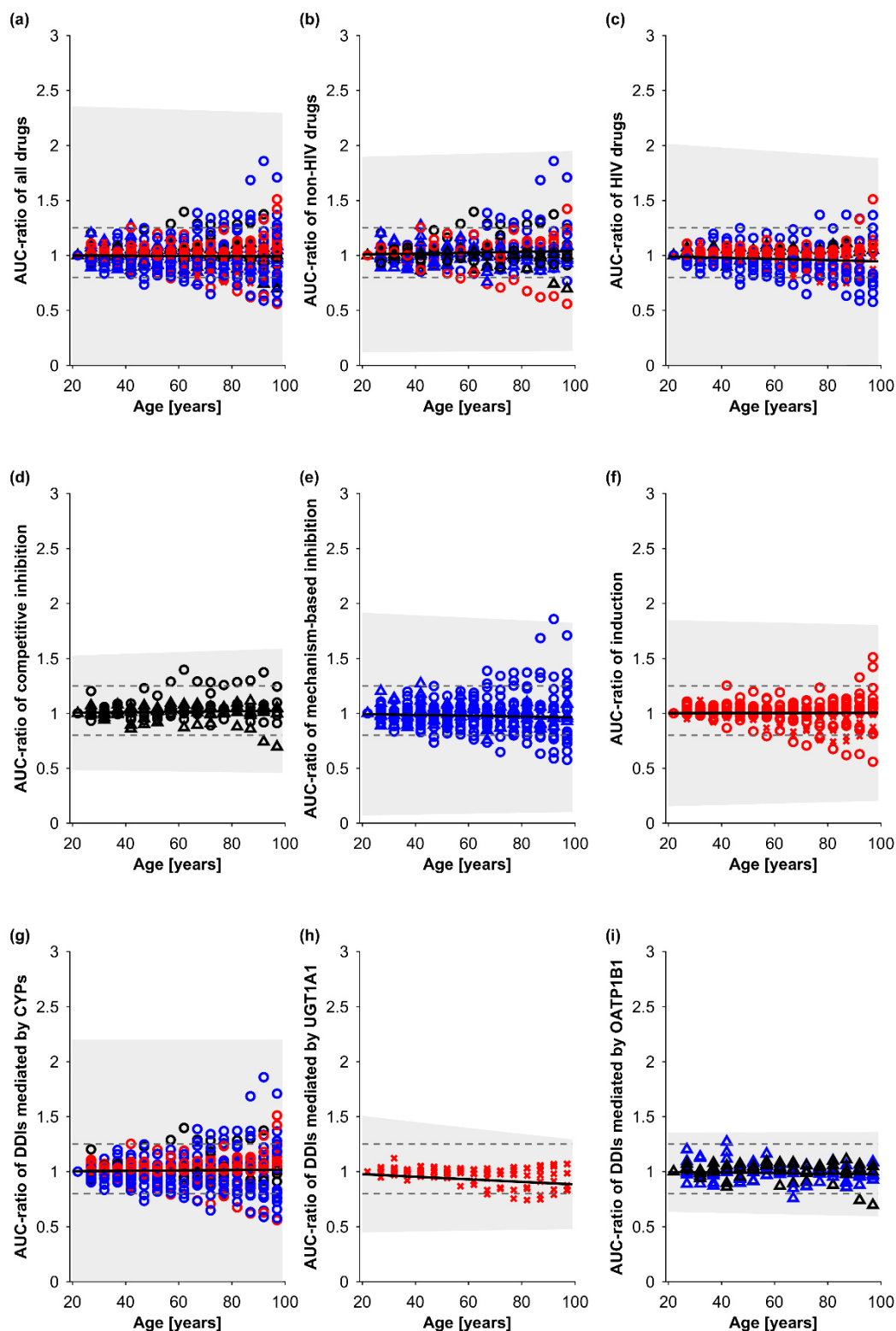


Figure 6.6: Area under the curve (AUC)-ratio normalized to the youngest investigated age group (20 to 24 years) for all drugs (a), for non-HIV drugs (b), for antiretroviral drugs (c), for competitive inhibition (d), for mechanism-based inhibition (e), for induction (f), for DDIs mediated by CYP enzymes (g), for DDIs mediated by UGT1A1 (h), and for DDIs mediated by OATP1B1 (i). Black, blue, and red markers represent competitive inhibition, mechanism-based inhibition, and induction. Circles, crosses, and triangles symbolize CYP-, UGT1A1-, and OATP1B1-mediated DDIs. The solid line and the shaded area show the mean \pm standard deviation. The dashed lines represent the 1.25-fold interval (bioequivalence criterion).

Table 6.9: Slope of mean prediction for DDI magnitudes across adulthood (20 to 99 years). P-values demonstrated that involved drug classes (non-HIV drugs vs. antiretroviral drugs), DDI mechanisms (competitive inhibition, mechanism-based inhibition, induction), mediator of the DDI (CYP enzymes, UGT enzymes, hepatic transporters) or the sex of the investigated individual did not influence the impact of aging on DDI magnitudes.

		C_{max}	t_{max}	AUC	CLF	VdF	$t_{1/2}$
slope	mean	5.17E-05	-1.42E-04	-9.62E-05	3.54E-04	1.58E-04	-1.98E-04
	95% CI	[-8.68E-05; 9.72E-05]	[-1.51E-04; -1.34E-04]	[-2.00E-04; 7.40E-06]	[2.52E-04; 4.56E-04]	[2.64E-05; 2.90E-04]	[-3.28E-04; -6.80E-05]
p-value	drug class	0.77	0.03	0.08	0.17	0.60	0.11
p-value	mechanism	0.65	0.38	0.57	0.60	0.58	0.79
p-value	mediator	0.18	0.77	0.77	0.48	0.12	0.18
p-value	mechanism*mediator	0.22	0.62	0.58	0.34	0.54	0.77
p-value	sex	0.76	0.93	0.61	0.95	0.88	0.45

Key: AUC = area under the curve, C_{max} = peak concentration, CI = confidence interval, CLF = clearance, t_{max} = time to C_{max} , $t_{1/2}$ = elimination half-life, VdF = apparent volume of distribution.

Independent clinically observed data proofed the estimated impact of aging on DDI magnitudes

In a last step, a literature search was performed to seek for studies investigating AUC-ratios in young and elderly subjects to proof the obtained general model-based hypothesis that DDI magnitudes are not affected by advanced aging. Our performed literature search yielded 20 studies that investigated DDI magnitudes in the elderly. Six studies were excluded, because there was no direct comparison between young and elderly individuals and one study was excluded because the age of study participants was not defined. The remaining 13 studies investigated 17 DDIs in elderly compared with young healthy subjects. The DDI mechanism was competitive in five cases, mechanism-based inhibition in three cases, induction in seven cases, and mechanism-based inhibition combined with induction in two cases. Ten of the investigated DDIs were mediated by CYP1A2, four by CYP3A, and three were not specified to a single enzyme. All included studies demonstrated no changes of DDI magnitudes with advanced aging (Figure 6.7). The average ratio elderly (n: 274; age: 68.3 years) / young (n = 298; age = 28.4 years) for the AUC-ratio was 1.01 ± 0.64 , which confirmed our general PBPK model estimates.

6.2.5 Discussion

Clinical data investigating the impact of aging on DDI magnitudes are sparse, leading to uncertainty how to manage DDIs in aging individuals in clinical practice. In this study, we demonstrated based on clinical data in combination with modelling and simulation that DDI magnitudes are not impacted by aging regardless of the drugs being involved in the DDI, the DDI mechanism, the mediator of the DDI, or the

sex of the studied individual. Thus, the clinical management of DDIs can a priori be similar in the elderly compared with young men and women in the absence of severe comorbidities.

The investigation of age-related changes in DDI magnitudes are especially important for PLWH given the increased life expectancy [510], high prevalence of polypharmacy [92], and the high DDI potential of antiretroviral drugs [576]. We previously conducted a clinical study in aging PLWH at least 55 years, who participated in the Swiss HIV Cohort Study, to investigate for the first time DDI magnitudes between antiretroviral drugs and comedications in elderly PLWH [577]. The comparison to historical data in young individuals receiving the same drug combination yielded no age-related changes in the magnitude of the investigated DDIs [577], comparable to studies conducted with midazolam and clarithromycin and rifampicin [111, 112, 573]. However, we could not include enough participants to adequately power the study and thus, interpretation must be careful. In general, clinical studies in the elderly are ethically difficult to undertake, because necessary treatments (i.e. antiretroviral drugs in our study) cannot be disrupted to establish a controlled scenario, the medication of interest cannot be added, and participants should not receive any other medication affecting the DDI of interest. Furthermore, it is not feasible or pragmatic to study every single drug combination in elderly individuals.

We used the PBPK approach to overcome all mentioned limitations in the DDI study design in elderly subjects. Before extrapolating to unknown scenarios of interest, it is crucial to verify the PBPK model for the population and the clinical scenario of interest [118]. A strength of the present study is the wide range of DDI mechanism (competitive inhibition, mechanism-based inhibition, and induction) and DDI mediators (CYP enzymes, UGT1A1, and OATP1B1) included in the PBPK model verification. All clinically observed data of altered plasma concentrations caused by a DDI were generally within the 95% confidence interval of the PBPK model predictions for young and elderly individuals (Figure 6.1-6.3), which demonstrated the predictive power of the used approach to simulate DDIs in aging subjects.

After proofing the predictive potential of the used PBPK model to simulate DDIs in the elderly, we performed sensitivity analyses on age for 50 DDIs with 42 DDIs that could only be verified in adults aged 20 to 50 years in the absence of clinical data in the elderly. The verified PBPK model estimated that DDI magnitudes are unchanged across adulthood (20 to 99 years) regardless of the involved drugs, DDI mechanism, the mediator of the DDI, and the sex of the studied individual.

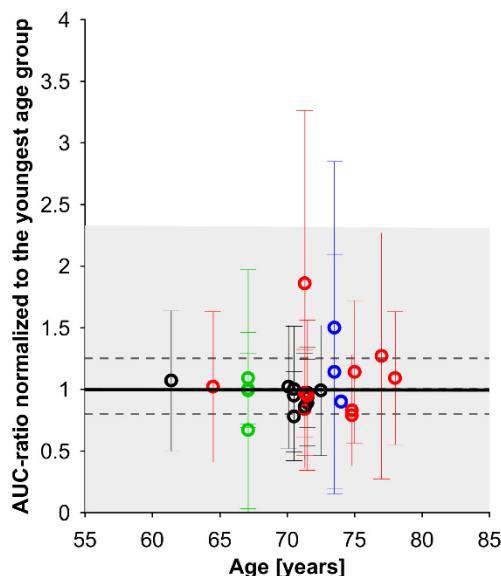


Figure 6.7: Impact of aging on the area under the curve (AUC) ratios normalized to the youngest age group for independent clinically observed data (mean \pm standard deviation; Table 6.5). Black, blue, red, and green markers symbolize competitive inhibition, mechanism-based inhibition, induction, and mechanism-based inhibition combined with induction, respectively. All investigated DDIs were mediated by CYP enzymes. The solid line and the shaded area show the mean \pm standard deviation. The dashed lines represent the 1.25-fold interval (bioequivalence criterion).

One advantage of the used PBPK approach over traditional clinical studies is that aging can be analyzed as a continuous process through sensitivity analysis. Longitudinal clinical studies are not practical, affordable, and ethically difficult to conduct. Thus, traditional clinical studies compare observed data of an elderly with a young group, ignoring the continuous physiological changes that impact the pharmacokinetics of drugs and the magnitudes of drug interactions throughout adulthood [58].

DDI magnitudes could potentially be affected by advanced aging, because of higher concentration of the inhibitor and inducer and age-related alterations in the regulation of transcription and translation. Drug exposure increases with advanced aging due to a decline of drug clearance that is caused by the age-related decrease in hepatic and renal blood flow as well as in the glomerular filtration rate and is independent of drug characteristic [512, 578]. The higher exposures of inhibitors or inducers with advanced aging appears not to lead to an elevated interaction potential in the elderly. Possible explanation could be that higher perpetrator concentrations cannot lead to an increased effect for strong inhibitors and inducers such as clarithromycin, ritonavir, or rifampicin. Strong inhibitors such as ritonavir achieve already a maximal effect in young individuals; therefore, an increased ritonavir concentration in the elderly is not expected to result in greater inhibition. The strong inducer rifampicin binds to PXR,

forms a complex with the retinoid X receptor, the complex binds to the DNA response element, and enhances the transcription of metabolizing enzymes such as CYP3A [635]. Higher rifampicin concentrations in the elderly might not lead to an increased CYP3A level, because the amount of PXR could be a limiting factor. Even if PXR transcription and translation would be enhanced, a negative feedback loop prevents higher PXR concentrations, and thus, induction of metabolizing enzymes such as CYP3A [636]. Other regulations to prevent high induction of metabolizing enzymes might exist but were not studied so far. For moderate perpetrators like nilotinib or etravirine, the predicted DDI magnitudes were 10% higher with advanced aging and thus, the effect appears to be marginal.

In contrast to CYP3A4 [220-222], uncertainty exists whether the transcription/translation of CYP2C9 and CYP1A2 are impacted by advanced aging [66-68], which would result in impaired enzyme activity and subsequently lower DDI magnitudes. The majority of DDIs collected in the fourth step of the present study to prove the general PBPK model-based hypothesis regarding the impact of aging on DDI magnitudes, were mediated by CYP1A2. CYP1A2 was either induced (smoking, phenytoin) or competitively inhibited (cimetidine, ciprofloxacin). The ratio elderly/young of the AUC-ratio ranged from 0.70 ± 0.57 [623] to 1.14 ± 0.58 [627], demonstrating that drug interactions mediated by CYP1A2 are likely not affected by advanced aging. The results are consistent with our previous work, in which we demonstrated that age-related changes in drug clearance are not determined by the clearance pathway, amongst others CYP3A, CYP2C9, and CYP1A2 [512]. However, there are reports in the literature indicating that enzyme inducibility might be different as shown exemplarily for antipyrine with rifampicin [637], where the elderly showed a six-fold lower DDI magnitude than the young group. Differences to other studies investigating age-related changes in DDI magnitudes are not explainable by frailty as all investigated participants were healthy. The comparison between young and elderly subjects was indirect, because the study in young individuals was conducted earlier, which led to the exclusion in our meta-analysis. The reduced inducibility cannot be assigned to a specific hepatic enzyme, because antipyrine is metabolized by several different hepatic enzymes, which can be induced by rifampicin. In two other studies investigating the effect of smoking and dichloralphenazone on antipyrine with advanced aging, there was no difference in the DDI magnitude between the two investigated age groups (AUC-ratio elderly/young: 1.02 and 0.78 ± 0.62 , respectively) [628, 634]. Studies using rifampicin as an inducer were in general heterogeneous with the found minimal and maximal DDI magnitude ratio elderly/young of 0.67 and 1.86 (Table 6.5). Both studies showed high variability, which might be

explained by the small sample size. These findings indicate no systematic effect of a certain DDI mechanism or involved enzyme. The found heterogeneity of data represents therefore patient variability in clinical practice. Taken together, uncertainty regarding the inducibility of hepatic enzymes exists in the literature probably based on the high variability of enzyme activity [217, 218] and the low number of subjects included in clinical studies. Overall, the clinically observed data for various DDIs (Table 6.2, Table 6.5) proofs our PBPK model estimates of unchanged DDI magnitudes with advanced aging; however, in between patient variability up to twofold might be possible.

As DDI magnitudes are not impacted by aging, static methods can be applied if an elderly patient receives two drugs with an uncharacterized DDI magnitude. Estimates are based on the degree of metabolism by a specific enzyme and the strength of an inhibitor or inducer [110, 387]. A PBPK model used in our study is not intended for the daily management of DDI queries in the clinic, but the static method provides a more straightforward supportive tool to rationalize dose adjustments to overcome a given DDI.

We used a sequential multi-step approach, that might have the risk to propagate assumptions and errors from one step to the next. Using a mathematical model, it is of tremendous importance to clearly mention all underlying assumptions, which we have done previously for our developed aging population and PBPK model [58, 118]. The model and its predictive power to simulate pharmacokinetics in elderly individuals was verified against clinically observed data for 20 non-HIV and HIV drugs, which had different drugs characteristics, and clinically observed drug concentrations were generally within the 95% confidence interval of the model predictions [512, 578]. Thus, a systematic over- or underprediction based on assumptions or errors in the population and model can be excluded. In the present study, we simulated 50 different DDI scenarios in adults aged 20 to 50 years, involving different DDI mechanisms (competitive inhibition, mechanism-based inhibition, and induction), enzymes (CYP3A, CYP2D6, CYP2B6, CYP2C9, UGT1A1), and active drug transporter (OATP1B1) and 74.5%, 93.6%, and 100% of AUC-ratios were predicted within 1.25-, 1.5-, 2.0-fold of clinically observed data, respectively. The average predicted:observed ratio was 0.99 ± 0.21 , indicating no systematic over- or underprediction of AUC-ratios. The predictive power of our model to simulate DDIs in aging individuals was verified against data from our own clinical study and independent, published data [111, 112, 573, 577] and all observed data were predicted within the 95% confidence interval. Furthermore, we verified the predicted impact

of advance aging on DDI magnitudes against independent clinically observed data, which verified our general model-based hypothesis. In conclusion, all performed verification with independent data verified the model assumptions and led to the exclusion of systematic errors in the PBPK model.

There are several limitations of our study. Firstly, physiological data to inform the PBPK model are sparse over the age of 85 years and therefore, simulation results in the very old need to be viewed with caution.

Secondly, individuals over the age of 65 years are generally excluded from clinical studies and if included have no major health problems [122, 379]. Thus, results might not be applicable to frail elderly individuals or aging subjects with severe comorbidities such as advanced renal impairment stage 4 to 5. However, our study delivers a comprehensive overview of conducted DDI studies in the elderly and uses a verified modelling approach to interpret the existing data broadly. Furthermore, the included aging PLWH in our own clinical study are representative of 75% of all elderly PLWH at least 75 years [564], who have mild to moderate renal impairment, hypertension, and receiving combined antiretroviral therapy as well as other comedications. The investigation if severe comorbidities impact age-related changes in DDI magnitudes is the next logical step for future clinical studies.

Thirdly, in vitro data regarding the induction of UGT1A1 by antiretroviral drugs were not available in the literature and based on the same molecular modulation of UGT1A1 and CYP3A [605], the same induction values were assumed for both enzymes. Clinically observed data of DDIs involving UGT1A1 induction were always predicted within the 95% confidence interval of the PBPK model, thus qualifying the used assumption.

Fourthly, the impact of aging on transporter mediated DDIs were only studied for the hepatic uptake transporter OATP1B1, but other hepatic, intestinal or renal transporters were not investigated and hence translation must be careful.

Fifthly, we used the commonly accepted twofold margin [326] to assess the accuracy of predicted pharmacokinetic parameters; however, the twofold limit might be too permissive for the interpretation of AUC-ratios, because it could lead to a misclassification of DDI magnitudes [638]. We focused on clinical

relevance, when analyzing the successful prediction of DDI magnitudes. The AUC-ratios that were predicted outside of the 1.5-fold margin were midazolam + rifampicin (predicted:observed: 1.69), dolutegravir + atazanavir/ritonavir (predicted:observed: 0.63), and atorvastatin + etravirine (predicted:observed: 1.54). The differences between predictions and clinically observed data were not judged to be of clinical relevance given the safety margin of dolutegravir and atorvastatin. In contrast, an under- or overprediction of the DDI magnitude with the anticoagulant rivaroxaban by twofold could have clinical consequences for the treated patient [391]. In the case of rivaroxaban, all AUC-ratios were predicted within the 1.25-fold margin (rivaroxaban + ketoconazole: 0.85, rivaroxaban + clarithromycin: 0.96, and rivaroxaban + ritonavir: 0.99). However, the 1.25-fold margin is still too permissive for narrow therapeutic index drugs for which the 1.11-fold margin is recommended by the health authorities [639].

In conclusion, by combining clinical data with modelling and simulation we elucidated that aging does not impact the magnitudes of DDIs regardless of the DDI mechanism, the DDI mediators (enzymes, transporters) or the involved drugs. Thus, the clinical management of DDIs can a priori be similar in aging men and women compared with young individuals in the absence of severe comorbidities.

6.2.6 Study Highlights

What is the current knowledge on the topic?

Age-related comorbidities are highly prevalent in the elderly, leading to polypharmacy and consequently, an increased risk for drug-drug interactions (DDIs). However, clinical studies investigating DDIs are generally not conducted in the elderly, resulting in missing guidance regarding the clinical management of DDIs with advanced aging.

What question did this study address?

We combined clinical data with physiologically based pharmacokinetic (PBPK) modelling to investigate the impact of aging on DDI magnitudes across the entire adulthood.

What does the study add to our knowledge?

The PBPK approach has the predictive power to simulate DDIs in the elderly. Predicted DDI magnitudes are not affected by advanced aging regardless of the involved drugs, DDI mechanism or the sex of the investigated individual. This model-based hypothesis was further verified by independent clinically observed AUC-ratios for 17 DDIs being studied in young and elderly individuals.

How might this change clinical pharmacology or translational science?

The clinical management of DDIs can a priori be similar in elderly compared with young men and women in the absence of severe comorbidities.

6.2.7 Appendix

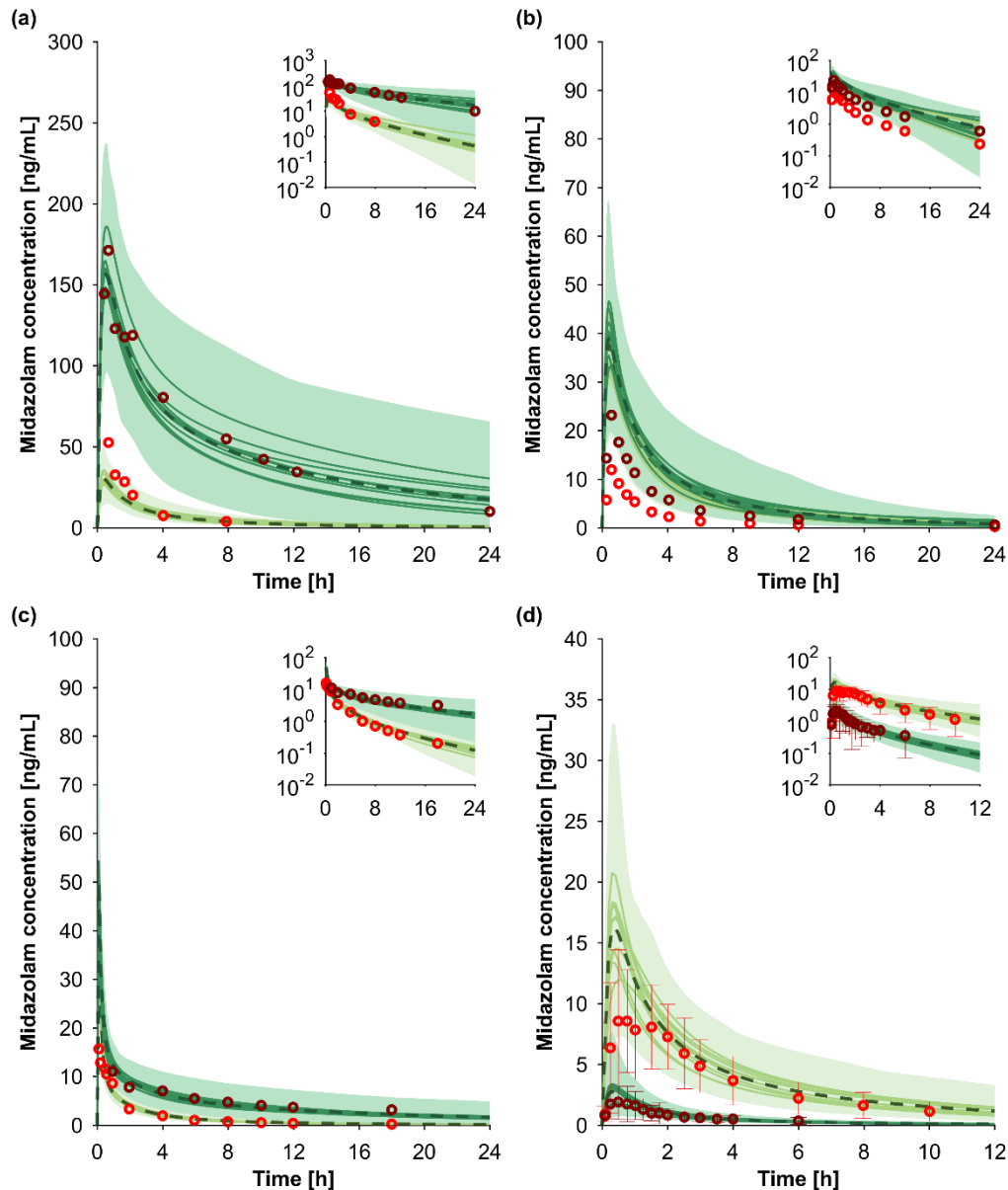


Figure A6.1: Predicted vs. observed concentration-time profiles of midazolam with ketoconazole (a), nilotinib (b), ritonavir (c), and rifampicin (d) in young individuals aged 20 to 50 years. The design of the simulated DDI scenarios is detailed in the Table 6.2. Red markers show the clinically observed data. The solid lines, the dashed lines, and the shaded area represent the mean of each virtual trial, the mean, and the 95% confidence interval of all virtual individuals, respectively. Brighter and darker colors show midazolam in the absence and in the presence of the perpetrator.

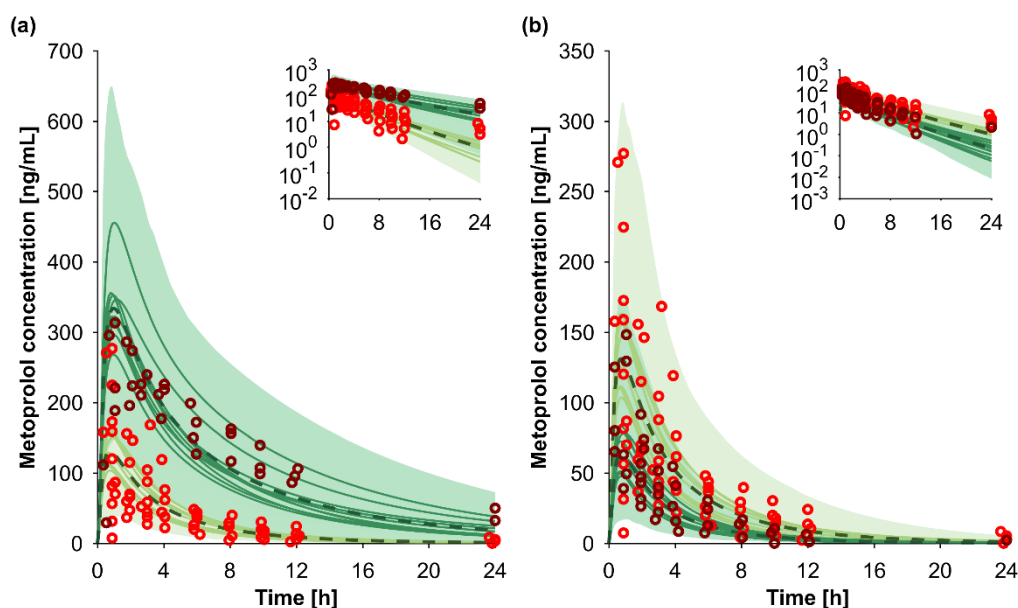


Figure A6.2: Predicted vs. observed concentration-time profiles of metoprolol in poor (a) and ultrarapid metabolizer of CYP2D6 (b) aged 20 to 50 years. The design of the simulated DDI scenarios is detailed in Table 6.2. Red markers show the clinically observed data from different individuals. The solid lines, the dashed lines, and the shaded area represent the mean of each virtual trial, the mean, and the 95% confidence interval of all virtual individuals, respectively. Brighter and darker colors show metoprolol in extensive metabolizers of CYP2D6 and in poor and ultrarapid metabolizers.

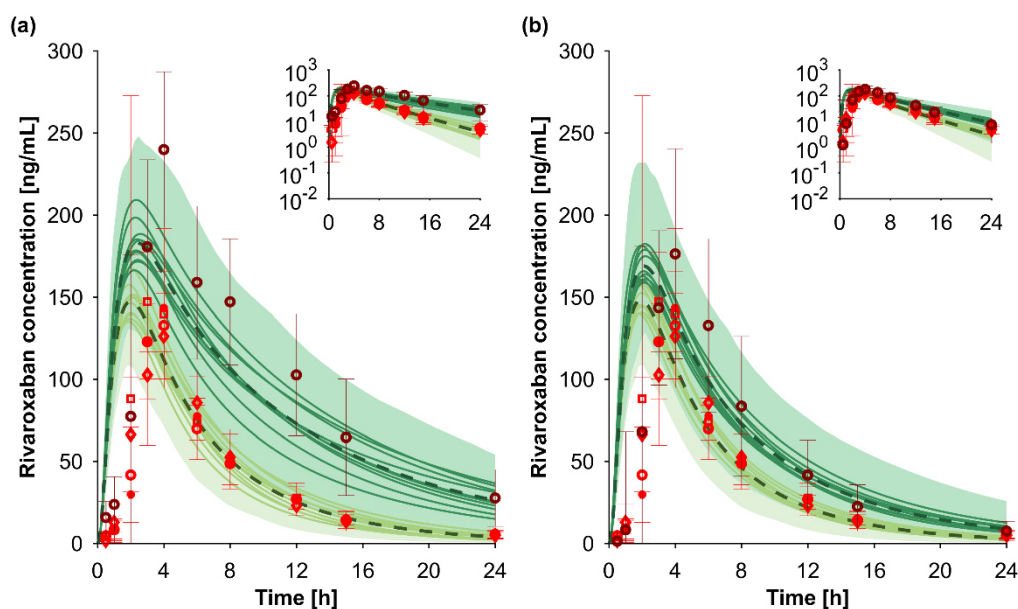


Figure A6.3: Predicted vs. observed concentration-time profiles of rivaroxaban with ketoconazole (a) and clarithromycin (b) in young subjects aged 20 to 50 years. The design of the simulated DDI scenarios is detailed in Table 6.2. Red markers show the clinically observed data with different markers representing different clinical studies. The solid lines, the dashed lines, and the shaded area represent the mean of each virtual trial, the mean, and the 95% confidence interval of all virtual individuals, respectively. Brighter and darker colors show rivaroxaban in the absence and in the presence of the perpetrator.

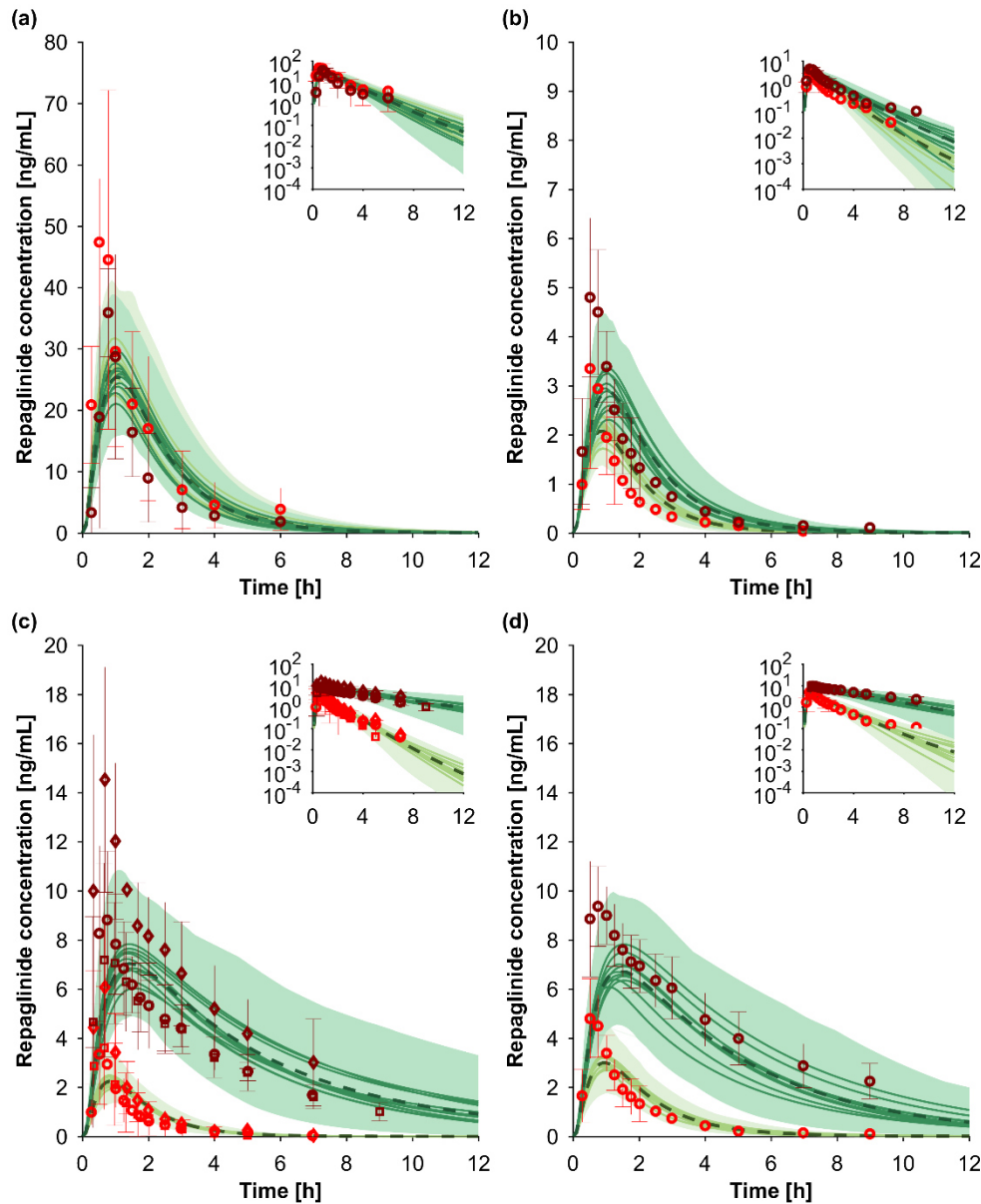


Figure A6.4: Predicted vs. observed concentration-time profiles of repaglinide in ultrarapid metabolizers of CYP2C8 (a), in subjects with a poor transporter phenotype of OATP1B1 (b), with gemfibrozil (c), and with gemfibrozil in subjects with a poor transporter phenotype of OATP1B1 (d). All subjects were 20 to 50 years old. The design of the simulated DDI scenarios is detailed in Table 6.2. Red markers show the clinically observed data with different markers representing different clinical studies. The solid lines, the dashed lines, and the shaded area represent the mean of each virtual trial, the mean, and the 95% confidence interval of all virtual individuals, respectively. Brighter and darker colors show the control and DDI scenario for repaglinide simulations.

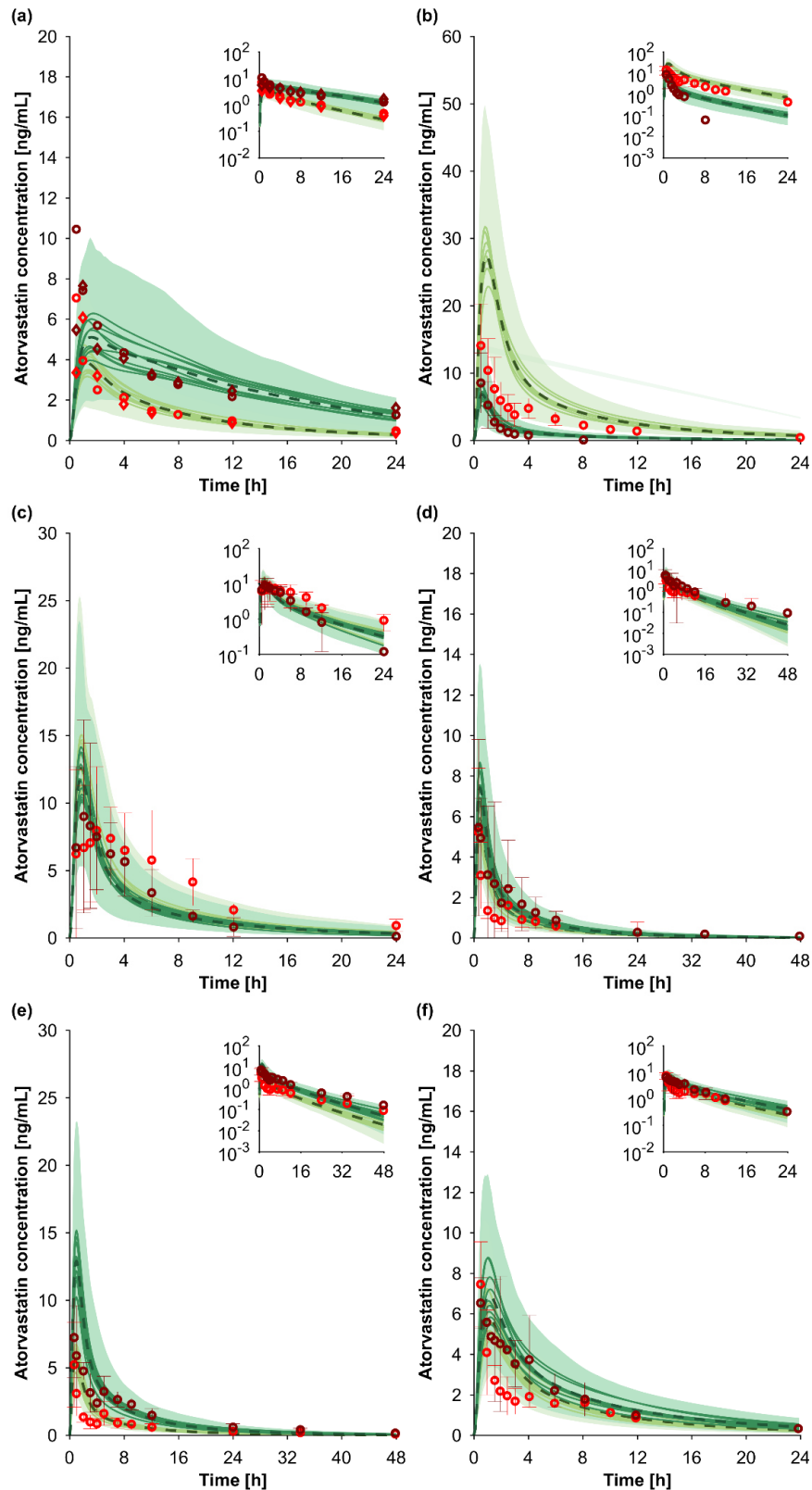


Figure A6.5: Predicted vs. observed concentration-time profiles of atorvastatin with clarithromycin (a), with rifampicin (b), with etravirine (c), in subjects with intermediate (d) and poor (e) transporter phenotype of OATP1B1, and with gemfibrozil (f). All subjects were 20 to 50 years old. The design of the simulated DDI scenarios is detailed in Table 6.2. Red markers show the clinically observed data with different markers representing different clinical studies. The solid lines, the dashed lines, and the shaded area represent the mean of each virtual trial, the mean, and the 95% confidence interval of all virtual individuals, respectively. Brighter and darker colors show the control and DDI scenario of atorvastatin.

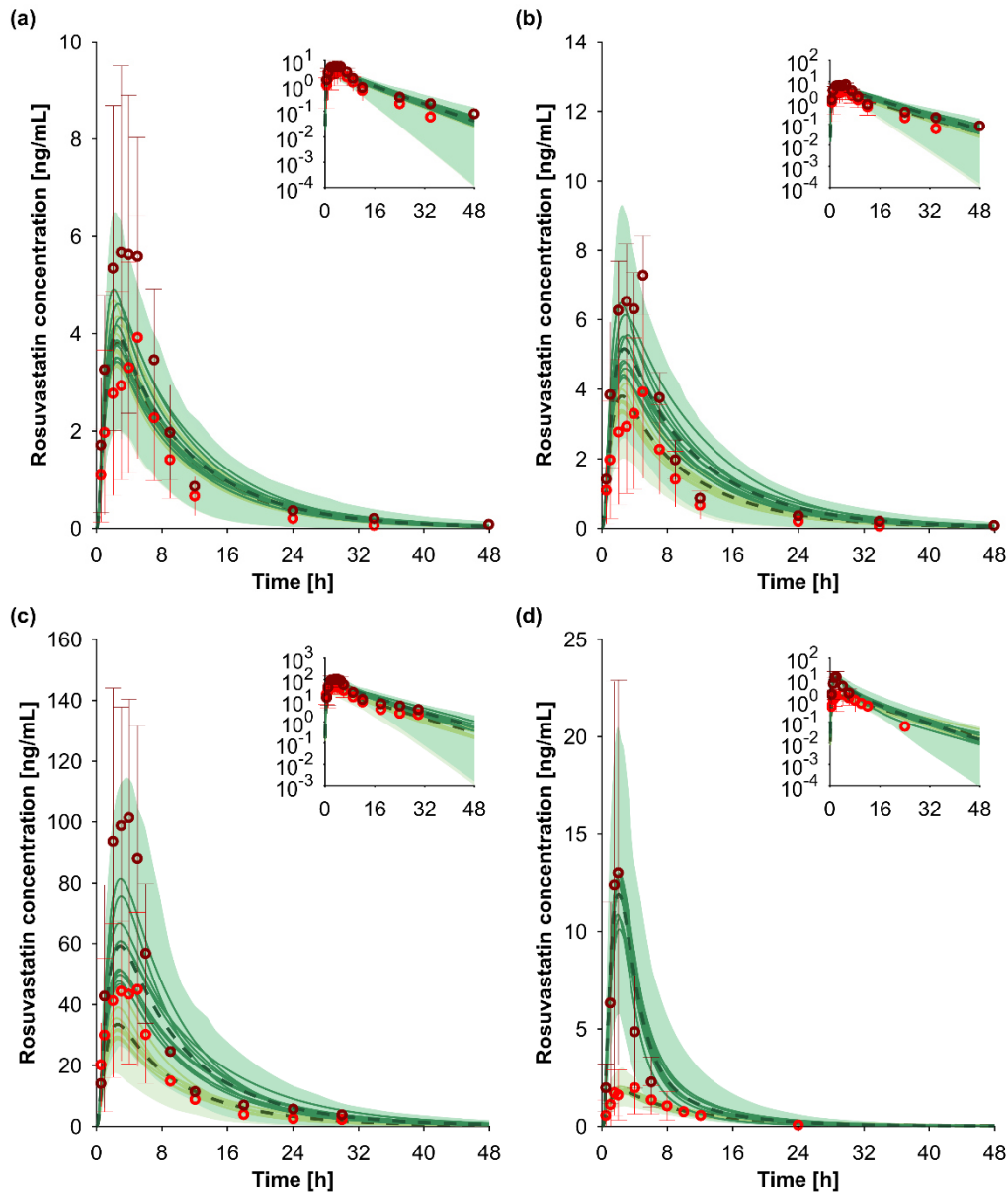


Figure A6.6: Predicted vs. observed concentration-time profiles of rosuvastatin in subjects with intermediate (a) and poor (b) transporter phenotype of OATP1B1, with gemfibrozil (c) and boosted atazanavir (d). All subjects were 20 to 50 years old. The design of the simulated DDI scenarios is detailed in Table 6.2. Red markers show the clinically observed data. The solid lines, the dashed lines, and the shaded area represent the mean of each virtual trial, the mean, and the 95% confidence interval of all virtual individuals, respectively. Brighter and darker colors show the control and DDI scenario of rosuvastatin.

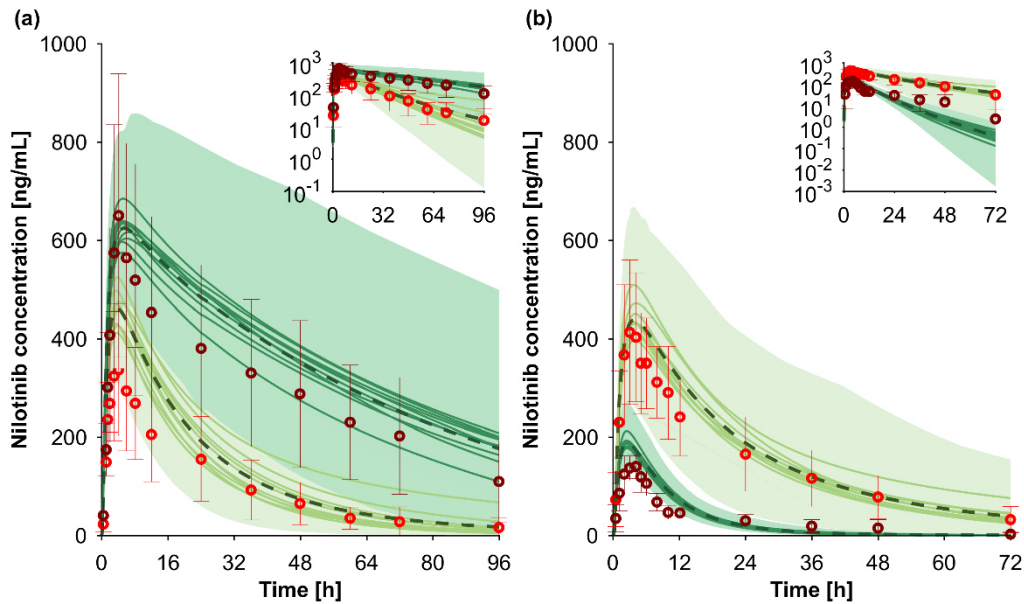


Figure A6.7: Predicted vs. observed concentration-time profiles of nilotinib with ketoconazole (a) and rifampicin (b) in young adults aged 20 to 50 years. The design of the simulated DDI scenarios is detailed in Table 6.2. Red markers show the clinically observed data. The solid lines, the dashed lines, and the shaded area represent the mean of each virtual trial, the mean, and the 95% confidence interval of all virtual individuals, respectively. Brighter and darker colors show nilotinib in the absence and in the presence of the perpetrator.

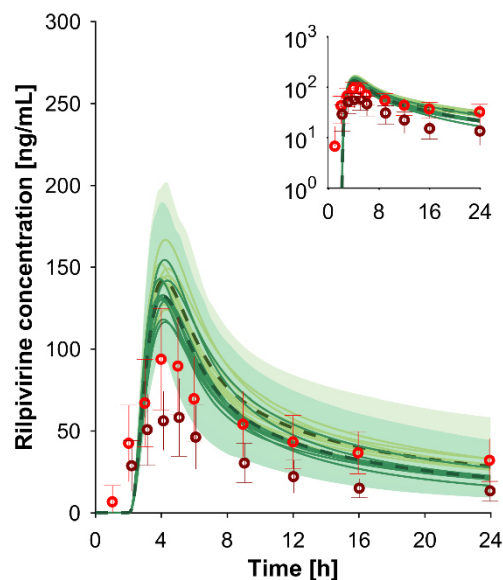


Figure A6.8: Predicted vs. observed concentration-time profile of rilpivirine with efavirenz in individuals aged 20 to 50 years. The design of the simulated DDI scenario is detailed in Table 6.2. Red markers show the clinically observed data. The solid lines, the dashed lines, and the shaded area represent the mean of each virtual trial, the mean, and the 95% confidence interval of all virtual individuals, respectively. Brighter and darker colors show rilpivirine in the absence and in the presence of efavirenz.

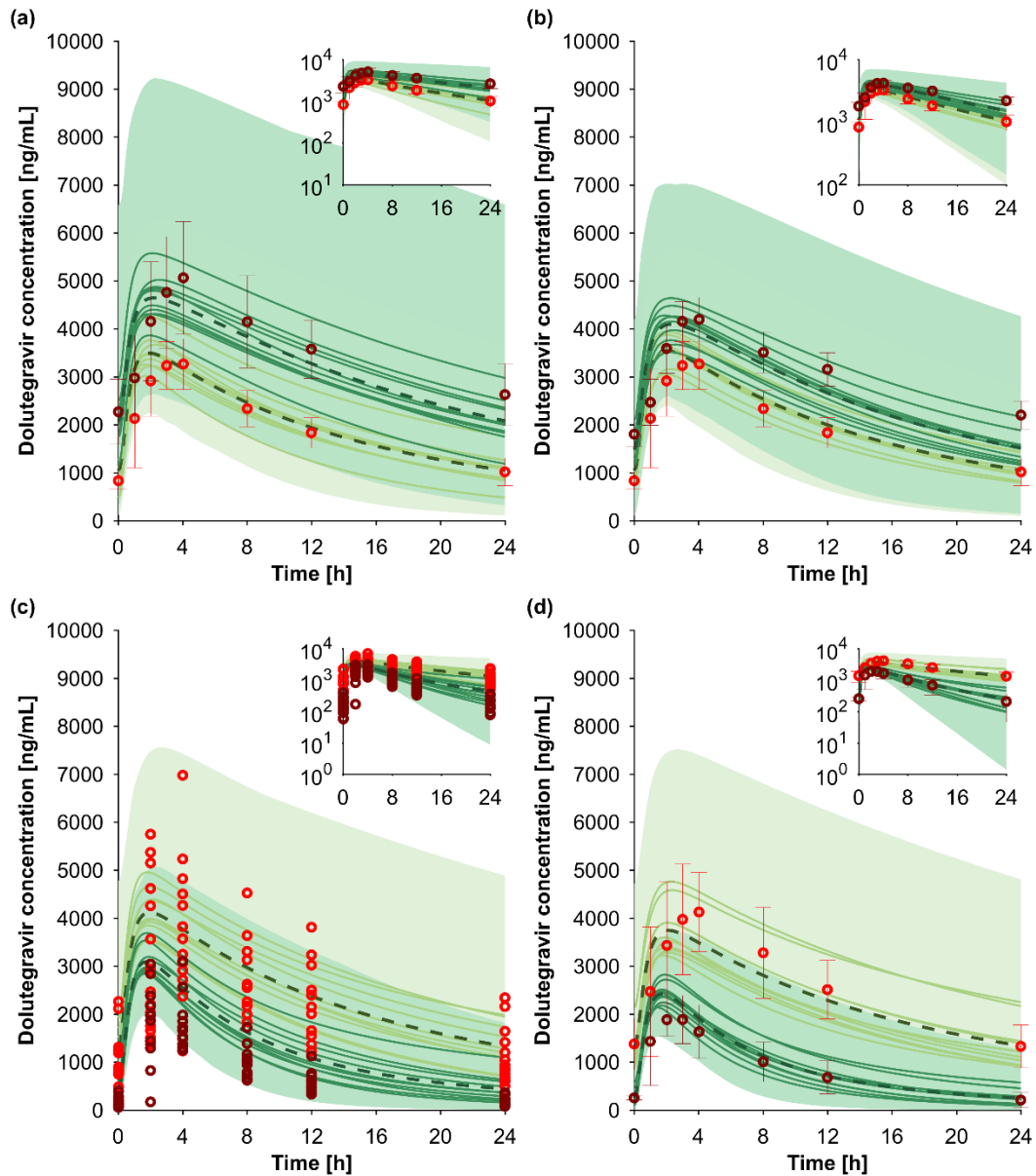


Figure A6.9: Predicted vs. observed concentration-time profiles of dolutegravir with atazanavir (a), boosted atazanavir (b), rifampicin (c), and etravirine (d) in young adults aged 20 to 50 years. The design of the simulated DDI scenarios is detailed in Table 6.2. Red markers show the clinically observed data with different markers representing different investigated individuals. The solid lines, the dashed lines, and the shaded area represent the mean of each virtual trial, the mean, and the 95% confidence interval of all virtual individuals, respectively. Brighter and darker colors show dolutegravir in the absence and in the presence of the perpetrator.

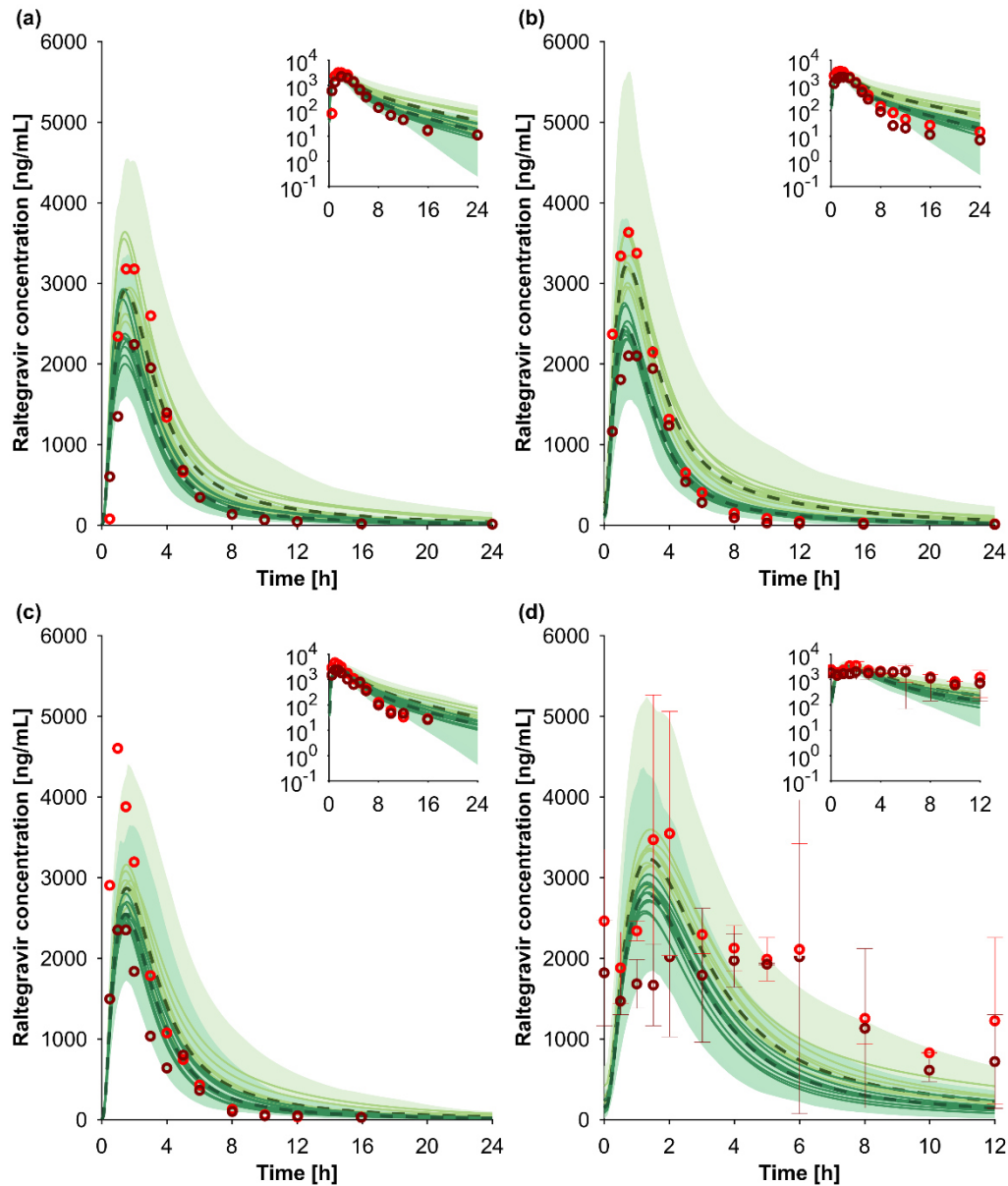


Figure A6.10: Predicted vs. observed concentration-time profiles of raltegravir with ritonavir (a), rifampicin (b), efavirenz (c), and etravirine (d) in young adults aged 20 to 50 years. The design of the simulated DDI scenarios is detailed in Table 6.2. Red markers show the clinically observed data. The solid lines, the dashed lines, and the shaded area represent the mean of each virtual trial, the mean, and the 95% confidence interval of all virtual individuals, respectively. Brighter and darker colors show raltegravir in the absence and in the presence of the perpetrator.

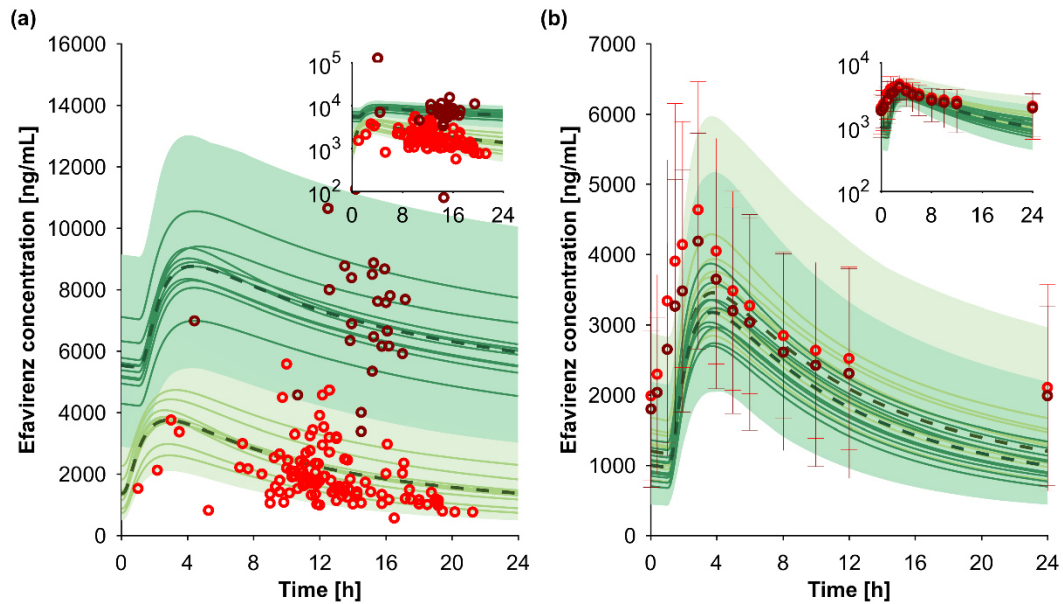


Figure A6.11: Predicted vs. observed concentration-time profiles of efavirenz in poor metabolizers of CYP2B6 (a) and with rifampicin (b) in young adults aged 20 to 50 years. The design of the simulated DDI scenarios is detailed in Table 6.2. Red markers show the clinically observed data with different markers representing different individuals. The solid lines, the dashed lines, and the shaded area represent the mean of each virtual trial, the mean, and the 95% confidence interval of all virtual individuals, respectively. Brighter and darker colors show the control and DDI scenario of efavirenz.

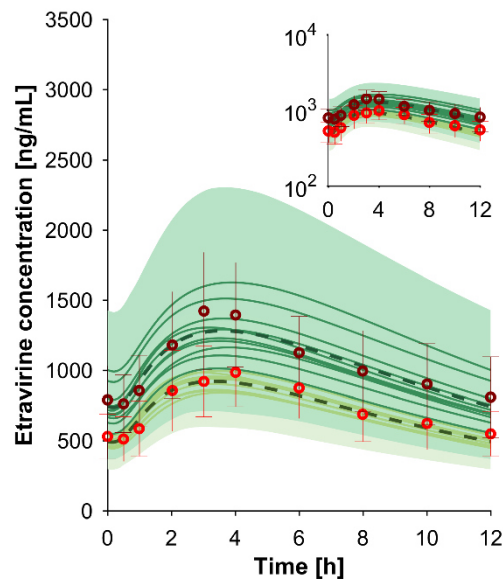


Figure A6.12: Predicted vs. observed concentration-time profile of etravirine with clarithromycin in young individuals aged 20 to 50 years. The design of the simulated DDI scenario is detailed in Table 6.2. Red markers show the clinically observed data. The solid lines, the dashed lines, and the shaded area represent the mean of each virtual trial, the mean, and the 95% confidence interval of all virtual individuals, respectively. Brighter and darker colors show etravirine in the absence and in the presence of clarithromycin.

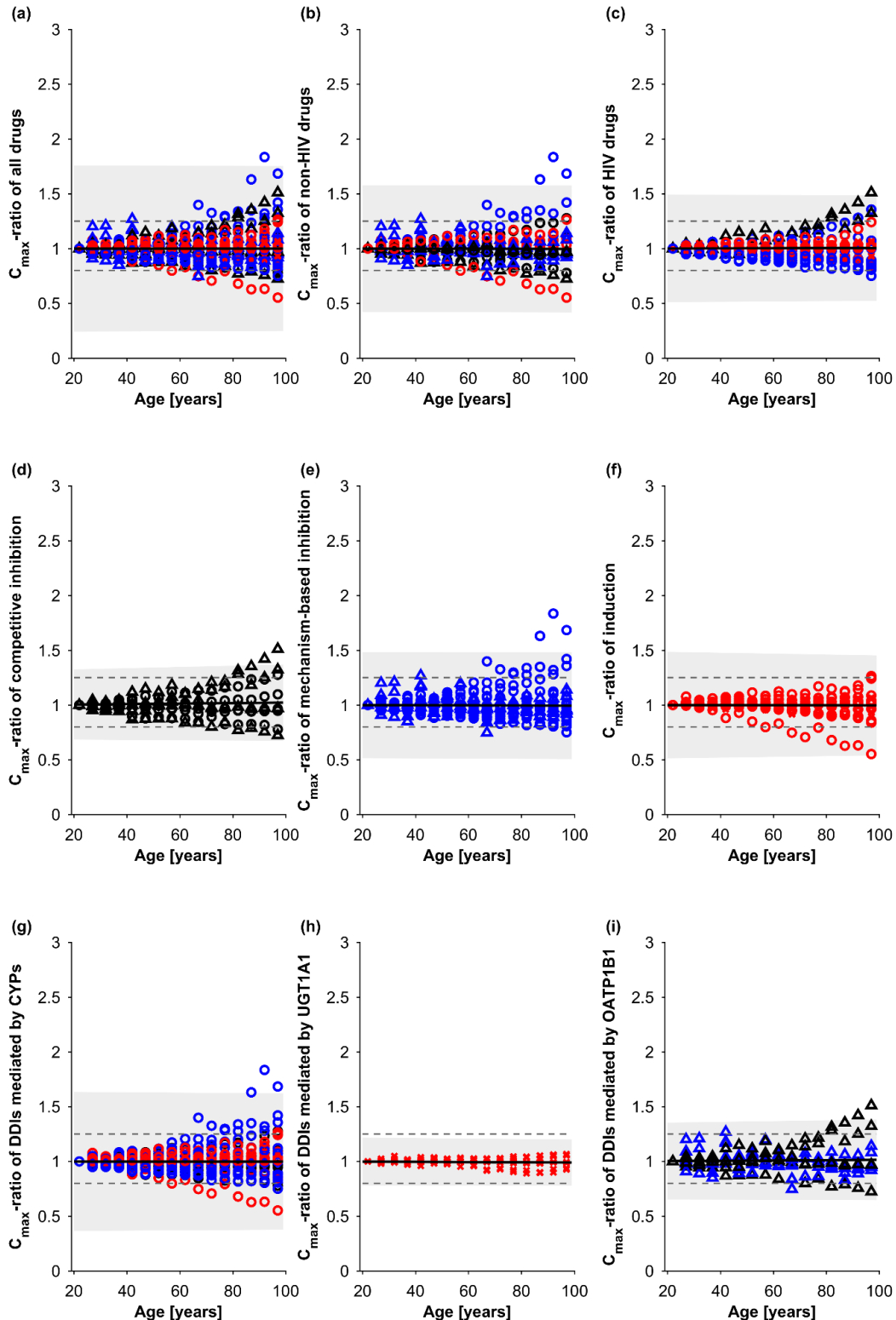


Figure A6.13: Peak concentration (C_{\max})-ratio normalized to the youngest investigated age group (20 to 24 years) for all drugs (a), for non-HIV drugs (b), for antiretroviral drugs (c), for competitive inhibition (d), for mechanism-based inhibition (e), for induction (f), for DDIs mediated by CYP enzymes (g), for DDIs mediated by UGT1A1 (h), and for DDIs mediated by OATP1B1 (i). Black, blue, and red markers represent competitive inhibition, mechanism-based inhibition, and induction. Circles, crosses, and triangles symbolize CYP-, UGT1A1-, and OATP1B1-mediated DDIs. The solid line and the shaded area show the mean \pm standard deviation. The dashed lines represent the 1.25-fold interval (bioequivalence criterion).

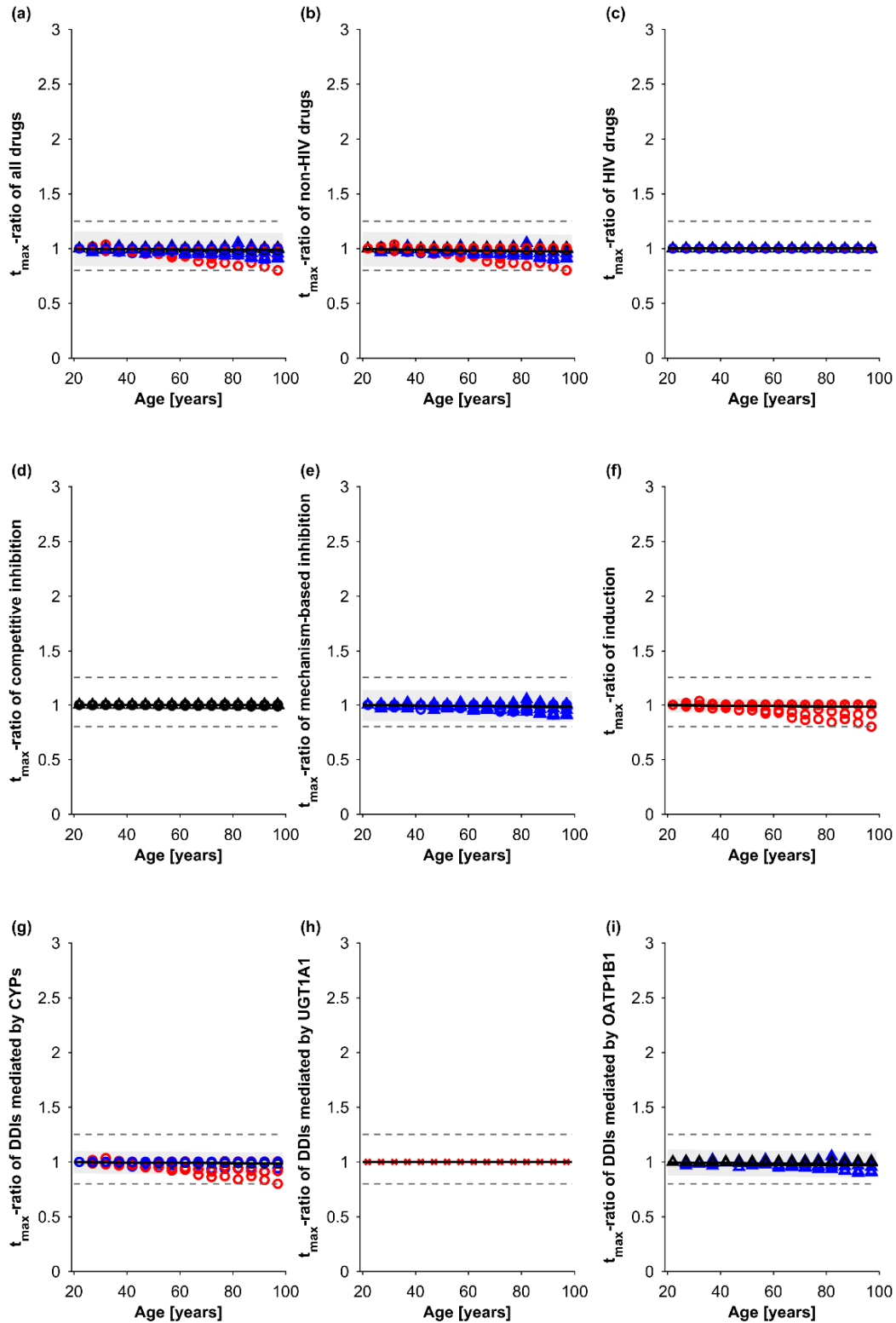


Figure A6.14: Time to peak concentration (t_{\max})-ratio normalized to the youngest investigated age group (20 to 24 years) for all drugs (a), for non-HIV drugs (b), for antiretroviral drugs (c), for competitive inhibition (d), for mechanism-based inhibition (e), for induction (f), for DDIs mediated by CYP enzymes (g), for DDIs mediated by UGT1A1 (h), and for DDIs mediated by OATP1B1 (i). Black, blue, and red markers represent competitive inhibition, mechanism-based inhibition, and induction. Circles, crosses, and triangles symbolize CYP-, UGT1A1-, and OATP1B1-mediated DDIs. The solid line and the shaded area show the mean \pm standard deviation. The dashed lines represent the 1.25-fold interval (bioequivalence criterion).

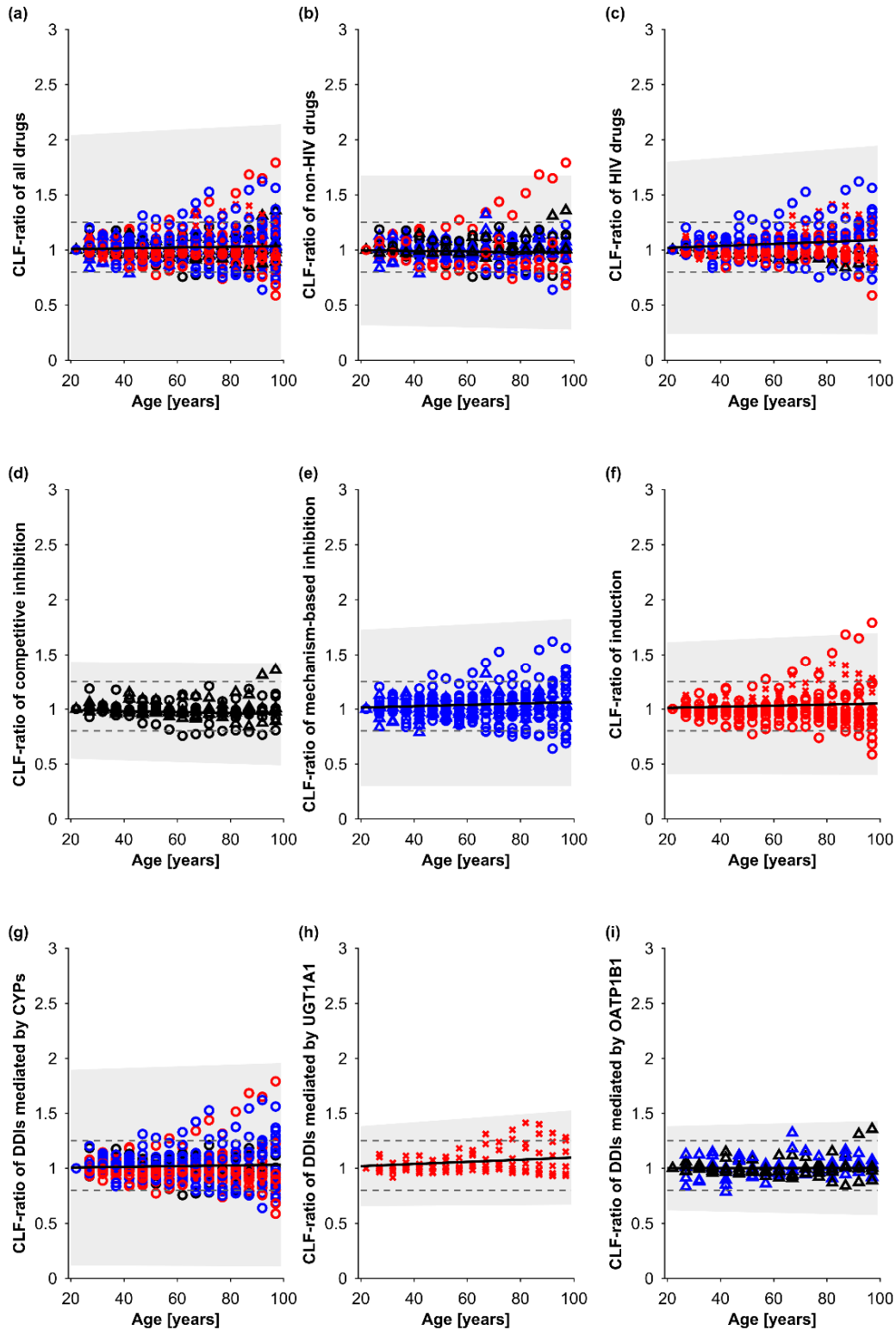


Figure A6.15: Clearance (CLF)-ratio normalized to the youngest investigated age group (20 to 24 years) for all drugs (a), for non-HIV drugs (b), for antiretroviral drugs (c), for competitive inhibition (d), for mechanism-based inhibition (e), for induction (f), for DDIs mediated by CYP enzymes (g), for DDIs mediated by UGT1A1 (h), and for DDIs mediated by OATP1B1 (i). Black, blue, and red markers represent competitive inhibition, mechanism-based inhibition, and induction. Circles, crosses, and triangles symbolize CYP-, UGT1A1-, and OATP1B1-mediated DDIs. The solid line and the shaded area show the mean \pm standard deviation. The dashed lines represent the 1.25-fold interval (bioequivalence criterion).

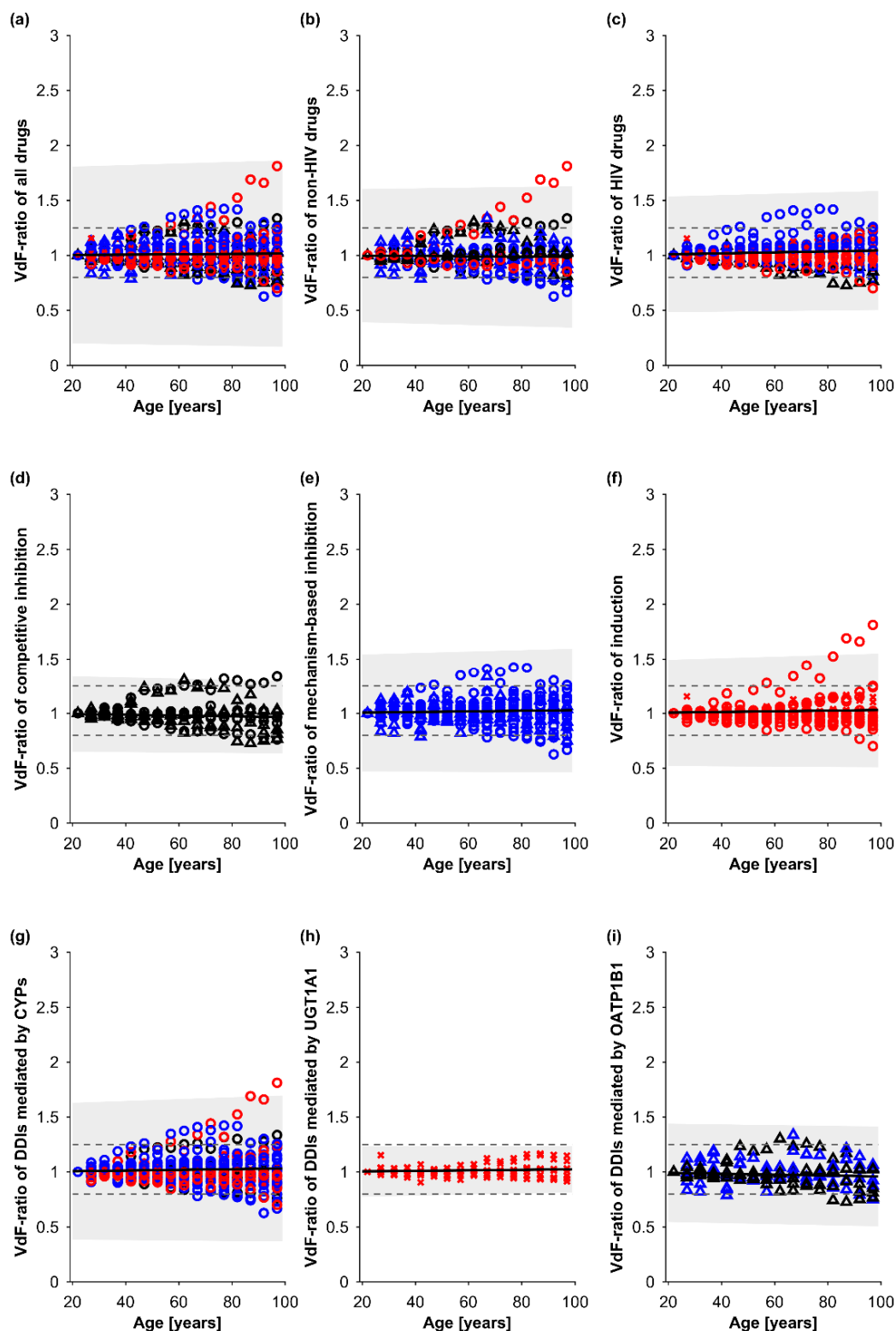


Figure A6.16: Apparent volume of distribution (VdF)-ratio normalized to the youngest investigated age group (20 to 24 years) for all drugs (a), for non-HIV drugs (b), for antiretroviral drugs (c), for competitive inhibition (d), for mechanism-based inhibition (e), for induction (f), for DDIs mediated by CYP enzymes (g), for DDIs mediated by UGT1A1 (h), and for DDIs mediated by OATP1B1 (i). Black, blue, and red markers represent competitive inhibition, mechanism-based inhibition, and induction. Circles, crosses, and triangles symbolize CYP-, UGT1A1-, and OATP1B1-mediated DDIs. The solid line and the shaded area show the mean \pm standard deviation. The dashed lines represent the 1.25-fold interval (bioequivalence criterion).

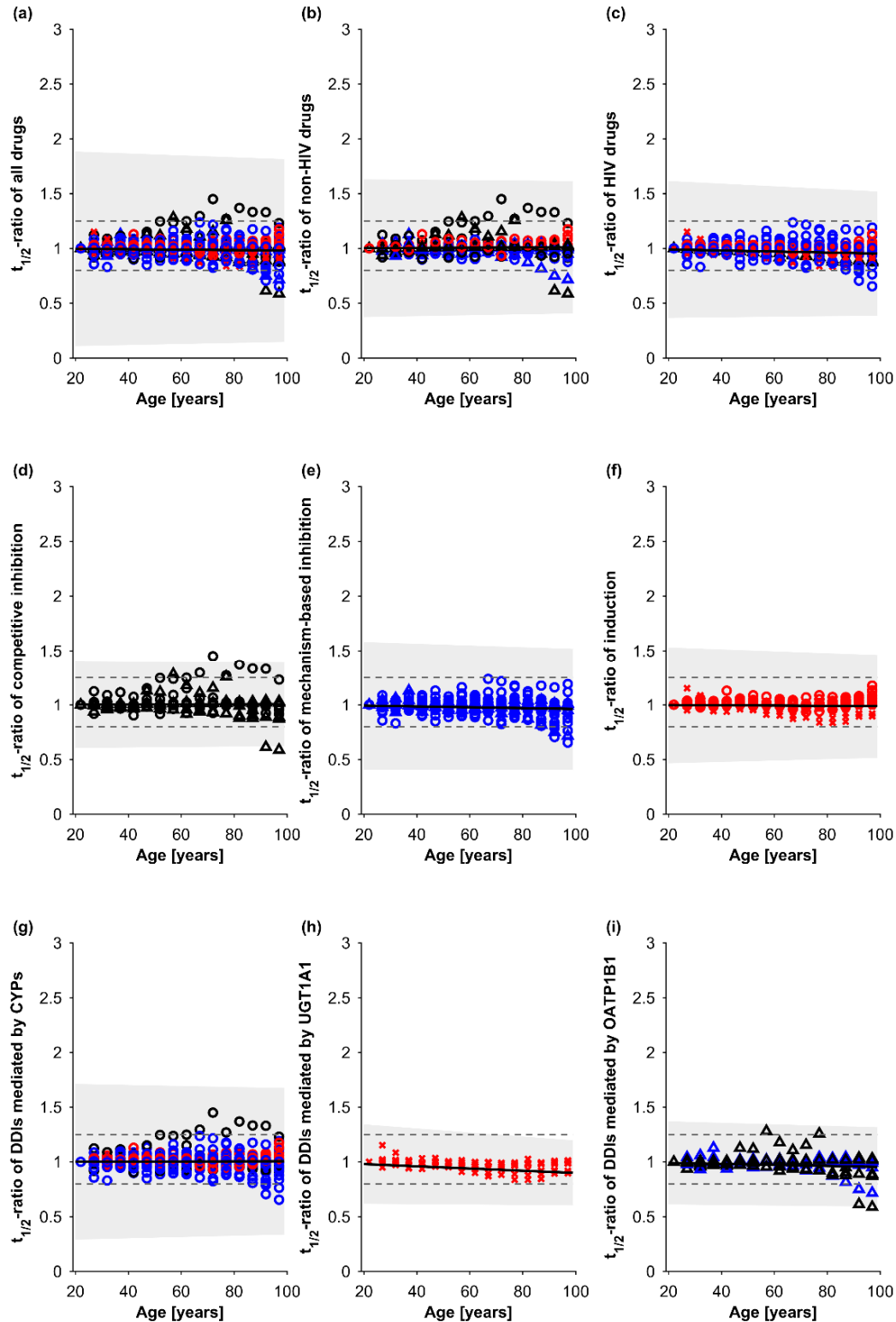


Figure A6.17: Elimination half-life ($t_{1/2}$)-ratio normalized to the youngest investigated age group (20 to 24 years) for all drugs (a), for non-HIV drugs (b), for antiretroviral drugs (c), for competitive inhibition (d), for mechanism-based inhibition (e), for induction (f), for DDIs mediated by CYP enzymes (g), for DDIs mediated by UGT1A1 (h), and for DDIs mediated by OATP1B1 (i). Black, blue, and red markers represent competitive inhibition, mechanism-based inhibition, and induction. Circles, crosses, and triangles symbolize CYP-, UGT1A1-, and OATP1B1-mediated DDIs. The solid line and the shaded area show the mean \pm standard deviation. The dashed lines represent the 1.25-fold interval (bioequivalence criterion).

Table A6.1: Observed vs. predicted drug pharmacokinetics in the control (victim in the absence of the perpetrator or extensive metabolizers/transporter phenotype) and DDI (victim in the presence of the perpetrator or different phenotype) scenario and the DDI ratio (DDI scenario / control scenario).

	Control scenario		DDI scenario		DDI ratio	
	observed	predicted	observed	predicted	observed	predicted
Midazolam + Ketoconazole						
C_{max} [ng/mL]	52.5 ± 22.1	31.1 ± 10.7	171 ± 49	163 ± 47	3.26 ± 1.66	5.23 ± 2.34
$t_{1/2}$ [h]	5.2 ± 6.0	4.7 ± 2.0	15.2 ± 5.1	9.5 ± 7.1	2.93 ± 3.56	2.04 ± 1.75
Rivaroxaban + Ketoconazole						
C_{max} [ng/mL]	138 ± 31	150 ± 30	237 ± 48	186 ± 38	1.72 ± 0.51	1.24 ± 0.35
$t_{1/2}$ [h]	6.7 ± 2.7	6.4 ± 1.0	6.5 ± 1.6	7.5 ± 2.6	0.97 ± 0.45	1.18 ± 0.45
Nilotinib + Ketoconazole						
C_{max} [ng/mL]	337 ± 134	472 ± 122	651 ± 289	637 ± 121	1.93 ± 1.15	1.35 ± 0.43
$t_{1/2}$ [h]	23.4 ± 13.8	14.6 ± 8.2	51.1 ± 24.3	44.8 ± 48.7	2.18 ± 1.65	3.07 ± 3.76
Midazolam + Nilotinib						
C_{max} [ng/mL]	38.5 ± 16.1	38.6 ± 15.0	45.0 ± 17.5	40.1 ± 15.2	1.17 ± 0.67	1.04 ± 0.56
$t_{1/2}$ [h]	5.8 ± 2.5	5.1 ± 2.3	6.8 ± 4.2	5.2 ± 2.4	1.17 ± 0.88	1.02 ± 0.66
Repaglinide + Gemfibrozil in PT of OATP1B1						
C_{max} [ng/mL]	5.2 ± 0.9	3.1 ± 1.0	9.8 ± 1.4	6.9 ± 1.8	1.88 ± 0.42	2.26 ± 0.95
$t_{1/2}$ [h]	1.9 ± 0.4	1.0 ± 0.3	2.8 ± 1.2	2.3 ± 1.1	1.47 ± 0.70	2.28 ± 1.28
Rivaroxaban + Clarithromycin						
C_{max} [ng/mL]	139 ± 23	151 ± 30	194 ± 42	172 ± 34	1.39 ± 0.38	1.14 ± 0.32
$t_{1/2}$ [h]	4.8 ± 1.0	3.9 ± 1.0	5.7 ± 1.0	5.0 ± 1.4	1.19 ± 0.32	1.30 ± 0.48
Atorvastatin + Clarithromycin						
C_{max} [ng/mL]	5.5 ± 4.1	4.0 ± 1.8	8.4 ± 2.4	5.4 ± 2.7	1.53 ± 1.24	1.35 ± 0.91
$t_{1/2}$ [h]	5.9 ± 2.3	8.2 ± 2.7	9.6 ± 4.3	8.8 ± 2.4	1.61 ± 0.96	1.08 ± 0.46
Etravirine + Clarithromycin						
C_{max} [ng/mL]	986 ± 242	926 ± 258	1,423 ± 419	1,288 ± 557	1.44 ± 0.55	1.39 ± 0.72
$t_{1/2}$ [h]	9.3 ± 2.7	7.4 ± 0.8	12.8 ± 3.8	7.8 ± 1.1	1.38 ± 0.57	1.05 ± 0.19
Midazolam + Ritonavir						
$t_{1/2}$ [h]	5.7	6.1 ± 2.6	18.4	12.9 ± 8.3	3.25	2.12 ± 1.64
Rilpivirine + Darunavir/r						
C_{max} [ng/mL]					1.79	1.70 ± 0.86
Atorvastatin + Rifampicin						
C_{max} [ng/mL]	15.8 ± 4.1	8.0 ± 3.1	9.5 ± 3.7	3.9 ± 1.6	0.60 ± 0.31	0.49 ± 0.28
$t_{1/2}$ [h]	10.3 ± 1.2	8.3 ± 3.0	2.7 ± 0.9	3.7 ± 1.8	0.26 ± 0.09	0.45 ± 0.28
Nilotinib + Rifampicin						
C_{max} [ng/mL]	413 ± 147	445 ± 123	140 ± 25	191 ± 40	0.34 ± 0.13	0.43 ± 0.15
$t_{1/2}$ [h]	20.7 ± 9.0	19.3 ± 11.7	14.5 ± 7.3	16.3 ± 5.2	0.70 ± 0.47	0.85 ± 0.58
Efavirenz + Rifampicin						
C_{max} [ng/mL]	4,571 ± 2,663	3,490 ± 1,154	3,882 ± 1,015	3,214 ± 982	0.85 ± 0.54	0.92 ± 0.41
$t_{1/2}$ [h]	46.4 ± 40.2	46.6 ± 12.6	55.9 ± 50.9	43.4 ± 10.6	1.20 ± 1.51	0.93 ± 0.34
Rilpivirine + Efavirenz						
C_{max} [ng/mL]	100 ± 28	146 ± 32	65 ± 21	136 ± 30	0.65 ± 0.28	0.93 ± 0.29
$t_{1/2}$ [h]	41.4 ± 22.6	44.2 ± 13.3	46.8 ± 28.5	37.6 ± 9.8	1.13 ± 0.92	0.85 ± 0.34
Atorvastatin + Efavirenz						
C_{max} [ng/mL]					1.06 ± 0.56	0.90 ± 0.56
Atorvastatin + Etravirine						
C_{max} [ng/mL]	11.0 ± 5.9	13.0 ± 6.0	11.5 ± 6.0	12.2 ± 5.7	1.05 ± 0.78	0.94 ± 0.62
$t_{1/2}$ [h]	6.9 ± 3.8	8.2 ± 2.5	3.8 ± 2.3	8.2 ± 2.5	0.55 ± 0.45	1.00 ± 0.43
Dolutegravir + Atazanavir						
C_{max} [ng/mL]	3,320 ± 531	3,543 ± 1,320	5,110 ± 1,022	4,686 ± 2,068	1.54 ± 0.39	1.32 ± 0.76
$t_{1/2}$ [h]	13.0 ± 2.5	11.8 ± 8.3	23.8 ± 5.0	16.7 ± 11.8	1.83 ± 0.52	1.41 ± 1.40
Dolutegravir + Atazanavir/r						
C_{max} [ng/mL]	3,320 ± 531	3,597 ± 1,102	4,290 ± 19	4,144 ± 1,463	1.29 ± 0.21	1.15 ± 0.54
$t_{1/2}$ [h]	13.0 ± 2.5	11.6 ± 6.2	24.1 ± 11.0	13.8 ± 8.8	1.85 ± 0.92	1.19 ± 0.99

Table A6.1: con't.

	Control scenario		DDI scenario		DDI ratio	
	observed	predicted	observed	predicted	observed	predicted
Raltegravir + Ritonavir						
C_{max} [ng/mL]	3,176	2,980 ± 866	2,240	2409 ± 598	0.71	0.81 ± 0.31
$t_{1/2}$ [h]	12.5	10.8 ± 4.0	12.4	9.9 ± 3.7	0.99	0.92 ± 0.48
Raltegravir + Rifampicin						
C_{max} [ng/mL]	3,833	3,303 ± 1,112	2,377	2,515 ± 715	0.62	0.76 ± 0.34
$t_{1/2}$ [h]	8.5	11.0 ± 4.3	9.6	9.8 ± 4.2	1.13	0.89 ± 0.52
Raltegravir + Efavirenz						
C_{max} [ng/mL]	4,602	2,949 ± 856	2,350	2,610 ± 680	0.51	0.89 ± 0.35
$t_{1/2}$ [h]	10.9	11.1 ± 4.4	10.8	10.7 ± 4.4	1.00	0.96 ± 0.55
Raltegravir + Etravirine						
C_{max} [ng/mL]	1,576 ± 2,248	1,588 ± 505	897 ± 456	1,380 ± 385	0.57 ± 0.86	0.87 ± 0.37
$t_{1/2}$ [h]	8.3 ± 9.3	10.5 ± 4.0	6.5 ± 6.0	9.9 ± 3.8	0.79 ± 1.15	0.95 ± 0.51
Dolutegravir + Rifampicin						
C_{max} [ng/mL]	3,969 ± 1,349	4,169 ± 1,652	2,569 ± 796	3,146 ± 1,076	0.65 ± 0.30	0.75 ± 0.40
$t_{1/2}$ [h]	8.9 ± 0.7	12.7 ± 9.4	6.7 ± 1.2	7.2 ± 5.1	0.75 ± 0.15	0.57 ± 0.58
Dolutegravir + Etravirine						
C_{max} [ng/mL]	4,340 ± 825	3,793 ± 1,513	2100 ± 24	2,476 ± 691	0.48 ± 0.09	0.65 ± 0.32
$t_{1/2}$ [h]	12.4 ± 2.6	13.9 ± 10.6	6.4 ± 22.0	5.6 ± 4.2	0.52 ± 1.78	0.40 ± 0.43
Repaglinide + Gemfibrozil						
C_{max} [ng/mL]	4.5 ± 2.7	2.3 ± 0.7	10.7 ± 4.6	7.3 ± 1.8	2.40 ± 1.77	3.16 ± 1.24
$t_{1/2}$ [h]	1.3 ± 0.4	0.9 ± 0.3	2.9 ± 1.2	2.7 ± 1.6	2.13 ± 1.09	3.07 ± 2.07
Atorvastatin + Gemfibrozil						
C_{max} [ng/mL]	8.2 ± 3.5	6.1 ± 2.7	9.6 ± 4.0	7.2 ± 3.3	1.17 ± 0.70	1.19 ± 0.76
$t_{1/2}$ [h]	10.7 ± 2.2	8.2 ± 2.5	9.0 ± 1.8	8.7 ± 2.9	0.84 ± 0.24	1.06 ± 0.48
Rosuvastatin + Gemfibrozil						
C_{max} [ng/mL]	49.5 ± 23.6	34.1 ± 13.9	109 ± 47	60.3 ± 28.9	2.20 ± 1.41	1.77 ± 1.11
$t_{1/2}$ [h]	17.1 ± 1.1	13.4 ± 4.5	23.3 ± 4.1	13.3 ± 4.5	1.36 ± 0.26	0.99 ± 0.47
Rosuvastatin + Atazanavir/r						
C_{max} [ng/mL]	2.0 ± 1.4	1.9 ± 0.6	13.0 ± 9.9	12.2 ± 4.6	6.61 ± 6.76	6.52 ± 3.23
$t_{1/2}$ [h]	9.1 ± 7.8	14.0 ± 4.7	8.3 ± 5.9	13.5 ± 4.7	0.92 ± 1.02	0.96 ± 0.46
Metoprolol in PM of CYP2D6						
C_{max} [ng/mL]	143 ± 65	135 ± 89	264 ± 26	348 ± 166	1.85 ± 0.87	2.57 ± 2.09
$t_{1/2}$ [h]	4.9 ± 1.5	3.1 ± 0.8	8.4 ± 1.1	5.0 ± 2.3	1.70 ± 0.57	1.61 ± 0.83
Metoprolol in UM of CYP2D6						
C_{max} [ng/mL]	143 ± 65	135 ± 89	80.0 ± 32.5	65.0 ± 51.1	0.56 ± 0.34	0.48 ± 0.49
$t_{1/2}$ [h]	4.9 ± 1.5	3.1 ± 0.8	4.3 ± 3.0	2.8 ± 0.7	0.88 ± 0.67	0.90 ± 0.31
Repaglinide in UM of CYP2C8						
C_{max} [ng/mL]	47.4 ± 10.4	27.6 ± 7.8	35.9 ± 7.2	25.9 ± 7.3	0.76 ± 0.22	0.94 ± 0.37
$t_{1/2}$ [h]	1.2 ± 0.12	1.1 ± 0.3	1.3 ± 0.3	1.0 ± 0.3	1.08 ± 0.26	0.95 ± 0.36
Repaglinide in PT of OATP1B1						
C_{max} [ng/mL]	3.5 ± 1.7	2.1 ± 0.5	5.2 ± 0.9	3.3 ± 1.0	1.49 ± 0.77	1.55 ± 0.60
$t_{1/2}$ [h]	1.5 ± 0.4	1.0 ± 0.4	1.9 ± 0.4	1.1 ± 0.4	1.27 ± 0.43	1.14 ± 0.62
Atorvastatin in IT of OATP1B1						
C_{max} [ng/mL]	5.7 ± 2.6	6.0 ± 2.4	8.0 ± 3.7	7.6 ± 3.1	1.41 ± 0.91	1.28 ± 0.73
$t_{1/2}$ [h]	10.0 ± 2.6	8.0 ± 2.8	9.2 ± 3.6	8.1 ± 2.9	0.92 ± 0.43	1.01 ± 0.50
Atorvastatin in PT of OATP1B1						
C_{max} [ng/mL]	5.7 ± 2.6	6.0 ± 2.4	10.1 ± 9.0	13.2 ± 5.5	1.76 ± 1.77	2.23 ± 1.28
$t_{1/2}$ [h]	10.0 ± 2.6	8.0 ± 2.8	10.4 ± 2.9	8.3 ± 2.9	1.04 ± 0.40	1.03 ± 0.51
Rosuvastatin in IT of OATP1B1						
C_{max} [ng/mL]	4.2 ± 2.4	3.9 ± 1.3	6.4 ± 3.2	4.0 ± 1.5	1.52 ± 1.15	1.04 ± 0.53
$t_{1/2}$ [h]	13.7 ± 8.5	13.9 ± 4.4	24.4 ± 13.7	14.1 ± 4.4	1.78 ± 1.49	1.02 ± 0.45
Rosuvastatin in PT of OATP1B1						
C_{max} [ng/mL]	4.2 ± 2.4	3.9 ± 1.3	7.5 ± 1.2	5.3 ± 2.3	1.79 ± 1.06	1.36 ± 0.75
$t_{1/2}$ [h]	13.7 ± 8.5	13.9 ± 4.4	24.4 ± 6.3	23.2 ± 8.9	1.78 ± 1.20	1.67 ± 0.83

Key: C_{max} = peak concentration, IT = intermediate transporter phenotype, PM = poor metabolizer, PT = poor transporter phenotype, $t_{1/2}$ = elimination half-life, UM = ultrarapid metabolizer.

6.2.8 **Supplementary Material**

The online version of this article contains supplementary material:

<https://doi.org/10.1002/cpt.2017>

Table S1: Published clinical studies used to verify drug-drug interaction predictions. See Table 6.2.

Table S2: Parameters for ketoconazole, nilotinib, gemfibrozil, and its glucuronide metabolite. See Table 6.3.

Table S3: Published clinical studies used to verify the developed PBPK models for ketoconazole, nilotinib, and gemfibrozil. See Table 6.4.

Table S4: Published studies comparing DDI magnitudes between young and elderly study participants. See Table 6.5.

Table S5: Observed vs. predicted parameters for ketoconazole, nilotinib, gemfibrozil, and its glucuronide metabolite in young (20 to 50 years) and elderly (at least 65 years) adults. See Table 6.7.

Table S6: Observed vs. predicted drug pharmacokinetics in the control (victim in the absence of the perpetrator or extensive metabolizers/transporter phenotype) and DDI (victim in the presence of the perpetrator or different phenotype) scenario and the DDI ratio (DDI scenario / control scenario). See Table A61.

Table S7: Slope of mean prediction for DDI magnitudes across adulthood (20 to 99 years). See Table 6.9.

Figure S1: Predicted vs. observed concentration time profiles for ketoconazole (200 mg once daily) in young and elderly subjects. See Figure 6.5.

Figure S2: Predicted vs. observed concentration time profiles for nilotinib (400 mg single dose), gemfibrozil (600 mg twice daily), and gemfibrozil glucuronide in young individuals aged 20 to 50 years. See Figure 6.4.

Figure S3ff: See Appendix Figures A6.1ff.

Chapter 7:

Effective Method to Predict Drug Interactions

7. Effective Method to Predict Drug Interactions

7.1	Abstract	Page 202
7.2	Introduction	Page 203
7.3	Methods	Page 204
7.3.1	Data source for clinical studies to verify the method	Page 205
7.3.2	Calculation of parameters (DPI and $\ln R$ / $\ln R_{3A}$) used for the prediction of DDI magnitudes	Page 205
7.4	Results	Page 207
7.4.1	Calculation of parameters (DPI_{3A} and $\ln R_{3A}$ / $\ln R_{3A}$) needed for the prediction of DDI magnitudes	Page 207
7.4.2	Verification of the method	Page 207
7.4.3	Impact and interplay of DPI_{3A} and $\ln R_{3A}$ / $\ln R_{3A}$	Page 210
7.4.4	Autoinhibition and autoinduction of antiretrovirals	Page 211
7.4.5	Prediction of DDIs between tyrosine kinase inhibitors and antiretrovirals	Page 213
7.5	Discussion	Page 214
7.6	Appendix	Page 218

This chapter is a pre-printed version of a peer-reviewed original research article published under the following reference:

Analysis of clinical drug-drug interaction data to predict magnitudes of uncharacterized interactions between antiretroviral drugs and comedications

Felix Stader, Hannah Kinvig, Manuel Battegay, Saye Khoo, Andrew Owen, Marco Siccardi, & Catia Marzolini

Antimicrobial Agents and Chemotherapy 2018; 62(7): e00717-18.

DOI: 10.1128/AAC.00717-18.

7.1 Abstract

Despite their high potential for drug-drug-interactions (DDI), clinical DDI studies of antiretroviral drugs are often lacking, because the full range of potential interactions cannot feasibly or pragmatically be studied, with some high-risk DDI studies also ethically difficult to undertake. Thus, a robust method to screen and to predict the likelihood of DDIs is required.

We developed a method to predict DDIs based on two parameters: the degree of metabolism by specific enzymes, such as cytochrome P-450 (CYP) 3A, and the strength of an inhibitor or inducer. These parameters were derived from existing clinical studies utilizing paradigm substrates, inducers and inhibitors of CYP3A, to assess the predictive performance of this method by verifying predicted magnitudes of changes in drug exposure against clinical DDI studies involving antiretroviral drugs.

The derived parameters were consistent with the FDA classification of sensitive CYP3A substrates and the strength of CYP3A inhibitors and inducers. Characterized DDI magnitudes ($n = 68$) between antiretroviral drugs and comedications were successfully quantified meaning 53%, 85%, and 98% of the predictions were within 1.25-fold (0.80 to 1.25), 1.5-fold (0.66 to 1.48), and 2.0-fold (0.66 to 1.94) of the observed clinical data. In addition, the method identifies CYP3A substrates likely to be highly or conversely, minimally impacted by CYP3A inhibitors or inducers, thus categorizing the magnitude of DDIs.

The developed effective and robust method has the potential to support a more rational identification of dose adjustment to overcome DDIs, being particularly relevant in an HIV-setting, given the treatment's complexity, high DDI risk, and limited guidance on the management of DDIs.

7.2 Introduction

Drug-drug interactions (DDIs) are an increasing burden for patients infected with the human immunodeficiency virus (HIV), because DDIs can lead to drug toxicity and treatment failure. Most antiretroviral drugs are substrates and inhibitors or inducers of cytochrome P-450 (CYP) enzymes, especially the CYP3A family [640], comprised of CYP3A, CYP3A5, CYP3A7, and CYP3A43 [641]. Antiretroviral drugs are considered to be amongst the therapeutic agents with the highest DDI potential [642]. Large surveys suggest around a quarter of HIV patients on treatment are at risk of a clinically significant DDIs even with modern antiretroviral therapies [576, 643, 644]. The risk for DDIs increases significantly with age, multiple morbidities, and polypharmacy [86, 645, 646].

It is not feasible, practical, or affordable for every potential DDI to be clinically studied, either during drug development or post licensing. Some DDIs (e.g. those resulting in increased exposure of narrow therapeutic index drugs) cannot easily or ethically be studied. However, the ability to quantitatively predict the likelihood of any DDI remains important to understand the clinical significance and whether any DDI can be safely managed through dose modification and to prevent unnecessary denial of important therapies to patients. Where data are lacking, empirical expert opinion prevails based on: (a) the metabolic pathway of the drugs involved, (b) in vitro drug metabolism data, and (c) prior knowledge from other DDI studies investigating the effect of paradigm agents on the drug of interest. However, it is challenging to scale these data in any quantitatively useful manner. Furthermore, in vitro data as well as clinical DDI trials are often undertaken only for strong, paradigm CYP3A inhibitors (e.g. ketoconazole, itraconazole) and inducers (e.g. rifampicin). It is difficult to estimate if and to what extent the dose of the victim drug should be adjusted when administered with a weaker CYP3A inhibitor than ketoconazole or inducer than rifampicin. Therefore, a quantitative tool for estimating DDIs involving antiretroviral drugs could support a more rational dose adjustment to overcome DDIs.

Physiologically based pharmacokinetic models (PBPK) can be used to simulate the magnitude of change in exposure of any given victim drug in a virtual patient population [360], using data obtained from in vitro experiments about the susceptibility of victim and the strength of perpetrator drugs. However, PBPK models are intended to be generally used for predicting DDIs [325] and not to manage daily DDI queries in the clinic.

An alternative method to predict DDIs is to analyze clinical pharmacokinetic data from similar drug combinations with known DDI magnitudes [110, 647]. This method can provide a valuable evaluation and prediction of a DDI magnitude, delineating a potential dose adjustment to overcome the DDI effect and ensure a safe and effective treatment of the patient.

The objective of this work was to investigate if DDIs between antiretroviral drugs and comedications can be quantified from existing clinical pharmacokinetic data of similar drug combinations, providing a rational framework to support necessary dose optimization for HIV-infected patients.

7.3 Methods

This study extends the method to estimate DDIs from clinical data to antiretroviral drugs [110, 647]. The common metric to quantify a DDI is the ratio of the area under the curve (AUC) of a victim drug in the presence of a perpetrator (AUC*) to the AUC of the victim drug in the absence of the perpetrator. The AUC ratio can be expressed in the following way for inhibitors (equation 1) and inducers (equation 2):

$$\frac{AUC^*}{AUC} = \frac{1}{1 - DPI_x \times InR_x} \quad (1)$$

$$\frac{AUC^*}{AUC} = \frac{1}{\frac{DPI_x}{1 - IcR_x} + (1 - DPI_x)} \quad (2)$$

where *DPI* is the fraction of the disposition pathway mediated by a specific enzyme *x* such as CYP3A, and *InR* and *IcR* are the inhibitor and inducer ratio, respectively. CYP3A was chosen because it is a major contributor to the metabolism of drugs in clinical use and is therefore often involved in DDIs. A detailed description of the used method and the deviation of the equation can be found in the appendix of chapter 7 (Section 7.7).

DPI represents the importance of a metabolic pathway of interest. A DPI_{3A} of 1 means that 100% of the drug is metabolized by CYP3A, hence no other enzyme or transporter is involved in the disposition of the drug, while a DPI_{3A} of 0 means that CYP3A is not involved in the metabolism at all. *InR* / *IcR* reflects the potential of a perpetrator to inhibit or induce the metabolic pathway of interest. An InR_{3A} / IcR_{3A} of 1 indicates a high inhibition / induction potential, while a low InR_{3A} / IcR_{3A} value translates to a weak inhibition / induction potential.

7.3.1 Data source for clinical studies to verify the method

A structured literature search was performed using the MEDLINE database to screen for DDI studies to develop and verify the method. Key words were “drug-drug-interaction”, “effect”, and the victim and perpetrator drug of interest. Chosen victim drugs should be highly, intermediately, and weakly metabolized by CYP3A, and chosen perpetrators should inhibit or induce CYP3A strongly, moderately, or weakly. Data were included if subjects were healthy volunteers or HIV-infected patients but did not have any severe disease affecting metabolizing enzymes (i.e. liver cirrhosis). At least 80% of the subjects of one study were white, because different ethnicities can have an impact on CYP abundance, and drug administration was oral. If more than one study reported an AUC ratio for the same victim-perpetrator drug combination, the weighted mean was calculated.

7.3.2 Calculation of parameters (DPI and InR / IcR) used for the prediction of DDI magnitudes

With a given AUC ratio determined in a clinical study, DPI and InR / IcR of victim and perpetrator drugs can be estimated. Therefore, equations 1 and 2 are rearranged to calculate DPI (equation 3), InR (equation 4), and IcR (equation 5).

$$DPI_x = \frac{1 - \frac{AUC}{AUC^*}}{InR_x} \quad (3)$$

$$InR_x = \frac{1 - \frac{AUC}{AUC^*}}{DPI_x} \quad (4)$$

$$IcR_x = \frac{1 - \frac{AUC}{AUC^*}}{1 - \frac{AUC}{AUC^*} - DPI_x} \quad (5)$$

To start the method, a model drug with a known DPI_{3A} is needed (Figure 7.1). We used midazolam as a probe substrate, which is highly metabolized by CYP3A4/3A5 and, to a less extent by UGT1A4 [648]. In the first step, InR_{3A} of strong, moderate, and weak inhibitors and IcR_{3A} of strong, moderate, and weak inducers were calculated from DDI studies with midazolam. In the second step, DPI_{3A} was calculated for drugs being highly, intermediately, or weakly metabolized by CYP3A. In the third step, characterized DDI magnitudes were calculated using the derived DPI_{3A} and InR_{3A} / IcR_{3A} values in equation 1 or 2, and the predicted results were compared to observed clinical data. Judgement if a prediction was

successful was assessed by the 1.25-, 1.5-, and 2.0-fold method as recommended by the FDA [556]. In the last step, uncharacterized DDI magnitudes were predicted for tyrosine kinase inhibitors being weakly, intermediately, or highly metabolized by CYP3A (sorafenib, imatinib, sunitinib, pazopanib, gefitinib, nilotinib, lapatinib, dasatinib, and ibrutinib), ritonavir as a potent CYP3A inhibitor, and etravirine as a moderate CYP3A inducer. Predicted DDI magnitudes were classified into no DDIs (AUC-ratio of 0.8 to 1.25), weak DDIs (AUC-ratio of 1.25 to 2.0 for inhibition and 0.5 to 0.8 for induction), moderate DDIs (AUC-ratio of 2.0 to 5.0 for inhibition and 0.2 to 0.5 for induction), and strong DDIs (AUC-ratio above 5.0 for inhibitors and below 0.2 for inducers) according to the FDA [649].

To capture the observed variability in clinical DDI studies, Monte-Carlo simulations ($n = 10,000$) were performed to calculate the equation parameters ($DP_{I_{3A}}$ and $\ln R_{3A} / \ln R_{3A}$) and AUC ratios of characterized DDIs to verify the method as well as uncharacterized DDIs between tyrosine kinase inhibitors and antiretroviral drugs. Results are reported as the geometric mean [95% confidence interval].

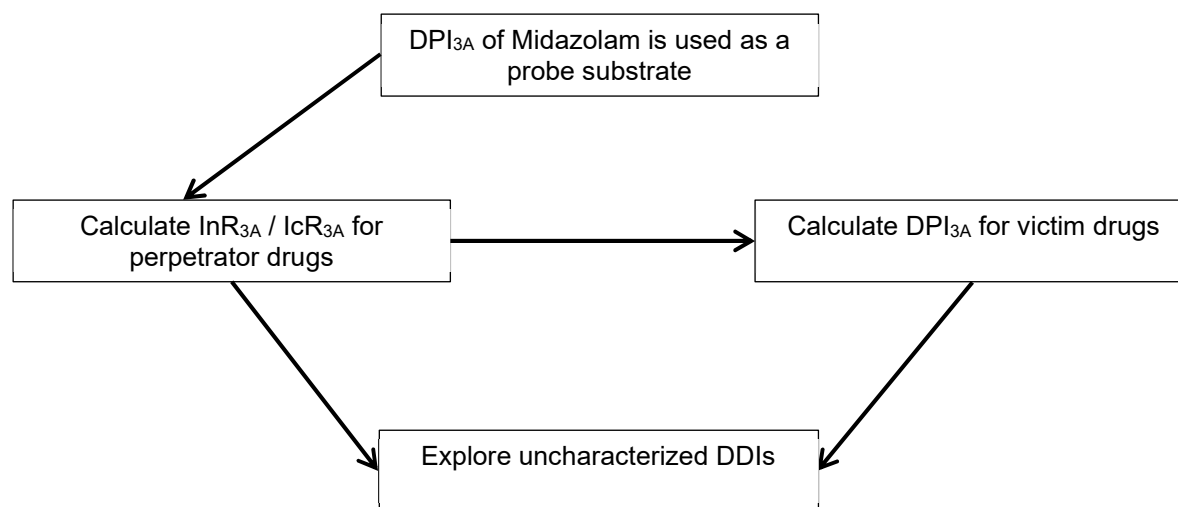


Figure 7.1: Verification of the developed effective method to estimate uncharacterized DDI magnitudes.

Key: $DP_{I_{3A}}$ = fraction of disposition pathway mediated by CYP3A, $\ln R_{3A}$ = inhibitor ratio, $\ln R_{3A}$ = inducer ratio.

7.4 Results

7.4.1 Calculation of parameters (DPI_{3A} and $\ln R_{3A} / I_c R_{3A}$) needed for the prediction of DDI magnitudes

A total of 68 DDIs issued from clinical studies involving antiretroviral drugs were identified including 13 involving competitive inhibition (whereby the inhibitor binds to the active site of the enzyme and thereby blocks the binding of the victim drug), 33 involving mechanism-based inhibition (whereby the inhibitor represses the transcription or translation of the metabolizing enzyme thereby leading to the loss of the enzyme), and 22 involving induction.

The fraction of CYP3A-mediated metabolism for victim drugs (Table 7.1) and the strength of perpetrators (Table 7.2) have been calculated for antiretroviral drugs using published, clinical AUC ratios of characterized DDIs. Drugs being highly metabolized by CYP3A (results are reported as geometric means and the 95% confidence interval) were triazolam ($DPI_{3A} = 0.966$ [0.898, 1.0]), midazolam ($DPI_{3A} = 0.940$ [0.909, 0.971]), quetiapine ($DPI_{3A} = 0.845$ [0.645, 1.0]), tacrolimus ($DPI_{3A} = 0.831$ [0.531, 1.0]), and maraviroc ($DPI_{3A} = 0.792$ [0.559, 0.998]), whereas CYP3A was only responsible for 30.3% of zolpidem disposition ($DPI_{3A} = 0.303$ [0.065, 0.661]).

Ritonavir ($\ln R_{3A} = 0.963$ [0.873, 1.0]), cobicistat ($\ln R_{3A} = 0.936$ [0.810, 1.0]), and ketoconazole ($\ln R_{3A} = 0.943$ [0.823, 1.0]) were estimated to be potent CYP3A inhibitors, whereas cimetidine was the weakest inhibitor of CYP3A in this study ($\ln R_{3A} = 0.256$ [0.049, 0.570]). The moderate inducers efavirenz and etravirine had $I_c R_{3A}$ values of 0.539 [0.282, 0.850] and 0.644 [0.433, 0.882] compared to the strong inducer rifampicin with an $I_c R_{3A}$ of 0.906 [0.846, 0.967].

7.4.2 Verification of the method

Characterized DDIs with antiretroviral drugs were calculated by using the derived DPI and $\ln R / I_c R$ values to verify the method and investigate its potential to predict uncharacterized DDIs (Figure 7.2). More than half of the predictions (53%) were within 1.25-fold (ratio predicted/observed: 0.90 to 1.25), 85% of the predicted values were within 1.5-fold (ratio predicted/observed: 0.66 to 1.48) and 98% of the

Table 7.1: Calculated fraction of the disposition pathway mediated by CYP3A (DPI_{3A}) of victim drugs sorted by their CYP3A sensitivities^b.

Drug	DPI _{3A}					Predicted AUC*/AUC with			
				Reference(s) ^a		Ritonavir (inhibitor)		Etravirine (inducer)	
	Single calculation	Monte Carlo simulation				Single calculation	Monte Carlo simulation	Single calculation	Monte Carlo simulation
Simvastatin	0.978	0.979	[0.916, 1.0]	[110]		45.97	34.54 [5.33, 100.0]	0.34	0.31 [0.12, 0.44]
Triazolam	0.959	0.966	[0.898, 1.0]	[650, 651]		24.39	24.97 [4.91, 100.0]	0.35	0.31 [0.12, 0.44]
Midazolam	0.940	0.940	[0.909, 0.971]	[652-655]		16.67	12.36 [5.40, 20.64]	0.35	0.32 [0.13, 0.45]
Quetiapine	0.896	0.845	[0.645, 1.0]	[656]		9.66	7.97 [2.42, 62.46]	0.36	0.34 [0.14, 0.47]
Tacrolimus	0.875	0.831	[0.531, 1.0]	[657]		8.03	10.20 [1.79, 100.0]	0.37	0.34 [0.14, 0.48]
Maraviroc	0.828	0.792	[0.559, 0.998]	[658]		5.80	5.85 [1.98, 31.26]	0.38	0.35 [0.14, 0.49]
Saquinavir	0.638	0.580	[0.258, 0.849]	[659]		2.76	2.88 [1.31, 6.04]	0.44	0.42 [0.18, 0.57]
Darunavir	0.602	0.543	[0.215, 0.817]	[660]		2.51	2.62 [1.26, 5.19]	0.46	0.43 [0.18, 0.59]
Macitentan	0.585	0.524	[0.200, 0.810]	[661]		2.41	2.55 [1.24, 4.98]	0.47	0.43 [0.19, 0.59]
Amlodipine	0.468	0.464	[0.117, 1.0]	[662]		1.88	2.75 [1.12, 30.13]	0.52	0.46 [0.19, 0.64]
Etravirine	0.340	0.336	[0.077, 0.701]	[100]		1.52	1.79 [1.08, 3.18]	0.60	0.52 [0.24, 0.71]
Rilpivirine	0.324	0.334	[0.079, 0.656]	[105]		1.48	1.73 [1.08, 2.84]	0.61	0.53 [0.24, 0.71]
Zolpidem	0.268	0.303	[0.065, 0.661]	[663]		1.37	1.66 [1.06, 2.79]	0.66	0.55 [0.25, 0.73]
Ritonavir	0.156	0.231	[0.038, 0.552]	[664]		1.19	1.46 [1.04, 2.19]	0.77	0.60 [0.29, 0.78]

^a References reporting observed AUC ratios used to calculate DPI_{3A} according to equation 3. If more than one study reported the AUC ratio for the same drug combination, the weighted mean was used to derive DPI_{3A}.

^b Single calculations not considering variability and Monte Carlo simulations (n = 10,000) were performed to predict DDI magnitudes with the inhibitor ritonavir and the inducer etravirine. Results of the Monte Carlo simulations are presented as geometric means [95% confidence intervals].

Key: AUC = area under the curve.

Table 7.2: Calculated inhibitor ($\ln R_{3A}$) and inducer ($\text{Ic}R_{3A}$) ratios sorted by their strengths^b.

Drug	$\ln R_{3A} / \text{Ic}R_{3A}$				Predicted AUC*/AUC with			
					Maraviroc		Rilpivirine	
	Single calculation	Monte Carlo simulation	Reference(s) ^a		Single calculation	Monte Carlo simulation	Single calculation	Monte Carlo simulation
Ritonavir	1.0	0.963	[0.873, 1.0]	[665-669] [580, 646, 654,	5.80	5.85 [1.98, 7.63]	1.48	1.73 [1.08, 2.06]
Ketoconazole	0.981	0.943	[0.823, 1.0]	670-672]	5.32	4.61 [1.93, 6.25]	1.47	1.64 [1.08, 2.00]
Cobicistat	0.967	0.936	[0.810, 1.0]	[673]	5.00	5.35 [1.91, 7.04]	1.46	1.71 [1.08, 2.00]
Voriconazole	0.951	0.916	[0.768, 1.0]	[674]	4.69	4.67 [1.78, 6.26]	1.45	1.67 [1.08, 1.98]
Itraconazole	0.920	0.877	[0.691, 0.986]	[675]	4.19	4.14 [1.72, 5.46]	1.43	1.62 [1.07, 1.92]
Clarithromycin	0.912	0.870	[0.680, 0.982]	[111]	4.08	3.98 [1.66, 5.24]	1.42	1.61 [1.07, 1.89]
Saquinavir	0.858	0.803	[0.557, 0.946]	[676]	3.45	3.32 [1.53, 4.34]	1.39	1.54 [1.07, 1.80]
Posaconazole	0.852	0.797	[0.551, 0.944]	[671, 677]	3.39	3.28 [1.53, 4.29]	1.38	1.54 [1.06, 1.79]
Diltiazem	0.780	0.715	[0.427, 0.898]	[678]	2.82	2.70 [1.36, 3.46]	1.34	1.46 [1.05, 1.68]
Fluconazole	0.768	0.700	[0.403, 0.893]	[653]	2.74	2.62 [1.34, 3.38]	1.33	1.45 [1.05, 1.66]
Cimetidine	0.213	0.256	[0.049, 0.570]	[679-681]	1.21	1.38 [1.04, 1.57]	1.07	1.15 [1.01, 1.23]
Efavirenz	0.566	0.539	[0.282, 0.850]	[589]	0.48	0.43 [0.18, 0.61]	0.70	0.60 [0.29, 0.79]
Etravirine	0.662	0.644	[0.433, 0.882]	[100]	0.38	0.35 [0.14, 0.49]	0.61	0.53 [0.24, 0.71]
Rifampicin	0.946	0.906	[0.846, 0.967]	[659]	0.06	0.10 [0.04, 0.20]	0.15	0.20 [0.07, 0.29]

^a References reporting observed AUC ratios used to calculate $\ln R_{3A}$ and $\text{Ic}R_{3A}$ according to equations 4 and 5. If more than one study reported the AUC ratio for the same drug combination, the weighted mean was used to derive $\ln R_{3A} / \text{Ic}R_{3A}$.

^b Single calculations not considering variability and Monte Carlo simulations ($n = 10,000$) were performed to predict DDI magnitudes with the victim drugs maraviroc, a sensitive CYP3A substrate, and rilpivirine, a moderate CYP3A substrate. Results of the Monte Carlo simulations are presented as geometric means [95% confidence intervals].

Key: AUC = area under the curve.

predictions were within 2.0-fold (ratio predicted/observed: 0.66 to 1.94) of the observed clinical data for all investigated DDI mechanisms. Overall, predictions were equally performant for antiretroviral drugs acting as perpetrators (ritonavir, cobicistat, darunavir, saquinavir, etravirine and efavirenz) or as victim drugs (maraviroc, rilpivirine).

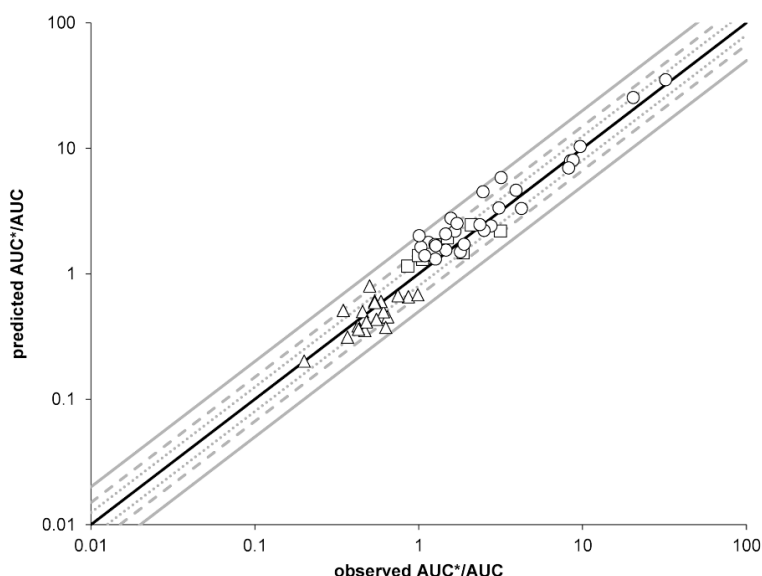


Figure 7.2: Predicted vs. observed AUC ratios for competitive inhibition (open squares), mechanism-based inhibition (open circles), and induction (open triangles). The solid line is the line of identity, the dotted lines represent the 80% and 125% margins, and the dashed lines represent the 50% and 200% margins. The interaction between saquinavir and cimetidine was calculated by using the $\ln R_{3A}$ of the stronger inhibitor saquinavir rather than of cimetidine, as explained in the discussion (Section 7.5).

7.4.3 Impact and interplay of DPI_{3A} and $\ln R_{3A} / I_c R_{3A}$

To analyze the impact of DPI_{3A} , the interaction magnitude with the potent inhibitor ritonavir ($\ln R_{3A} = 0.963$ [0.873, 1.0]) and the moderate inducer etravirine ($I_c R_{3A} = 0.644$ [0.433, 0.882]) have been calculated (Table 7.1). Drugs being highly metabolized by CYP3A like triazolam and maraviroc showed >5-fold increase in exposure when given with ritonavir and roughly a 65% decrease in the AUC when administered with etravirine. Monte-Carlo simulations allowed us to investigate the variability of predictions, which can be remarkably high for some interactions (e.g. tacrolimus when administered with ritonavir or etravirine).

The impact of $\ln R_{3A}$ and $I_c R_{3A}$ was investigated by calculating the DDI potential with the victim drugs maraviroc for which CYP3A is responsible for 79.2% of the disposition ($DPI_{3A} = 0.792$ [0.559, 0.998]), and rilpivirine, which is less metabolized by CYP3A ($DPI_{3A} = 0.334$ [0.079, 0.656], Table 7.2). Strong

CYP3A inhibitors such as ritonavir and cobicistat led to a 5-fold increase in the AUC of maraviroc and to a 1.5-fold increase of rilpivirine exposure, showing also the impact of DPI_{3A} . This holds true for inducers, because CYP3A substrates such as maraviroc and rilpivirine were more impacted by rifampicin than by efavirenz and etravirine. The predicted variability was greater for maraviroc being highly metabolized by CYP3A, particularly for inhibitors and inducers impacting CYP3A strongly, than for rilpivirine.

To investigate the interplay between the role CYP3A plays in the metabolism of drugs (represented by DPI_{3A}) and the inhibitor strength (represented by lnR_{3A}), the DDI magnitude between five victim drugs with increasing DPI_{3A} (zolpidem < macitentan < maraviroc < triazolam < simvastatin) and inhibitors with increasing lnR_{3A} (cimetidine < fluconazole < itraconazole < ritonavir) have been investigated and compared to observed clinical data, if available (Figure 7.3). The strong inhibitors ritonavir and itraconazole led to a >5-fold increase of exposure for victim drugs being highly metabolized by CYP3A, whereas drugs that were not as sensitive to CYP3A like zolpidem ($DPI_{3A} = 0.303$ [0.065, 0.661]) resulted in a weak AUC ratio increase of less than 2.0-fold. Moderate CYP3A inhibitors like fluconazole gave rise to a moderate DDI magnitude (2- to 5-fold) and CYP3A inhibitors with low lnR_{3A} values such as cimetidine resulted in small DDI magnitudes (<1.25) when administered with a drug being highly metabolized by CYP3A (e.g. maraviroc, triazolam, and simvastatin). Therefore, the magnitude of a DDI depends on the sensitivity of a substrate towards a specific metabolic pathway represented by DPI and the strength of an inhibitor or inducer represented by lnR and lcR .

7.4.4 Autoinhibition and autoinduction of antiretroviral drugs

It should be highlighted that some antiretroviral drugs, for instance, ritonavir and etravirine, can inhibit or induce their own metabolism (autoinhibition / autoinduction), which is important to consider when quantifying DDIs involving those drugs. The inhibitor ritonavir ($lnR_{3A} = 0.963$ [0.873, 1.0]; $DPI_{3A} = 0.231$ [0.038, 0.552]) and the inducer etravirine ($lcR_{3A} = 0.644$ [0.433, 0.882]; $DPI_{3A} = 0.336$ [0.077, 0.701]) were used as victim drugs and the effect of the CYP3A inhibitors cimetidine (weak inhibitor), fluconazole (moderate inhibitor), and ketoconazole (strong inhibitor) on ritonavir and etravirine exposures were investigated (Figure 7.4). Even with strong inhibitors like ketoconazole, there was only a minor effect on ritonavir and etravirine exposure, which is in accordance with observed clinical data.

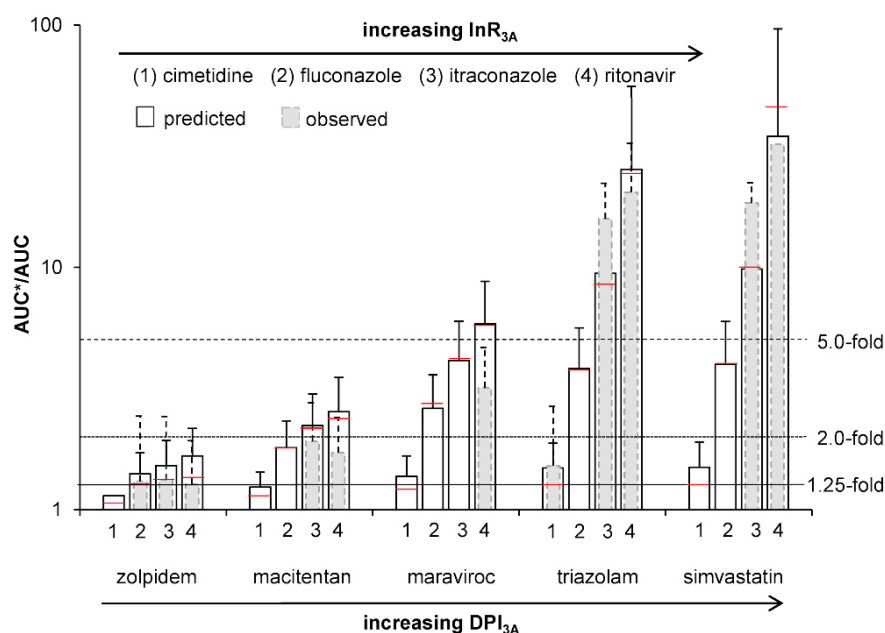


Figure 7.3: Comparison of predicted (white bars) and observed AUC ratios (grey bars) for the five victim drugs zolpidem ($DPI_{3A} = 0.303$ [0.065, 0.661]), macitentan ($DPI_{3A} = 0.524$ [0.200, 0.810]), maraviroc ($DPI_{3A} = 0.792$ [0.559, 0.998]), triazolam ($DPI_{3A} = 0.966$ [0.898, 1.0]), and simvastatin ($DPI_{3A} = 0.979$ [0.916, 1.0]) administered together with the four CYP3A inhibitors cimetidine ($\ln R_{3A} = 0.256$ [0.049, 0.570]), fluconazole ($\ln R_{3A} = 0.700$ [0.403, 0.893]), itraconazole ($\ln R_{3A} = 0.877$ [0.691, 0.986]), and ritonavir ($\ln R_{3A} = 0.963$ [0.873, 1.0]). The red line represents the calculated value without using Monte Carlo simulations. The solid line, the dotted line, and the dashed line represent the 1.25-fold, 2.0-fold and 5.0-fold increase in the AUC ratio according to the FDA classification of DDI magnitudes [649].

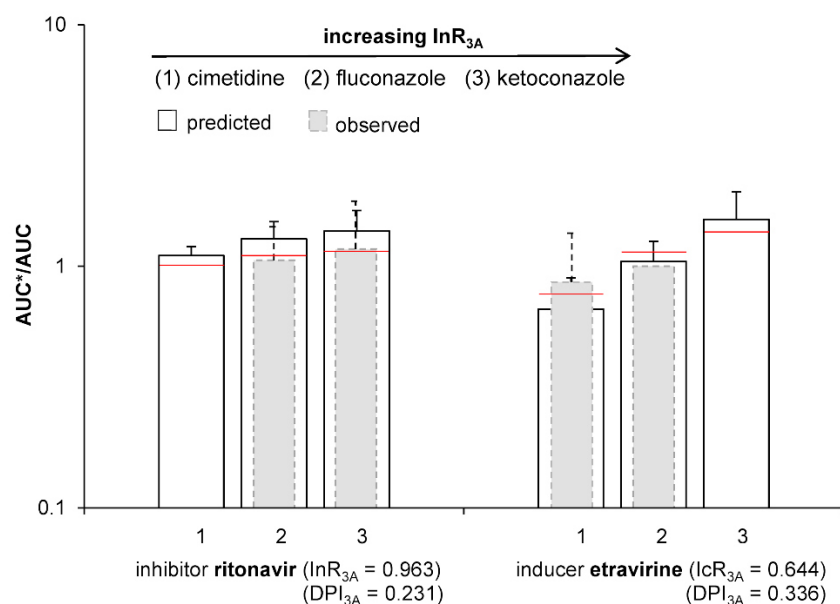


Figure 7.4: Comparison of the predicted (white bars) and observed (grey bars) AUC ratio plus standard deviations for the two victim drugs with intrinsic inhibitory (ritonavir) and inducing (etravirine) properties administered together with the three CYP3A inhibitors cimetidine ($\ln R_{3A} = 0.256$ [0.049, 0.570]), fluconazole ($\ln R_{3A} = 0.700$ [0.403, 0.893]), and ketoconazole ($\ln R_{3A} = 0.943$ [0.823, 1.0]). The red line represents the calculated value without using Monte Carlo simulations.

7.4.5 Prediction of DDIs between tyrosine kinase inhibitors and antiretroviral drugs

Tyrosine kinase inhibitors being highly metabolized by CYP3A (ibrutinib and dasatinib with DPI_{3A} values of 0.971 [0.916, 1.0] and 0.779 [0.524, 1.0]) given with the potent CYP3A inhibitor ritonavir led to strong DDIs, with AUC ratios > 5-fold (Figure 7.5). Considering variability estimated by Monte Carlo simulations, all predicted AUC ratios of ibrutinib given with ritonavir were above 5-fold. Moderate DDIs were predicted for tyrosine kinase inhibitors being intermediately metabolized by CYP3A (lapatinib, nilotinib, and gefitinib with DPI_{3A} values of 0.696 [0.403, 0.936], 0.646 [0.333, 0.895], and 0.534 [0.197, 0.884], respectively), although some AUC ratios were above 5-fold and therefore, categorized as strong DDIs. Tyrosine kinase inhibitors for which CYP3A is a minor pathway (pazopanib, sunitinib, and imatinib with DPI_{3A} values of 0.383 [0.106, 0.700], 0.336 [0.079, 0.661], and 0.301 [0.064, 0.627]) showed weak DDIs when administered with ritonavir, although considering variability, some predicted AUC ratios had a magnitude greater than 2.0-fold, classifying them as moderate DDIs. Sorafenib is almost not metabolized by CYP3A (DPI_{3A} of 0.054 [0.006, 0.391]) and showed no DDI with ritonavir.

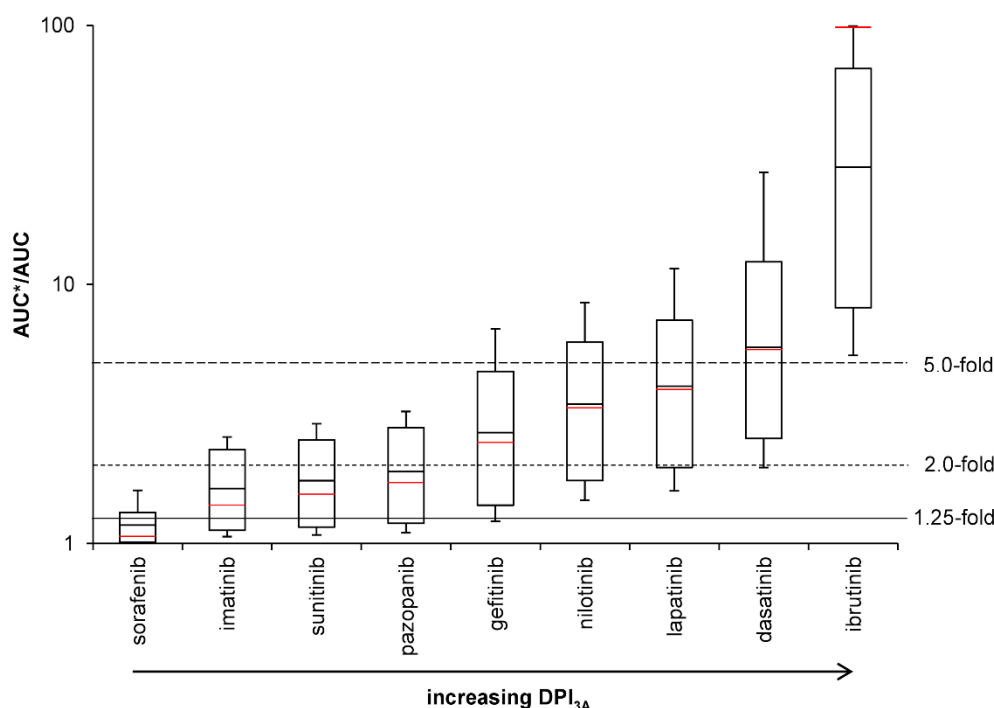


Figure 7.5: DDI magnitudes between tyrosine kinase inhibitors with increasing DPI_{3A} and the potent CYP3A inhibitor ritonavir predicted by running 10,000 Monte Carlo simulations. The solid red line shows the calculated value without using Monte Carlo predictions. The solid line, the dotted line, and the dashed line represent the 1.25-fold, 2.0-fold, and 5.0-fold increases in the AUC ratio, respectively, according to the FDA classification of DDI magnitudes [649].

Results for the tyrosine kinase inhibitors were similar when administered with the moderate inducer etravirine (Figure 7.6). Tyrosine kinase inhibitors being highly or intermediately metabolized by CYP3A showed moderate DDIs when given with etravirine, with some predicted AUC ratios being above 5-fold. Administration of etravirine with imatinib, sunitinib, and pazopanib led to weak DDIs. The combination of sorafenib and etravirine showed no DDI potential.

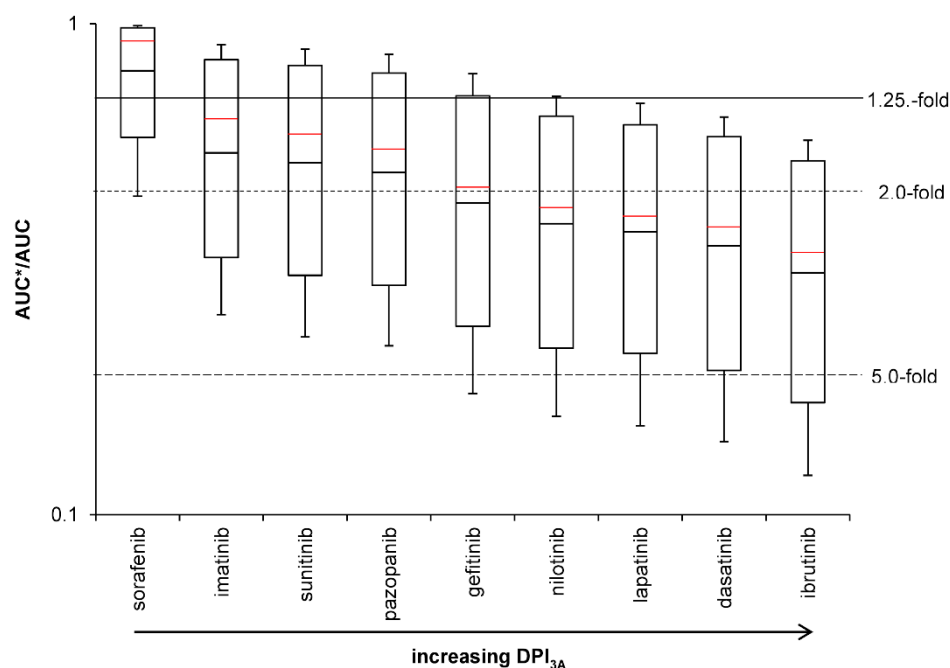


Figure 7.6: DDI magnitudes between tyrosine kinase inhibitors with increasing DPI_{3A} and the moderate CYP3A inducer etravirine predicted by running 10,000 Monte Carlo simulations. The solid red line shows calculated values without using Monte Carlo predictions. The solid line, the dotted line, and the dashed line represent the 1.25-fold, 2.0-fold, and 5.0-fold increase in the AUC ratio, respectively, according to the FDA classification of DDI magnitudes [649].

7.5 Discussion

The management of DDIs involving antiretroviral drugs is often problematic in clinical practice, as guidance on dosing recommendations is only provided for a limited number of evaluated drug combinations. We present a robust and reproducible method to predict uncharacterized DDIs between antiretroviral drugs and comedications. Of interest, the method discriminates between CYP3A substrates likely to be significantly, or else marginally, impacted by CYP3A inhibitors and inducers, and therefore categorizes DDIs according to their magnitude. The method has the potential to support a more rational identification of dose adjustment to overcome DDIs with the perspective to support clinical DDI management in the future. In addition, this approach can help to minimize and rationalize future clinical studies, providing a valuable characterization of the interaction potential. The integration with

modelling techniques such as PBPK will additionally allow to have a comprehensive prediction of DDI magnitude as well as identify drug combination that might require more detailed laboratory and clinical investigations.

The method predicts DDIs based on the degree of metabolism by a specific enzyme such as CYP3A (represented by DPI), and the strength of an inhibitor or inducer (represented by InR and IcR). These parameters can be estimated from existing clinical pharmacokinetic studies and are used, in turn, to estimate uncharacterized DDIs involving antiretroviral drugs. The derived parameters, DPI_{3A} and InR_{3A} / IcR_{3A} , were consistent with the FDA classifications [682]. CYP3A sensitive substrates such as triazolam, midazolam, and tacrolimus had DPI_{3A} values close to 1. Conversely, drugs being partly metabolized by CYP3A, such as zolpidem, had lower DPI_{3A} values and were shown to be less sensitive to CYP3A inhibitors or inducers, because metabolism can still occur through unaffected CYPs. This example highlights how multiple metabolic pathways can modulate the magnitude of DDIs. Furthermore, ritonavir, cobicistat, and ketoconazole were predicted to be strong inhibitors, whereas fluconazole was found to be a moderate inhibitor. The strength of inducers was also correctly predicted, with rifampicin characterized as a strong inducer and etravirine and efavirenz as moderate inducers. Thus, the parameters necessary for the method can be reliably derived from existing clinical DDI studies.

The derived parameters were used subsequently to predict DDIs and were compared against existing clinical DDI studies to assess the predictive performance of the method. All predicted AUC ratios were within 2.0-fold of the observed data, apart from saquinavir and cimetidine. Additionally, 53% and 85% of all predictions fell within the 1.25-fold and 1.5-fold interval (Figure 7.2). The reason for the underprediction of the saquinavir-cimetidine interaction could be that cimetidine is a weaker inhibitor of CYP3A than saquinavir. It is likely that CYP3A is not fully inhibited by cimetidine, thus the inhibitory effect of the protease inhibitor saquinavir adds to the total inhibition effect, while strong CYP3A inhibitors like ketoconazole inhibit the enzyme completely, thus an additive effect by protease inhibitors would not be detectable [360]. Therefore, in the situation of two combined drugs having both the potential to inhibit CYP3A, it is recommended to use the inhibitor ratio (InR) of the stronger inhibitor among the two drugs to obtain a more accurate prediction. In this case, the InR_{3A} of saquinavir should be used to calculate the DDI magnitude between saquinavir and cimetidine leading to a predicted AUC-ratio of 2.23, which is in accordance to the observed one of 2.48 (ratio predicted/observed: 0.90).

Of importance, this method allows to categorize the magnitude of DDIs. DDIs of large magnitude are expected for drugs being highly metabolized by a given enzyme in the presence of strong and moderate inhibitors and inducers of this enzyme (Figure 7.3). Therefore, in this situation, depending on the dose-exposure relationship of the victim drug, dose adjustment and/or close clinical monitoring might be needed unless the drug combination leads to deleterious effects, for instance, the combination of dasatinib or ibrutinib and ritonavir, which consequently should be avoided (Figure 7.5) [683]. Conversely, drugs metabolized by multiple enzymes are expected to be weakly impacted by strong inhibitors or inducers and not affected by moderate and weak perpetrators. Therefore, no dose adjustment would be needed a priori unless the drug has a narrow therapeutic index [683]. Furthermore, our results illustrate that drugs with strong or at least moderate inhibitory or inducing properties on their own metabolism (e.g. ritonavir or etravirine) are minimally impacted by other inhibitors or inducers, as their own effect on CYPs counteracts the effect of other drugs (Figure 7.4).

The strengths of this method are that it can potentially be applied to any given CYP enzyme and for any given DDI, and that results shown for tyrosine kinase inhibitors can be translated to other drug classes. One clinical example would be an HIV-infected patient receiving ritonavir who suffers from hypertension which requires treatment with amlodipine, a calcium channel inhibitor. Amlodipine is metabolized by CYP3A, and therefore an interaction would be expected with ritonavir. To get an idea about the DDI magnitude, the presented approach is used. The package insert usually contains information about known DDIs and can therefore be used to estimate DPI_{3A} of the chosen drug. The package insert of amlodipine contains the information that diltiazem, a strong CYP3A inhibitor [682], increases amlodipine exposure by 60% and other strong CYP3A inhibitors like ketoconazole and ritonavir may increase amlodipine concentration to a greater extent without further details on the potential DDI magnitude and guidance on how to adjust the amlodipine dose to prevent hypotension and edemas [662]. By deriving the inhibitory strength of diltiazem ($\ln R_{3A} = 0.715$ [0.427, 0.898] by Monte-Carlo simulations or 0.802 by single calculation) using an existing midazolam/diltiazem DDI study [678], the fraction of CYP3A-mediated metabolism of amlodipine can be calculated to be 0.464 [0.117, 1.0] by using Monte Carlo simulations or 0.468 by single calculation. The inhibitory strength of ritonavir was 0.963 [0.873, 1.0] by Monte-Carlo simulations or 1 by single calculations has been derived from midazolam/ritonavir DDI studies [665-669]. Both the fraction of amlodipine metabolism mediated by CYP3A and the inhibitory strength of ritonavir were used to calculate the magnitude of the DDI (AUC ratio) using equation 1. The

parameters derived from Monte Carlo simulations or single calculations provided similar DDI predictions. A 90% increase in amlodipine exposure is expected, suggesting a 50% dose reduction would be required when amlodipine is given with ritonavir, which is in agreement with findings from a published DDI study [570]. It should be noted that the decision to adjust the dose should not be based only on the pharmacokinetic change but should also take into account the possibility to monitor the DDI effect, drug-response relationship, and the therapeutic index to safely manage DDIs.

Some limitations should be acknowledged. Perpetrators are never completely selective and therefore affect more than one pathway. Thus, the method cannot distinguish between effects attributed exclusively to the specific CYP enzyme of interest or if the DDI results from a combined effect from other CYPs, uridine diphosphate-glucuronosyltransferases (UGTs) and/or drug transporters. In addition, the method cannot separate effects from different locations (e.g. intestinal vs. hepatic). However, the multiple combined effects of several enzymes and drug transporters and the contribution of different sites to a DDI are accounted for in the prediction, because clinical data of similar DDIs with similar pathways are used. DDIs of drug pairs can be quantified, but in clinical reality subjects may receive concomitantly several drugs, which may interact mutually. The method does not account for the genetic background and comorbidities (e.g. liver cirrhosis), which all can impact DDI magnitudes. PBPK models are necessary to answer these questions, which are highly established in the field of DDI predictions [684, 685]. Our method was verified using the common twofold limit, which might be considered as too permissive for drugs with a narrow therapeutic index [638]. However, the potential underprediction of a DDI would occur only if the inhibitor / inducer of interest alters a pathway other than that of the paradigm perpetrator used to derive the necessary parameters (DPI and $\ln R/\ln R$). It is therefore recommended that DPI and $\ln R/\ln R$ are derived using several perpetrators for the prediction of uncharacterized DDIs involving drugs with a narrow therapeutic index and that results are compared to exclude this possibility.

In conclusion, the developed robust method can minimize and rationalize future clinical studies, providing an effective prediction of DDI magnitudes. Additionally, it has the potential to support a more rational identification of dose adjustment to overcome DDIs, being particularly relevant in an HIV-setting giving the treatment's complexity, high DDI risk, and limited guidance on the management of DDIs. In the future, the method could be extended to other drug classes and prediction of multiple DDIs.

7.6 Appendix

A full deviation of the used equation is provided here. The oral clearance of a drug A is defined as follows:

$$CL_{oral} = \frac{CL_{tot}}{F} = \frac{CL_{hep} + CL_{ren} + CL_{add}}{f_a \times F_G \times F_H}, \quad (1)$$

where CL_{tot} = total clearance, F = bioavailability, CL_{hep} = total hepatic clearance, CL_{ren} = renal clearance, CL_{add} = additional clearance not via liver or kidney, f_a = fraction absorbed, F_G = fraction escaping gut metabolism and F_H = fraction escaping first pass metabolism.

The following assumptions hold true.

- 1) The main route of metabolism is the liver. Renal or other pathways are assumed to be negligible:

$$CL_{ren} = CL_{add} = 0. \quad (2)$$

- 2) The orally administered drug is fully absorbed:

$$f_a = 1. \quad (3)$$

- 3) The well-stirred liver model holds true:

$$CL_{hep} = \frac{Q_H \times CL_{int} \times fu_B}{Q_H + CL_{int} \times fu_B}, \quad (4)$$

$$F_H = \frac{Q_H}{Q_H + CL_{int} \times fu_B}, \quad (5)$$

where Q_H = liver blood flow, CL_{int} = total intrinsic hepatic clearance, fu_B = fraction unbound in blood.

- 4) Unbound concentration in the intracellular space of the liver and the plasma are similar
- 5) The metabolic pathway follows Michaelis-Menten kinetics.
- 6) The intracellular, unbound substrate concentration is below K_M and therefore clearance of the substrate is independent of the dose.

Considering the assumptions and equations 2, 3, 4 and 5, equation 1 changes as follows:

$$CL_{oral} = \frac{\frac{Q_H \times CL_{int} \times fu_B}{Q_H + CL_{int} \times fu_B} + 0 + 0}{1 \times F_G \times \frac{Q_H}{Q_H + CL_{int} \times fu_B}} = \frac{CL_{int} \times fu_B}{F_G}. \quad (6)$$

In the presence of a perpetrator, oral clearance of drug A changes as follows:

$$CL_{oral}^* = \frac{CL_{int}^* \times fu_B}{F_G^*}. \quad (7)$$

where the superscript * stands for in the presence of the perpetrator.

The common metric to assess an interaction of drug A and the perpetrator is the AUC ratio:

$$\frac{AUC^*}{AUC} = \frac{\frac{Dose}{CL_{oral}^*}}{\frac{Dose}{CL_{oral}}} = \frac{CL_{oral}}{CL_{oral}^*} = \frac{\frac{CL_{int} \times fu_B}{F_G}}{\frac{CL_{int}^* \times fu_B}{F_G^*}} = \frac{CL_{int} \times F_G^*}{CL_{int}^* \times F_G}. \quad (8)$$

It is assumed that gut metabolism is not affected by the interaction:

$$\frac{F_G^*}{F_G} = 1. \quad (9)$$

The total intrinsic hepatic clearance depends on enzymes, which metabolize drug A. In this work, we are interested in CYP3A, but the method is general and can potentially be used for all CYP enzymes:

$$CL_{int} = fm_{3A} \times CL_{int} + (1 - fm_{3A}) \times CL_{int}, \quad (10)$$

where fm = fraction metabolized by a certain enzyme.

Now we assume to have a perpetrator only affecting the CYP3A pathway:

$$CL_{int}^* = \frac{fm_{3A} \times CL_{int}}{FR_{3A}} + (1 - fm_{3A}) \times CL_{int}, \quad (11)$$

where FR is the fold reduction by the perpetrator. FR depends on the type of interaction, which can be competitive inhibition (equation 12), mechanism-based inhibition (equation 13) or induction (equation 14):

$$FR_{3A} = 1 + \frac{[I]}{K_i}, \quad (12)$$

$$FR_{3A} = 1 + \frac{k_{inact}^*[I]}{k_{deg}^*(K_{app} + [I])}, \quad (13)$$

$$FR_{3A} = \frac{1}{1 + \frac{IndMax*[I]}{[I] + IC_{50}}}, \quad (14)$$

where $[I]$ = inhibitor concentration at steady state, K_i = inhibition constant, k_{deg} = enzyme degradation rate, k_{inact} = inactivation rate of an enzyme for mechanism-based inhibition, K_{app} = apparent enzyme inhibition constant for mechanism-based inhibition (concentration of the inhibitor associated with half maximum inactivation rate), $IndMax$ = maximum fold of induction and IC_{50} = half maximum inhibitory concentration.

Considering equation 9, 10 and 11, the AUC ratio can be written as follows:

$$\frac{AUC^*}{AUC} = \frac{CL_{int}}{CL_{int}^*} = \frac{CL_{int}}{\frac{fm_{3A} \times CL_{int}}{FR_{3A}} + (1 - fm_{3A}) \times CL_{int}} = \frac{CL_{int}}{CL_{int} \times \left(\frac{fm_{3A}}{FR_{3A}} + (1 - fm_{3A}) \right)} = \frac{1}{\frac{fm_{3A}}{FR_{3A}} + 1 - fm_{3A}}. \quad (15)$$

The inhibitor ratio (InR) was defined by Hisaka *et al.* [686] for competitive inhibition, but can be used for mechanism-based inhibition as well:

$$InR_{3A} = 1 - \frac{1}{1 + \frac{[I]}{K_i}} = 1 - \frac{1}{FR_{3A}}. \quad (16)$$

The inducer ratio (IcR) can be defined in a similar way as the inhibitor ratio, but the reciprocal needs to be used:

$$IcR_{3A} = 1 - FR_{3A}. \quad (17)$$

FR in equation 15 can now be replaced by InR (equation 16) and IcR (equation 17). Because the method cannot distinguish between different inhibited enzymes and transporters, fm_{3A} needs to be replaced by the broadly defined fraction of disposition pathway altered by the perpetrator (DPI_{3A}).

For CYP3A inhibitors, the AUC-ratio can be calculated according to equation 18 and for inducers according to equation 19:

$$\frac{AUC^*}{AUC} = \frac{1}{\frac{DPI_{3A}}{FR_{3A}} + (1 - DPI_{3A})} = \frac{1}{1 - DPI_{3A} \left(1 - \frac{1}{FR_{3A}} \right)} = \frac{1}{1 - DPI_{3A} \cdot InR_{3A}}, \quad (18)$$

$$\frac{AUC^*}{AUC} = \frac{1}{\frac{DPI_{3A}}{1 - IcR_{3A}} + (1 - DPI_{3A})}. \quad (19)$$

Chapter 8:

General Discussion

8. General Discussion

8.1	The impact of aging on drug pharmacokinetics is marginal	Page 223
8.2	Can clinical pharmacology for elderly individuals do any better?	Page 225
8.3	Pharmacodynamic changes with advanced aging	Page 228
8.4	Conclusion and future perspective	Page 230

Aging people living with HIV (PLWH) are generally excluded from clinical studies leading to a knowledge gap how antiretroviral drug pharmacokinetics and drug-drug interaction (DDI) magnitudes are impacted by advanced aging. Clinically observed data in combination with modelling and simulation elucidated marginal age-related pharmacokinetic changes of antiretroviral drugs and no impact of advanced aging on DDI magnitudes. Thus, antiretroviral doses and the clinical management of DDIs can a priori be similar in aging men and women living with HIV in the absence of severe comorbidities.

8.1 The impact of aging on drug pharmacokinetics is marginal

Effective antiretroviral therapies have led to the same life expectancy of PLWH than the general population [38, 39], but no current HIV treatment can eradicate the virus and thus, HIV therapy is a life-long treatment. In 2018, 37.9 million people lived globally with HIV and 16% were older than 50 years [1]. The number is projected to increase in the future showing the importance to establish guidelines for safe and effective HIV and geriatric care in aging PLWH [57]. Most product labels of antiretrovirals give no dose recommendations for the elderly [76-83], except for atazanavir [85] for which doses do not need to be adjusted based on the age of the treated individual. In general, clinical data in this vulnerable population are lacking leading to missing guidance whether dose adjustment is necessary based on the age of the treated PLWH.

Age-related pharmacokinetic changes of antiretrovirals were found to be marginally, considering the large therapeutic index of the current first-line treatment [578]. Thus, a dose adjustment would a priori not be necessary in aging male and female PLWH in the absence of severe comorbidities. The results presented in this thesis are in line with four studies that investigated age-related pharmacokinetic changes of antiretrovirals in aging PLWH. The first clinical study was a pilot study investigating the pharmacokinetics of two common antiretroviral regimens in 12 PLWH aged 55 to 65 years. Dumond *et al.* found marginal alterations in drug exposure within the expected interindividual variability for tenofovir, efavirenz, and atazanavir. Emtricitabine and ritonavir exposures were increased by 19% to 78% in two different groups, demonstrating high variability [71]. A limitation of this pilot study is the small sample size and the exclusion of PLWH at least 65 years. In the second study, single sample time points from 2,447 PLWH aged 20 to 80 years, who participated in the UK Collaborative HIV Cohort Study, were analyzed. In agreement with the first study, plasma concentrations of protease inhibitors (e.g. lopinavir,

saquinavir, and atazanavir) were increased and concentrations of non-nucleoside reverse transcriptase inhibitors (e.g. efavirenz) were not affected by the age of the studied participants [73]. However, most of the samples came from PLWH aged 20 to 50 years and therefore, an extrapolation to the elderly is hardly possible. In a third clinical study, Elliot *et al.* investigated dolutegravir exposure in PLWH aged 60 to 79 years, which was marginally increased by 8% in the elderly compared with young controls [72]. The fourth study investigated renally excreted antiretrovirals in young (20 to 49 years) and elderly (65 to 74 years) PLWH by a physiologically based pharmacokinetic (PBPK) model and found on average a 40%, 42%, and 48% increase in drug exposure for emtricitabine, lamivudine, and tenofovir, respectively [75].

In contrast to the aforementioned clinical studies, this thesis describes for the first time antiretroviral drug exposure for all currently recommended antiretrovirals in non-frail PLWH at least 55 years, who are representative for the majority of elderly PLWH as observed by the French HIV Cohort [564]. The combination of clinically observed data with modelling and simulation allowed to analyze aging as a continuous process. Furthermore, age-related pharmacokinetic changes could be understood mechanistically; therefore, allowing a general model-based conclusion of the conducted clinical studies. The linear increase in drug exposure with an average rate of 0.9% per year throughout adulthood was caused by reduced drug elimination resulting from the progressive decline of hepatic and renal blood flow and the glomerular filtration rate with advanced aging. Age-related changes of drug pharmacokinetics are independent of drug characteristics and thus, are similar for antiretroviral and non-HIV drugs [512, 578]. Therefore, results of this thesis are broadly applicable and because age-related changes in drug exposure are independent of the drug, the general conclusion is valid for future therapies.

The cutting-edge concept that pharmacokinetic alterations in the elderly depend only on physiological changes and are independent of drug characteristics [512] can probably not be translated to other special populations. As soon as enzyme and transporter activities change compared with healthy, young adults (e.g. in children [687, 688], in pregnant women [555], in hepatic [332], and renal impairment [333]), the difference in drug clearance between the investigated special population and the control group will depend on the enzyme(s) metabolizing the drug of interest.

8.2 *Can clinical pharmacology for elderly individuals do any better?*

Clinical pharmacology of elderly individuals faces several challenges. Firstly, conducted clinical studies have a selection bias towards more healthy individuals. Secondly, longitudinal data in the same subject are missing and thus, aging is often treated as a discrete (young group vs. elderly group) and not as a continuous variable in statistical analysis of the clinically observed data. Thirdly, there is a huge time gap between the drug entering the market and first study results being published in the scientific literature by mostly academic groups. Fourthly, the full range of prescribed drugs and individuals requiring drug treatment cannot feasible or pragmatical be studied

Aging individuals take most of the prescribed drugs [378] and have the highest prevalence for DDIs [95], but the elderly are generally excluded from clinical studies for pragmatical and ethical concerns [122]. If elderly subjects are included, there is usually a clear selection bias towards “apparently” healthy aged study participants [379, 689] and thus, conducted clinical studies are too restrictive, not covering the entire range of elderly individuals being frail or suffering from highly prevalent age-related comorbidities such as severe renal impairment stage 4 to 5. Therapeutic drug monitoring in the elderly might help to measure real-life plasma concentrations of drugs, covering the entire variability of the aged patient population. One strength of the clinical study described in Chapter 6 is the inclusion of aging PLWH at least 55 years who had a declined kidney function (i.e. the glomerular filtration rate was 65.6 ± 19.2 mL/min/1.73m²) and common comorbidities (i.e. hypertension) and thus, being representative of the majority of elderly PLWH [564].

Longitudinal studies to investigate the impact of aging on drug pharmacokinetics in the same individual are entirely missing. Instead, current clinical studies usually compare the pharmacokinetics between a young and an elderly group of subjects. There are three concerns: Firstly, what is the definition and the starting age for being “elderly”? The studied “elderly” group often starts at the age of 65 years being the age of retirement in most Western Countries; however, there is no pharmacological or clinical definition for an “elderly” individual [55]. Studies presented in this thesis assessed when aging leads to differences in the pharmacokinetics that are higher than expected from the interindividual variability. Compared with a 20 years old, this was the case at the age of 55 years for antiretroviral and non-HIV drugs [512, 578]. If the young group in the clinical study would have a mean age older than 20 years, the start age for the

“elderly” group would need to be higher, because aging is a continuous process [58]. Secondly, calculating the ratio between two group can be impacted by the interindividual variability that is higher in the elderly compared with young individuals [690]. Thirdly, statistical differences are assessed by comparing data from the two investigated age groups by a parametric t-test, which has a limited meaning, because in contrast to for instance sex, aging is a continuous process and not a discrete variable. The PBPK approach, verified by the clinically observed data in young and elderly subjects for a certain drug, extrapolates pharmacokinetics across adulthood and allows to investigate the continuous effect of aging on the pharmacokinetics of the drug of interest [512].

The regulations to conduct clinical trials are strict before drug approval, because firstly safety and effectiveness of a novel agent need to be proven. After drug approval, the pharmaceutical industry has often no interest to invest more money in clinical trials for special populations unless there could be a potential novel indication. Therefore, clinical studies in special populations are often conducted by academic groups and networks like for instance The Pharmacokinetic and Clinical Observations in PeoPle Over fifty (POPPY) study [691] to investigate the effect of aging on antiretroviral treatment in elderly PLWH. It needs time to design the clinical studies, establish networks between different study sites, include patients, analyze the clinically observed data, and publish the results. There is a huge time gap between the drug entering the market after successful approval by the health authorities and the first published study in a special population. After market access of a novel drug, there are two possibilities to give the drug to special populations in clinical practice: Firstly, the approved drug is given “off-label” as drug labels do usually not contain enough information regarding dosing recommendations for special population, demonstrating the lack of clinically available data. Clinicians are faced with the challenge to adjust the dose based on empirical “guesses” such as the 25 to 50% dose reduction in the elderly [502]. However, if the mechanism behind those rules of thumbs are not completely understood, it remains challenging to extrapolate those to every patient and every therapy. In case of severe side effects, those can be reported to the drug safety of the relevant pharmaceutical company, but again it will take time till the information circulates back to the clinics and reaches other patients. Secondly, important therapies might be denied for special populations if the prescribing physician follows a more conservative approach to wait until clinically observed data are publicly available. Both scenarios could harm patients. Therefore, it is proposed to study the safety and efficacy of drugs in special population

at a later stage in clinical development in a rigorously controlled environment to guide dosing recommendations in the drug label at the time of drug approval.

However, even if more clinical studies would be conducted in the elderly in the future, it would still not be feasible or pragmatical to study every single drug or drug combination in the elderly. In clinical practice, more drug combinations are prescribed than the usual paradigm substrates, strong inhibitors/inducers of enzymes and transporters, that are used in clinical studies before drug approval. It is difficult to scale DDI magnitudes obtain for a strong inhibitor in young adults to a moderate inhibitor of the same enzyme in an elderly patient without having further data. Modelling and simulation provides the possibility to predict DDI scenarios for moderate perpetrator when being appropriately verified with existing clinical data (e.g. with DDIs involving strong inhibitors/inducers) [387]. Thus, model-informed drug development is important to support the clinical care of patients. The few clinical studies that need to be conducted can verify predictive models, which can subsequently be used to explore unknown clinical scenarios of interest [118]. One example for model-informed drug development is the study investigating the impact of aging on DDI magnitudes in this thesis (Chapter 6). A clinical study in aging PLWH at least 55 years was conducted to assess DDI magnitudes between antiretrovirals and commonly prescribed cardiovascular agents [577]. The study was underpowered, because not enough patients could be included. Nevertheless, the clinical data obtained in this study represent real-life plasma concentrations from aging PLWH representative for the majority of elderly PLWH [564] and described for the first time DDI magnitudes of antiretrovirals in the elderly. The data served for the verification of the PBPK approach to assess the predictive potential to simulate DDIs in the elderly. Having a verified model, DDIs that were only investigated in young adults, including moderate inhibitors such as nilotinib or etravirine, could be extrapolated to the elderly. The modelling approach allowed for a virtual longitudinal study; thus, DDI magnitudes could be investigated across the entire adult lifespan. Therefore, the combination of the limited clinical DDI data in aging PLWH for a couple of DDI scenarios with modelling and simulation helped to understand that DDI magnitudes are not impacted by advanced aging and support the clinical management of DDIs in the elderly [692].

Another challenge in clinical practice is the huge interindividual variability that can potentially not be covered in clinical trials even if more studies would be conducted. The same dose of a drug can lead to an inefficacious or unsafe therapy in different patients. It is also necessary to account for the patient's

individual lifestyle such as smoking and genotypes to fully assess and understand the pharmacokinetic variability seen in clinical practice. With advanced aging, interindividual variability increases because of frailty [690]. Frailty is defined as the cumulative physiological alterations and the subsequent changes in health status after a minor stressor event [693]. PLWH are considered to be frail, but the quantification of frailty is difficult in this context, because antiretroviral therapy is so effective [694]. Frail individuals, despite living with HIV, were not included in our conducted clinical study [74, 577]. There are reports indicating that the association between age and altered drug metabolism and elimination are stronger with frailty [695]. More studies are warranted to study the combined effect of aging and frailty on drug pharmacokinetics and compare them to the results obtained in this thesis for aging alone [512, 578].

Taken together, the studies in this thesis support the clinical pharmacology for elderly individuals. Firstly, with the inclusion of aging PLWH at least 55 years, having a declined kidney function and common comorbidities, real-life plasma concentrations from representative elderly PLWH [564] were obtained for the first time. Secondly, modelling and simulation helped to extrapolate the limited clinical data obtained in two distinct age groups across adulthood. Thirdly, the PBPK approach determined physiological alterations with advanced aging as the cause for age-related pharmacological changes. Generally, doses would need to be reduced by 25% at 60 years, by 50% at 75 years, and by 75% at 95 years depending on the therapeutic index of the drug of interest. As being independent of drug characteristics, this rule can be applied to future drugs after marketing authorization and reduces the publication time gap.

8.3 Pharmacodynamic changes of antiretroviral drugs with advanced aging

Aging can not only affect pharmacokinetic processes, but also the pharmacodynamics of a drug. Clinical studies regarding the effect of aging on antiretroviral pharmacodynamics are scarce. Studies presented in this thesis focused mainly on drug pharmacokinetics, which are essential to establish the dose-response-relationship. Furthermore, intracellular and unbound concentrations are important for target binding and the effect of the drug.

As drug targets are often not in plasma, it is important to understand age-related changes in intracellular drug exposure. Intracellular concentration of tenofovir diphosphate (after administration of tenofovir

disoproxil fumarate) and emtricitabine diphosphate were measured in peripheral blood mononuclear cells of 12 PLWH aged 55 to 65 years. Intracellular tenofovir diphosphate exposure was increased by 57.7% and emtricitabine exposure was decreased by 22.4% compared to historical controls in young PLWH [71]. The age-related changes in intracellular drug exposure are contradictory for both investigated drugs. As more clinical data are missing, a common age-related trend like for plasma exposure cannot be given [578]. In the future, more studies investigating intracellular antiretroviral drug concentrations in the elderly are warranted. A whole-body PBPK model used in this thesis [118] could help to understand age-related changes in intracellular concentration mechanistically that could lead to pharmacodynamic alterations with advanced aging. However, the PBPK model needs to be verified against existing clinical data, which are currently not available.

Considering the free-binding hypothesis, only the unbound drug can bind to a target and lead to a pharmacodynamic action [696]. Albumin concentration declines by 1.5% in each age decade in elderly individuals, who have no severe illness or malnutrition, that can both substantially affect albumin levels [58]. The age-related changes of albumin are unlikely to be of clinical relevance [697]. The fraction unbound of several benzodiazepines (e.g. midazolam, lorazepam, oxazepam, and temazepam) [499, 698], warfarin [699, 700], and phenytoin [701] was found to be similar between elderly and young individuals. However, in a different study the fraction unbound of phenytoin was statistically significantly increased in the elderly (12.8% vs. 11.1%), but the increase was of no clinical relevance [702]. The free fraction of valproic acid increased from 6.4% in adults aged 20 to 25 years to 10.7% in adults aged 60 to 88 years [703]. But the unbound concentration of valproic acid was found to be elevated with increasing plasma concentrations in young subjects and thus might be more explained by the general age-related increase in drug exposure [512] rather than changes in the albumin concentration [704]. Alpha-acid glycoprotein, important for the plasma binding of protease inhibitors, is unaltered in the elderly [58]. Taken together, it is unlikely that age-related changes in free antiretroviral concentration would lead to pharmacodynamic alterations. As the targets of antiretrovirals are intracellular, it is also important to consider the passive and active uptake of drugs into cells and the intracellular drug binding.

Once the unbound antiretroviral drug enters the cell, it can bind to the viral target and suppresses the HI virus. The molecular structure of viral proteins such as the reverse transcriptase, the HIV protease, and the HIV integrase, are unlikely to be changed with advanced aging of the human host. It can be

assumed that the binding affinity between antiretrovirals and viral proteins is not altered based on the age of the treated PLWH. Transcription and translation could be altered with advanced aging in the human host leading to an altered level of viral proteins. Horvath & Levine demonstrated that epigenetic methylation patterns in the blood and the brain of PLWH corresponded to accelerated aging of at least five years [705]. These epigenetic alterations as well as age-related changes in the histone methylation pattern potentially affect the transcription process [706]. The age-related effects on the transcription and translation would lead presumably to less viral protein and therefore to an enhanced pharmacodynamic effect.

Pharmacodynamic studies in elderly PLWH are barely conducted. In the French HIV Cohort Study, suppression of the HIV virus was similar between 16,436 PLWH aged 50 to 74 years and 572 PLWH at least 75 years [88], indicating that pharmacodynamic effect of antiretrovirals are not affected with advanced aging to a clinically relevant extend. Pharmacodynamic alterations of comedications need careful considerations [502] to support the overall care of elderly PLWH beyond HIV.

8.4 Conclusion and future perspective

PLWH are aging with high prevalence for age-related comorbidities [93], polypharmacy [92], and consequently an increased risk for DDIs [94]. To support the clinical care of elderly PLWH, it is necessary to investigate the continuous effect of aging of drug pharmacokinetics and DDI magnitudes.

The studies presented in this thesis demonstrated that age-related pharmacokinetic changes are driven by a decline in drug clearance of maximal 1.7-fold difference across adulthood, which itself is caused by the physiological decline of the hepatic and renal blood flow as well as of the glomerular filtration rate, but is independent of drug characteristics [512, 578]. Given the high therapeutic window of the current first line antiretroviral treatment, dose adjustment would a priori not be necessary in aging male and female PLWH. Dose adjustment for non-HIV drugs would depend on the therapeutic index of the drug of interest. Generally, the “start low and go slow” strategy is recommended when starting drug treatment in the elderly. Drug dose should be reduced by 25% at the age of 60 years, by 50% at the age of 75 years, and by 75% at the age of 95 years compared with young individuals.

DDI magnitudes were not affected by advanced aging regardless of the involved drugs or DDI mechanism [692]. Thus, the clinical management of a given DDI (i.e. to reduce or increase the dose to overcome a drug inhibition or induction) can a priori be similar in aging men and women.

The conducted studies describe pharmacokinetic alterations in aging individuals, who had a declined kidney function (i.e. a reduced glomerular filtration rate) and common comorbidities (i.e. hypertension), and thus being representative for the majority of aging PLWH [564]. Future clinical studies are warranted to investigate the combined effects of aging and frailty or severe comorbidities on the physiology, pharmacokinetics, and DDI magnitudes.

Aging of PLWH is a global phenomenon [1] and the number of PLWH at least 50 years is estimated to increase especially in Eastern and Southern Africa [44]. Ethnicity did not impact the age-related decrease in drug clearance, driving age-related pharmacokinetic changes; however, only clinical data in Asians were found [578]. Clinical studies analyzing the age-related pharmacokinetic and pharmacodynamic changes of antiretrovirals in other ethnic groups than Europeans, especially in Africans, are highly needed to support the care of elderly PLWH globally.

Pharmacodynamic changes with advanced aging need careful consideration when prescribing treatments in the elderly and giving recommendations to adjust drug regimens. Pharmacokinetic predictions can be linked to pharmacodynamic models using the PBPK approach [381]; however, because of a lack of understanding the molecular mechanisms driving pharmacodynamic effects, these models are often empirical rather than mechanistic. Furthermore, the effect of aging on these molecular mechanisms is crucial to understand age-dependent pharmacodynamic alterations. In the future more pharmacodynamic studies in aging PLWH are warranted.

Intracellular antiretroviral drug concentrations are usually not obtained in clinical studies and thus, knowledge regarding the passive and active uptake of antiretrovirals into cells remains sparse. More studies are warranted in the future to understand age-dependent changes of the intracellular drug concentrations driving the pharmacodynamic effect, also for preexposure prophylaxes.

With the “graying” of the HIV epidemics, the clinical care of PLWH needs to be merged with geriatric care. Virologic suppression and antiretroviral management remain important for safe and effective HIV therapy, but geriatric screening including amongst others an assessment of frailty will become more and more important to support the overall care of aging PLWH beyond HIV [57]. Guidelines for geriatric care to support HIV clinicians will become more important in the future and need to be properly implemented.

Overall, the studies reported in this thesis support antiretroviral and comorbidity treatments in aging male and female PLWH in the absence of severe comorbidities.

References

1. **UNAIDS.** Global HIV & AIDS statistics - 2019 fact sheet. 2019. Available from: <https://www.unaids.org/en/resources/fact-sheet>. Accessed on 10/10/2019.
2. **UNAIDS.** Report on the global HIV/AIDS epidemic. 2000. Available from: http://data.unaids.org/pub/report/2000/2000_gr_en.pdf. Accessed on 13/12/2019.
3. **Jaffe HW, Bregman DJ, & Selik RM.** Acquired immune deficiency syndrome in the United States: the first 1,000 cases. *Journal of Infectious Diseases*, **1983**. 148(2): 339-345.
4. **Palmisano L & Vella S.** A brief history of antiretroviral therapy of HIV infection: success and challenges. *Annali dell'Istituto superiore di sanità*, **2011**. 47: 44-48.
5. **Zhang JL & Crumpacker C.** Eradication of HIV and cure of AIDS, now and how? *Frontiers in Immunology*, **2013**. 4(337): 1-9.
6. **Weiss RA.** HIV and AIDS: looking ahead. *Nature Medicine*, **2003**. 9(7): 887-891.
7. **Flexner C.** Antiretroviral agents and treatment of HIV infection, in Goodman and Gilman's the Pharmacological Basis of Therapeutics. **2018**, New York: McGraw Hill. p. 1623-1663.
8. **Bukrinsky MI.** HIV life cycle and inherited co-receptors. Encyclopedia of Life Science. **2014**: John Wiley & Sons Ltd.
9. **Turner BG & Summers MF.** Structural biology of HIV. *Journal of Molecular Biology*, **1999**. 285(1): 1-32.
10. **Gelderblom HR, Hausmann EH, Özel M, Pauli G, & Koch MA.** Fine structure of human immunodeficiency virus (HIV) and immunolocalization of structural proteins. *Virology*, **1987**. 156(1): 171-176.
11. **Wilén CB, Tilton JC, & Doms RW.** HIV: cell binding and entry. *Cold Spring Harbor Perspectives in Medicine*, **2012**. 2(8): a006866.
12. **Walker BD & Xu GY.** Unravelling the mechanisms of durable control of HIV-1. *Nature Reviews Immunology*, **2013**. 13(7): 487-498.
13. **Telesnitsky A & Goff S.** Reverse transcriptase and the generation of retroviral DNA, in Retroviruses. **1997**, Cold Spring Harbor Laboratory Press: Cold Spring Harbor, New York.
14. **Jayappa KD, Ao Z, & Yao X.** The HIV-1 passage from cytoplasm to nucleus: the process involving a complex exchange between the components of HIV-1 and cellular machinery to access nucleus and successful integration. *International Journal of Biochemistry and Molecular Biology*, **2012**. 3(1): 70-85.
15. **Hindmarsh P & Leis J.** Retroviral DNA integration. *Microbiology and Molecular Biology Reviews*, **1999**. 63(4): 836-843.
16. **Darke PL, Nutt RF, Brady SF, Garsky VM, Ciccarone TM, Leu C-T, Lumma PK, Freidinger RM, Veber DF, & Sigal IS.** HIV-1 protease specificity of peptide cleavage is sufficient for processing of gag and pol polyproteins. *Biochemical and Biophysical Research Communications*, **1988**. 156(1): 297-303.
17. **Sayer JM, Agniswamy J, Weber IT, & Louis JM.** Autocatalytic maturation, physical/chemical properties, and crystal structure of group N HIV-1 protease: Relevance to drug resistance. *Protein Science*, **2010**. 19(11): 2055-2072.
18. **Modrow S, Falke D, Truyen U, & Schätzl H.** Molecular virology. **2013**: Springer.
19. **Erb P, Battegay M, Zimmerli W, Rickenbach M, & Egger M.** Effect of antiretroviral therapy on viral load, CD4 cell count, and progression to acquired immunodeficiency syndrome in a community human immunodeficiency virus-infected cohort. *Archives of Internal Medicine*, **2000**. 160(8): 1134-1140.

20. **Pau AK & George JM.** Antiretroviral therapy: current drugs. *Infectious Disease Clinics*, **2014**. 28(3): 371-402.
21. **Anderson PL, Kakuda TN, & Lichtenstein KA.** The cellular pharmacology of nucleoside-and nucleotide-analogue reverse-transcriptase inhibitors and its relationship to clinical toxicities. *Clinical Infectious Diseases*, **2004**. 38(5): 743-753.
22. **Tressler R & Godfrey C.** NRTI backbone in HIV treatment. *Drugs*, **2012**. 72(16): 2051-2062.
23. **Merluzzi VJ, Hargrave KD, Labadia M, Grozinger K, Skoog M, Wu JC, Shih C-K, Eckner K, Hattox S, & Adams J.** Inhibition of HIV-1 replication by a nonnucleoside reverse transcriptase inhibitor. *Science*, **1990**. 250(4986): 1411-1413.
24. **Adams J, Patel N, Mankaryous N, Tadros M, & Miller CD.** Nonnucleoside reverse transcriptase inhibitor resistance and the role of the second-generation agents. *Annals of Pharmacotherapy*, **2010**. 44(1): 157-165.
25. **Feng M, Wang D, Grobler JA, Hazuda DJ, Miller MD, & Lai M-T.** In vitro resistance selection with doravirine (MK-1439), a novel nonnucleoside reverse transcriptase inhibitor with distinct mutation development pathways. *Antimicrobial Agents and Chemotherapy*, **2015**. 59(1): 590-598.
26. **Hare S, Vos AM, Clayton RF, Thuring JW, Cummings MD, & Cherepanov P.** Molecular mechanisms of retroviral integrase inhibition and the evolution of viral resistance. *Proceedings of the National Academy of Sciences*, **2010**. 107(46): 20057-20062.
27. **Flexner C.** HIV-protease inhibitors. *New England Journal of Medicine*, **1998**. 338(18): 1281-1293.
28. **Jones A.** HIV treatment. Types of antiretroviral medications. 2019. Available from: <http://www.aidsmap.com/about-hiv/types-antiretroviral-medications>. Accessed on 15/12/2019.
29. **Gandhi M & Gandhi RT.** Single-pill combination regimens for treatment of HIV-1 infection. *New England Journal of Medicine*, **2014**. 371(3): 248-259.
30. **Lieberman-Blum SS, Fung HB, & Bandres JC.** Maraviroc: a CCR5-receptor antagonist for the treatment of HIV-1 infection. *Clinical Therapeutics*, **2008**. 30(7): 1228-1250.
31. **Chong H, Yao X, Zhang C, Cai L, Cui S, Wang Y, & He Y.** Biophysical property and broad anti-HIV activity of albuvirtide, a 3-maleimidopropionic acid-modified peptide fusion inhibitor. *PloS One*, **2012**. 7(3): 1-10.
32. **Bruno CJ & Jacobson JM.** Ibalizumab: an anti-CD4 monoclonal antibody for the treatment of HIV-1 infection. *Journal of Antimicrobial Chemotherapy*, **2010**. 65(9): 1839-1841.
33. **Hardy H & Skolnik PR.** Enfuvirtide, a new fusion inhibitor for therapy of human immunodeficiency virus infection. *Pharmacotherapy: The Journal of Human Pharmacology and Drug Therapy*, **2004**. 24(2): 198-211.
34. **Rathbun RC & Rossi DR.** Low-dose ritonavir for protease inhibitor pharmacokinetic enhancement. *Annals of Pharmacotherapy*, **2002**. 36(4): 702-706.
35. **Shah BM, Schafer JJ, Priano J, & Squires KE.** Cobicistat: a new boost for the treatment of human immunodeficiency virus infection. *Pharmacotherapy: The Journal of Human Pharmacology and Drug Therapy*, **2013**. 33(10): 1107-1116.
36. **Battegay M & Ryom L.** European AIDS Clinical Society Guidelines Version 10.0. 2019. Available from: https://www.eacsociety.org/files/2019_guidelines-10.0_final.pdf. Accessed on 15/12/2019.

37. **McCormack S, Dunn DT, Desai M, Dolling DI, Gafos M, Gilson R, Sullivan AK, Clarke A, Reeves I, & Schembri G.** Pre-exposure prophylaxis to prevent the acquisition of HIV-1 infection (PROUD): effectiveness results from the pilot phase of a pragmatic open-label randomised trial. *The Lancet*, **2016**. 387(10013): 53-60.
38. **Trickey A, May MT, Vehreschild J, Obel N, Gill MJ, Crane HM, Boesecke C, Patterson S, Grabar S, & Cazanave C.** Survival of HIV-positive patients starting antiretroviral therapy between 1996 and 2013: a collaborative analysis of cohort studies. *The Lancet HIV*, **2017**. 4(8): e349-e356.
39. **Gueler A, Moser A, Calmy A, Günthard HF, Bernasconi E, Furrer H, Fux CA, Battegay M, Cavassini M, & Vernazza P.** Life expectancy in HIV-positive persons in Switzerland: matched comparison with general population. *AIDS*, **2017**. 31(3): 427-436.
40. **Swiss HIV Cohort Study.** Current status. 2017. Available from: <http://www.shcs.ch/232-current-status>. Accessed on 10/10/2019.
41. **Wing EJ.** The aging population with HIV infection. *Transactions of the American Clinical and Climatological Association*, **2017**. 128: 131-144.
42. **Smit M, Brinkman K, Geerlings S, Smit C, Thyagarajan K, van Sighem A, de Wolf F, & Hallett TB.** Future challenges for clinical care of an ageing population infected with HIV: a modelling study. *The Lancet Infectious Diseases*, **2015**. 15(7): 810-818.
43. **World Health Organisation.** Life expectancy increased by 5 years since 2000, but health inequalities persist. 2016. Available from: <https://www.who.int/en/news-room/detail/19-05-2016-life-expectancy-increased-by-5-years-since-2000-but-health-inequalities-persist>. Accessed on 28/09/2019.
44. **Autenrieth CS, Beck EJ, Stelzle D, Mallouris C, Mahy M, & Ghys P.** Global and regional trends of people living with HIV aged 50 and over: Estimates and projections for 2000–2020. *PloS One*, **2018**. 13(11): 1-11.
45. **Centers for Disease Control and Prevention.** HIV and older Americans. 2019. Available from: <https://www.cdc.gov/hiv/group/age/olderamericans/index.html>. Accessed on 10/10/2019.
46. **Guaraldi G, Orlando G, Zona S, Menozzi M, Carli F, Garlassi E, Berti A, Rossi E, Roverato A, & Palella F.** Premature age-related comorbidities among HIV-infected persons compared with the general population. *Clinical Infectious Diseases*, **2011**. 53(11): 1120-1126.
47. **Önen NF, Overton ET, Seyfried W, Stumm ER, Snell M, Mondy K, & Tebas P.** Aging and HIV infection: a comparison between older HIV-infected persons and the general population. *HIV clinical trials*, **2010**. 11(2): 100-109.
48. **Tseng A, Szadkowski L, Walmsley S, Salit I, & Raboud J.** Association of age with polypharmacy and risk of drug interactions with antiretroviral medications in HIV-positive patients. *Annals of Pharmacotherapy*, **2013**. 47(11): 1429-1439.
49. **Morgan EE, Iudicello JE, Weber E, Duarte NA, Riggs PK, Delano-Wood L, Ellis R, Grant I, & Woods SP.** Synergistic effects of HIV infection and older age on daily functioning. *Journal of Acquired Immune Deficiency Syndromes*, **2012**. 61(3): 341-348.
50. **Chirch LM, Hasham M, & Kuchel GA.** HIV and aging: a clinical journey from Koch's postulate to the chronic disease model and the contribution of geriatric syndromes. *Current Opinion in HIV and AIDS*, **2014**. 9(4): 405-411.
51. **Friis-Møller N, Reiss P, Sabin C, Weber R, Monforte A, El-Sadr W, Thiebaut R, De Wit S, Kirk O, Fontas E, Law M, Phillips A, & Lundgren J.** Class of antiretroviral drugs and the risk of myocardial infarction. *The New England Journal of Medicine*, **2007**. 356(17): 1723-1735.

52. **Calza L, Colangeli V, Manfredi R, Bon I, Re MC, & Viale P.** Clinical management of dyslipidaemia associated with combination antiretroviral therapy in HIV-infected patients. *Journal of Antimicrobial Chemotherapy*, **2016**. 71(6): 1451-1465.
53. **Mocroft A, Lundgren JD, Ross M, Fux CA, Reiss P, Moranne O, Morlat P, Monforte A, Kirk O, & Ryom L.** Cumulative and current exposure to potentially nephrotoxic antiretrovirals and development of chronic kidney disease in HIV-positive individuals with a normal baseline estimated glomerular filtration rate: a prospective international cohort study. *The Lancet HIV*, **2016**. 3(1): e23-e32.
54. **Sabin CA & Reiss P.** Epidemiology of ageing with HIV: what can we learn from cohorts? *AIDS*, **2017**. 31(Suppl 2): S121-S128.
55. **Singh S & Bajorek B.** Defining 'elderly' in clinical practice guidelines for pharmacotherapy. *Pharmacy Practice*, **2014**. 12(4): 489-498.
56. **World Health Organisation.** Definition of an older or elderly person. 2010. WHO. Available from: <http://www.who.int/healthinfo/survey/ageingdefolder/en/index.html> Accessed on 23/02/2018.
57. **Guaraldi G & Palella Jr FJ.** Clinical implications of aging with HIV infection: perspectives and the future medical care agenda. *AIDS*, **2017**. 31: S129-S135.
58. **Stader F, Siccardi M, Battegay M, Kinzig H, Penny MA, & Marzolini C.** Repository describing an aging population to inform physiologically based pharmacokinetic models considering anatomical, physiological, and biological age-dependent changes. *Clinical Pharmacokinetics*, **2019**. 58(4): 483-501.
59. **Evans MA, Triggs EJ, Cheung M, Broe GA, & Creasey H.** Gastric emptying rate in the elderly: implications for drug therapy. *Journal of the American Geriatrics Society*, **1981**. 29(5): 201-205.
60. **Horowitz M, Maddern GJ, Chatterton BE, Collins PJ, Harding PE, & Shearman DJ.** Changes in gastric emptying rates with age. *Clinical Science*, **1984**. 67(2): 213-218.
61. **Gainsborough N, Maskrey V, Nelson M, Keating J, Sherwood R, Jackson S, & Swift C.** The association of age with gastric emptying. *Age and Ageing*, **1993**. 22(1): 37-40.
62. **Madsen JL.** Effects of gender, age, and body mass index on gastrointestinal transit times. *Digestive Diseases and Sciences*, **1992**. 37(10): 1548-1553.
63. **Graff J, Brinch K, & Madsen JL.** Gastrointestinal mean transit times in young and middle-aged healthy subjects. *Clinical Physiology*, **2001**. 21(2): 253-259.
64. **Kupfer R, Heppell M, Haggith J, & Bateman D.** Gastric emptying and small-bowel transit rate in the elderly. *Journal of the American Geriatrics Society*, **1985**. 33(5): 340-343.
65. **Fülöp T, Worum I, Csongor J, Foris G, & Leövey A.** Body composition in elderly people. *Gerontology*, **1985**. 31(1): 6-14.
66. **Achour B, Russell MR, Barber J, & Rostami-Hodjegan A.** Simultaneous quantification of the abundance of several cytochrome P450 and uridine 5'-diphospho-glucuronosyltransferase enzymes in human liver microsomes using multiplexed targeted proteomics. *Drug Metabolism and Disposition*, **2014**. 42(4): 500-510.
67. **Parkinson A, Mudra D, Johnson C, Dwyer A, & Carroll K.** The effects of gender, age, ethnicity, and liver microsomes and inducibility in cultured human hepatocytes. *Toxicology & Applied Pharmacology*, **2004**. 199(3): 193-209.
68. **Simon T, Becquemont L, Hamon B, Nouyrigat E, Chodjania Y, Poirier J, Funck-Brentano C, & Jaillon P.** Variability of cytochrome P450 1A2 activity over time in young and elderly healthy volunteers. *British Journal of Clinical Pharmacology*, **2001**. 52(5): 601-604.

69. **Swift CG, Homeida M, Halliwell M, & Roberts C.** Antipyrine disposition and liver size in the elderly. *European Journal of Clinical Pharmacology*, **1978**. 14(2): 149-152.
70. **McLachlan M.** The ageing kidney. *The Lancet*, **1978**. 312(8081): 143-146.
71. **Dumond JB, Adams JL, Prince HM, Kendrick RL, Wang R, Jennings SH, Malone S, White N, Sykes C, & Corbett AH.** Pharmacokinetics of two common antiretroviral regimens in older HIV-infected patients: a pilot study. *HIV Medicine*, **2013**. 14(7): 401-409.
72. **Elliot ER, Wang X, Singh S, Simmons B, Vera JH, Miller RF, Fitzpatrick C, Moyle G, McClure M, & Boffito M.** Increased dolutegravir peak concentrations in people living with HIV aged 60 and over and analysis of sleep quality and cognition. *Clinical Infectious Diseases*, **2018**. 68(1): 87-95.
73. **Winston A, Jose S, Gibbons S, Back D, Stohr W, Post F, Fisher M, Gazzard B, Nelson M, & Gilson R.** Effects of age on antiretroviral plasma drug concentration in HIV-infected subjects undergoing routine therapeutic drug monitoring. *Journal of Antimicrobial Chemotherapy*, **2013**. 68(6): 1354-1359.
74. **Courlet P, Stader F, Guidi M, Saldanha SA, Stoeckle M, Cavassini M, Battegay M, Buclin T, Decosterd LA, & Marzolini C.** Pharmacokinetic profiles of boosted darunavir, dolutegravir and lamivudine in aging patients enrolled in the Swiss HIV Cohort Study. *AIDS*, **2019**. 34(1): 103-108.
75. **De Sousa Mendes M & Chetty M.** Are standard doses of renally-excreted antiretrovirals in older patients appropriate: A PBPK study comparing exposures in the elderly population with those in renal impairment. *Drugs in R&D*, **2019**. 19(4): 339-350.
76. **U.S. Food and Drug Administration.** PREZISTA. Highlights of prescribing information. 2011. Available from: https://www.accessdata.fda.gov/drugsatfda_docs/label/2012/021976s021lbl.pdf. Accessed on 22/11/2019.
77. **U.S. Food and Drug Administration.** NORVIR. Highlights of prescribing information. 2012. Available from: https://www.accessdata.fda.gov/drugsatfda_docs/label/2012/020945s033lbl.pdf. Accessed on 22/11/2019.
78. **U.S. Food and Drug Administration.** TIVICAY. Highlights of prescribing information. 2013. Available from: https://www.accessdata.fda.gov/drugsatfda_docs/label/2013/204790lbl.pdf. Accessed on 22/11/2019.
79. **U.S. Food and Drug Administration.** EDURANT. Highlights of prescribing information. 2011. Available from: https://www.accessdata.fda.gov/drugsatfda_docs/label/2011/202022s000lbl.pdf. Accessed on 22/11/2019.
80. **U.S. Food and Drug Administration.** SUSTIVA. Highlights of prescribing information. 2011. Available from: https://www.accessdata.fda.gov/drugsatfda_docs/label/2011/020972s038lbl.pdf. Accessed on 22/11/2019.
81. **U.S. Food and Drug Administration.** INTELENCE. Highlights of prescribing information. 2011. Available from: https://www.accessdata.fda.gov/drugsatfda_docs/label/2011/022187s008lbl.pdf. Accessed on 22/11/2019.
82. **U.S. Food and Drug Administration.** VIREAD. Highlights of prescribing information. 2012. Available from: https://www.accessdata.fda.gov/drugsatfda_docs/label/2012/022577lbl.pdf. Accessed on 22/11/2019.

83. **U.S. Food and Drug Administration.** EMTRIVA. Highlights of prescribing information. 2012. Available from: https://www.accessdata.fda.gov/drugsatfda_docs/label/2012/021500s019lbl.pdf. Accessed on 22/11/2019.
84. **U.S. Food and Drug Administration.** ISENTRESS. Highlights of prescribing information. 2013. Available from: https://www.accessdata.fda.gov/drugsatfda_docs/label/2013/022145s029lbl.pdf. Accessed on 16/12/2019.
85. **U.S. Food and Drug Administration.** REYATAZ. Highlights of prescribing information. 2011. Available from: https://www.accessdata.fda.gov/drugsatfda_docs/label/2011/021567s026lbl.pdf. Accessed on 22/11/2019.
86. **Greene M, Steinman MA, McNicholl IR, & Valcour V.** Polypharmacy, drug–drug interactions, and potentially inappropriate medications in older adults with human immunodeficiency virus infection. *Journal of the American Geriatrics Society*, **2014**. 62(3): 447-453.
87. **Hasse B, Ledergerber B, Furrer H, Battegay M, Hirschel B, Cavassini M, Bertisch B, Bernasconi E, & Weber R.** Morbidity and aging in HIV-infected persons: the Swiss HIV cohort study. *Clinical Infectious Diseases*, **2011**. 53(11): 1130-1139.
88. **Allavena C, Hanf M, Rey D, Duvivier C, BaniSadr F, Poizot-Martin I, Jacomet C, Pugliese P, Delobel P, & Katlama C.** Antiretroviral exposure and comorbidities in an aging HIV-infected population: The challenge of geriatric patients. *PloS One*, **2018**. 13(9): 1-11.
89. **Ziere G, Dieleman J, Hofman A, Pols HA, Van Der Cammen T, & Stricker BC.** Polypharmacy and falls in the middle age and elderly population. *British Journal of Clinical Pharmacology*, **2006**. 61(2): 218-223.
90. **Krentz HB & Gill MJ.** The impact of non-antiretroviral polypharmacy on the continuity of antiretroviral therapy (ART) among HIV patients. *AIDS Patient Care and Sexual Transmitted Diseases*, **2016**. 30(1): 11-17.
91. **Justice AC, Gordon KS, Skanderson M, Edelman EJ, Akgün KM, Gibert CL, Re III VL, Rimland D, Womack JA, & Wyatt CM.** Nonantiretroviral polypharmacy and adverse health outcomes among HIV-infected and uninfected individuals. *AIDS*, **2018**. 32(6): 739.
92. **López-Centeno B, Badenes-Olmedo C, Mataix-Sanjuan Á, McAllister K, Bellón JM, Gibbons S, Balsalobre P, Pérez-Latorre L, Benedí J, & Marzolini C.** Polypharmacy and drug-drug interactions in HIV-infected subjects in the region of Madrid, Spain: a population-based study. *Clinical Infectious Diseases*, **2019**. [Epub ahead of print].
93. **Guaraldi G, Malagoli A, Calcagno A, Mussi C, Celesia B, Carli F, Piconi S, De Socio G, Cattelan A, & Orofino G.** The increasing burden and complexity of multi-morbidity and polypharmacy in geriatric HIV patients: a cross sectional study of people aged 65–74 years and more than 75 years. *BMC Geriatrics*, **2018**. 18(1): 99-109.
94. **Marzolini C, Back D, Weber R, Furrer H, Cavassini M, Calmy A, Vernazza P, Bernasconi E, Khoo S, & Battegay M.** Aging with HIV: medication use and risk for potential drug–drug interactions. *Journal of Antimicrobial Chemotherapy*, **2011**. 66(9): 2107-2111.
95. **Johnell K & Klarin I.** The relationship between number of drugs and potential drug-drug interactions in the elderly. *Drug Safety*, **2007**. 30(10): 911-918.
96. **Burger D, Back D, Buggisch P, Buti M, Craxí A, Foster G, Klinker H, Larrey D, Nikitin I, & Pol S.** Clinical management of drug–drug interactions in HCV therapy: challenges and solutions. *Journal of Hepatology*, **2013**. 58(4): 792-800.

97. **U.S. Food and Drug Administration.** BIKTARVY. Highlights of prescribing information. . 2018. Available from: https://www.accessdata.fda.gov/drugsatfda_docs/label/2018/210251s000lbl.pdf. Accessed on 16/12/2019.
98. **U.S. Food and Drug Administration.** DELSTRIGO. Highlight of prescribing information. 2018. Available from: https://www.accessdata.fda.gov/drugsatfda_docs/label/2018/210807s000lbl.pdf. Accessed on 16/12/2019.
99. **U.S. Food and Drug Administration.** SELZENTRY. Highlights of prescribing information. 2007. Available from: https://www.accessdata.fda.gov/drugsatfda_docs/label/2007/022128lbl.pdf. Accessed on 16/12/2019.
100. **Schöller-Gyüre M, Kakuda TN, Raoof A, De Smedt G, & Hoetelmans RM.** Clinical pharmacokinetics and pharmacodynamics of etravirine. *Clinical Pharmacokinetics*, **2009**. 48(9): 561-574.
101. **Marzolini C, Rajoli R, Battegay M, Elzi L, Back D, & Sicaardi M.** Physiologically based pharmacokinetic modeling to predict drug–drug interactions with efavirenz involving simultaneous inducing and inhibitory effects on cytochromes. *Clinical Pharmacokinetics*, **2017**. 56(4): 409-420.
102. **Tseng A, Hughes CA, Wu J, Seet J, & Phillips EJ.** Cobicistat versus ritonavir: similar pharmacokinetic enhancers but some important differences. *Annals of Pharmacotherapy*, **2017**. 51(11): 1008-1022.
103. **Annaert P, Ye Z, Stieger B, & Augustijns P.** Interaction of HIV protease inhibitors with OATP1B1, 1B3, and 2B1. *Xenobiotica*, **2010**. 40(3): 163-176.
104. **Zhu L, Persson A, Mahnke L, Eley T, Li T, Xu X, Agarwala S, Dragone J, & Bertz R.** Effect of low-dose omeprazole (20 mg daily) on the pharmacokinetics of multiple-dose atazanavir with ritonavir in healthy subjects. *The Journal of Clinical Pharmacology*, **2011**. 51(3): 368-377.
105. **Crauwels H, Van Heeswijk R, Stevens M, Buelens A, Vanveggel S, Boven K, & Hoetelmans R.** Clinical perspective on drug-drug interactions with the non-nucleoside reverse transcriptase inhibitor rilpivirine. *AIDS Reviews*, **2012**. 15(2): 87-101.
106. **Song I, Borland J, Arya N, Wynne B, & Piscitelli S.** Pharmacokinetics of dolutegravir when administered with mineral supplements in healthy adult subjects. *The Journal of Clinical Pharmacology*, **2015**. 55(5): 490-496.
107. **Holtzman C, Armon C, Tedaldi E, Chmiel JS, Buchacz K, Wood K, & Brooks JT.** Polypharmacy and risk of antiretroviral drug interactions among the aging HIV-infected population. *Journal of General Internal Medicine*, **2013**. 28(10): 1302-1310.
108. **Ranzani A, Oreni L, Agrò M, van den Bogaart L, Milazzo L, Giacomelli A, Cattaneo D, Gervasoni C, & Ridolfo AL.** Burden of exposure to potential interactions between antiretroviral and non-antiretroviral medications in a population of HIV-positive patients aged 50 years or older. *Journal of Acquired Immune Deficiency Syndromes*, **2018**. 78(2): 193-201.
109. **Deutschmann E, Bucher H, Jaekel S, Gibbons S, McAllister K, Scherrer A, Braun D, Cavassini M, Hachfeld A, Calmy A, Battegay M, Ciprani M, Elzi L, Young J, Lopéz-Centeno B, Berenguer J, Khoo S, Moffa G, & Marzolini C.** Prevalence of potential drug-drug interactions in patients of the Swiss HIV cohort study in the era of HIV integrase inhibitors. in 17th European AIDS Conference. **2019**. Basel: Wiley.
110. **Ohno Y, Hisaka A, & Suzuki H.** General framework for the quantitative prediction of CYP3A4-mediated oral drug interactions based on the AUC increase by coadministration of standard drugs. *Clinical Pharmacokinetics*, **2007**. 46(8): 681-696.

111. **Gorski JC, Jones DR, Haehner-Daniels BD, Hamman MA, O'Mara EM, & Hall SD.** The contribution of intestinal and hepatic CYP3A to the interaction between midazolam and clarithromycin. *Clinical Pharmacology & Therapeutics*, **1998**. 64(2): 133-143.
112. **Quinney SK, Haehner BD, Rhoades MB, Lin Z, Gorski JC, & Hall SD.** Interaction between midazolam and clarithromycin in the elderly. *British Journal of Clinical Pharmacology*, **2008**. 65(1): 98-109.
113. **Li X, Margolick JB, Conover CS, Badri S, Riddler SA, Witt MD, & Jacobson LP.** Interruption and discontinuation of highly active antiretroviral therapy in the multicenter AIDS cohort study. *Journal of Acquired Immune Deficiency Syndromes*, **2005**. 38(3): 320-328.
114. **Schmitt W & Willmann S.** Physiology-based pharmacokinetic modeling: ready to be used. *Drug Discovery Today: Technologies*, **2004**. 1(4): 449-456.
115. **Edginton AN, Theil F-P, Schmitt W, & Willmann S.** Whole body physiologically-based pharmacokinetic models: their use in clinical drug development. *Expert Opinion on Drug Metabolism & Toxicology*, **2008**. 4(9): 1143-1152.
116. **Jamei M, Dickinson GL, & Rostami-Hodjegan A.** A framework for assessing inter-individual variability in pharmacokinetics using virtual human populations and integrating general knowledge of physical chemistry, biology, anatomy, physiology and genetics: a tale of 'bottom-up' vs 'top-down' recognition of covariates. *Drug Metabolism and Pharmacokinetics*, **2009**. 24(1): 53-75.
117. **Khalil F & Läer S.** Physiologically based pharmacokinetic modeling: methodology, applications, and limitations with a focus on its role in pediatric drug development. *BioMed Research International*, **2011**. 2011: 1-13.
118. **Stader F, Penny MA, Siccardi M, & Marzolini C.** A comprehensive framework for physiologically based pharmacokinetic modelling in Matlab®. *CPT: Pharmacometrics & Systems Pharmacology*, **2019**. 8(7): 444-459.
119. **United Nations.** World Population Ageing. 2015. Available from: http://www.un.org/en/development/desa/population/publications/pdf/ageing/WPA2015_Report.pdf. Accessed on 23/01/2018.
120. **Maher RL, Hanlon J, & Hajjar ER.** Clinical consequences of polypharmacy in elderly. *Expert Opinion on Drug Safety*, **2014**. 13(1): 57-65.
121. **Barnett K, Mercer SW, Norbury M, Watt G, Wyke S, & Guthrie B.** Epidemiology of multimorbidity and implications for health care, research, and medical education: a cross-sectional study. *The Lancet*, **2012**. 380(9836): 37-43.
122. **Watts G.** Why the exclusion of older people from clinical research must stop. *British Medical Journal*, **2012**. 344: 1-3.
123. **Dunnill M & Halley W.** Some observations on the quantitative anatomy of the kidney. *The Journal of Pathology*, **1973**. 110(2): 113-121.
124. **Hollenberg NK, Adams DF, Solomon HS, Rashid A, Abrams HL, & Merrill JP.** Senescence and the renal vasculature in normal man. *Circulation Research*, **1974**. 34(3): 309-316.
125. **Cockcroft DW & Gault H.** Prediction of creatinine clearance from serum creatinine. *Nephron*, **1976**. 16(1): 31-41.
126. **Koff R, Garvey A, Burney S, & Bell B.** Absence of an age effect on sulfobromophthalein retention in healthy men. *Gastroenterology*, **1973**. 65(2): 300-302.
127. **Marchesini G, Bua V, Brunori A, Bianchi G, Pisi P, Fabbri A, Zoli M, & Pisi E.** Galactose elimination capacity and liver volume in aging man. *Hepatology*, **1988**. 8(5): 1079-1083.

128. **Wynne HA, Cope LH, Mutch E, Rawlins MD, Woodhouse KW, & James OF.** The effect of age upon liver volume and apparent liver blood flow in healthy man. *Hepatology*, **1989**. 9(2): 297-301.
129. **Safar M.** Ageing and its effects on the cardiovascular system. *Drugs*, **1990**. 39(1): 1-8.
130. **Thompson CM, Johns DO, Sonawane B, Barton HA, Hattis D, Tardif R, & Krishnan K.** Database for physiologically based pharmacokinetic (PBPK) modeling: physiological data for healthy and health-impaired elderly. *Journal of Toxicology and Environmental Health, Part B*, **2009**. 12(1): 1-24.
131. **Schlender J-F, Meyer M, Thelen K, Krauss M, Willmann S, Eissing T, & Jaehde U.** Development of a whole-body physiologically based pharmacokinetic approach to assess the pharmacokinetics of drugs in elderly individuals. *Clinical Pharmacokinetics*, **2016**. 55(12): 1573-1589.
132. **O'Carroll R, Ebmeier K, Dougall N, Murray C, Goodwin G, Hayes P, Bouchier I, & Best J.** Regional cerebral blood flow and cognitive function in patients with chronic liver disease. *The Lancet*, **1991**. 337(8752): 1250-1253.
133. **Hozo SP, Djulbegovic B, & Hozo I.** Estimating the mean and variance from the median, range, and the size of a sample. *BMC Medical Research Methodology*, **2005**. 5(13): 1-10.
134. **Wan X, Wang W, Liu J, & Tong T.** Estimating the sample mean and standard deviation from the sample size, median, range and/or interquartile range. *BMC Medical Research Methodology*, **2014**. 14(1): 135-159.
135. **Williams L & Leggett R.** Reference values for resting blood flow to organs of man. *Clinical Physics and Physiological Measurement*, **1989**. 10(3): 187-217.
136. **DuBois D & DuBois EF.** Fifth paper the measurement of the surface area of man. *Archives of Internal Medicine*, **1915**. 15(5): 868-881.
137. **Burnham KP & Anderson DR.** Model selection and multimodel inference: a practical information-theoretic approach. **2003**, New York (USA): *Springer Science & Business Media*.
138. **European Union.** Eurostat - Population. 2013. Available from: <http://ec.europa.eu/eurostat/data/database>. Accessed on 23/02/2017.
139. **Bundesamt für Statistik (Schweiz).** Permanent resident population by age, sex and category of citizenship. 2016. Available from: <https://www.bfs.admin.ch/bfs/de/home/statistiken/bevoelkerung.assetdetail.299701.html>. Accessed on 01/05/2017.
140. **Bedogni G, Pietrobelli A, Heymsfield SB, Borghi A, Manzieri AM, Morini P, Battistini N, & Salvioli G.** Is body mass index a measure of adiposity in elderly women? *Obesity Research*, **2001**. 9(1): 17-20.
141. **Bosy-Westphal A, Mast M, Eichhorn C, Becker C, Kutzner D, Heller M, & Müller MJ.** Validation of air-displacement plethysmography for estimation of body fat mass in healthy elderly subjects. *European Journal of Nutrition*, **2003**. 42(4): 207-216.
142. **Brown E, Hopper Jr J, Hodges Jr J, Bradley B, Wennesland R, & Yamauchi H.** Red cell, plasma, and blood volume in healthy women measured by radiochromium cell-labeling and hematocrit. *Journal of Clinical Investigation*, **1962**. 41(12): 2182-2190.
143. **Statistisches Bundesamt der Bundesrepublik Deutschland.** Mikrozensus - Fragen zur Gesundheit. Körpermaße der Bevölkerung. 2013. Available from: https://www.destatis.de/DE/Publikationen/Thematisch/Gesundheit/Gesundheitszustand/Koerpermasse5239003099004.pdf?__blob=publicationFile. Accessed on 31/05/2017.

144. **Calloway N, Foley C, & Lagerbloom P.** Uncertainties in geriatric data. II. Organ size. *Journal of the American Geriatrics Society*, **1965**. 13(1): 20-28.
145. **Chien S, Usami S, Simmons R, McAllister F, & Gregersen M.** Blood volume and age: repeated measurements on normal men after 17 years. *Journal of Applied Physiology*, **1966**. 21(2): 583-588.
146. **Cohn JE & Shock NW.** Blood volume studies in middle-aged and elderly males. *American Journal of Medical Sciences*, **1949**. 217: 388-391.
147. **Corish CA & Kennedy NP.** Anthropometric measurements from a cross-sectional survey of Irish free-living elderly subjects with smoothed centile curves. *British Journal of Nutrition*, **2003**. 89(1): 137-145.
148. **De Groot C, Perdigao A, & Deurenberg P.** Longitudinal changes in anthropometric characteristics of elderly Europeans. SENECA Investigators. *European Journal of Clinical Nutrition*, **1996**. 50(Spl2): S9-15.
149. **Delarue J, Constans T, Malvy D, Pradignac A, Couet C, & Lamisse F.** Anthropometric values in an elderly French population. *British Journal of Nutrition*, **1994**. 71(2): 295-302.
150. **Dey DK, Rothenberg E, Sundh V, Bosaeus I, & Steen B.** Height and body weight in the elderly. I. A 25-year longitudinal study of a population aged 70 to 95 years. *European Journal of Clinical Nutrition*, **1999**. 53(12): 905-914.
151. **Dey D, Bosaeus I, Lissner L, & Steen B.** Body composition estimated by bioelectrical impedance in the Swedish elderly. Development of population-based prediction equation and reference values of fat-free mass and body fat for 70-and 75-y olds. *European Journal of Clinical Nutrition*, **2003**. 57(8): 909-916.
152. **Dey DK, Bosaeus I, Lissner L, & Steen B.** Changes in body composition and its relation to muscle strength in 75-year-old men and women: a 5-year prospective follow-up study of the NORA cohort in Göteborg, Sweden. *Nutrition*, **2009**. 25(6): 613-619.
153. **Eiben G, Dey D, Rothenberg E, Steen B, Björkelund C, Bengtsson C, & Lissner L.** Obesity in 70-year-old Swedes: secular changes over 30 years. *International Journal of Obesity*, **2005**. 29(7): 810-817.
154. **Farinatti PT & Soares PP.** Cardiac output and oxygen uptake relationship during physical effort in men and women over 60 years old. *European Journal of Applied Physiology*, **2009**. 107(6): 625-631.
155. **Gallagher D, Visser M, De Meersman RE, Sepúlveda D, Baumgartner RN, Pierson RN, Harris T, & Heymsfield SB.** Appendicular skeletal muscle mass: effects of age, gender, and ethnicity. *Journal of Applied Physiology*, **1997**. 83(1): 229-239.
156. **Gallagher D, Belmonte D, Deurenberg P, Wang Z, Krasnow N, Pi-Sunyer FX, & Heymsfield SB.** Organ-tissue mass measurement allows modeling of REE and metabolically active tissue mass. *American Journal of Physiology-Endocrinology And Metabolism*, **1998**. 275(2): E249-E258.
157. **Gallagher D, Allen A, Wang Z, Heymsfield SB, & Krasnow N.** Smaller organ tissue mass in the elderly fails to explain lower resting metabolic rate. *Annals of the New York Academy of Sciences*, **2000**. 904(1): 449-455.
158. **Gavriilidou N, Pihlsgård M, & Elmståhl S.** Anthropometric reference data for elderly Swedes and its disease-related pattern. *European Journal of Clinical Nutrition*, **2015**. 69(9): 1066-1075.
159. **Gibson JG & Evans WA.** Clinical studies of the blood volume. II. The relation of plasma and total blood volume to venous pressure, blood velocity rate, physical measurements, age and sex in ninety normal humans. *Journal of Clinical Investigation*, **1937**. 16(3): 317-328.

160. **Gillette-Guyonnet S, Nourhashemi F, Lauque S, Grandjean H, & Vellas B.** Body composition and osteoporosis in elderly women. *Gerontology*, **2000**. 46(4): 189-193.
161. **Gnudi S, Sitta E, & Fiumi N.** Relationship between body composition and bone mineral density in women with and without osteoporosis: relative contribution of lean and fat mass. *Journal of Bone and Mineral Metabolism*, **2007**. 25(5): 326-332.
162. **Henche SA, Torres RR, & Pellico LG.** An evaluation of patterns of change in total and regional body fat mass in healthy Spanish subjects using dual-energy X-ray absorptiometry (DXA). *European Journal of Clinical Nutrition*, **2008**. 62(12): 1440-1448.
163. **Horber FF, Gruber B, Thomi F, Jensen EX, & Jaeger P.** Effect of sex and age on bone mass, body composition and fuel metabolism in humans. *Nutrition*, **1997**. 13(6): 524-534.
164. **Launer LJ & Harris T.** Weight, height and body mass index distributions in geographically and ethnically diverse samples of older persons. *Age and Ageing*, **1996**. 25(4): 300-306.
165. **Legrand D, Adriaensen W, Vaes B, Matheï C, Wallemacq P, & Degryse J.** The relationship between grip strength and muscle mass (MM), inflammatory biomarkers and physical performance in community-dwelling very old persons. *Archives of Gerontology and Geriatrics*, **2013**. 57(3): 345-351.
166. **Molina DK & DiMaio VJ.** Normal organ weights in men: part II - the brain, lungs, liver, spleen, and kidneys. *The American Journal of Forensic Medicine and Pathology*, **2012**. 33(4): 368-372.
167. **Molina DK & DiMaio VJ.** Normal organ weights in women: Part II - the brain, lungs, liver, spleen, and kidneys. *The American Journal of Forensic Medicine and Pathology*, **2015**. 36(3): 182-187.
168. **Olivetti G, Giordano G, Corradi D, Melissari M, Lagrasta C, Gambert SR, & Anversa P.** Gender differences and aging: effects on the human heart. *Journal of the American College of Cardiology*, **1995**. 26(4): 1068-1079.
169. **Perissinotto E, Pisent C, Sergi G, Grigoletto F, & Enzi G.** Anthropometric measurements in the elderly: age and gender differences. *British Journal of Nutrition*, **2002**. 87(2): 177-186.
170. **Puggaard L, Bjørnsbo KS, Kock K, Lüders K, Thobo-Carlsen B, & Lammert O.** Age-related decrease in energy expenditure at rest parallels reductions in mass of internal organs. *American Journal of Human Biology*, **2002**. 14(4): 486-493.
171. **Ravaglia G, Morini P, Forti P, Maioli F, Boschi F, Bernardi M, & Gasbarrini G.** Anthropometric characteristics of healthy Italian nonagenarians and centenarians. *British Journal of Nutrition*, **1997**. 77(1): 9-17.
172. **Ravaglia G, Forti P, Maioli F, Boschi F, Cicognani A, & Gasbarrini G.** Measurement of body fat in healthy elderly men: a comparison of methods. *The Journals of Gerontology Series A: Biological Sciences and Medical Sciences*, **1999**. 54(2): M70-M76.
173. **Rea I, Gillen S, & Clarke E.** Anthropometric measurements from a cross-sectional survey of community dwelling subjects aged over 90 years of age. *European Journal of Clinical Nutrition*, **1997**. 51(2): 102-106.
174. **Santana H, Zoico E, Turcato E, Tosoni P, Bissoli L, Olivieri M, Bosello O, & Zamboni M.** Relation between body composition, fat distribution, and lung function in elderly men. *The American Journal of Clinical Nutrition*, **2001**. 73(4): 827-831.
175. **Schutz Y, Kyle U, & Pichard C.** Fat-free mass index and fat mass index percentiles in Caucasians aged 18-98 y. *International Journal of Obesity*, **2002**. 26(7): 953-960.
176. **Smith HL.** The relation of the weight of the heart to the weight of the body and of the weight of the heart to age. *American Heart Journal*, **1928**. 4(1): 79-93.

177. **Svendsten OL, Hassager C, & Christiansen C.** Age- and menopause-associated variations in body composition and fat distribution in healthy women as measured by dual-energy X-ray absorptiometry. *Metabolism*, **1995**. 44(3): 369-373.
178. **Tanner J.** The construction of normal standards for cardiac output in man. *Journal of Clinical Investigation*, **1949**. 28(3): 567-582.
179. **Tichet J, Goxe D, Sallé A, Berrut G, & Ritz P.** Prevalence of sarcopenia in the French senior population. *The Journal of Nutrition Health and Aging*, **2008**. 12(3): 202-206.
180. **Vache C, Rousset P, Gachon P, Gachon A, Morio B, Boulieu A, Coudert J, Beaufrere B, & Ritz P.** Bioelectrical impedance analysis measurements of total body water and extracellular water in healthy elderly subjects. *International Journal of Obesity*, **1998**. 22(6): 537-543.
181. **Wennesland R, Brown E, Hopper Jr J, Hodges Jr J, Guttentag O, Scott K, Tucker I, & Bradley B.** Red cell, plasma and blood volume in healthy men measured by radiochromium (Cr51) cell tagging and hematocrit: influence of age, somatotype and habits of physical activity on the variance after regression of volumes to height and weight combined. *Journal of Clinical Investigation*, **1959**. 38(7): 1065-1077.
182. **Whimster WF & Macfarlane AJ.** Normal lung weights in a white population. *American Review of Respiratory Disease*, **1974**. 110(4): 478-483.
183. **Ylihärsilä H, Kajantie E, Osmond C, Forsén T, Barker DJ, & Eriksson JG.** Body mass index during childhood and adult body composition in men and women aged 56–70 y. *The American Journal of Clinical Nutrition*, **2008**. 87(6): 1769-1775.
184. **de la Grandmaison GL, Clairand I, & Durigon M.** Organ weight in 684 adult autopsies: new tables for a Caucasoid population. *Forensic Science International*, **2001**. 119(2): 149-154.
185. **Starr I, Donal J, Margolies A, Shaw R, Collins L, & Gamble C.** Studies of the heart and circulation in disease; estimations of basal cardiac output, metabolism, heart size, and blood pressure in 235 subjects. *Journal of Clinical Investigation*, **1934**. 13(4): 561-592.
186. **Bartali B, Benvenuti E, Corsi AM, Bandinelli S, Russo CR, Di Iorio A, Lauretani F, & Ferrucci L.** Changes in anthropometric measures in men and women across the life-span: findings from the InCHIANTI study. *Sozial-und Präventivmedizin*, **2002**. 47(5): 336-348.
187. **Chouker A, Martignoni A, Dugas M, Eisenmenger W, Schauer R, Kaufmann I, Schelling G, Löhle F, Jauch KW, & Peter K.** Estimation of liver size for liver transplantation: the impact of age and gender. *Liver Transplantation*, **2004**. 10(5): 678-685.
188. **Clarys J, Martin A, & Drinkwater D.** Gross tissue weights in the human body by cadaver dissection. *Human Biology*, **1984**. 56(3): 459-473.
189. **Cournand A, Riley R, Breed E, Baldwin ED, Richards Jr D, Lester M, & Jones M.** Measurement of cardiac output in man using the technique of catheterization of the right auricle or ventricle. *Journal of Clinical Investigation*, **1945**. 24(1): 106-116.
190. **Davy KP & Seals DR.** Total blood volume in healthy young and older men. *Journal of Applied Physiology*, **1994**. 76(5): 2059-2062.
191. **Gillette-Guyonnet S, Nourhashemi F, Andrieu S, Cantet C, Albarède JL, Vellas B, & Grandjean H.** Body composition in French women 75+ years of age: the EPIDOS study. *Mechanisms of Ageing and Development*, **2003**. 124(3): 311-316.
192. **Ho C, Beard J, Farrell P, Minson C, & Kenney W.** Age, fitness, and regional blood flow during exercise in the heat. *Journal of Applied Physiology*, **1997**. 82(4): 1126-1135.
193. **Ishii T & Sternby NH.** Pathology of centenarians. I. The cardiovascular system and lungs. *Journal of the American Geriatrics Society*, **1978**. 26(3): 108-115.

194. **Janssen I, Heymsfield SB, Wang Z, & Ross R.** Skeletal muscle mass and distribution in 468 men and women aged 18–88 yr. *Journal of Applied Physiology*, **2000**. 89(1): 81-88.
195. **Kasiske B & Umen A.** The influence of age, sex, race, and body habitus on kidney weight in humans. *Archives of Pathology & Laboratory Medicine*, **1986**. 110(1): 55-60.
196. **Kemmler W, Teschler M, Goisser S, Bebenek M, von Stengel S, Bollheimer LC, Sieber CC, & Freiburger E.** Prevalence of sarcopenia in Germany and the corresponding effect of osteoarthritis in females 70 years and older living in the community: results of the FORMoSA study. *Clinical Interventions in Aging*, **2015**. 10: 1565-1573.
197. **Kumar NT, Liestøl K, Løberg EM, Reims HM, & Mæhlen J.** Postmortem heart weight: relation to body size and effects of cardiovascular disease and cancer. *Cardiovascular Pathology*, **2014**. 23(1): 5-11.
198. **Masanés Toran F, Culla A, Navarro-Gonzalez M, Navarro-Lopez M, Sacanella E, Torres B, & Lopez-Soto A.** Prevalence of sarcopenia in healthy community-dwelling elderly in an urban area of Barcelona (Spain). *The Journal of Nutrition, Health & Aging*, **2012**. 16(2): 184-187.
199. **Mezzani A, Grassi B, Giordano A, Corrà U, Colombo S, & Giannuzzi P.** Age-related prolongation of phase I of Vo₂ on-kinetics in healthy humans. *American Journal of Physiology*, **2010**. 299(3): R968-R976.
200. **Nyengaard J & Bendtsen T.** Glomerular number and size in relation to age, kidney weight, and body surface in normal man. *The Anatomical Record*, **1992**. 232(2): 194-201.
201. **Sprogøe-Jakobsen S & Sprogøe-Jakobsen U.** The weight of the normal spleen. *Forensic Science International*, **1997**. 88(3): 215-223.
202. **Thompson EN & Williams R.** Effect of age on liver function with particular reference to bromsulphalein excretion. *Gut*, **1965**. 6(3): 266-269.
203. **Meyer W, Peter B, & Solth K.** The weight of organs in the older age groups (70-92 years) and their relation to age and body weight. *Virchows Archiv für pathologische Anatomie und Physiologie und für klinische Medizin*, **1963**. 337: 17-32.
204. **Carlisle K, Halliwell M, Read A, & Wells P.** Estimation of total hepatic blood flow by duplex ultrasound. *Gut*, **1992**. 33(1): 92-97.
205. **Minson CT, Wladkowski SL, Cardell AF, Pawelczyk JA, & Kenney WL.** Age alters the cardiovascular response to direct passive heating. *Journal of Applied Physiology*, **1998**. 84(4): 1323-1332.
206. **Nakamura T, Moriyasu F, Ban N, Nishida O, Tamada T, Kawasaki T, Sakai M, & Uchino H.** Quantitative measurement of abdominal arterial blood flow using image-directed Doppler ultrasonography: superior mesenteric, splenic, and common hepatic arterial blood flow in normal adults. *Journal of Clinical Ultrasound*, **1989**. 17(4): 261-268.
207. **Vanis L, Gentilcore D, Lange K, Gilja OH, Rigda RS, Trahair LG, Feinle-Bisset C, Rayner CK, Horowitz M, & Jones KL.** Effects of variations in intragastric volume on blood pressure and splanchnic blood flow during intraduodenal glucose infusion in healthy older subjects. *American Journal of Physiology*, **2012**. 302(4): R391-R399.
208. **Zoli M, Iervese T, Abbati S, Bianchi G, Marchesini G, & Pisi E.** Portal blood velocity and flow in aging man. *Gerontology*, **1989**. 35(2-3): 61-65.
209. **Dunbar SL & Kenney WL.** Effects of hormone replacement therapy on hemodynamic responses of postmenopausal women to passive heating. *Journal of Applied Physiology*, **2000**. 89(1): 97-103.

-
210. **Robertson D, Waller D, Renwick A, & George C.** Age-related changes in the pharmacokinetics and pharmacodynamics of nifedipine. *British Journal of Clinical Pharmacology*, **1988**. 25(3): 297-305.
211. **Castleden CM & George CF.** The effect of ageing on the hepatic clearance of propranolol. *British Journal of Clinical Pharmacology*, **1979**. 7(1): 49-54.
212. **Greenblatt DJ, Harmatz JS, Shapiro L, Engelhardt N, Gouthro TA, & Shader RI.** Sensitivity to triazolam in the elderly. *New England Journal of Medicine*, **1991**. 324(24): 1691-1698.
213. **Tygstrup N, Winkler K, Mellemgaard K, & Andreassen M.** Determination of the hepatic arterial blood flow and oxygen supply in man by clamping the hepatic artery during surgery. *Journal of Clinical Investigation*, **1962**. 41(3): 447-454.
214. **Howgate E, Rowland Yeo K, Proctor N, Tucker G, & Rostami-Hodjegan A.** Prediction of in vivo drug clearance from in vitro data. I: impact of inter-individual variability. *Xenobiotica*, **2006**. 36(6): 473-497.
215. **Barter ZE, Bayliss MK, Beaune PH, Boobis AR, Carlile DJ, Edwards RJ, Brian Houston J, Lake BG, Lipscomb JC, & Pelkonen OR.** Scaling factors for the extrapolation of in vivo metabolic drug clearance from in vitro data: reaching a consensus on values of human microsomal protein and hepatocellularity per gram of liver. *Current Drug Metabolism*, **2007**. 8(1): 33-45.
216. **Barter ZE, Chowdry JE, Harlow JR, Snawder JE, Lipscomb JC, & Rostami-Hodjegan A.** Covariation of human microsomal protein per gram of liver with age: absence of influence of operator and sample storage may justify interlaboratory data pooling. *Drug Metabolism and Disposition*, **2008**. 36(12): 2405-2409.
217. **Rowland-Yeo K.** Abundance of cytochrome P450 in human liver: a meta-analysis. *British Journal of Clinical Pharmacology*, **2004**. 57(5): 687-688.
218. **Achour B, Barber J, & Rostami-Hodjegan A.** Expression of hepatic drug-metabolizing cytochrome p450 enzymes and their intercorrelations: a meta-analysis. *Drug Metabolism and Disposition*, **2014**. 42(8): 1349-1356.
219. **Shimada T, Yamazaki H, Mimura M, Inui Y, & Guengerich FP.** Interindividual variations in human liver cytochrome P-450 enzymes involved in the oxidation of drugs, carcinogens and toxic chemicals: studies with liver microsomes of 30 Japanese and 30 Caucasians. *Journal of Pharmacology and Experimental Therapeutics*, **1994**. 270(1): 414-423.
220. **Schwartz JB.** Erythromycin breath test results in elderly, very elderly, and frail elderly persons. *Clinical Pharmacology & Therapeutics*, **2006**. 79(5): 440-448.
221. **Hunt CM, Westerkam WR, & Stave GM.** Effect of age and gender on the activity of human hepatic CYP3A. *Biochemical Pharmacology*, **1992**. 44(2): 275-283.
222. **Schmucker DL, Woodhouse KW, Wang RK, Wynne H, James OF, McManus M, & Kremers P.** Effects of age and gender on in vitro properties of human liver microsomal monooxygenases. *Clinical Pharmacology & Therapeutics*, **1990**. 48(4): 365-374.
223. **Polasek TM, Patel F, Jensen BP, Sorich MJ, Wiese MD, & Doogue MP.** Predicted metabolic drug clearance with increasing adult age. *British Journal of Clinical Pharmacology*, **2013**. 75(4): 1019-1028.
224. **Morgan E.** Impact of infectious and inflammatory disease on cytochrome P450-mediated drug metabolism and pharmacokinetics. *Clinical Pharmacology & Therapeutics*, **2009**. 85(4): 434-438.
225. **Court MH.** Interindividual variability in hepatic drug glucuronidation: studies into the role of age, sex, enzyme inducers, and genetic polymorphism using the human liver bank as a model system. *Drug Metabolism Reviews*, **2010**. 42(1): 209-224.
-

-
226. **Herd B, Wynne H, Wright P, James O, & Woodhouse K.** The effect of age on glucuronidation and sulphation of paracetamol by human liver fractions. *British Journal of Clinical Pharmacology*, **1991**. 32(6): 768-770.
227. **Villesen HH, Banning A-M, Petersen RH, Weinelt S, Poulsen JB, Hansen SH, & Christrup LL.** Pharmacokinetics of morphine and oxycodone following intravenous administration in elderly patients. *Therapeutics and Clinical Risk Management*, **2007**. 3(5): 961-967.
228. **Burt HJ, Riedmaier AE, Harwood MD, Crewe HK, Gill KL, & Neuhoff S.** Abundance of hepatic transporters in Caucasians: a meta-analysis. *Drug Metabolism and Disposition*, **2016**. 44(10): 1550-1561.
229. **Bauer JH, Brooks CS, & Burch RN.** Renal function and hemodynamic studies in low-and normal-renin essential hypertension. *Archives of Internal Medicine*, **1982**. 142(7): 1317-1323.
230. **Davies DF & Shock NW.** Age changes in glomerular filtration rate, effective renal plasma flow, and tubular excretory capacity in adult males. *Journal of Clinical Investigation*, **1950**. 29(5): 496-507.
231. **Fliser D, Zeier M, Nowack R, & Ritz E.** Renal functional reserve in healthy elderly subjects. *Journal of the American Society of Nephrology*, **1993**. 3(7): 1371-1377.
232. **Fliser D, Franek E, Joest M, Block S, Mutschler E, & Ritz E.** Renal function in the elderly: impact of hypertension and cardiac function. *Kidney International*, **1997**. 51(4): 1196-1204.
233. **Ghose K & Burch A.** Measurement of renal functions by double isotope techniques in elderly patients during tenoxicam therapy. *Archives of Gerontology and Geriatrics*, **1989**. 9(2): 115-122.
234. **Goldring W, Chasis H, Ranges HA, & Smith HW.** Relations of effective renal blood flow and glomerular filtration to tubular excretory mass in normal man. *Journal of Clinical Investigation*, **1940**. 19(5): 739-750.
235. **McDonald RK, Solomon DH, & Shock NW.** Aging as a factor in the renal hemodynamic changes induced by a standardized pyrogen. *Journal of Clinical Investigation*, **1951**. 30(5): 457-462.
236. **Miller JH, McDonald RK, & Shock NW.** The renal extraction of p-aminohippurate in the aged individual. *Journal of Gerontology*, **1951**. 6(3): 213-216.
237. **Fuiano G, Sund S, Mazza G, Rosa M, Caglioti A, Gallo G, Natale G, Andreucci M, Memoli B, & De Nicola L.** Renal hemodynamic response to maximal vasodilating stimulus in healthy older subjects. *Kidney International*, **2001**. 59(3): 1052-1058.
238. **Stevens LA, Coresh J, Greene T, & Levey AS.** Assessing kidney function - measured and estimated glomerular filtration rate. *New England Journal of Medicine*, **2006**. 354(23): 2473-2483.
239. **Christensson A & Elmståhl S.** Estimation of the age-dependent decline of glomerular filtration rate from formulas based on creatinine and cystatin C in the general elderly population. *Nephron Clinical Practice*, **2011**. 117(1): c40-c50.
240. **Van Den Noortgate NJ, Janssens WH, Delanghe JR, Afschrift MB, & Lameire NH.** Serum cystatin C concentration compared with other markers of glomerular filtration rate in the old old. *Journal of the American Geriatrics Society*, **2002**. 50(7): 1278-1282.
241. **DeSanto N, Anastasio P, Coppola S, Barba G, Jadanza A, & Capasso G.** Age-related changes in renal reserve and renal tubular function in healthy humans. *Child Nephrology and Urology*, **1991**. 11(1): 33-40.
242. **Levey AS, Bosch JP, Lewis JB, Greene T, Rogers N, & Roth D.** A more accurate method to estimate glomerular filtration rate from serum creatinine: a new prediction equation. *Annals of Internal Medicine*, **1999**. 130(6): 461-470.
-

243. **Musso CG & Oreopoulos DG.** Aging and physiological changes of the kidneys including changes in glomerular filtration rate. *Nephron Physiology*, **2011**. 119(Suppl. 1): p1-p5.
244. **Zoico E, Di Francesco V, Guralnik J, Mazzali G, Bortolani A, Guariento S, Sergi G, Bosello O, & Zamboni M.** Physical disability and muscular strength in relation to obesity and different body composition indexes in a sample of healthy elderly women. *International Journal of Obesity*, **2004**. 28(2): 234-241.
245. **Lesser GT & Deutsch S.** Measurement of adipose tissue blood flow and perfusion in man by uptake of 85Kr. *Journal of Applied Physiology*, **1967**. 23(5): 621-630.
246. **Andersson J, Karpe F, Sjöström L-G, Riklund K, Söderberg S, & Olsson T.** Association of adipose tissue blood flow with fat depot sizes and adipokines in women. *International Journal of Obesity*, **2012**. 36(6): 783-789.
247. **Proctor DN, Newcomer SC, Koch DW, Le KU, MacLean DA, & Leuenberger UA.** Leg blood flow during submaximal cycle ergometry is not reduced in healthy older normally active men. *Journal of Applied Physiology*, **2003**. 94(5): 1859-1869.
248. **Amery A, Bossaert H, & Verstraete M.** Muscle blood flow in normal and hypertensive subjects: influence of age, exercise, and body position. *American Heart Journal*, **1969**. 78(2): 211-216.
249. **Johnson JM, Brengelmann GL, & Rowell LB.** Interactions between local and reflex influences on human forearm skin blood flow. *Journal of Applied Physiology*, **1976**. 41(6): 826-831.
250. **Proctor DN, Koch DW, Newcomer SC, Le KU, & Leuenberger UA.** Impaired leg vasodilation during dynamic exercise in healthy older women. *Journal of Applied Physiology*, **2003**. 95(5): 1963-1970.
251. **Spann W & Dustmann H.** Weight of the human brain and its dependence on age, body length, cause of death and occupation. *Deutsche Zeitschrift für die gesamte gerichtliche Medizin*, **1964**. 56(5): 299-317.
252. **Bertsch K, Hagemann D, Hermes M, Walter C, Khan R, & Naumann E.** Resting cerebral blood flow, attention, and aging. *Brain Research*, **2009**. 1267: 77-88.
253. **Chen JJ, Rosas HD, & Salat DH.** Age-associated reductions in cerebral blood flow are independent from regional atrophy. *Neuroimage*, **2011**. 55(2): 468-478.
254. **Davis SM, Ackerman RH, Correia JA, Alpert NM, Chang J, Buonanno F, Kelley RE, Rosner B, & Taveras JM.** Cerebral blood flow and cerebrovascular CO₂ reactivity in stroke-age normal controls. *Neurology*, **1983**. 33(4): 391-391.
255. **Devous M, Stokely E, Chehabi H, & Bonte F.** Normal distribution of regional cerebral blood flow measured by dynamic single-photon emission tomography. *Journal of Cerebral Blood Flow & Metabolism*, **1986**. 6(1): 95-104.
256. **Hagstadius S & Risberg J.** Regional cerebral blood flow characteristics and variations with age in resting normal subjects. *Brain and Cognition*, **1989**. 10(1): 28-43.
257. **Leenders K, Perani D, Lammertsma A, Heather J, Buckingham P, Jones T, Healy M, Gibbs J, Wise R, & Hatazawa J.** Cerebral blood flow, blood volume and oxygen utilization. *Brain*, **1990**. 113(1): 27-47.
258. **Lu H, Xu F, Rodrigue KM, Kennedy KM, Cheng Y, Flicker B, Hebrank AC, Uh J, & Park DC.** Alterations in cerebral metabolic rate and blood supply across the adult lifespan. *Cerebral Cortex*, **2011**. 21(6): 1426-1434.
259. **Martin AJ, Friston KJ, Colebatch JG, & Frackowiak RS.** Decreases in regional cerebral blood flow with normal aging. *Journal of Cerebral Blood Flow & Metabolism*, **1991**. 11(4): 684-689.

-
260. **Parkes LM, Rashid W, Chard DT, & Tofts PS.** Normal cerebral perfusion measurements using arterial spin labeling: reproducibility, stability, and age and gender effects. *Magnetic Resonance in Medicine*, **2004**. 51(4): 736-743.
261. **Scheinberg P, Blackburn I, Rich M, & Saslaw M.** Effects of aging on cerebral circulation and metabolism. *AMA Archives of Neurology & Psychiatry*, **1953**. 70(1): 77-85.
262. **Shaw TG, Mortel KF, Meyer JS, Rogers RL, Hardenberg J, & Cutaia MM.** Cerebral blood flow changes in benign aging and cerebrovascular disease. *Neurology*, **1984**. 34(7): 855-855.
263. **Shin W, Horowitz S, Ragin A, Chen Y, Walker M, & Carroll TJ.** Quantitative cerebral perfusion using dynamic susceptibility contrast MRI: evaluation of reproducibility and age- and gender-dependence with fully automatic image postprocessing algorithm. *Magnetic Resonance in Medicine*, **2007**. 58(6): 1232-1241.
264. **Molina DK & DiMaio VJ.** Normal organ weights in men: part I - the heart. *The American Journal of Forensic Medicine and Pathology*, **2012**. 33(4): 362-367.
265. **Molina DK & DiMaio VJ.** Normal organ weights in women: part I - the heart. *The American Journal of Forensic Medicine and Pathology*, **2015**. 36(3): 176-181.
266. **Baliga RR, Rosen SD, Camici PG, & Kooner JS.** Regional myocardial blood flow redistribution as a cause of postprandial angina pectoris. *Circulation*, **1998**. 97(12): 1144-1149.
267. **Bergmann SR, Herrero P, Markham J, Weinheimer CJ, & Walsh MN.** Noninvasive quantitation of myocardial blood flow in human subjects with oxygen-15-labeled water and positron emission tomography. *Journal of the American College of Cardiology*, **1989**. 14(3): 639-652.
268. **Chan SY, Brunken RC, Czernin J, Porenta G, Kuhle W, Krivokapich J, Phelps ME, & Schelbert HR.** Comparison of maximal myocardial blood flow during adenosine infusion with that of intravenous dipyridamole in normal men. *Journal of the American College of Cardiology*, **1992**. 20(4): 979-985.
269. **Duvernoy CS, Meyer C, Seifert-Klauss V, Dayanikli F, Matsunari I, Rattenhuber J, Höss C, Graeff H, & Schwaiger M.** Gender differences in myocardial blood flow dynamics: lipid profile and hemodynamic effects. *Journal of the American College of Cardiology*, **1999**. 33(2): 463-470.
270. **Leight L, Defazio V, Talmers FN, Regan TJ, & Hellems HK.** Coronary blood flow, myocardial oxygen consumption, and myocardial metabolism in normal and hyperthyroid human subjects. *Circulation*, **1956**. 14(1): 90-99.
271. **Senneff MJ, Geltman EM, & Bergmann SR.** Noninvasive delineation of the effects of moderate aging on myocardial perfusion. *Journal of Nuclear Medicine*, **1991**. 32(11): 2037-2042.
272. **Brandfonbrener M, Landowne M, & Shock NW.** Changes in cardiac output with age. *Circulation*, **1955**. 12(4): 557-566.
273. **Lewis WH.** Changes with age in the cardiac output in adult men. *American Journal of Physiology*, **1938**. 121(2): 517-527.
274. **Smith RH.** Normal blood volumes in men and women over sixty years of age as determined by a modified Cr51 method. *The Journal of the American Society of Anesthesiologists*, **1958**. 19(6): 752-756.
275. **Smith WW, Wikler NS, & Fox AC.** Hemodynamic studies of patients with myocardial infarction. *Circulation*, **1954**. 9(3): 352-362.
276. **Tietz NW, Shuey DF, & Wekstein DR.** Laboratory values in fit aging individuals - sexagenarians through centenarians. *Clinical Chemistry*, **1992**. 38(6): 1167-1185.
-

-
277. **Zauber NP & Zauber AG.** Hematologic data of healthy very old people. *Jama*, **1987**. 257(16): 2181-2184.
278. **Timiras ML & Brownstein H.** Prevalence of anemia and correlation of hemoglobin with age in a geriatric screening clinic population. *Journal of the American Geriatrics Society*, **1987**. 35(7): 639-643.
279. **Sklaroff D.** Isotopic determination of blood volume in the normal aged. *American Journal of Roentgenology*, **1956**. 75: 1082-1083.
280. **Jernigan JA, Gudat JC, Blake JL, Bowen L, & Lezotte DC.** Reference values for blood findings in relatively fit elderly persons. *Journal of the American Geriatrics Society*, **1980**. 28(7): 308-314.
281. **Campion EW, Delabry LO, & Glynn RJ.** The effect of age on serum albumin in healthy males: report from the Normative Aging Study. *Journal of Gerontology*, **1988**. 43(1): M18-M20.
282. **Fu A & Nair KS.** Age effect on fibrinogen and albumin synthesis in humans. *American Journal of Physiology-Endocrinology And Metabolism*, **1998**. 275(6): E1023-E1030.
283. **Gardner M & Scott R.** Age-and sex-related reference ranges for eight plasma constituents derived from randomly selected adults in a Scottish new town. *Journal of Clinical Pathology*, **1980**. 33(4): 380-385.
284. **Garry PJ, Hunt WC, Van der Jagt DJ, & Rhyne RL.** Clinical chemistry reference intervals for healthy elderly subjects. *The American Journal of Clinical Nutrition*, **1989**. 50(5): 1219-1230.
285. **Gersovitz M, Munro HN, Udall J, & Young VR.** Albumin synthesis in young and elderly subjects using a new stable isotope methodology: response to level of protein intake. *Metabolism*, **1980**. 29(11): 1075-1086.
286. **Pickart L.** Increased ratio of plasma free fatty acids to albumin during normal aging and in patients with coronary heart disease. *Atherosclerosis*, **1983**. 46(1): 21-28.
287. **Reed A, Cannon D, Winkelman J, Bhasin Y, Henry R, & Pileggi V.** Estimation of normal ranges from a controlled sample survey. I. Sex and age-related influence on the SMA 12/60 screening group of tests. *Clinical Chemistry*, **1972**. 18(1): 57-66.
288. **Veering BT, Burm A, Souverijn J, Serree J, & Spierdijk J.** The effect of age on serum concentrations of albumin and alpha 1-acid glycoprotein. *British Journal of Clinical Pharmacology*, **1990**. 29(2): 201-206.
289. **Wallace S & Whiting B.** Factors affecting drug binding in plasma of elderly patients. *British Journal of Clinical Pharmacology*, **1976**. 3(2): 327-330.
290. **Denko CW & Gabriel P.** Age and sex related levels of albumin, ceruloplasmin, alpha 1 antitrypsin, alpha 1 acid glycoprotein, and transferrin. *Annals of Clinical & Laboratory Science*, **1981**. 11(1): 63-68.
291. **Routledge P, Stargel W, Kitchell B, Barchowsky A, & Shand D.** Sex-related differences in the plasma protein binding of lignocaine and diazepam. *British Journal of Clinical Pharmacology*, **1981**. 11(3): 245-250.
292. **Paxton J & Briant R.** Alpha 1-acid glycoprotein concentrations and propranolol binding in elderly patients with acute illness. *British Journal of Clinical Pharmacology*, **1984**. 18(5): 806-810.
293. **Blain P, Mucklow J, Rawlins M, Roberts D, Routledge P, & Shand D.** Determinants of plasma alpha 1-acid glycoprotein (AAG) concentrations in health. *British Journal of Clinical Pharmacology*, **1985**. 20(5): 500-502.
-

-
294. **Boddy K, King PC, Hume R, & Weyers E.** The relation of total body potassium to height, weight, and age in normal adults. *Journal of Clinical Pathology*, **1972**. 25(6): 512-517.
295. **Bruce A, Andersson M, Arvidsson B, & Isaksson B.** Body composition. Prediction of normal body potassium, body water and body fat in adults on the basis of body height, body weight and age. *Scandinavian Journal of Clinical and Laboratory Investigation*, **1980**. 40(5): 461-473.
296. **Cornish B, Ward L, Thomas B, Jebb S, & Elia M.** Evaluation of multiple frequency bioelectrical impedance and Cole-Cole analysis for the assessment of body water volumes in healthy humans. *European Journal of Clinical Nutrition*, **1996**. 50(3): 159-164.
297. **Hume R & Weyers E.** Relationship between total body water and surface area in normal and obese subjects. *Journal of Clinical Pathology*, **1971**. 24(3): 234-238.
298. **Schoeller DA.** Changes in total body water with age. *The American Journal of Clinical Nutrition*, **1989**. 50(5): 1176-1181.
299. **St-Onge M-P, Wang Z, Horlick M, Wang J, & Heymsfield SB.** Dual-energy X-ray absorptiometry lean soft tissue hydration: independent contributions of intra-and extracellular water. *American Journal of Physiology-Endocrinology and Metabolism*, **2004**. 287(5): E842-E847.
300. **Steen B.** Body composition and aging. *Nutrition Reviews*, **1988**. 46(2): 45-51.
301. **Chumlea WC, Guo SS, Zeller CM, Reo NV, Baumgartner RN, Garry PJ, Wang J, Pierson RN, Heymsfield SB, & Siervogel RM.** Total body water reference values and prediction equations for adults. *Kidney International*, **2001**. 59(6): 2250-2258.
302. **Gill KL, Gardner I, Li L, & Jamei M.** A bottom-up whole-body physiologically based pharmacokinetic model to mechanistically predict tissue distribution and the rate of subcutaneous absorption of therapeutic proteins. *The AAPS Journal*, **2016**. 18(1): 156-170.
303. **Snyder W, Cook M, Nasset E, Karhausen L, Howells GP, & Tipton I.** Report of the Task Group on Reference Man. **1975**, Oxford (UK): *Pergamon Press*.
304. **Valentin J.** Basic anatomical and physiological data for use in radiological protection: reference values: ICRP Publication 89. *Annals of the ICRP*, **2002**. 32(3): 1-277.
305. **Dressman JB, Berardi RR, Dermentzoglou LC, Russell TL, Schmaltz SP, Barnett JL, & Jarvenpaa KM.** Upper gastrointestinal (GI) pH in young, healthy men and women. *Pharmaceutical Research*, **1990**. 7(7): 756-761.
306. **Russell TL, Berardi RR, Barnett JL, Dermentzoglou LC, Jarvenpaa KM, Schmaltz SP, & Dressman JB.** Upper gastrointestinal pH in seventy-nine healthy, elderly, North American men and women. *Pharmaceutical Research*, **1993**. 10(2): 187-196.
307. **Fallingborg J, Christensen L, Ingeman-Nielsen M, Jacobsen B, Abildgaard K, & Rasmussen H.** pH-profile and regional transit times of the normal gut measured by a radiotelemetry device. *Alimentary Pharmacology & Therapeutics*, **1989**. 3(6): 605-614.
308. **Jamei M, Turner D, Yang J, Neuhoﬀ S, Polak S, Rostami-Hodjegan A, & Tucker G.** Population-based mechanistic prediction of oral drug absorption. *The AAPS Journal*, **2009**. 11(2): 225-237.
309. **Morihara M, Aoyagi N, Kaniwa N, Kojima S, & Ogata H.** Assessment of gastric acidity of Japanese subjects over the last 15 years. *Biological and Pharmaceutical Bulletin*, **2001**. 24(3): 313-315.
310. **Chaw C, Yazaki E, & Evans D.** The effect of pH change on the gastric emptying of liquids measured by electrical impedance tomography and pH-sensitive radiotelemetry capsule. *International Journal of Pharmaceutics*, **2001**. 227(1): 167-175.
-

311. **Moore JG, Tweedy C, Christian PE, & Datz FL.** Effect of age on gastric emptying of liquid-solid meals in man. *Digestive Diseases and Sciences*, **1983**. 28(4): 340-344.
312. **Goo R, Moore J, Greenberg E, & Alazraki N.** Circadian variation in gastric emptying of meals in humans. *Gastroenterology*, **1987**. 93(3): 515-518.
313. **Henderson JM, Heymsfield SB, Horowitz J, & Kutner MH.** Measurement of liver and spleen volume by computed tomography. Assessment of reproducibility and changes found following a selective distal splenorenal shunt. *Radiology*, **1981**. 141(2): 525-527.
314. **Fischer M & Fadda HM.** The effect of sex and age on small intestinal transit times in humans. *Journal of Pharmaceutical Sciences*, **2016**. 105(2): 682-686.
315. **Husebye E & Engedal K.** The patterns of motility are maintained in the human small intestine throughout the process of aging. *Scandinavian Journal of Gastroenterology*, **1992**. 27(5): 397-404.
316. **Bender AD.** Effect of age on intestinal absorption: implications for drug absorption in the elderly. *Journal of the American Geriatrics Society*, **1968**. 16(12): 1331-1339.
317. **Warren P, Pepperman M, & Montgomery R.** Age changes in small-intestinal mucosa. *The Lancet*, **1978**. 312(8094): 849-850.
318. **Saltzman JR, Kowdley KV, Perrone G, & Russell RM.** Changes in small-intestine permeability with aging. *Journal of the American Geriatrics Society*, **1995**. 43(2): 160-164.
319. **Valentini L, Ramminger S, Haas V, Postrach E, Werich M, Fischer A, Koller M, Swidsinski A, Bereswill S, & Lochs H.** Small intestinal permeability in older adults. *Physiological Reports*, **2014**. 2(4): 1-10.
320. **Barter ZE, Tucker GT, & Rowland-Yeo K.** Differences in cytochrome p450-mediated pharmacokinetics between chinese and caucasian populations predicted by mechanistic physiologically based pharmacokinetic modelling. *Clinical Pharmacokinetics*, **2013**. 52(12): 1085-1100.
321. **Abduljalil K, Jamei M, Rostami-Hodjegan A, & Johnson TN.** Changes in individual drug-independent system parameters during virtual paediatric pharmacokinetic trials: introducing time-varying physiology into a paediatric PBPK model. *The AAPS Journal*, **2014**. 16(3): 568-576.
322. **Ludin H.** Radiologic estimation of kidney weight. *Acta Radiologica. Diagnosis*, **1967**. 6(6): 561-574.
323. **McLachlan M & Wasserman P.** Changes in sizes and distensibility of the aging kidney. *The British Journal of Radiology*, **1981**. 54(642): 488-491.
324. **Centers for Disease Control and Prevention.** HIV among people aged 50 and over. 2018. Available from: <https://www.cdc.gov/hiv/group/age/olderamericans/index.html>. Accessed on 26/02/2018.
325. **Jamei M.** Recent advances in development and application of physiologically-based pharmacokinetic (PBPK) models: a transition from academic curiosity to regulatory acceptance. *Current Pharmacology Reports*, **2016**. 2(3): 161-169.
326. **U.S. Food and Drug Administration.** Physiologically based pharmacokinetic analysis - format and content. Guidance for industry. 2016. Available from: <https://www.fda.gov/downloads/Drugs/GuidanceComplianceRegulatoryInformation/Guidances/UCM531207.pdf>. Accessed on 02/01/2018.

327. **European Medicines Agency.** Guideline on the qualification and reporting of physiologically based pharmacokinetic (PBPK) modelling and simulation. Draft. 2016. Available from: http://www.ema.europa.eu/docs/en_GB/document_library/Scientific_guideline/2016/07/WC500211315.pdf. Accessed on 02/01/2018.
328. **Rowland-Yeo K, Jamei M, & Rostami-Hodjegan A.** Predicting drug–drug interactions: application of physiologically based pharmacokinetic models under a systems biology approach. *Expert Review of Clinical Pharmacology*, **2013**. 6(2): 143-157.
329. **Stader F, Würthwein G, Groll AH, Vehreschild JJ, Cornely OA, & Hempel G.** Physiology-based pharmacokinetics of caspofungin for adults and paediatrics. *Pharmaceutical Research*, **2015**. 32(6): 2029-2037.
330. **Ke AB, Nallani S, Zhao P, Rostami-Hodjegan A, Isoherranen N, & Unadkat JD.** A PBPK model to predict disposition of P450 2D6 and P450 1A2 metabolized drugs in pregnant women. *Drug Metabolism and Disposition*, **2013**. 41: 801-813.
331. **Olagunju A, Rajoli RK, Atoyebi SA, Khoo S, Owen A, & Siccardi M.** Physiologically-based pharmacokinetic modelling of infant exposure to efavirenz through breastfeeding. *AAS Open Research*, **2018**. 1: 1-16.
332. **Johnson TN, Boussery K, Rowland-Yeo K, Tucker GT, & Rostami-Hodjegan A.** A semi-mechanistic model to predict the effects of liver cirrhosis on drug clearance. *Clinical Pharmacokinetics*, **2010**. 49(3): 189-206.
333. **Rowland Yeo K, Aarabi M, Jamei M, & Rostami-Hodjegan A.** Modeling and predicting drug pharmacokinetics in patients with renal impairment. *Expert Review of Clinical Pharmacology*, **2011**. 4(2): 261-274.
334. **Rajoli RK, Back DJ, Rannard S, Meyers CLF, Flexner C, Owen A, & Siccardi M.** Physiologically based pharmacokinetic modelling to inform development of intramuscular long-acting nanoformulations for HIV. *Clinical Pharmacokinetics*, **2015**. 54(6): 639-650.
335. **Barton HA, Chiu WA, Setzer RW, Andersen ME, Bailer AJ, Bois FY, DeWoskin RS, Hays S, Johanson G, & Jones N.** Characterizing uncertainty and variability in physiologically based pharmacokinetic models: state of the science and needs for research and implementation. *Toxicological Sciences*, **2007**. 99(2): 395-402.
336. **Jamei M, Marciniak S, Feng K, Barnett A, Tucker G, & Rostami-Hodjegan A.** The Simcyp® population-based ADME simulator. *Expert Opinion on Drug Metabolism & Toxicology*, **2009**. 5(2): 211-223.
337. **Willmann S, Lippert J, Sevestre M, Solodenko J, Fois F, & Schmitt W.** PK-Sim®: a physiologically based pharmacokinetic ‘whole-body’ model. *Biosilico*, **2003**. 1(4): 121-124.
338. **Gastro Plus.** Product of Simulations Plus. Available from: www.simulationsplus.com. Accessed on 02/01/2018.
339. **Johnson TN, Rostami-Hodjegan A, & Tucker GT.** Prediction of the clearance of eleven drugs and associated variability in neonates, infants and children. *Clinical Pharmacokinetics*, **2006**. 45(9): 931-956.
340. **Jones H & Rowland-Yeo K.** Basic concepts in physiologically based pharmacokinetic modeling in drug discovery and development. *CPT: Pharmacometrics & Systems Pharmacology*, **2013**. 2(8): 1-12.
341. **Pomerantz RJ.** Reservoirs of human immunodeficiency virus type 1: the main obstacles to viral eradication. *Clinical Infectious Diseases*, **2002**. 34(1): 91-97.
342. **Yu LX & Amidon GL.** A compartmental absorption and transit model for estimating oral drug absorption. *International Journal of Pharmaceutics*, **1999**. 186(2): 119-125.

343. **Darwich A, Neuhoff S, Jamei M, & Rostami-Hodjegan A.** Interplay of metabolism and transport in determining oral drug absorption and gut wall metabolism: a simulation assessment using the “Advanced Dissolution, Absorption, Metabolism (ADAM)” model. *Current Drug Metabolism*, **2010**. 11(9): 716-729.
344. **Estudante M, Morais JG, Soveral G, & Benet LZ.** Intestinal drug transporters: an overview. *Advanced Drug Delivery Reviews*, **2013**. 65(10): 1340-1356.
345. **Sun D, Lennernäs H, Welage LS, Barnett JL, Landowski CP, Foster D, Fleisher D, Lee K-D, & Amidon GL.** Comparison of human duodenum and Caco-2 gene expression profiles for 12,000 gene sequences tags and correlation with permeability of 26 drugs. *Pharmaceutical Research*, **2002**. 19(10): 1400-1416.
346. **Helander HF & Fändriks L.** Surface area of the digestive tract—revisited. *Scandinavian Journal of Gastroenterology*, **2014**. 49(6): 681-689.
347. **Sugano K.** Artificial membrane technologies to assess transfer and permeation of drugs in drug discovery. *Comprehensive Medicinal Chemistry II*, **2007**. 5: 453-487.
348. **Crowe PT & Marsh MN.** Morphometric analysis of small intestinal mucosa IV. Determining cell volumes. *Virchows Archiv*, **1993**. 422(6): 459-466.
349. **Wasan KM.** The role of lymphatic transport in enhancing oral protein and peptide drug delivery. *Drug Development and Industrial Pharmacy*, **2002**. 28(9): 1047-1058.
350. **Poulin P & Theil FP.** Prediction of pharmacokinetics prior to in vivo studies. 1. Mechanism-based prediction of volume of distribution. *Journal of Pharmaceutical Sciences*, **2002**. 91(1): 129-156.
351. **Poulin P & Theil FP.** Prediction of pharmacokinetics prior to in vivo studies. 2. Generic physiologically based pharmacokinetic models of drug disposition. *Journal of Pharmaceutical Sciences*, **2002**. 91(5): 1358-1370.
352. **Rodgers T, Leahy D, & Rowland M.** Physiologically based pharmacokinetic modeling. 1. Predicting the tissue distribution of moderate-to-strong bases. *Journal of Pharmaceutical Sciences*, **2005**. 94(6): 1259-1276.
353. **Rodgers T & Rowland M.** Physiologically based pharmacokinetic modelling. 2. Predicting the tissue distribution of acids, very weak bases, neutrals and zwitterions. *Journal of Pharmaceutical Sciences*, **2006**. 95(6): 1238-1257.
354. **Rodgers T & Rowland M.** Mechanistic approaches to volume of distribution predictions: understanding the processes. *Pharmaceutical Research*, **2007**. 24(5): 918-933.
355. **Schmitt W.** General approach for the calculation of tissue to plasma partition coefficients. *Toxicology in Vitro*, **2008**. 22(2): 457-467.
356. **Rippe B & Haraldsson B.** Fluid and protein fluxes across small and large pores in the microvasculature. Application of two-pore equations. *Acta Physiologica*, **1987**. 131(3): 411-428.
357. **Tachibana T, Kato M, Takano J, & Sugiyama Y.** Predicting drug-drug interactions involving the inhibition of intestinal CYP3A4 and P-glycoprotein. *Current Drug Metabolism*, **2010**. 11(9): 762-777.
358. **Jamei M, Bajot F, Neuhoff S, Barter Z, Yang J, Rostami-Hodjegan A, & Rowland-Yeo K.** A mechanistic framework for in vitro–in vivo extrapolation of liver membrane transporters: prediction of drug–drug interaction between rosuvastatin and cyclosporine. *Clinical Pharmacokinetics*, **2014**. 53(1): 73-87.

359. **Noé J, Portmann R, Brun M-E, & Funk C.** Substrate-dependent drug-drug interactions between gemfibrozil, fluvastatin and other organic anion-transporting peptide (OATP) substrates on OATP1B1, OATP2B1, and OATP1B3. *Drug Metabolism and Disposition*, **2007**. 35(8): 1308-1314.
360. **Rostami-Hodjegan A & Tucker G.** 'In silico' simulations to assess the 'in vivo' consequences of 'in vitro' metabolic drug-drug interactions. *Drug Discovery Today: Technologies*, **2004**. 1(4): 441-448.
361. **Pang KS & Rowland M.** Hepatic clearance of drugs. I. Theoretical considerations of a "well-stirred" model and a "parallel tube" model. Influence of hepatic blood flow, plasma and blood cell binding, and the hepatocellular enzymatic activity on hepatic drug clearance. *Journal of Pharmacokinetics and Biopharmaceutics*, **1977**. 5(6): 625-653.
362. **Neuhoff S, Gaohua L, Burt H, Jamei M, Li L, Tucker GT, & Rostami-Hodjegan A.** Accounting for transporters in renal clearance: towards a mechanistic kidney model (Mech KiM), in *Transporters in Drug Development*. **2013**, Springer. p. 155-177.
363. **Edginton AN, Schmitt W, Voith B, & Willmann S.** A mechanistic approach for the scaling of clearance in children. *Clinical Pharmacokinetics*, **2006**. 45(7): 683-704.
364. **Cubitt HE, Rowland-Yeo K, Howgate EM, Rostami-Hodjegan A, & Barter ZE.** Sources of interindividual variability in IVIVE of clearance: an investigation into the prediction of benzodiazepine clearance using a mechanistic population-based pharmacokinetic model. *Xenobiotica*, **2011**. 41(8): 623-638.
365. **Almond LM, Mukadam S, Gardner I, Okialda K, Wong S, Hatley O, Tay S, Rowland-Yeo K, Jamei M, & Rostami-Hodjegan A.** Prediction of drug-drug interactions arising from CYP3A induction using a physiologically based dynamic model. *Drug Metabolism and Disposition*, **2016**. 44(6): 821-832.
366. **Shampine LF & Reichelt MW.** The Matlab ode suite. *SIAM Journal on Scientific Computing*, **1997**. 18(1): 1-22.
367. **Paine MF, Khalighi M, Fisher JM, Shen DD, Kunze KL, Marsh CL, Perkins JD, & Thummel KE.** Characterization of interintestinal and intrainestinal variations in human CYP3A-dependent metabolism. *Journal of Pharmacology and Experimental Therapeutics*, **1997**. 283(3): 1552-1562.
368. **Moltó J, Rajoli R, Back D, Valle M, Miranda C, Owen A, Clotet B, & Siccardi M.** Use of a physiologically based pharmacokinetic model to simulate drug-drug interactions between antineoplastic and antiretroviral drugs. *Journal of Antimicrobial Chemotherapy*, **2016**. 72(3): 805-811.
369. **Mueck W, Kubitzka D, & Becka M.** Co-administration of rivaroxaban with drugs that share its elimination pathways: pharmacokinetic effects in healthy subjects. *British Journal of Clinical Pharmacology*, **2013**. 76(3): 455-466.
370. **Kakuda TN, Opsomer M, Timmers M, Iterbeke K, Van De Casteele T, Hillewaert V, Petrovic R, & Hoetelmans RM.** Pharmacokinetics of darunavir in fixed-dose combination with cobicistat compared with coadministration of darunavir and ritonavir as single agents in healthy volunteers. *The Journal of Clinical Pharmacology*, **2014**. 54(8): 949-957.
371. **DeJesus E, Lalezari JP, Osileyemi OO, Ruane PJ, Ryan R, Kakuda TN, & Witek J.** Pharmacokinetics of once-daily etravirine without and with once-daily darunavir/ritonavir in antiretroviral-naïve HIV type-1-infected adults. *Antiviral Therapy*, **2010**. 15(5): 711.
372. **Boffito M, Miralles D, & Hill A.** Pharmacokinetics, efficacy, and safety of darunavir/ritonavir 800/100 mg once-daily in treatment-naïve and-experienced patients. *HIV Clinical Trials*, **2008**. 9(6): 418-427.

373. **Mathias A, West S, Hui J, & Kearney B.** Dose-response of ritonavir on hepatic CYP3A activity and elvitegravir oral exposure. *Clinical Pharmacology & Therapeutics*, **2009**. 85(1): 64-70.
374. **Burger D, Agarwala S, Child M, Been-Tiktak A, Wang Y, & Bertz R.** Effect of rifampin on steady-state pharmacokinetics of atazanavir with ritonavir in healthy volunteers. *Antimicrobial Agents and Chemotherapy*, **2006**. 50(10): 3336-3342.
375. **Ortman JM, Velkoff VA, & Hogan H.** An aging nation: the older population in the United States. 2014. United States Census Bureau, Economics and Statistics Administration. Available from: <https://www.census.gov/library/publications/2014/demo/p25-1140.html>. Accessed on 10/07/2020.
376. **European Union - Eurostats.** People in the EU - population projections. 2017. Available from: https://ec.europa.eu/eurostat/statistics-explained/index.php/People_in_the_EU_-_population_projections#Age_dependency_ratios. Accessed on 06/02/2019.
377. **Jaul E & Barron J.** Age-related diseases and clinical and public health implications for the 85 years old and over population. *Frontiers in Public Health*, **2017**. 5: 335-341.
378. **Eurostat.** Medicine use statistics. 2014. Available from: https://ec.europa.eu/eurostat/statistics-explained/index.php/Medicine_use_statistics. Accessed on 15/11/2018.
379. **U.S. Food and Drug Administration.** Diversity in clinical trials. 2018. Available from: <https://www.fda.gov/ForConsumers/ConsumerUpdates/ucm535306.htm>. Accessed on 15/11/2018.
380. **Chetty M, Johnson TN, Polak S, Salem F, Doki K, & Rostami-Hodjegan A.** Physiologically based pharmacokinetic modelling to guide drug delivery in older people. *Advanced Drug Delivery Reviews*, **2018**. 135: 85-96.
381. **Chetty M, Rose RH, Abduljalil K, Patel N, Lu G, Cain T, Jamei M, & Rostami-Hodjegan A.** Applications of linking PBPK and PD models to predict the impact of genotypic variability, formulation differences, differences in target binding capacity and target site drug concentrations on drug responses and variability. *Frontiers in Pharmacology*, **2014**. 5(258): 1-14.
382. **Mukherjee D, Zha J, Menon RM, & Shebley M.** Guiding dose adjustment of amlodipine after co-administration with ritonavir containing regimens using a physiologically-based pharmacokinetic/pharmacodynamic model. *Journal of Pharmacokinetics and Pharmacodynamics*, **2018**. 45(3): 443-456.
383. **Zhang T.** Physiologically based pharmacokinetic modeling of disposition and drug–drug interactions for atorvastatin and its metabolites. *European Journal of Pharmaceutical Sciences*, **2015**. 77: 216-229.
384. **Rowland-Yeo K, Walsky R, Jamei M, Rostami-Hodjegan A, & Tucker G.** Prediction of time-dependent CYP3A4 drug–drug interactions by physiologically based pharmacokinetic modelling: impact of inactivation parameters and enzyme turnover. *European Journal of Pharmaceutical Sciences*, **2011**. 43(3): 160-173.
385. **Varma MV, Lai Y, Kimoto E, Goosen TC, El-Kattan AF, & Kumar V.** Mechanistic modeling to predict the transporter-and enzyme-mediated drug-drug interactions of repaglinide. *Pharmaceutical Research*, **2013**. 30(4): 1188-1199.
386. **Faulkner J, McGibney D, Chasseaud L, Perry J, & Taylor I.** The pharmacokinetics of amlodipine in healthy volunteers after single intravenous and oral doses and after 14 repeated oral doses given once daily. *British Journal of Clinical Pharmacology*, **1986**. 22(1): 21-25.
387. **Stader F, Kinvig H, Battegay M, Khoo S, Owen A, Siccardi M, & Marzolini C.** Analysis of clinical drug-drug interaction data to predict uncharacterized interaction magnitudes between antiretroviral drugs and co-medications. *Antimicrobial Agents and Chemotherapy*, **2018**. 62(7): 1-12.

388. **Zhu Y, Wang F, Li Q, Zhu M, Du A, Tang W, & Chen W.** Amlodipine metabolism in human liver microsomes and roles of CYP3A4/5 in the dihydropyridine dehydrogenation. *Drug Metabolism and Disposition*, **2014**. 42(2): 245-249.
389. **Varma MV, Lai Y, Feng B, Litchfield J, Goosen TC, & Bergman A.** Physiologically based modeling of pravastatin transporter-mediated hepatobiliary disposition and drug-drug interactions. *Pharmaceutical Research*, **2012**. 29(10): 2860-2873.
390. **Wishart DS.** DrugBank: Lisinopril. 2005. Available from: <https://www.drugbank.ca/drugs/DB00722>. Accessed on 13/12/2018.
391. **Mueck W, Stampfuss J, Kubitza D, & Becka M.** Clinical pharmacokinetic and pharmacodynamic profile of rivaroxaban. *Clinical Pharmacokinetics*, **2014**. 53(1): 1-16.
392. **Wishart DS.** DrugBank: Midazolam. 2005. Available from: <https://www.drugbank.ca/drugs/DB00683>. Accessed on 13/12/2018.
393. **Royal Society of Chemistry.** The Merck Index Online. 2018. Available from: <https://www.rsc.org/Merck-Index/monograph/m6842/lisinopril?q=unauthorize>. Accessed on 13/12/2018.
394. **McFarland JW, Berger CM, Froshauer SA, Hayashi SF, Hecker SJ, Jaynes BH, Jefson MR, Kamicker BJ, Lipinski CA, & Lundy KM.** Quantitative structure - activity relationships among macrolide antibacterial agents: in vitro and in vivo potency against *Pasteurella multocida*. *Journal of Medicinal Chemistry*, **1997**. 40(9): 1340-1346.
395. **Walser A, Benjamin LE, Flynn T, Mason C, Schwartz R, & Fryer RI.** Quinazolines and 1, 4-benzodiazepines. 84. Synthesis and reactions of imidazo [1, 5-a][1, 4] benzodiazepines. *The Journal of Organic Chemistry*, **1978**. 43(5): 936-944.
396. **Wan H, Holmén AG, Wang Y, Lindberg W, Englund M, Någård MB, & Thompson RA.** High-throughput screening of pKa values of pharmaceuticals by pressure-assisted capillary electrophoresis and mass spectrometry. *Rapid Communications in Mass Spectrometry*, **2003**. 17(23): 2639-2648.
397. **Çelebier M, Reçber T, Koçak E, Altınöz S, & Kır S.** Determination of rivaroxaban in human plasma by solid-phase extraction-high performance liquid chromatography. *Journal of Chromatographic Science*, **2015**. 54(2): 216-220.
398. **Mandić Z & Gabelica V.** Ionization, lipophilicity and solubility properties of repaglinide. *Journal of Pharmaceutical and Biomedical Analysis*, **2006**. 41(3): 866-871.
399. **Wishart DS.** DrugBank: Clarithromycin. 2005. Available from: <https://www.drugbank.ca/drugs/DB01211>. Accessed on 29/05/2019.
400. **Grillo JA, Zhao P, Bullock J, Booth BP, Lu M, Robie-Suh K, Berglund EG, Pang KS, Rahman A, & Zhang L.** Utility of a physiologically-based pharmacokinetic (PBPK) modeling approach to quantitatively predict a complex drug-drug-disease interaction scenario for rivaroxaban during the drug review process: implications for clinical practice. *Biopharmaceutics & Drug Disposition*, **2012**. 33(2): 99-110.
401. **Obach RS, Lombardo F, & Waters NJ.** Trend analysis of a database of intravenous pharmacokinetic parameters in humans for 670 drug compounds. *Drug Metabolism and Disposition*, **2008**. 36(7): 1385-1405.
402. **Björkman S.** Prediction of drug disposition in infants and children by means of physiologically based pharmacokinetic (PBPK) modelling: theophylline and midazolam as model drugs. *British Journal of Clinical Pharmacology*, **2005**. 59(6): 691-704.
403. **Maddi S, Yamsani MR, Seeling A, & Scriba GK.** Stereoselective plasma protein binding of amlodipine. *Chirality: The Pharmacological, Biological, and Chemical Consequences of Molecular Asymmetry*, **2010**. 22(2): 262-266.

-
404. **Seedher N & Kanojia M.** Reversible binding of antidiabetic drugs, repaglinide and gliclazide, with human serum albumin. *Chemical Biology & Drug Design*, **2008**. 72(4): 290-296.
405. **Wang Q, Huang C, Jiang M, Zhu Y, Wang J, Chen J, & Shi J.** Binding interaction of atorvastatin with bovine serum albumin: spectroscopic methods and molecular docking. *Spectrochimica Acta Part A: Molecular and Biomolecular Spectroscopy*, **2016**. 156: 155-163.
406. **Yago K, Kuroyama M, Motohashi S, & Kumano K.** Protein binding of clarithromycin in patients with chronic renal failure. *The Japanese Journal of Antibiotics*, **1996**. 49(3): 256-263.
407. **Boman G & Ringberger V.** Binding of rifampicin by human plasma proteins. *European Journal of Clinical Pharmacology*, **1974**. 7(5): 369-373.
408. **Artursson P & Karlsson J.** Correlation between oral drug absorption in humans and apparent drug permeability coefficients in human intestinal epithelial (Caco-2) cells. *Biochemical and Biophysical Research Communications*, **1991**. 175(3): 880-885.
409. **Miezeiewski B.** Biopharmaceutical classification system: defining a permeability class. 2011. Absorption Systems. Available from: <http://www.as-lat.com/wp-content/uploads/2014/06/BCS-Defining-a-Permeability-Class.pdf>. Accessed on 21/11/2018.
410. **Kudo T, Goda H, Yokosuka Y, Tanaka R, Komatsu S, & Ito K.** Estimation of the contribution of CYP2C8 and CYP3A4 in repaglinide metabolism by human liver microsomes under various buffer conditions. *Journal of Pharmaceutical Sciences*, **2017**. 106(9): 2847-2852.
411. **Martin PD, Warwick MJ, Dane AL, Hill SJ, Giles PB, Phillips PJ, & Lenz E.** Metabolism, excretion, and pharmacokinetics of rosuvastatin in healthy adult male volunteers. *Clinical Therapeutics*, **2003**. 25(11): 2822-2835.
412. **Sagirli O & Ersoy L.** An HPLC method for the determination of lisinopril in human plasma and urine with fluorescence detection. *Journal of Chromatography B*, **2004**. 809(1): 159-165.
413. **Ke A, Barter Z, Rowland-Yeo K, & Almond L.** Towards a best practice approach in PBPK modeling: case example of developing a unified efavirenz model accounting for induction of CYPs 3A4 and 2B6. *CPT: Pharmacometrics & Systems Pharmacology*, **2016**. 5(7): 367-376.
414. **Kendall M, Brown D, & Yates R.** Plasma metoprolol concentrations in young, old and hypertensive subjects. *British Journal of Clinical Pharmacology*, **1977**. 4(4): 497-499.
415. **Gautam P, Vargas E, & Lye M.** Pharmacokinetics of lisinopril (MK521) in healthy young and elderly subjects and in elderly patients with cardiac failure. *Journal of Pharmacy and Pharmacology*, **1987**. 39(11): 929-931.
416. **Gomez HJ, Cirillo VJ, & Moncloa F.** The clinical pharmacology of lisinopril. *Journal of Cardiovascular Pharmacology*, **1987**. 9: S27-S34.
417. **Ulm E, Hichens M, Gomez H, Till A, Hand E, Vassil T, Biollaz J, Brunner H, & Schelling J.** Enalapril maleate and a lysine analogue (MK-521): disposition in man. *British Journal of Clinical Pharmacology*, **1982**. 14(3): 357-362.
418. **Acocella G, Pagani V, Marchetti M, Baroni G, & Nicolis F.** Kinetic studies on rifampicin. I. Serum concentration analysis in subjects treated with different oral doses over a period of two weeks. *Chemotherapy*, **1971**. 16(6): 356-370.
419. **Quarterman C, Kendall M, & Jack D.** The effect of age on the pharmacokinetics of metoprolol and its metabolites. *British Journal of Clinical Pharmacology*, **1981**. 11(3): 287-294.
420. **Abernethy DR, Gutkowska J, & Winterbottom LM.** Effects of amlodipine, a long-acting dihydropyridine calcium antagonist in aging hypertension: pharmacodynamics in relation to disposition. *Clinical Pharmacology & Therapeutics*, **1990**. 48(1): 76-86.
-

-
421. **Kubitza D, Becka M, Roth A, & Mueck W.** The influence of age and gender on the pharmacokinetics and pharmacodynamics of rivaroxaban - an oral, direct factor Xa inhibitor. *The Journal of Clinical Pharmacology*, **2013**. 53(3): 249-255.
422. **Kubitza D, Becka M, Wensing G, Voith B, & Zuehlisdorf M.** Safety, pharmacodynamics, and pharmacokinetics of BAY 59-7939—an oral, direct Factor Xa inhibitor—after multiple dosing in healthy male subjects. *European Journal of Clinical Pharmacology*, **2005**. 61(12): 873-880.
423. **Hatorp V, Huang W-C, & Strange P.** Repaglinide pharmacokinetics in healthy young adult and elderly subjects. *Clinical Therapeutics*, **1999**. 21(4): 702-710.
424. **Gibson DM, Bron NJ, Richens MA, Hounslow NJ, Sedman AJ, & Whitfield LR.** Effect of age and gender on pharmacokinetics of atorvastatin in humans. *The Journal of Clinical Pharmacology*, **1996**. 36(3): 242-246.
425. **Backman JT, Luurila H, Neuvonen M, & Neuvonen PJ.** Rifampin markedly decreases and gemfibrozil increases the plasma concentrations of atorvastatin and its metabolites. *Clinical Pharmacology & Therapeutics*, **2005**. 78(2): 154-167.
426. **Kantola T, Kivistö KT, & Neuvonen PJ.** Effect of itraconazole on the pharmacokinetics of atorvastatin. *Clinical Pharmacology & Therapeutics*, **1998**. 64(1): 58-65.
427. **Lau Y, Huang Y, Frassetto L, & Benet L.** Effect of OATP1B transporter inhibition on the pharmacokinetics of atorvastatin in healthy volunteers. *Clinical Pharmacology & Therapeutics*, **2007**. 81(2): 194-204.
428. **Pham P, La Porte C, Lee L, Van Heeswijk R, Sabo J, Elgadi M, Piliero P, Barditch-Crovo P, Fuchs E, & Flexner C.** Differential effects of tipranavir plus ritonavir on atorvastatin or rosuvastatin pharmacokinetics in healthy volunteers. *Antimicrobial Agents and Chemotherapy*, **2009**. 53(10): 4385-4392.
429. **Martin PD, Dane AL, Nwose OM, Schneck DW, & Warwick MJ.** No effect of age or gender on the pharmacokinetics of rosuvastatin: a new HMG-CoA reductase inhibitor. *The Journal of Clinical Pharmacology*, **2002**. 42(10): 1116-1121.
430. **Martin PD, Warwick MJ, Dane AL, & Cantarini MV.** A double-blind, randomized, incomplete crossover trial to assess the dose proportionality of rosuvastatin in healthy volunteers. *Clinical Therapeutics*, **2003**. 25(8): 2215-2224.
431. **Martin PD, Warwick MJ, Dane AL, Brindley C, & Short T.** Absolute oral bioavailability of rosuvastatin in healthy white adult male volunteers. *Clinical Therapeutics*, **2003**. 25(10): 2553-2563.
432. **Lee E, Ryan S, Birmingham B, Zalikowski J, March R, Ambrose H, Moore R, Lee C, Chen Y, & Schneck D.** Rosuvastatin pharmacokinetics and pharmacogenetics in white and Asian subjects residing in the same environment. *Clinical Pharmacology & Therapeutics*, **2005**. 78(4): 330-341.
433. **Chu Sy, Wilson DS, Guay DR, & Craft C.** Clarithromycin pharmacokinetics in healthy young and elderly volunteers. *The Journal of Clinical Pharmacology*, **1992**. 32(11): 1045-1049.
434. **Chandler M, Toler S, Rapp R, Muder R, & Korvick J.** Multiple-dose pharmacokinetics of concurrent oral ciprofloxacin and rifampin therapy in elderly patients. *Antimicrobial Agents and Chemotherapy*, **1990**. 34(3): 442-447.
435. **Turnheim K, Krivanek P, & Oberbauer R.** Pharmacokinetics and pharmacodynamics of allopurinol in elderly and young subjects. *British Journal of Clinical Pharmacology*, **1999**. 48(4): 501.
436. **Kaplan GB, Greenblatt DJ, Ehrenberg BL, Goddard JE, Harmatz JS, & Shader RI.** Single-dose pharmacokinetics and pharmacodynamics of alprazolam in elderly and young subjects. *The Journal of Clinical Pharmacology*, **1998**. 38(1): 14-21.
-

-
437. **Hayden F, Minocha A, Spyker D, & Hoffman H.** Comparative single-dose pharmacokinetics of amantadine hydrochloride and rimantadine hydrochloride in young and elderly adults. *Antimicrobial Agents and Chemotherapy*, **1985**. 28(2): 216-221.
438. **Sabanathan K, Castleden C, Adam H, Ryan J, & Fitzsimons T.** A comparative study of the pharmacokinetics and pharmacodynamics of atenolol, hydrochlorothiazide and amiloride in normal young and elderly subjects and elderly hypertensive patients. *European Journal of Clinical Pharmacology*, **1987**. 32(1): 53-60.
439. **Rho JP, Jones A, Woo M, Castle S, Smith K, Bawdon RE, & Norman DC.** Single-dose pharmacokinetics of intravenous ampicillin plus sulbactam in healthy elderly and young adult subjects. *Journal of Antimicrobial Chemotherapy*, **1989**. 24(4): 573-580.
440. **Meyers BR, Wilkinson P, Mendelson M, Walsh S, Bournazos C, & Hirschman S.** Pharmacokinetics of ampicillin-sulbactam in healthy elderly and young volunteers. *Antimicrobial Agents and Chemotherapy*, **1991**. 35(10): 2098-2101.
441. **Rigby J, Scott A, Hawksworth G, & Petrie J.** A comparison of the pharmacokinetics of atenolol, metoprolol, oxprenolol and propranolol in elderly hypertensive and young healthy subjects. *British Journal of Clinical Pharmacology*, **1985**. 20(4): 327-331.
442. **Tarral A & Merdjan H.** Effect of age and sex on the pharmacokinetics and safety of avibactam in healthy volunteers. *Clinical Therapeutics*, **2015**. 37(4): 877-886.
443. **Coates P, Daniel R, Houston A, Antrobus J, & Taylor T.** An open study to compare the pharmacokinetics, safety and tolerability of a multiple-dose regimen of azithromycin in young and elderly volunteers. *European Journal of Clinical Microbiology and Infectious Diseases*, **1991**. 10(10): 850-852.
444. **Blanchard J & Sowers SJ.** Comparative pharmacokinetics of caffeine in young and elderly men. *Journal of Pharmacokinetics and Pharmacodynamics*, **1983**. 11(2): 109-126.
445. **Faulkner R, Bohaychuk W, Lanc R, Haynes J, Desjardins R, Yacobi A, & Silber B.** Pharmacokinetics of cefixime in the young and elderly. *Journal of Antimicrobial Chemotherapy*, **1988**. 21(6): 787-794.
446. **Tremblay D, Dupront A, Ho C, Coussediere D, & Lenfant B.** Pharmacokinetics of cefpodoxime in young and elderly volunteers after single doses. *Journal of Antimicrobial Chemotherapy*, **1990**. 26(Suppl E): 21-28.
447. **Williams P, Brown A, Rajaguru S, Walters G, McEwen J, & Durnin C.** A pharmacokinetic study of cilazapril in elderly and young volunteers. *British Journal of Clinical Pharmacology*, **1989**. 27(S2): 211S-215S.
448. **Shah A, Lettieri J, Nix D, Wilton J, & Heller A.** Pharmacokinetics of high-dose intravenous ciprofloxacin in young and elderly and in male and female subjects. *Antimicrobial Agents and Chemotherapy*, **1995**. 39(4): 1003-1006.
449. **Gutierrez M & Abramowitz W.** Steady-state pharmacokinetics of citalopram in young and elderly subjects. *Pharmacotherapy: The Journal of Human Pharmacology and Drug Therapy*, **2000**. 20(12): 1441-1447.
450. **Abernethy D, Greenblatt D, & Shader R.** Imipramine and desipramine disposition in the elderly. *Journal of Pharmacology and Experimental Therapeutics*, **1985**. 232(1): 183-188.
451. **Klotz U, Avant G, Hoyumpa A, Schenker S, & Wilkinson G.** The effects of age and liver disease on the disposition and elimination of diazepam in adult man. *The Journal of Clinical Investigation*, **1975**. 55(2): 347-359.
452. **Scavone JM, Greenblatt DJ, Harmatz JS, Engelhardt N, & Shader RI.** Pharmacokinetics and pharmacodynamics of diphenhydramine 25 mg in young and elderly volunteers. *The Journal of Clinical Pharmacology*, **1998**. 38(7): 603-609.
-

-
453. **Simons KJ, Watson WT, Martin TJ, Chen MXY, & Simons FER.** Diphenhydramine: pharmacokinetics and pharmacodynamics in elderly adults, young adults, and children. *The Journal of Clinical Pharmacology*, **1990**. 30(7): 665-671.
454. **Hockings N, Ajayi A, & Reid J.** Age and the pharmacokinetics of angiotensin converting enzyme inhibitors enalapril and enalaprilat. *British Journal of Clinical Pharmacology*, **1986**. 21(4): 341-348.
455. **Almeida L, Falcão A, Maia J, Mazur D, Gellert M, & Soares-da-Silva P.** Single-dose and steady-state pharmacokinetics of eslicarbazepine acetate (BIA 2-093) in healthy elderly and young subjects. *The Journal of Clinical Pharmacology*, **2005**. 45(9): 1062-1066.
456. **Harvey AT & Preskorn SH.** Fluoxetine pharmacokinetics and effect on CYP2C19 in young and elderly volunteers. *Journal of Clinical Psychopharmacology*, **2001**. 21(2): 161-166.
457. **Abernethy DR & Greenblatt DJ.** Impairment of lidocaine clearance in elderly male subjects. *Journal of Cardiovascular Pharmacology*, **1983**. 5(6): 1093-1096.
458. **Greenblatt DJ, Allen MD, Locniskar A, Harmatz JS, & Shader RI.** Lorazepam kinetics in the elderly. *Clinical Pharmacology & Therapeutics*, **1979**. 26(1): 103-113.
459. **Ljungberg B & Nilsson-Ehle I.** Pharmacokinetics of meropenem and its metabolite in young and elderly healthy men. *Antimicrobial Agents and Chemotherapy*, **1992**. 36(7): 1437-1440.
460. **Sambol NC, Chiang J, Lin ET, Goodman AM, Liu CY, Benet LZ, & Cogan MG.** Kidney function and age are both predictors of pharmacokinetics of metformin. *The Journal of Clinical Pharmacology*, **1995**. 35(11): 1094-1102.
461. **Tornatore KM, Logue G, Venuto RC, & Davis PJ.** Pharmacokinetics of methylprednisolone in elderly and young healthy males. *Journal of the American Geriatrics Society*, **1994**. 42(10): 1118-1122.
462. **Zhao JJ, Rogers JD, Holland SD, Larson P, Amin RD, Haesen R, Freeman A, Seiberling M, Merz M, & Cheng H.** Pharmacokinetics and bioavailability of montelukast sodium (MK-0476) in healthy young and elderly volunteers. *Biopharmaceutics & Drug Disposition*, **1997**. 18(9): 769-777.
463. **Baillie S, Bateman D, Coates P, & Woodhouse K.** Age and the pharmacokinetics of morphine. *Age and Ageing*, **1989**. 18(4): 258-262.
464. **Jaillon P, Gardin M, Lecocq B, Richard M, Meignan S, Blondel Y, Grippat J, Bergnieres J, & Vergnoux O.** Pharmacokinetics of nalbuphine in infants, young healthy volunteers, and elderly patients. *Clinical Pharmacology & Therapeutics*, **1989**. 46(2): 226-233.
465. **Upton R, Williams R, Kelly J, & Jones R.** Naproxen pharmacokinetics in the elderly. *British Journal of Clinical Pharmacology*, **1984**. 18(2): 207-214.
466. **Crome P, Müller F, Wijayawardhana P, Groenewoud G, Hundt H, Leighton G, Luus H, Schall R, & Van Dyk M.** Single dose and steady-state pharmacokinetic profiles of nifedipine GITS tablets in healthy elderly and young volunteers. *Drug Investigation*, **1993**. 5(4): 193-199.
467. **Landahl S, Andersson T, Larsson M, Lernfeldt B, Lundborg P, Regårdh C-G, Sixt E, & Skånberg I.** Pharmacokinetic study of omeprazole in elderly healthy volunteers. *Clinical Pharmacokinetics*, **1992**. 23(6): 469-476.
468. **Liukas A, Kuusniemi K, Aantaa R, Virolainen P, Neuvonen M, Neuvonen P, & Olkkola K.** Plasma concentrations of oral oxycodone are greatly increased in the elderly. *Clinical Pharmacology & Therapeutics*, **2008**. 84(4): 462-467.
469. **Dörwald FZ.** Lead optimization for medicinal chemists: pharmacokinetic properties of functional groups and organic compounds. **2012**: John Wiley & Sons.
-

-
470. **Rakhit A, Kochak G, Tipnis V, Radensky P, Hurley M, & Williams R.** Pharmacokinetics of pentopril in the elderly. *British Journal of Clinical Pharmacology*, **1987**. 24(3): 351-357.
471. **Pan HY, Wacławski AP, Funke PT, & Whigan D.** Pharmacokinetics of pravastatin in elderly versus young men and women. *Annals of Pharmacotherapy*, **1993**. 27(9): 1029-1033.
472. **Rubin PC, Scott P, & Reid JL.** Prazosin disposition in young and elderly subjects. *British Journal of Clinical Pharmacology*, **1981**. 12(3): 401-404.
473. **Andros E, Detmar-Hanna D, Suteaparuk S, Gal J, & Gerber J.** The effect of aging on the pharmacokinetics and pharmacodynamics of prazosin. *European Journal of Clinical Pharmacology*, **1996**. 50(1-2): 41-46.
474. **Castleden C, Kaye C, & Parsons R.** The effect of age on plasma levels of propranolol and practolol in man. *British Journal of Clinical Pharmacology*, **1975**. 2(4): 303-306.
475. **Snoeck E, Van Peer A, Mannens G, Woestenborghs R, Heykants J, Sack M, Horton M, & Meibach R.** Influence of age, renal and liver impairment on the pharmacokinetics of risperidone in man. *Psychopharmacology*, **1995**. 122(3): 223-229.
476. **Ronfeld RA, Tremaine LM, & Wilner KD.** Pharmacokinetics of sertraline and its N-demethyl metabolite in elderly and young male and female volunteers. *Clinical Pharmacokinetics*, **1997**. 32(1): 22-30.
477. **Hind I, Mangham J, Ghani S, Haddock R, Garratt C, & Jones R.** Sibutramine pharmacokinetics in young and elderly healthy subjects. *European Journal of Clinical Pharmacology*, **1999**. 54(11): 847-849.
478. **Perret C, Lenfant B, Weinling E, Wessels D, Scholtz H, Montay G, & Sultan E.** Pharmacokinetics and absolute oral bioavailability of an 800 mg oral dose of telithromycin in healthy young and elderly volunteers. *Chemotherapy*, **2002**. 48(5): 217-223.
479. **Shin SG, Juan D, & Rammohan M.** Theophylline pharmacokinetics in normal elderly subjects. *Clinical Pharmacology & Therapeutics*, **1988**. 44(5): 522-530.
480. **Antal E, Kramer PA, Mercik SA, Chapron D, & Lawson I.** Theophylline pharmacokinetics in advanced age. *British Journal of Clinical Pharmacology*, **1981**. 12(5): 637-645.
481. **Shah J, Teitelbaum P, Molony B, Gabuzda T, & Massey I.** Single and multiple dose pharmacokinetics of ticlopidine in young and elderly subjects. *British Journal of Clinical Pharmacology*, **1991**. 32(6): 761-764.
482. **Greenblatt DJ, Harmatz JS, Moltke LL, Wright CE, & Shader RI.** Age and gender effects on the pharmacokinetics and pharmacodynamics of triazolam, a cytochrome P450 3A substrate. *Clinical Pharmacology & Therapeutics*, **2004**. 76(5): 467-479.
483. **Greenblatt D, Divoll M, Abernethy DR, Moschitto L, Smith R, & Shader R.** Reduced clearance of triazolam in old age: relation to antipyrine oxidizing capacity. *British Journal of Clinical Pharmacology*, **1983**. 15(3): 303-309.
484. **Bryson S, Verma N, Scott P, & Rubin P.** Pharmacokinetics of valproic acid in young and elderly subjects. *British Journal of Clinical Pharmacology*, **1983**. 16(1): 104-105.
485. **Gupta S, Atkinson L, Tu T, & Longstreth J.** Age and gender related changes in stereoselective pharmacokinetics and pharmacodynamics of verapamil and norverapamil. *British Journal of Clinical Pharmacology*, **1995**. 40(4): 325-331.
486. **Wilner K, Tensfeldt T, Baris B, Smolarek T, Turncliff R, Colburn W, & Hansen R.** Single- and multiple-dose pharmacokinetics of ziprasidone in healthy young and elderly volunteers. *British Journal of Clinical Pharmacology*, **2000**. 49(S1): 15-20.
-

-
487. **Olubodun JO, Ochs HR, Von Moltke LL, Roubenoff R, Hesse LM, Harmatz JS, Shader RI, & Greenblatt DJ.** Pharmacokinetic properties of zolpidem in elderly and young adults: possible modulation by testosterone in men. *British Journal of Clinical Pharmacology*, **2003**. 56(3): 297-304.
488. **Wishart DS, Knox C, Guo AC, Cheng D, Shrivastava S, Tzur D, Gautam B, & Hassanali M.** DrugBank: a knowledgebase for drugs, drug actions and drug targets. *Nucleic Acids Research*, **2007**. 36(Suppl. 1): D901-D906.
489. **Abernethy DR, Gutkowska J, & Lambert MD.** Amlodipine in elderly hypertensive patients: pharmacokinetics and pharmacodynamics. *Journal of Cardiovascular Pharmacology*, **1988**. 12: S67-71.
490. **Rodvold KA.** Clinical pharmacokinetics of clarithromycin. *Clinical Pharmacokinetics*, **1999**. 37(5): 385-398.
491. **Acocella G.** Clinical pharmacokinetics of rifampicin. *Clinical Pharmacokinetics*, **1978**. 3(2): 108-127.
492. **Regårdh C, Landahl S, Larsson M, Lundborg P, Steen B, Hoffmann K-J, & Lagerström P-O.** Pharmacokinetics of metoprolol and its metabolite α -OH-metoprolol in healthy, non-smoking, elderly individuals. *European Journal of Clinical Pharmacology*, **1983**. 24(2): 221-226.
493. **Beermann B.** Pharmacokinetics of lisinopril. *The American Journal of Medicine*, **1988**. 85(3): 25-30.
494. **Lennernas H.** Clinical pharmacokinetics of atorvastatin. *Clinical Pharmacokinetics*, **2003**. 42(13): 1141-1160.
495. **Vestal RE, McGuire EA, Tobin JD, Andres R, Norris AH, & Mezey E.** Aging and ethanol metabolism. *Clinical Pharmacology & Therapeutics*, **1977**. 21(3): 343-354.
496. **Redolfi A, Borgogelli E, & Lodola E.** Blood level of cimetidine in relation to age. *European Journal of Clinical Pharmacology*, **1979**. 15(4): 257-261.
497. **Cusack B, Kelly J, O'Malley K, Noel J, Lavan J, & Horgan J.** Digoxin in the elderly: pharmacokinetic consequences of old age. *Clinical Pharmacology & Therapeutics*, **1979**. 25(6): 772-776.
498. **Vestal R, Wood A, Branch R, Shand D, & Wilkinson G.** Effects of age and cigarette smoking on propranolol disposition. *Clinical Pharmacology & Therapeutics*, **1979**. 26(1): 8-15.
499. **Greenblatt DJ, Abernethy DR, Locniskar A, Harmatz JS, Limjuco RA, & Shader RI.** Effect of age, gender, and obesity on midazolam kinetics. *Anesthesiology*, **1984**. 61(1): 27-35.
500. **Soldin OP & Mattison DR.** Sex differences in pharmacokinetics and pharmacodynamics. *Clinical Pharmacokinetics*, **2009**. 48(3): 143-157.
501. **Rodighiero V.** Effects of cardiovascular disease on pharmacokinetics. *Cardiovascular Drugs and Therapy*, **1989**. 3(5): 711-730.
502. **Wooten JM.** Pharmacotherapy considerations in elderly adults. *Southern Medical Journal*, **2012**. 105(8): 437-445.
503. **Albrecht S, Ihmsen H, Hering W, Geisslinger G, Dingemanse J, Schwilden H, & Schüttler J.** The effect of age on the pharmacokinetics and pharmacodynamics of midazolam. *Clinical Pharmacology & Therapeutics*, **1999**. 65(6): 630-639.
504. **Goa KL, Balfour JA, & Zuanetti G.** Lisinopril. A review of its pharmacology and clinical efficacy in the early management of acute myocardial infarction. *Drugs*, **1996**. 52(4): 564-588.
-

505. **Leenen FH & Coletta E.** Pharmacokinetic and antihypertensive profile of amlodipine and felodipine-ER in younger versus older patients with hypertension. *Journal of Cardiovascular Pharmacology*, **2010**. 56(6): 669-675.
506. **Kubitza D, Becka M, Voith B, Zuehlisdorf M, & Wensing G.** Safety, pharmacodynamics, and pharmacokinetics of single doses of BAY 59-7939, an oral, direct factor Xa inhibitor. *Clinical Pharmacology & Therapeutics*, **2005**. 78(4): 412-421.
507. **Kubitza D, Becka M, Roth A, & Mueck W.** Dose-escalation study of the pharmacokinetics and pharmacodynamics of rivaroxaban in healthy elderly subjects. *Current Medical Research and Opinion*, **2008**. 24(10): 2757-2765.
508. **Szadkowska I, Stanczyk A, Aronow WS, Kowalski J, Pawlicki L, Ahmed A, & Banach M.** Statin therapy in the elderly: a review. *Archives of Gerontology and Geriatrics*, **2010**. 50(1): 114-118.
509. **Vass M & Hendriksen C.** Medication for older people. *Zeitschrift für Gerontologie und Geriatrie*, **2005**. 38(3): 190-195.
510. **Hogg R, Lima V, Sterne J, Grabar S, Battegay M, Bonarek M, D'Arminio Monforte A, Esteve A, Gill M, & Harris R.** Antiretroviral therapy cohort collaboration: life expectancy of individuals on combination antiretroviral therapy in high-income countries: a collaborative analysis of 14 cohort studies. *Lancet*, **2008**. 372(9635): 293-299.
511. **Wagner C, Zhao P, Pan Y, Hsu V, Grillo J, Huang S, & Sinha V.** Application of physiologically based pharmacokinetic (PBPK) modeling to support dose selection: report of an FDA public workshop on PBPK. *CPT: Pharmacometrics & Systems Pharmacology*, **2015**. 4(4): 226-230.
512. **Stader F, Kinvig H, Penny MA, Battegay M, Siccardi M, & Marzolini C.** Physiologically based pharmacokinetic modelling to identify pharmacokinetic parameters driving drug exposure changes in the elderly. *Clinical Pharmacokinetics*, **2020**. 59(3): 383-401.
513. **Csajka C, Marzolini C, Fattinger K, Décosterd LA, Fellay J, Telenti A, Biollaz J, & Buclin T.** Population pharmacokinetics and effects of efavirenz in patients with human immunodeficiency virus infection. *Clinical Pharmacology & Therapeutics*, **2003**. 73(1): 20-30.
514. **Burger D, Huisman A, Van Ewijk N, Neisingh H, Van Uden P, Rongen G, Koopmans P, & Bertz R.** The effect of atazanavir and atazanavir/ritonavir on UDP-glucuronosyltransferase using lamotrigine as a phenotypic probe. *Clinical Pharmacology & Therapeutics*, **2008**. 84(6): 698-703.
515. **McCance-Katz EF, Moody DE, Morse GD, Ma Q, DiFrancesco R, Friedland G, Pade P, & Rainey PM.** Interaction between buprenorphine and atazanavir or atazanavir/ritonavir. *Drug and Alcohol Dependence*, **2007**. 91(2-3): 269-278.
516. **Ford SL, Gould E, Chen S, Margolis D, Spreen W, Crauwels H, & Piscitelli S.** Lack of pharmacokinetic interaction between rilpivirine and integrase inhibitors dolutegravir and GSK1265744. *Antimicrobial Agents and Chemotherapy*, **2013**. 57(11): 5472-5477.
517. **Song I, Borland J, Min S, Lou Y, Chen S, Patel P, Wajima T, & Piscitelli SC.** The effect of etravirine alone and with ritonavir-boosted protease inhibitors on the pharmacokinetics of dolutegravir. *Antimicrobial Agents and Chemotherapy*, **2011**. 55(7): 3517-3521.
518. **Anderson MS, Kakuda TN, Hanley W, Miller J, Kost JT, Stoltz R, Wenning LA, Stone JA, Hoetelmans RM, & Wagner JA.** Minimal pharmacokinetic interaction between the human immunodeficiency virus nonnucleoside reverse transcriptase inhibitor etravirine and the integrase inhibitor raltegravir in healthy subjects. *Antimicrobial Agents and Chemotherapy*, **2008**. 52(12): 4228-4232.
519. **Cattaneo D, Ripamonti D, Baldelli S, Cozzi V, Conti F, & Clementi E.** Exposure-related effects of atazanavir on the pharmacokinetics of raltegravir in HIV-1-infected patients. *Therapeutic Drug Monitoring*, **2010**. 32(6): 782-786.

520. Iwamoto M, Wenning LA, Mistry GC, Petry AS, Liou SY, Ghosh K, Breidinger S, Azrolan N, Gutierrez MJ, & Bridson WE. Atazanavir modestly increases plasma levels of raltegravir in healthy subjects. *Clinical Infectious Diseases*, **2008**. 47(1): 137-140.
521. Iwamoto M, Wenning LA, Petry AS, Laethem M, De Smet M, Kost JT, Breidinger SA, Mangin EC, Azrolan N, & Greenberg HE. Minimal effects of ritonavir and efavirenz on the pharmacokinetics of raltegravir. *Antimicrobial Agents and Chemotherapy*, **2008**. 52(12): 4338-4343.
522. Dickinson L, Yapa HM, Jackson A, Moyle G, Else L, Amara A, Khoo S, Back D, Karolia Z, & Higgs C. Plasma tenofovir, emtricitabine, and rilpivirine and intracellular tenofovir diphosphate and emtricitabine triphosphate pharmacokinetics following drug intake cessation. *Antimicrobial Agents and Chemotherapy*, **2015**. 59(10): 6080-6086.
523. Villani P, Regazzi M, Castelli F, Viale P, Torti C, Seminari E, & Maserati R. Pharmacokinetics of efavirenz (EFV) alone and in combination therapy with nelfinavir (NFV) in HIV-1 infected patients. *British Journal of Clinical Pharmacology*, **1999**. 48(5): 712-715.
524. Blum MR, Chittick GE, Begley JA, & Zong J. Steady-state pharmacokinetics of emtricitabine and tenofovir disoproxil fumarate administered alone and in combination in healthy volunteers. *The Journal of Clinical Pharmacology*, **2007**. 47(6): 751-759.
525. Ramanathan S, Shen G, Cheng A, & Kearney BP. Pharmacokinetics of emtricitabine, tenofovir, and GS-9137 following coadministration of emtricitabine/tenofovir disoproxil fumarate and ritonavir-boosted GS-9137. *Journal of Acquired Immune Deficiency Syndromes*, **2007**. 45(3): 274-279.
526. Wang LH, Begley J, St. Claire III RL, Harris J, Wakeford C, & Rousseau FS. Pharmacokinetic and pharmacodynamic characteristics of emtricitabine support its once daily dosing for the treatment of HIV infection. *AIDS Research & Human Retroviruses*, **2004**. 20(11): 1173-1182.
527. Winiwarter S, Bonham NM, Ax F, Hallberg A, Lennernäs H, & Karlén A. Correlation of human jejunal permeability (in vivo) of drugs with experimentally and theoretically derived parameters. A multivariate data analysis approach. *Journal of Medicinal Chemistry*, **1998**. 41(25): 4939-4949.
528. Vermeir M, Lachau-Durand S, Mannens G, Cuyckens F, van Hoof B, & Raoof A. Absorption, metabolism, and excretion of darunavir, a new protease inhibitor, administered alone and with low-dose ritonavir in healthy subjects. *Drug Metabolism and Disposition*, **2009**. 37(4): 809-820.
529. ViiV Healthcare Company. Dolutegravir - Full prescribing information. 2018. Available from: <https://aidsinfo.nih.gov/drugs/509/dolutegravir/167/professional>. Accessed on 02/04/2019.
530. U.S. Food and Drug Administration. Rilpivirine - Clinical pharmacology and biopharmaceutics review(s). 2010. Available from: https://www.accessdata.fda.gov/drugsatfda_docs/nda/2011/202022Orig1s000ClinPharmR.pdf. Accessed on 01/04/2019.
531. European Medicines Agency. Emtriva - Summary of product characteristics. 2003. Available from: https://www.ema.europa.eu/en/documents/product-information/emtriva-epar-product-information_en.pdf. Accessed on 03/01/2020.
532. Moss DM, Siccardi M, Back DJ, & Owen A. Predicting intestinal absorption of raltegravir using a population-based ADME simulation. *Journal of Antimicrobial Chemotherapy*, **2013**. 68(7): 1627-1634.
533. Wishart DS. DrugBank: Dolutegravir. 2013. Available from: <https://www.drugbank.ca/drugs/DB08930>. Accessed on 01/04/2019.
534. Ursu O, Oprea T, & Holmes J. Raltegravir. 2018. Available from: <http://drugcentral.org/drugcard/2352?q=raltegravir>. Accessed on 03/01/2020.

535. **Wishart DS.** DrugBank: Etravirine. 2008. Available from: <https://www.drugbank.ca/drugs/DB06414>. Accessed on 01/04/2019.
536. **Wishart DS.** DrugBank: Tenofovir. 2018. Available from: <https://www.drugbank.ca/drugs/DB14126>. Accessed on 01/04/2019.
537. **Wishart DS.** DrugBank: Emtricitabine. 2005. Available from: <https://www.drugbank.ca/drugs/DB00879>. Accessed on 01/04/2019.
538. **De Sousa Mendes M, Hirt D, Urien S, Valade E, Bouazza N, Foissac F, Blanche S, Treluyer JM, & Benaboud S.** Physiologically-based pharmacokinetic modeling of renally excreted antiretroviral drugs in pregnant women. *British Journal of Clinical Pharmacology*, **2015**. 80(5): 1031-1041.
539. **Colbers A, Greupink R, Litjens C, Burger D, & Russel FG.** Physiologically based modelling of darunavir/ritonavir pharmacokinetics during pregnancy. *Clinical Pharmacokinetics*, **2016**. 55(3): 381-396.
540. **Kobayashi M, Yoshinaga T, Seki T, Wakasa-Morimoto C, Brown KW, Ferris R, Foster SA, Hazen RJ, Miki S, & Suyama-Kagitani A.** In vitro antiretroviral properties of S/GSK1349572, a next-generation HIV integrase inhibitor. *Antimicrobial Agents and Chemotherapy*, **2011**. 55(2): 813-821.
541. **Barau C, Furlan V, Yazdanpanah Y, Fagard C, Molina J-M, Taburet A-M, & Barrail-Tran A.** Characterization of binding of raltegravir to plasma proteins. *Antimicrobial Agents and Chemotherapy*, **2013**. 57(10): 5147-5150.
542. **Wanke R, Harjivan SG, Pereira SA, Marques MM, & Antunes AM.** The role of competitive binding to human serum albumin on efavirenz-warfarin interaction: a nuclear magnetic resonance study. *International Journal of Antimicrobial Agents*, **2013**. 42(5): 443-446.
543. **Kaspera R, Kirby BJ, Sahele T, Collier AC, Kharasch ED, Unadkat JD, & Totah RA.** Investigating the contribution of CYP2J2 to ritonavir metabolism in vitro and in vivo. *Biochemical Pharmacology*, **2014**. 91(1): 109-118.
544. **Kozawa O, Uematsu T, Matsuno H, Niwa M, Nagashima S, & Kanamaru M.** Comparative study of pharmacokinetics of two new fluoroquinolones, balofloxacin and grepafloxacin, in elderly subjects. *Antimicrobial Agents and Chemotherapy*, **1996**. 40(12): 2824-2828.
545. **Kozawa O, Uematsu T, Matsuno H, Niwa M, Takiguchi Y, Matsumoto S, Minamoto M, Niida Y, Yokokawa M, & Nagashima S.** Pharmacokinetics and safety of a new parenteral carbapenem antibiotic, biapenem (L-627), in elderly subjects. *Antimicrobial Agents and Chemotherapy*, **1998**. 42(6): 1433-1436.
546. **Ohnishi A, Mihara M, Kamakura H, Tomono Y, Hasegawa J, Yamazaki K, Morishita N, & Tanaka T.** Comparison of the pharmacokinetics of E2020, a new compound for Alzheimer's disease, in healthy young and elderly subjects. *The Journal of Clinical Pharmacology*, **1993**. 33(11): 1086-1091.
547. **Inotsume N, Nishimura M, Fujiyama S, Sagara K, Sato T, Imai Y, Matsui H, & Nakano M.** Pharmacokinetics of famotidine in elderly patients with and without renal insufficiency and in healthy young volunteers. *European Journal of Clinical Pharmacology*, **1989**. 36(5): 517-520.
548. **Jarivis B & Faulds D.** Lamivudine: a review of its therapeutic potential in chronic hepatitis B. *Drugs*, **1999**. 58(1): 101-141.
549. **Jang K, Chung H, Yoon Js, Moon SJ, Yoon SH, Yu KS, Kim K, & Chung JY.** Pharmacokinetics, safety, and tolerability of metformin in healthy elderly subjects. *The Journal of Clinical Pharmacology*, **2016**. 56(9): 1104-1110.

550. **Wang HY, Chen X, Jiang J, Shi J, & Hu P.** Evaluating a physiologically based pharmacokinetic model for predicting the pharmacokinetics of midazolam in Chinese after oral administration. *Acta Pharmacologica Sinica*, **2016**. 37(2): 276.
551. **Abe M, Smith J, Urae A, Barrett J, Kinoshita H, & Rayner CR.** Pharmacokinetics of oseltamivir in young and very elderly subjects. *Annals of Pharmacotherapy*, **2006**. 40(10): 1724-1730.
552. **Zhao X, Sun P, Zhou Y, Liu Y, Zhang H, Mueck W, Kubitz D, Bauer RJ, Zhang H, & Cui Y.** Safety, pharmacokinetics and pharmacodynamics of single/multiple doses of the oral, direct Factor Xa inhibitor rivaroxaban in healthy Chinese subjects. *British Journal of Clinical Pharmacology*, **2009**. 68(1): 77-88.
553. **Jiang J, Hu Y, Zhang J, Yang J, Mueck W, Kubitz D, Bauer RJ, Meng L, & Hu P.** Safety, pharmacokinetics and pharmacodynamics of single doses of rivaroxaban—an oral, direct factor Xa inhibitor—in elderly Chinese subjects. *Thrombosis and Haemostasis*, **2010**. 103(01): 234-241.
554. **Sasaki M, Tateishi T, & Ebihara A.** The effects of age and gender on the stereoselective pharmacokinetics of verapamil. *Clinical Pharmacology & Therapeutics*, **1993**. 54(3): 278-285.
555. **Dallmann A, Ince I, Coboeken K, Eissing T, & Hempel G.** A physiologically based pharmacokinetic model for pregnant women to predict the pharmacokinetics of drugs metabolized via several enzymatic pathways. *Clinical Pharmacokinetics*, **2018**. 57(6): 749-768.
556. **Wagner C, Pan Y, Hsu V, Grillo JA, Zhang L, Reynolds KS, Sinha V, & Zhao P.** Predicting the effect of cytochrome P450 inhibitors on substrate drugs: analysis of physiologically based pharmacokinetic modeling submissions to the US Food and Drug Administration. *Clinical Pharmacokinetics*, **2015**. 54(1): 117-127.
557. **Fortuna S, Fabbiani M, Digiambenedetto S, Ragazzoni E, Lisi L, Cauda R, & Navarra P.** Variability of raltegravir plasma levels in the clinical setting. *Pharmacology*, **2013**. 92(1-2): 43-48.
558. **Arab-Alameddine M, Fayet-Mello A, Lubomirov R, Neely M, di Iulio J, Owen A, Boffito M, Cavassini M, Günthard HF, & Rentsch K.** Population pharmacokinetic analysis and pharmacogenetics of raltegravir in HIV-positive and healthy individuals. *Antimicrobial Agents and Chemotherapy*, **2012**. 56(6): 2959-2966.
559. **Khanal A, Castelino R, Peterson G, & Jose M.** Dose adjustment guidelines for medications in patients with renal impairment: how consistent are drug information sources? *Internal Medicine Journal*, **2014**. 44(1): 77-85.
560. **Sato K, Kawamura T, & Wakusawa R.** Hepatic blood flow and function in elderly patients undergoing laparoscopic cholecystectomy. *Anesthesia & Analgesia*, **2000**. 90(5): 1198-1202.
561. **Imai E, Horio M, Yamagata K, Iseki K, Hara S, Ura N, Kiyohara Y, Makino H, Hishida A, & Matsuo S.** Slower decline of glomerular filtration rate in the Japanese general population: a longitudinal 10-year follow-up study. *Hypertension Research*, **2008**. 31(3): 433.
562. **Klein K, Lang T, Saussele T, Barbosa-Sicard E, Schunck W-H, Eichelbaum M, Schwab M, & Zanger UM.** Genetic variability of CYP2B6 in populations of African and Asian origin: allele frequencies, novel functional variants, and possible implications for anti-HIV therapy with efavirenz. *Pharmacogenetics and Genomics*, **2005**. 15(12): 861-873.
563. **Li J, Menard V, Benish RL, Jurevic RJ, Guillemette C, Stoneking M, Zimmerman PA, & Mehlotra RK.** Worldwide variation in human drug-metabolism enzyme genes CYP2B6 and UGT2B7: implications for HIV/AIDS treatment. *Pharmacogenomics*, **2012**. 13(5): 555-570.
564. **Bernaude C, Sécher S, Michau C, Perre P, Fialaire P, Vatan R, Raffi F, Allavena C, & Hitoto H.** HIV-infected patients aged above 75 years. *Medecine et Maladies Infectieuses*, **2019**. 50(1): 43-48.

565. **Welage LS, Carver PL, Revankar S, Pierson C, & Kauffman CA.** Alterations in gastric acidity in patients infected with human immunodeficiency virus. *Clinical Infectious Diseases*, **1995**. 21(6): 1431-1438.
566. **Merry C, Mulcahy F, Gibbons S, Lloyd J, Barry M, & Back D.** Alpha (1)-acid glycoprotein concentration in HIV disease: implications for treatment with protease inhibitors. *AIDS*, **1996**. 10: P21.
567. **Dickinson L, Khoo S, & Back D.** Differences in the pharmacokinetics of protease inhibitors between healthy volunteers and HIV-infected persons. *Current Opinion in HIV and AIDS*, **2008**. 3(3): 296-305.
568. **Marzolini C & Livio F.** Prescribing issues in elderly individuals living with HIV. *Expert Review of Clinical Pharmacology*, **2019**. 12(7): 643-659.
569. **Courlet P, Spaggiari D, Desfontaine V, Cavassini M, Alves Saldanha S, Buclin T, Marzolini C, Csajka C, & Decosterd LA.** UHPLC-MS/MS assay for simultaneous determination of amlodipine, metoprolol, pravastatin, rosuvastatin, atorvastatin with its active metabolites in human plasma, for population-scale drug-drug interactions studies in people living with HIV. *Journal of chromatography. B, Analytical technologies in the biomedical and life sciences*, **2019**. 1125: 121733.
570. **Glesby MJ, Aberg JA, Kendall MA, Fichtenbaum CJ, Hafner R, Hall S, Grosskopf N, Zolopa AR, & Gerber JG.** Pharmacokinetic interactions between indinavir plus ritonavir and calcium channel blockers. *Clinical Pharmacology & Therapeutics*, **2005**. 78(2): 143-153.
571. **Fichtenbaum CJ, Gerber JG, Rosenkranz SL, Segal Y, Aberg JA, Blaschke T, Alston B, Fang F, Kosel B, & Aweeka F.** Pharmacokinetic interactions between protease inhibitors and statins in HIV seronegative volunteers: ACTG Study A5047. *AIDS*, **2002**. 16(4): 569-577.
572. **Samineni D, Desai PB, Sallans L, & Fichtenbaum CJ.** Steady-state pharmacokinetic interactions of darunavir/ritonavir with lipid-lowering agent rosuvastatin. *The Journal of Clinical Pharmacology*, **2012**. 52(6): 922-931.
573. **Gorski JC, Vannaprasaht S, Hamman MA, Ambrosius WT, Bruce MA, Haehner-Daniels B, & Hall SD.** The effect of age, sex, and rifampin administration on intestinal and hepatic cytochrome P450 3A activity. *Clinical Pharmacology & Therapeutics*, **2003**. 74(3): 275-287.
574. **Kis O, Robillard K, Chan GN, & Bendayan R.** The complexities of antiretroviral drug–drug interactions: role of ABC and SLC transporters. *Trends in Pharmacological Sciences*, **2010**. 31(1): 22-35.
575. **Palella JF, Hart R, Armon C, Tedaldi E, Yangco B, Novak R, Battalora L, Ward D, Li J, & Buchacz K.** Non-AIDS comorbidity burden differs by sex, race, and insurance type in aging adults in HIV care. *AIDS* **2019**. 33(15): 2327-2335.
576. **Marzolini C, Elzi L, Gibbons S, Weber R, Fux C, Furrer H, Chave J-P, Cavassini M, Bernasconi E, Calmy A, Vernazza P, Khoo S, Ledergerber B, Back D, & Battegay M.** Prevalence of comedications and effect of potential drug-drug interactions in the Swiss HIV Cohort Study. *Antiviral Therapy*, **2010**. 15(3): 413-423.
577. **Stader F, Decosterd LA, Stoeckle M, Cavassini M, Battegay M, Saldanha SA, Marzolini C, Courlet P, & Swiss HIV Cohort Study.** Aging does not impact drug-drug interaction magnitudes with antiretrovirals: a Swiss HIV Cohort Study. *AIDS*, **2020**. 34(6): 949-952.
578. **Stader F, Courlet P, Kinvig H, Battegay M, Decosterd LA, Penny MA, Siccardi M, & Marzolini C.** Effect of ageing in antiretroviral drug pharmacokinetics using clinical data combined with modelling and simulation. *British Journal of Clinical Pharmacology* **2020**. [Epub ahead of print].

579. **Wojtyniak JG, Britz H, Selzer D, Schwab M, & Lehr T.** Data digitizing: accurate and precise data extraction for quantitative systems pharmacology and physiologically-based pharmacokinetic modeling. *CPT: Pharmacometrics & Systems Pharmacology*, **2020**. [Epub ahead of print].
580. **Lam Y, Alfaro CL, Ereshefsky L, & Miller M.** Pharmacokinetic and pharmacodynamic interactions of oral midazolam with ketoconazole, fluoxetine, fluvoxamine, and nefazodone. *The Journal of Clinical Pharmacology*, **2003**. 43(11): 1274-1282.
581. **Zhang H, Sheng J, Ko JH, Zheng C, Zhou W, Priess P, Lin W, & Novick S.** Inhibitory effect of single and repeated doses of nilotinib on the pharmacokinetics of CYP3A substrate midazolam. *The Journal of Clinical Pharmacology*, **2015**. 55(4): 401-408.
582. **Kirchheiner J, Heesch C, Bauer S, Meisel C, Seringer A, Goldammer M, Tzvetkov M, Meineke I, Roots I, & Brockmöller J.** Impact of the ultrarapid metabolizer genotype of cytochrome P450 2D6 on metoprolol pharmacokinetics and pharmacodynamics. *Clinical Pharmacology & Therapeutics*, **2004**. 76(4): 302-312.
583. **Menon RM, Badri PS, Wang T, Polepally AR, Zha J, Khatrri A, Wang H, Hu B, Coakley EP, & Podsadecki TJ.** Drug-drug interaction profile of the all-oral anti-hepatitis C virus regimen of paritaprevir/ritonavir, ombitasvir, and dasabuvir. *Journal of Hepatology*, **2015**. 63(1): 20-29.
584. **Tomalik-Scharte D, Fuhr U, Hellmich M, Frank D, Doroshenko O, Jetter A, & Stingl JC.** Effect of the CYP2C8 genotype on the pharmacokinetics and pharmacodynamics of repaglinide. *Drug Metabolism and Disposition*, **2011**. 39(5): 927-932.
585. **Kalliokoski A, Backman J, Kurkinen K, Neuvonen P, & Niemi M.** Effects of gemfibrozil and atorvastatin on the pharmacokinetics of repaglinide in relation to SLCO1B1 polymorphism. *Clinical Pharmacology & Therapeutics*, **2008**. 84(4): 488-496.
586. **Niemi M, Backman JT, Neuvonen M, & Neuvonen PJ.** Effects of gemfibrozil, itraconazole, and their combination on the pharmacokinetics and pharmacodynamics of repaglinide: potentially hazardous interaction between gemfibrozil and repaglinide. *Diabetologia*, **2003**. 46(3): 347-351.
587. **Tornio A, Niemi M, Neuvonen M, Laitila J, Kalliokoski A, Neuvonen PJ, & Backman JT.** The effect of gemfibrozil on repaglinide pharmacokinetics persists for at least 12 h after the dose: evidence for mechanism-based inhibition of CYP2C8 in vivo. *Clinical Pharmacology & Therapeutics*, **2008**. 84(3): 403-411.
588. **Shin J, Pauly DF, Pacanowski MA, Langaee T, Frye RF, & Johnson JA.** Effect of cytochrome P450 3A5 genotype on atorvastatin pharmacokinetics and its interaction with clarithromycin. *Pharmacotherapy: The Journal of Human Pharmacology and Drug Therapy*, **2011**. 31(10): 942-950.
589. **Gerber JG, Rosenkranz SL, Fichtenbaum CJ, Vega JM, Yang A, Alston BL, Brobst SW, Segal Y, & Aberg JA.** Effect of efavirenz on the pharmacokinetics of simvastatin, atorvastatin, and pravastatin: results of AIDS Clinical Trials Group 5108 Study. *Journal of Acquired Immune Deficiency Syndromes*, **2005**. 39(3): 307-312.
590. **Schöller-Gyüre M, Kakuda T, De Smedt G, Woodfall B, Bollen S, Peeters M, Vandermeulen K, & Hoetelmans R.** Pharmacokinetic interaction between the non-nucleoside reverse transcriptase inhibitors (NNRTI) TMC125 and atorvastatin in HIV-negative volunteers. *Age*, **2007**. 40: 19-53.
591. **Pasanen M, Fredrikson H, Neuvonen P, & Niemi M.** Different effects of SLCO1B1 polymorphism on the pharmacokinetics of atorvastatin and rosuvastatin. *Clinical Pharmacology & Therapeutics*, **2007**. 82(6): 726-733.
592. **Schneck DW, Birmingham BK, Zalikowski JA, Mitchell PD, Wang Y, Martin PD, Lasseter KC, Brown CD, Windass AS, & Raza A.** The effect of gemfibrozil on the pharmacokinetics of rosuvastatin. *Clinical Pharmacology & Therapeutics*, **2004**. 75(5): 455-463.

-
593. **Busti AJ, Bain AM, Hall RG, Bedimo RG, Leff RD, Meek C, & Mehvar R.** Effects of atazanavir/ritonavir or fosamprenavir/ritonavir on the pharmacokinetics of rosuvastatin. *Journal of Cardiovascular Pharmacology*, **2008**. 51(6): 605-610.
594. **Tanaka C, Yin OQ, Smith T, Sethuraman V, Grouss K, Galitz L, Harrell R, & Schran H.** Effects of rifampin and ketoconazole on the pharmacokinetics of nilotinib in healthy participants. *The Journal of Clinical Pharmacology*, **2011**. 51(1): 75-83.
595. **Boffito M, Else L, Back D, Taylor J, Khoo S, Sousa M, Pozniak A, Gazzard B, & Moyle G.** Pharmacokinetics of atazanavir/ritonavir once daily and lopinavir/ritonavir twice and once daily over 72 h following drug cessation. *Antiviral Therapy*, **2008**. 13(7): 901-907.
596. **Colombo S, Buclin T, Franc C, Guignard N, Khonkarly M, Tarr PE, Rochat B, Biollaz J, Telenti A, & Decosterd LA.** Ritonavir-boosted atazanavir-lopinavir combination: a pharmacokinetic interaction study of total, unbound plasma and cellular exposures. *Antiviral Therapy*, **2006**. 11(1): 53-62.
597. **Song I, Borland J, Chen S, Lou Y, Peppercorn A, Wajima T, Min S, & Piscitelli SC.** Effect of atazanavir and atazanavir/ritonavir on the pharmacokinetics of the next-generation HIV integrase inhibitor, S/GSK1349572. *British Journal of Clinical Pharmacology*, **2011**. 72(1): 103-108.
598. **Song I, Min SS, Borland J, Lou Y, Chen S, Patel P, Ishibashi T, & Piscitelli SC.** The effect of lopinavir/ritonavir and darunavir/ritonavir on the HIV integrase inhibitor S/GSK1349572 in healthy participants. *The Journal of Clinical Pharmacology*, **2011**. 51(2): 237-242.
599. **Wang X, Cerrone M, Ferretti F, Castrillo N, Maartens G, McClure M, & Boffito M.** Pharmacokinetics of dolutegravir 100 mg once daily with rifampicin. *International Journal of Antimicrobial Agents*, **2019**. 52(2): 202-206.
600. **Crauwels H, Vingerhoets J, Ryan R, Witek J, & Anderson D.** Pharmacokinetic parameters of once-daily rilpivirine following administration of efavirenz in healthy subjects. *Antiviral Therapy*, **2012**. 17(3): 439-446.
601. **Wenning LA, Hanley WD, Brainard DM, Petry AS, Ghosh K, Jin B, Mangin E, Marbury TC, Berg JK, & Chodakewitz JA.** Effect of rifampin, a potent inducer of drug-metabolizing enzymes, on the pharmacokinetics of raltegravir. *Antimicrobial Agents and Chemotherapy*, **2009**. 53(7): 2852-2856.
602. **Kwara A, Tashima KT, Dumond JB, Poethke P, Kurpewski J, Kashuba AD, & Greenblatt DJ.** Modest but variable effect of rifampin on steady-state plasma pharmacokinetics of efavirenz in healthy African-American and Caucasian volunteers. *Antimicrobial Agents and Chemotherapy*, **2011**. 55(7): 3527-3533.
603. **Kakuda TN, Woodfall B, De Marez T, Peeters M, Vandermeulen K, Aharchi F, & Hoetelmans RM.** Pharmacokinetic evaluation of the interaction between etravirine and rifabutin or clarithromycin in HIV-negative, healthy volunteers: results from two Phase 1 studies. *Journal of Antimicrobial Chemotherapy*, **2013**. 69(3): 728-734.
604. **Suzuki M, Hirata M, Takagi M, Watanabe T, Iguchi T, Koiwai K, Maezawa S, & Koiwai O.** Truncated UDP-glucuronosyltransferase (UGT) from a Crigler–Najjar syndrome type II patient colocalizes with intact UGT in the endoplasmic reticulum. *Journal of Human Genetics*, **2014**. 59(3): 158-162.
605. **Smith CM, Faucette SR, Wang H, & LeCluyse EL.** Modulation of UDP-glucuronosyltransferase 1A1 in primary human hepatocytes by prototypical inducers. *Journal of Biochemical and Molecular Toxicology*, **2005**. 19(2): 96-108.
606. **Liu B, Crewe HK, Ozdemir M, Rowland Yeo K, Tucker G, & Rostami-Hodjegan A.** The absorption kinetics of ketoconazole plays a major role in explaining the reported variability in the level of interaction with midazolam: interplay between formulation and inhibition of gut wall and liver metabolism. *Biopharmaceutics & Drug Disposition*, **2017**. 38: 260-270.
-

607. **Heimbach T, Lin W, Hourcade-Potelleret F, Tian X, Combes FP, Horvath N, & He H.** Physiologically based pharmacokinetic modeling to supplement nilotinib pharmacokinetics and confirm dose selection in pediatric patients. *Journal of Pharmaceutical Sciences*, **2019**. 108(6): 2191-2198.
608. **Wishart DS.** DrugBank: Ketoconazole. 2005. Available from: <https://www.drugbank.ca/drugs/DB01026>. Accessed on 25/10/2019.
609. **Manley PW, Stiefl N, Cowan-Jacob SW, Kaufman S, Mestan J, Wartmann M, Wiesmann M, Woodman R, & Gallagher N.** Structural resemblances and comparisons of the relative pharmacological properties of imatinib and nilotinib. *Bioorganic & Medicinal Chemistry*, **2010**. 18(19): 6977-6986.
610. **Xia B, Heimbach T, He H, & Lin TH.** Nilotinib preclinical pharmacokinetics and practical application toward clinical projections of oral absorption and systemic availability. *Biopharmaceutics & Drug Disposition*, **2012**. 33(9): 536-549.
611. **Zsila F, Fitos I, Bencze G, Keri G, & Orfi L.** Determination of human serum α 1-acid glycoprotein and albumin binding of various marketed and preclinical kinase inhibitors. *Current Medicinal Chemistry*, **2009**. 16(16): 1964-1977.
612. **Wishart DS.** DrugBank: Gemfibrozil. 2005. Available from: <https://www.drugbank.ca/drugs/DB01241>. Accessed on 01/11/2019.
613. **Sallustio BC, Fairchild BA, & Pannall PR.** Interaction of human serum albumin with the electrophilic metabolite 1-O-gemfibrozil- β -D-glucuronide. *Drug Metabolism and Disposition*, **1997**. 25(1): 55-60.
614. **European Medicines Agency.** Nilotinib - Scientific discussion. 2007. Available from: https://www.ema.europa.eu/en/documents/scientific-discussion/tasigna-epar-scientific-discussion_en.pdf. Accessed on 31/10/2019.
615. **Goosen TC, Bauman JN, Davis JA, Yu C, Hurst SI, Williams JA, & Loi C-M.** Atorvastatin glucuronidation is minimally and nonselectively inhibited by the fibrates gemfibrozil, fenofibrate, and fenofibric acid. *Drug Metabolism and Disposition*, **2007**. 35(8): 1315-1324.
616. **Van der Meer J, Keuning J, Scheijgrond H, Heykants J, Cutsem JV, & Brugmans J.** The influence of gastric acidity on the bio-availability of ketoconazole. *Journal of Antimicrobial Chemotherapy*, **1980**. 6(4): 552-554.
617. **Daneshmend TK, Warnock DW, Ene MD, Johnson EM, Potten M, Richardson M, & Williamson P.** Influence of food on the pharmacokinetics of ketoconazole. *Antimicrobial Agents and Chemotherapy*, **1984**. 25(1): 1-3.
618. **Daneshmend TK & Warnock DW.** Clinical pharmacokinetics of ketoconazole. *Clinical Pharmacokinetics*, **1988**. 14(1): 13-34.
619. **Hurwitz A, Ruhl CE, Kimler BF, Topp EM, & Mayo MS.** Gastric function in the elderly: effects on absorption of ketoconazole. *The Journal of Clinical Pharmacology*, **2003**. 43(9): 996-1002.
620. **Tanaka C, Yin O, Sethuraman V, Smith T, Wang X, Grouss K, Kantarjian H, Giles F, Ottmann O, & Galitz L.** Clinical pharmacokinetics of the BCR-ABL tyrosine kinase inhibitor nilotinib. *Clinical Pharmacology & Therapeutics*, **2010**. 87(2): 197-203.
621. **Okerholm R, Keeley F, Peterson F, & Glazko A.** The metabolism of gemfibrozil. *Proceedings of the Royal Society of Medicine*, **1976**. 69(2_suppl): 11-14.
622. **Loi C-M, Parker BM, Cusack BJ, & Vestal RE.** Aging and drug interactions. III. Individual and combined effects of cimetidine and ciprofloxacin on theophylline metabolism in healthy male and female nonsmokers. *Journal of Pharmacology and Experimental Therapeutics*, **1997**. 280(2): 627-637.

623. **Adebayo G & Coker H.** Cimetidine inhibition of theophylline elimination: the influence of adult age and the time course. *Biopharmaceutics & Drug Disposition*, **1987**. 8(2): 149-158.
624. **Vestal RE, Cusack BJ, Mercer GD, Dawson GW, & Park B.** Aging and drug interactions. I. Effect of cimetidine and smoking on the oxidation of theophylline and cortisol in healthy men. *Journal of Pharmacology and Experimental Therapeutics*, **1987**. 241(2): 488-500.
625. **Feely J, Pereira L, Guy E, & Hockings N.** Factors affecting the response to inhibition of drug metabolism by cimetidine-dose response and sensitivity of elderly and induced subjects. *British Journal of Clinical Pharmacology*, **1984**. 17(1): 77-81.
626. **Crowley J, Cusack B, Jue S, Koup J, Park B, & Vestal R.** Aging and drug interactions. II. Effect of phenytoin and smoking on the oxidation of theophylline and cortisol in healthy men. *Journal of Pharmacology and Experimental Therapeutics*, **1988**. 245(2): 513-523.
627. **Cusack B, Kelly J, Lavan J, Noel J, & O'Malley K.** Theophylline kinetics in relation to age: the importance of smoking. *British Journal of Clinical Pharmacology*, **1980**. 10(2): 109-114.
628. **Wood A, Vestal R, Wilkinson G, Branch R, & Shand D.** Effect of aging and cigarette smoking on antipyrine and indocyanine green elimination. *Clinical Pharmacology & Therapeutics*, **1979**. 26(1): 16-20.
629. **Liukas A, Hagelberg NM, Kuusniemi K, Neuvonen PJ, & Olkkola KT.** Inhibition of cytochrome P450 3A by clarithromycin uniformly affects the pharmacokinetics and pharmacodynamics of oxycodone in young and elderly volunteers. *Journal of Clinical Psychopharmacology*, **2011**. 31(3): 302-308.
630. **Montamat SC & Abernethy DR.** Calcium antagonists in geriatric patients: diltiazem in elderly persons with hypertension. *Clinical Pharmacology & Therapeutics*, **1989**. 45(6): 682-691.
631. **Miglioli P, Pivetta P, Strazzabosco M, Orlando R, Okolicsanyi L, & Palatini P.** Effect of age on single-and multiple-dose pharmacokinetics of erythromycin. *European Journal of Clinical Pharmacology*, **1990**. 39(2): 161-164.
632. **Fromm MF, Dilger K, Busse D, Kroemer HK, Eichelbaum M, & Klotz U.** Gut wall metabolism of verapamil in older people: effects of rifampicin-mediated enzyme induction. *British Journal of Clinical Pharmacology*, **1998**. 45(3): 247-255.
633. **Smith D, Chandler M, Shedlofsky S, Wedlund P, & Blouin R.** Age-dependent stereoselective increase in the oral clearance of hexobarbitone isomers caused by rifampicin. *British Journal of Clinical Pharmacology*, **1991**. 32(6): 735-739.
634. **Salem S, Rajjayabun P, Shepherd A, & Stevenson I.** Reduced induction of drug metabolism in the elderly. *Age and Ageing*, **1978**. 7(2): 68-73.
635. **Niemi M, Backman JT, Fromm MF, Neuvonen PJ, & Kivistö KT.** Pharmacokinetic interactions with rifampicin. *Clinical Pharmacokinetics*, **2003**. 42(9): 819-850.
636. **Bailey I, Gibson GG, Plant K, Graham M, & Plant N.** A PXR-mediated negative feedback loop attenuates the expression of CYP3A in response to the PXR agonist pregnenalone-16 α -carbonitrile. *PLoS One*, **2011**. 6(2): e16703.
637. **Twum-Barima Y, Finnigan T, Habash A, Cape R, & Carruthers S.** Impaired enzyme induction by rifampicin in the elderly. *British Journal of Clinical Pharmacology*, **1984**. 17(5): 595-597.
638. **Guest EJ, Aarons L, Houston JB, Rostami-Hodjegan A, & Galetin A.** Critique of the two-fold measure of prediction success for ratios: application for the assessment of drug-drug interactions. *Drug Metabolism and Disposition*, **2011**. 39(2): 170-173.

639. **U.S. Food and Drug Administration.** Quality and bioequivalence standards for narrow therapeutic index drugs. 2011. Available from: <https://www.fda.gov/downloads/drugs/developmentapprovalprocess/howdrugsaredevelopedanapproved/approvalapplications/abbreviatednewdrugapplicationandgenerics/ucm292676.pdf>. Accessed on 03/04/2018.
640. **Warnke D, Barreto J, & Temesgen Z.** Antiretroviral drugs. *The Journal of Clinical Pharmacology*, **2007**. 47(12): 1570-1579.
641. **de Wildt SN, Kearns GL, Leeder JS, & van den Anker JN.** Cytochrome P450 3A. *Clinical Pharmacokinetics*, **1999**. 37(6): 485-505.
642. **Barry M, Mulcahy F, Merry C, Gibbons S, & Back D.** Pharmacokinetics and potential interactions amongst antiretroviral agents used to treat patients with HIV infection. *Clinical Pharmacokinetics*, **1999**. 36(4): 289-304.
643. **Miller CD, El-Kholi R, Faragon JJ, & Lodise TP.** Prevalence and risk factors for clinically significant drug interactions with antiretroviral therapy. *Pharmacotherapy: The Journal of Human Pharmacology and Drug Therapy*, **2007**. 27(10): 1379-1386.
644. **Evans-Jones JG, Cottle LE, Back DJ, Gibbons S, Beeching NJ, Carey PB, & Khoo SH.** Recognition of risk for clinically significant drug interactions among HIV-infected patients receiving antiretroviral therapy. *Clinical Infectious Diseases*, **2010**. 50(10): 1419-1421.
645. **Darque A, Enel P, Petit N, Ravaux I, & Retornaz F.** Drug interactions in elderly individuals with the human immunodeficiency virus. *Journal of the American Geriatrics Society*, **2012**. 60(2): 382-384.
646. **Tsunoda SM, Velez RL, Moltke LL, & Greenblatt DJ.** Differentiation of intestinal and hepatic cytochrome P450 3A activity with use of midazolam as an in vivo probe: effect of ketoconazole. *Clinical Pharmacology & Therapeutics*, **1999**. 66(5): 461-471.
647. **Tod M, Goutelle S, Clavel-Grabit F, Nicolas G, & Charpiat B.** Quantitative prediction of cytochrome P450 (CYP) 2D6-mediated drug interactions. *Clinical Pharmacokinetics*, **2011**. 50(8): 519-530.
648. **Galetin A, Ito K, Hallifax D, & Houston JB.** CYP3A4 substrate selection and substitution in the prediction of potential drug-drug interactions. *Journal of Pharmacology and Experimental Therapeutics*, **2005**. 314(1): 180-190.
649. **U.S. Food and Drug Administration.** Clinical drug interaction studies - study design, data analysis, and clinical implications. Guidance for industry. 2017. Available from: <https://www.fda.gov/downloads/drugs/guidances/ucm292362.pdf>. Accessed on 22/03/2018.
650. **Greenblatt DJ, Wright CE, Moltke LL, Harmatz JS, Ehrenberg BL, Harrel LM, Corbett K, Counihan M, Tobias S, & Shader RI.** Ketoconazole inhibition of triazolam and alprazolam clearance: differential kinetic and dynamic consequences. *Clinical Pharmacology & Therapeutics*, **1998**. 64(3): 237-247.
651. **Varhe A, Olkkola KT, & Neuvonen PJ.** Oral triazolam is potentially hazardous to patients receiving systemic antimycotics ketoconazole or itraconazole. *Clinical Pharmacology & Therapeutics*, **1994**. 56(6): 601-607.
652. **Ahonen J, Olkkola KT, & Neuvonen PJ.** Effect of itraconazole and terbinafine on the pharmacokinetics and pharmacodynamics of midazolam in healthy volunteers. *British Journal of Clinical Pharmacology*, **1995**. 40(3): 270-272.
653. **Olkkola KT, Ahonen J, & Neuvonen PJ.** The effect of the systemic antimycotics, itraconazole and fluconazole, on the pharmacokinetics and pharmacodynamics of intravenous and oral midazolam. *Anesthesia & Analgesia*, **1996**. 82(3): 511-516.

-
654. **Oikkola KT, Backman JT, & Neuvonen PJ.** Midazolam should be avoided in patients receiving the systemic antimycotics ketoconazole or itraconazole. *Clinical Pharmacology & Therapeutics*, **1994**. 55(5): 481-485.
655. **Backman JT, Kivistö KT, Oikkola KT, & Neuvonen PJ.** The area under the plasma concentration–time curve for oral midazolam is 400-fold larger during treatment with itraconazole than with rifampicin. *European Journal of Clinical Pharmacology*, **1998**. 54(1): 53-58.
656. **Grimm SW, Richtand NM, Winter HR, Stams KR, & Reece SB.** Effects of cytochrome P450 3A modulators ketoconazole and carbamazepine on quetiapine pharmacokinetics. *British Journal of Clinical Pharmacology*, **2006**. 61(1): 58-69.
657. **Sansone-Parsons A, Krishna G, Martinho M, Kantesaria B, Gelone S, & Mant TG.** Effect of oral posaconazole on the pharmacokinetics of cyclosporine and tacrolimus. *Pharmacotherapy: The Journal of Human Pharmacology and Drug Therapy*, **2007**. 27(6): 825-834.
658. **Abel S, Russell D, Taylor-Worth RJ, Ridgway CE, & Muirhead GJ.** Effects of CYP3A4 inhibitors on the pharmacokinetics of maraviroc in healthy volunteers. *British Journal of Clinical Pharmacology*, **2008**. 65(s1): 27-37.
659. **Grub S, Bryson H, Goggin T, Lüdin E, & Jorga K.** The interaction of saquinavir (soft gelatin capsule) with ketoconazole, erythromycin and rifampicin: comparison of the effect in healthy volunteers and in HIV-infected patients. *European Journal of Clinical Pharmacology*, **2001**. 57(2): 115-121.
660. **Sekar VJ, Lefebvre E, De Pauw M, Vangeneugden T, & Hoetelmans RM.** Pharmacokinetics of darunavir/ritonavir and ketoconazole following co-administration in HIV–healthy volunteers. *British Journal of Clinical Pharmacology*, **2008**. 66(2): 215-221.
661. **Atsmon J, Dingemanse J, Shaikovich D, Volokhov I, & Sidharta PN.** Investigation of the effects of ketoconazole on the pharmacokinetics of macitentan, a novel dual endothelin receptor antagonist, in healthy subjects. *Clinical Pharmacokinetics*, **2013**. 52(8): 685-692.
662. **Pfizer Labs.** Package insert of Norvasc (amlodipine). 2011. Available from: https://www.accessdata.fda.gov/drugsatfda_docs/label/2011/019787s047lbl.pdf. Accessed on 12/09/2017.
663. **Greenblatt DJ, Moltke LL, Harmatz JS, Mertzanis P, Graf JA, Durol ALB, Counihan M, Roth-Schechter B, & Shader RI.** Kinetic and dynamic interaction study of zolpidem with ketoconazole, itraconazole, and fluconazole. *Clinical Pharmacology & Therapeutics*, **1998**. 64(6): 661-671.
664. **Bertz R, Wong C, Carothers L, Lauva I, Dennis S, & Valdes J.** Evaluation of the pharmacokinetics of multiple dose ritonavir and ketoconazole in combination. *Clinical Pharmacology & Therapeutics*, **1998**. 63(2): 230.
665. **Greenblatt DJ, Peters DE, Oleson LE, Harmatz JS, MacNab MW, Berkowitz N, Zinny MA, & Court MH.** Inhibition of oral midazolam clearance by boosting doses of ritonavir, and by 4, 4-dimethyl-benziso-(2H)-selenazine (ALT-2074), an experimental catalytic mimic of glutathione oxidase. *British Journal of Clinical Pharmacology*, **2009**. 68(6): 920-927.
666. **Yeh RF, Gaver VE, Patterson KB, Rezk NL, Baxter-Meheux F, Blake MJ, Eron Jr JJ, Klein CE, Rublein JC, & Kashuba AD.** Lopinavir/ritonavir induces the hepatic activity of cytochrome P450 enzymes CYP2C9, CYP2C19, and CYP1A2 but inhibits the hepatic and intestinal activity of CYP3A as measured by a phenotyping drug cocktail in healthy volunteers. *Journal of Acquired Immune Deficiency Syndromes*, **2006**. 42(1): 52-60.
-

-
667. **Schmitt C, Hofmann C, Riek M, Zwanziger E, & Patel A.** Effect of saquinavir-ritonavir on cytochrome P450 3A4 activity in healthy volunteers using midazolam as a probe. *Pharmacotherapy: The Journal of Human Pharmacology and Drug Therapy*, **2009**. 29(10): 1175-1181.
668. **Kirby BJ, Collier AC, Kharasch ED, Whittington D, Thummel KE, & Unadkat JD.** Complex drug interactions of HIV protease inhibitors 1: inactivation, induction and inhibition of cytochrome P450 3A by ritonavir or nelfinavir. *Drug Metabolism and Disposition*, **2011**. 39(6): 1070-1078.
669. **Knox TA, Oleson L, von Moltke LL, Kaufman RC, Wanke CA, & Greenblatt DJ.** Ritonavir greatly impairs CYP3A activity in HIV infection with chronic viral hepatitis. *Journal of Acquired Immune Deficiency Syndromes*, **2008**. 49(4): 358-368.
670. **Eap CB, Buclin T, Cucchia G, Zullino D, Hustert E, Bleiber G, Golay KP, Aubert AC, Baumann P, & Telenti A.** Oral administration of a low dose of midazolam (75 µg) as an in vivo probe for CYP3A activity. *European Journal of Clinical Pharmacology*, **2004**. 60(4): 237-246.
671. **Krishna G, Moton A, Ma L, Savant I, Martinho M, Seiberling M, & McLeod J.** Effects of oral posaconazole on the pharmacokinetic properties of oral and intravenous midazolam: a phase I, randomized, open-label, crossover study in healthy volunteers. *Clinical Therapeutics*, **2009**. 31(2): 286-298.
672. **Chung E, Nafziger AN, Kazierad DJ, & Bertino JS.** Comparison of midazolam and simvastatin as cytochrome P450 3A probes. *Clinical Pharmacology & Therapeutics*, **2006**. 79(4): 350-361.
673. **Sohlenius-Sternbeck A-K, Meyerson G, Hagbjörk A-L, Juric S, & Terelius Y.** A strategy for early-risk predictions of clinical drug–drug interactions involving the GastroPlus™ DDI module for time-dependent CYP inhibitors. *Xenobiotica*, **2017**. 15: 1-9.
674. **Saari TI, Laine K, Leino K, Valtonen M, Neuvonen PJ, & Olkkola KT.** Effect of voriconazole on the pharmacokinetics and pharmacodynamics of intravenous and oral midazolam. *Clinical Pharmacology & Therapeutics*, **2006**. 79(4): 362-370.
675. **Neuvonen PJ, Kantola T, & Kivistö KT.** Simvastatin but not pravastatin is very susceptible to interaction with the CYP3A4 inhibitor itraconazole. *Clinical Pharmacology & Therapeutics*, **1998**. 63(3): 332-341.
676. **Palkama VJ, Ahonen J, Neuvonen PJ, & Olkkola KT.** Effect of saquinavir on the pharmacokinetics and pharmacodynamics of oral and intravenous midazolam. *Clinical Pharmacology & Therapeutics*, **1999**. 66(1): 33-39.
677. **Krishna G, Ma L, Prasad P, Moton A, Martinho M, & O'Mara E.** Effect of posaconazole on the pharmacokinetics of simvastatin and midazolam in healthy volunteers. *Expert Opinion on Drug Metabolism & Toxicology*, **2012**. 8(1): 1-10.
678. **Backman JT, Olkkola KT, Aranko K, Himberg J-J, & Neuvonen PJ.** Dose of midazolam should be reduced during diltiazem and verapamil treatments. *British Journal of Clinical Pharmacology*, **1994**. 37(3): 221-225.
679. **Greenblatt DJ, Locniskar A, Scavone JM, Blyden GT, Ochs HR, Harmatz JS, & Shader RI.** Absence of interaction of cimetidine and ranitidine with intravenous and oral midazolam. *Anesthesia & Analgesia*, **1986**. 65(2): 176-180.
680. **Klotz U, Arvela P, & Rosenkranz B.** Effect of single doses of cimetidine and ranitidine on the steady-state plasma levels of midazolam. *Clinical Pharmacology & Therapeutics*, **1985**. 38(6): 652-655.
681. **Fee J, Collier P, Howard P, & Dundee J.** Cimetidine and ranitidine increase midazolam bioavailability. *Clinical Pharmacology & Therapeutics*, **1987**. 41(1): 80-84.
-

682. **U.S. Food and Drug Administration.** Drug development and drug interactions: Table of substrates, inhibitors and inducers. 2016. Available from: <https://www.fda.gov/drugs/developmentapprovalprocess/developmentresources/druginteractionlabeling/ucm093664.htm>. Accessed on 04/09/2017.
683. **Teo YL, Ho HK, & Chan A.** Metabolism-related pharmacokinetic drug– drug interactions with tyrosine kinase inhibitors: current understanding, challenges and recommendations. *British Journal of Clinical Pharmacology*, **2015**. 79(2): 241-253.
684. **Rowland-Yeo K, Jamei M, Yang J, Tucker GT, & Rostami-Hodjegan A.** Physiologically based mechanistic modelling to predict complex drug–drug interactions involving simultaneous competitive and time-dependent enzyme inhibition by parent compound and its metabolite in both liver and gut—the effect of diltiazem on the time-course of exposure to triazolam. *European Journal of Pharmaceutical Sciences*, **2010**. 39(5): 298-309.
685. **Rose R, Neuhoﬀ S, Abduljalil K, Chetty M, Rostami-Hodjegan A, & Jamei M.** Application of a physiologically based pharmacokinetic model to predict OATP1B1-related variability in pharmacodynamics of rosuvastatin. *CPT: Pharmacometrics & Systems Pharmacology*, **2014**. 3(7): 1-9.
686. **Hisaka A, Yoshiyuki O, Yamamoto T, & Suzuki H.** Theoretical considerations on quantitative prediction of drug-drug interactions. *Drug Metabolism and Pharmacokinetics*, **2010**. 25(1): 48-61.
687. **Salem F, Johnson TN, Abduljalil K, Tucker GT, & Rostami-Hodjegan A.** A re-evaluation and validation of ontogeny functions for cytochrome P450 1A2 and 3A4 based on in vivo data. *Clinical Pharmacokinetics*, **2014**. 53(7): 625-636.
688. **Upreti VV & Wahlstrom JL.** Meta-analysis of hepatic cytochrome P450 ontogeny to underwrite the prediction of pediatric pharmacokinetics using physiologically based pharmacokinetic modeling. *The Journal of Clinical Pharmacology*, **2016**. 56(3): 266-283.
689. **Ives DG, Traven ND, Kuller LH, & Schulz R.** Selection bias and nonresponse to health promotion in older adults. *Epidemiology*, **1994**. 5(4): 456-461.
690. **Mangoni AA & Jackson SH.** Age-related changes in pharmacokinetics and pharmacodynamics: basic principles and practical applications. *British Journal of Clinical Pharmacology*, **2004**. 57(1): 6-14.
691. **Bagkeris E, Burgess L, Mallon PW, Post FA, Boffito M, Sachikonye M, Anderson J, Asboe D, Garvey L, & Vera J.** Cohort profile: The Pharmacokinetic and clinical Observations in PeoPle over fifty (POPPY) study. *International Journal of Epidemiology*, **2018**. 47(5): 1391-1392e.
692. **Stader F, Courlet P, Kinvig H, Penny MA, Decosterd LA, Battegay M, Siccardi M, & Marzolini C.** Clinical data combined with modelling and simulation indicate unchanged drug drug interaction magnitudes in the elderly. *Clinical Pharmacology & Therapeutics*, **2020**. [Epub ahead of print].
693. **Clegg A, Young J, Iliffe S, Rikkert MO, & Rockwood K.** Frailty in elderly people. *The Lancet*, **2013**. 381(9868): 752-762.
694. **Brothers TD, Kirkland S, Guaraldi G, Falutz J, Theou O, Johnston BL, & Rockwood K.** Frailty in people aging with human immunodeficiency virus (HIV) infection. *Journal of Infectious Diseases*, **2014**. 210(8): 1170-1179.
695. **Gutiérrez-Valencia M & Martínez-Velilla N.** Frailty in the older person: Implications for pharmacists. *American Journal of Health-System Pharmacy*, **2019**. 76(23): 1980-1987.
696. **Schmidt S, Gonzalez D, & Derendorf H.** Significance of protein binding in pharmacokinetics and pharmacodynamics. *Journal of Pharmaceutical Sciences*, **2010**. 99(3): 1107-1122.

-
697. **Reeve E, Wiese MD, & Mangoni AA.** Alterations in drug disposition in older adults. *Expert Opinion on Drug Metabolism & Toxicology*, **2015**. 11(4): 491-508.
698. **Chin PK, Jensen BP, Larsen HS, & Begg EJ.** Adult age and ex vivo protein binding of lorazepam, oxazepam and temazepam in healthy subjects. *British Journal of Clinical Pharmacology*, **2011**. 72(6): 985-989.
699. **Jensen BP, Chin PKL, Roberts RL, & Begg EJ.** Influence of adult age on the total and free clearance and protein binding of (R)-and (S)-warfarin. *British Journal of Clinical Pharmacology*, **2012**. 74(5): 797-805.
700. **Shepherd AM, Hewick DS, Moreland TA, & Stevenson IH.** Age as a determinant of sensitivity to warfarin. *British Journal of Clinical Pharmacology*, **1977**. 4(3): 315-320.
701. **Bender AD, Post A, Meier JP, Higson JE, & Reichard Jr G.** Plasma protein binding of drugs as a function of age in adult human subjects. *Journal of Pharmaceutical Sciences*, **1975**. 64(10): 1711-1713.
702. **Patterson M, Heazelwood R, Smithurst B, & Eadie M.** Plasma protein binding of phenytoin in the aged: in vivo studies. *British Journal of Clinical Pharmacology*, **1982**. 13(3): 423-425.
703. **Bauer LA, Davis R, Wilensky A, Raisys V, & Levy RH.** Valproic acid clearance: unbound fraction and diurnal variation in young and elderly adults. *Clinical Pharmacology & Therapeutics*, **1985**. 37(6): 697-700.
704. **Riva R, Albani F, Baruzzi A, Galvani I, & Perucca E.** Determination of unbound valproic acid concentration in plasma by equilibrium dialysis and gas-liquid chromatography: methodological aspects and observations in epileptic patients. *Therapeutic Drug Monitoring*, **1982**. 4(4): 341-352.
705. **Horvath S & Levine AJ.** HIV-1 infection accelerates age according to the epigenetic clock. *The Journal of Infectious Diseases*, **2015**. 212(10): 1563-1573.
706. **D'Aquila P, Rose G, Bellizzi D, & Passarino G.** Epigenetics and aging. *Maturitas*, **2013**. 74(2): 130-136.

Appendix

Appendix

Abbreviations	Page 281
List of Figures	Page 283
List of Tables	Page 288
Classes at the University of Basel	Page 291
Curriculum vitae	Page 292

Abbreviations

The list contains the most used abbreviations in the thesis in alphabetical order.

AAG:	alpha-acid glycoprotein
AIDS:	acquired immunodeficiency syndrome
ANCOVA:	analysis of covariance
ANOVA:	analysis of variance
AUC:	area under the curve
AUC _{inf} :	area under the curve extrapolated to infinity
AUC _t :	area under the curve for one dosing interval
BSA:	body surface area
CCR:	chemokine receptor
CD:	cluster of differentiation
CLF:	apparent clearance
C _{max} :	peak concentration
CO:	cardiac output
CV:	coefficient of variance
CXCR:	CX-chemokine receptor
CYP:	cytochrome P-450
DDI:	drug-drug interaction
DMPK:	drug metabolism and pharmacokinetics
DNA:	deoxyribonucleic acid
DPI:	fraction of disposition pathway mediated by a specific enzyme
EM:	extensive metabolizer
ET:	extensive transporter-phenotype
f:	female
fm:	fraction metabolized
GFR:	glomerular filtration rate
GI:	gastrointestinal

gp:	glycoprotein
HIV:	human immunodeficiency virus
HPGL:	hepatocytes per gram liver
IcR:	inducer ratio
InR:	inhibitor ratio
IT:	intermediate transporter phenotype
m:	male
MPPGL:	microsomal protein per gram liver
NNRTI:	non-nucleoside reverse transcriptase inhibitors
NRTI:	nucleoside/nucleotide reverse transcriptase inhibitors
OATP:	organic anion transporting polypeptide
ODE:	ordinary differential equations
PBPK:	physiologically based pharmacokinetic modelling
PLWH:	people living with HIV
PM:	poor metabolizer
PT:	poor transporter phenotype
RNA:	ribonucleic acid
SD:	standard deviation
$t_{1/2}$:	elimination half-life
t_{max} :	time to peak concentration
UGT:	uridine diphosphate-glucuronosyltransferase
UM:	ultrarapid metabolizer
VdF:	apparent volume of distribution

List of Figures

Figure 1.1:	Schematic structure of HIV.	Page 12
Figure 1.2:	Reproductive cycle of HIV and targets for antiretroviral drugs.	Page 13
Figure 1.3:	Age distribution of active patients by year in the Swiss HIV Cohort Study, 1986-2016.	Page 15
Figure 1.4:	Structure of a whole-body PBPK model.	Page 20
Figure 2.1:	Proportion of subjects and proportion of women per age decade.	Page 32
Figure 2.2:	Body height and body weight per age decade in an aging population.	Page 34
Figure 2.3:	Liver weight and hepatic blood flow per age decade in an aging population.	Page 35
Figure 2.4:	Kidney weight, renal blood flow, and glomerular filtration rate per age decade in an aging population.	Page 37
Figure 2.5:	Cardiac output per age decade in an aging population.	Page 40
Figure 2.6:	Blood weight, hematocrit, albumin, and alpha-acid glycoprotein concentration per age decade in an aging population.	Page 41
Figure 2.7:	Sum of all organ weights in comparison to body weight in male and female subjects.	Page 42
Figure 2.8:	Total body water and total body cell mass per age decade in an aging population.	Page 43
Figure 2.9:	Comparison of a 50 and 70 years old man and women with a 30 years old subject.	Page 48
Figure 3.1:	Schematic illustration of the five steps to build a PBPK model.	Page 57
Figure 3.2:	Structure of an organ in the PBPK model.	Page 58
Figure 3.3:	Example of the organization of drug parameters with variability.	Page 58
Figure 3.4:	Steps from the user-defined drug to be simulated to the drug parameter that are loaded to inform the PBPK model.	Page 63

Figure 3.5:	PBPK simulations for a single dose of 10 mg rivaroxaban administered with 600 mg ritonavir twice daily and 800/100 mg darunavir/ritonavir once daily in steady state.	Page 81
Figure 3.6:	PBPK simulations for 800 mg darunavir once daily boosted with 100 mg ritonavir once daily and 100 mg ritonavir once daily.	Page 82
Figure 4.1:	Workflow for the verification of the used physiologically based pharmacokinetic framework.	Page 95
Figure 4.2:	Predicted vs. observed concentration-time profiles for midazolam, metoprolol, and lisinopril.	Page 104
Figure 4.3:	Predicted vs. observed concentration time profiles for amlodipine and rivaroxaban.	Page 105
Figure 4.4:	Predicted vs. observed concentration time profiles for repaglinide, atorvastatin, and rosuvastatin.	Page 107
Figure 4.5:	Predicted vs. observed concentration time profiles for clarithromycin and rifampicin.	Page 109
Figure 4.6:	Age-related changes of pharmacokinetic parameters for non-HIV drugs normalized to the youngest investigated age group (20 to 24 years).	Page 110
Figure 4.7:	Sensitivity analysis to analyze the impact of drug and physiological parameters on age-related pharmacokinetic changes.	Page 111
Figure 4.8:	Verification of derived pharmacokinetic parameter changes with age against 52 additional drugs.	Page 113
Figure 4.9:	Correlation between drug (octanol-water partition coefficient, fraction unbound in plasma) and physiological parameters (blood flow to respective organ, glomerular filtration rate) against age-related changes in apparent volume of distribution and clearance.	Page 114
Figure 5.1:	Predicted vs. observed concentration time profiles for ritonavir (100 mg once daily), darunavir/r (800/100 mg once daily), and atazanavir/r (300/100 mg once daily).	Page 133
Figure 5.2:	Predicted vs. observed concentration time profiles for dolutegravir (50 mg once daily) and raltegravir (400 mg twice daily).	Page 135

Figure 5.3:	Predicted vs. observed concentration time profiles for rilpivirine (25 mg once daily), efavirenz (600 mg once daily), and etravirine (400 mg once daily).	Page 137
Figure 5.4:	Predicted vs. observed concentration time profiles for tenofovir (300 mg once daily) and emtricitabine (200 mg once daily).	Page 138
Figure 5.5:	Pharmacokinetic parameters of antiretroviral drugs normalized to the youngest investigated age group (20 to 24 years).	Page 139
Figure 5.6:	Impact of ethnicities on age-related pharmacokinetic changes.	Page 144
Figure 6.1:	Predicted vs. observed concentration time profiles for midazolam in the absence and the presence of clarithromycin after intravenous administration and oral administration.	Page 165
Figure 6.2:	Predicted vs. observed concentration time profiles for amlodipine, atorvastatin, and rosuvastatin in the absence and the presence of boosted darunavir.	Page 168
Figure 6.3:	Predicted vs. observed concentration time profiles for dolutegravir in the absence and in the presence of boosted darunavir.	Page 169
Figure 6.4:	Predicted vs. observed concentration time profiles for nilotinib (400 mg single dose), gemfibrozil (600 mg twice daily), and gemfibrozil glucuronide in young individuals aged 20 to 50 years.	Page 169
Figure 6.5:	Predicted vs. observed concentration time profiles for ketoconazole (200 mg once daily).	Page 170
Figure 6.6:	Area under the curve ratio normalized to the youngest investigated age group (20 to 24 years).	Page 173
Figure 6.7:	Impact of aging on the normalized area under the curve ratios for independent clinically observed data (mean \pm standard deviation; Table 6.5).	Page 176
Figure A6.1:	Predicted vs. observed concentration-time profiles of midazolam with ketoconazole, nilotinib, ritonavir, and rifampicin in young individuals aged 20 to 50 years.	Page 182
Figure A6.2:	Predicted vs. observed concentration-time profiles of metoprolol in poor and ultrarapid metabolizer of CYP2D6 aged 20 to 50 years.	Page 183

Figure A6.3:	Predicted vs. observed concentration-time profiles of rivaroxaban with ketoconazole and clarithromycin in young subjects aged 20 to 50 years.	Page 183
Figure A6.4:	Predicted vs. observed concentration-time profiles of repaglinide in ultrarapid metabolizers of CYP2C8, in subjects with a poor transporter phenotype of OATP1B1, with gemfibrozil, and with gemfibrozil in subjects with a poor transporter phenotype of OATP1B1.	Page 184
Figure A6.5:	Predicted vs. observed concentration-time profiles of atorvastatin with clarithromycin, with rifampicin, with etravirine, in subjects with intermediate and poor transporter phenotype of OATP1B1, and with gemfibrozil.	Page 185
Figure A6.6:	Predicted vs. observed concentration-time profiles of rosuvastatin in subjects with intermediate and poor transporter phenotype of OATP1B1, with gemfibrozil and boosted atazanavir.	Page 186
Figure A6.7:	Predicted vs. observed concentration-time profiles of nilotinib with ketoconazole and rifampicin in young adults aged 20 to 50 years.	Page 187
Figure A6.8:	Predicted vs. observed concentration-time profile of rilpivirine with efavirenz in individuals aged 20 to 50 years.	Page 187
Figure A6.9:	Predicted vs. observed concentration-time profiles of dolutegravir with atazanavir, boosted atazanavir, rifampicin, and etravirine in young adults aged 20 to 50 years.	Page 188
Figure A6.10:	Predicted vs. observed concentration-time profiles of raltegravir with ritonavir, rifampicin, efavirenz, and etravirine in young adults aged 20 to 50 years.	Page 189
Figure A6.11:	Predicted vs. observed concentration-time profiles of efavirenz in poor metabolizers of CYP2B6 and with rifampicin in young adults aged 20 to 50 years.	Page 190
Figure A6.12:	Predicted vs. observed concentration-time profile of etravirine with clarithromycin in young individuals aged 20 to 50 years.	Page 190
Figure A6.13:	Peak concentration ratio normalized to the youngest investigated age group (20 to 24 years).	Page 191
Figure A6.14:	Time to peak concentration ratio normalized to the youngest investigated age group (20 to 24 years).	Page 192

Figure A6.15:	Clearance ratio normalized to the youngest investigated age group (20 to 24 years).	Page 193
Figure A6.16:	Apparent volume of distribution ratio normalized to the youngest investigated age group (20 to 24 years).	Page 194
Figure A6.17:	Elimination half-life ratio normalized to the youngest investigated age group (20 to 24 years).	Page 195
Figure 7.1:	Verification of the developed effective method to estimate uncharacterized DDI magnitudes.	Page 206
Figure 7.2:	Predicted vs. observed AUC ratios for competitive inhibition, mechanism-based inhibition and induction.	Page 210
Figure 7.3:	Comparison of predicted and observed AUC ratios for the five victim drugs zolpidem ($DPI_{3A} = 0.303$ [0.065, 0.661]), macitentan ($DPI_{3A} = 0.524$ [0.200, 0.810]), maraviroc ($DPI_{3A} = 0.792$ [0.559, 0.998]), triazolam ($DPI_{3A} = 0.966$ [0.898, 1.0]) and simvastatin ($DPI_{3A} = 0.979$ [0.916, 1.0]) administered together with the four CYP3A inhibitors cimetidine ($lnR_{3A} = 0.256$ [0.049, 0.570]), fluconazole ($lnR_{3A} = 0.700$ [0.403, 0.893]), itraconazole ($lnR_{3A} = 0.877$ [0.691, 0.986]) and ritonavir ($lnR_{3A} = 0.963$ [0.873, 1.0]).	Page 211
Figure 7.4:	Comparison of the predicted and observed AUC ratio plus standard deviations for the two victim drugs with intrinsic inhibitory (ritonavir) and inducing (etravirine) properties administered together with the three CYP3A inhibitors cimetidine ($lnR_{3A} = 0.256$ [0.049, 0.570]), fluconazole ($lnR_{3A} = 0.700$ [0.403, 0.893]) and ketoconazole ($lnR_{3A} = 0.943$ [0.823, 1.0]).	Page 212
Figure 7.5:	DDI magnitudes between tyrosine kinase inhibitors with increasing DPI_{3A} and the potent CYP3A inhibitor ritonavir predicted by running 10,000 Monte Carlo simulations.	Page 213
Figure 7.6:	DDI magnitudes between tyrosine kinase inhibitors with increasing DPI_{3A} and the moderate CYP3A inducer etravirine predicted by running 10,000 Monte Carlo simulations.	Page 214

List of Tables

Table 1.1:	Antiretroviral drugs currently in use, their antiretroviral drug classes, and targets.	Page 12
Table 2.1:	System parameter necessary to describe a population of interest.	Page 29
Table 2.2:	Descriptive equations and population variability for anatomical, physiological, and biological parameters necessary to inform a PBPK model.	Page 33
Table 3.1:	Parameters required for a drug file to inform the PBPK model.	Page 64
Table 3.2:	Observed vs. predicted pharmacokinetic parameters for rivaroxaban (10 mg; single) in combination with ritonavir (600 mg once daily) and boosted darunavir (800/100 mg once daily), darunavir (800 mg once daily) boosted with ritonavir (100 mg once daily).	Page 83
Table A3.1:	Parameters with their abbreviation and units used to build the PBPK model.	Page 84
Table A3.2:	Subscripts and their abbreviation used to build the PBPK model.	Page 85
Table 4.1:	Parameter of the simulated non-HIV drugs.	Page 94
Table 4.2:	Published clinical studies used to verify the developed PBPK models.	Page 97
Table 4.3:	Studies for non-HIV drugs used to verify the derived age-related relationships of pharmacokinetic parameters	Page 100
Table 4.4:	Observed vs. predicted pharmacokinetic parameters for non-HIV drugs in young and elderly individuals.	Page 103
Table 4.5:	Results of the Pearson correlation for continuous variables to explain age-related pharmacokinetic changes of the clinical data for 52 drugs additionally collected.	Page 112
Table 5.1:	Published clinical studies for antiretroviral drugs used to verify the developed PBPK models.	Page 127
Table 5.2:	Parameters of the simulated antiretroviral drugs.	Page 129
Table 5.3:	Studies used to investigate the impact of ethnicity on age-related pharmacokinetic changes.	Page 132

Table 5.4:	Observed vs. predicted pharmacokinetic parameters of antiretroviral drugs for young (20 to 50 years) and elderly adults (55 to 85 years).	Page 134
Table 5.5:	P-values to analyze the differences in regression slopes of relative age-related pharmacokinetic changes for men and women by a t-test.	Page 140
Table 5.6:	Fold change (95% confidence interval) between the age of 85 years and 20 years for non-HIV and antiretroviral drugs.	Page 142
Table 6.1:	Comparison of DDI magnitudes of amlodipine, atorvastatin, and rosuvastatin combined with boosted darunavir in young (20 to 50 years) and aging individuals (56 to 80 years).	Page 154
Table 6.2:	Published clinical studies used to verify drug-drug interaction predictions of our developed PBPK model.	Page 159
Table 6.3:	Parameters of ketoconazole (KTZ), nilotinib (NIL), gemfibrozil (GEM), and its glucuronide metabolite (GEU).	Page 162
Table 6.4:	Published clinical studies used to verify the developed PBPK models for raltegravir, ketoconazole, nilotinib, and gemfibrozil.	Page 163
Table 6.5:	Published studies comparing DDI magnitudes between young and elderly study participants.	Page 166
Table 6.6:	Observed vs. predicted pharmacokinetics in the absence and presence of the perpetrator in young (20 to 50 years) and aging individuals (at least 55 years).	Page 167
Table 6.7:	Observed vs. predicted parameters for young (20 to 50 years) and elderly (at least 65 years) adults.	Page 171
Table 6.8:	Predicted vs. observed AUC of the control and DDI scenario and the AUC-ratio (DDI scenario / control scenario).	Page 172
Table 6.9:	Slope of mean prediction for DDI magnitudes across adulthood (20 to 99 years).	Page 174
Table A6.1:	Observed vs. predicted drug pharmacokinetics in the control (victim in the absence of the perpetrator or extensive metabolizers/transporter phenotype) and DDI (victim in the presence of the perpetrator or different phenotype) scenario and the DDI ratio (DDI scenario / control scenario).	Page 196

Table 7.1:	Calculated fraction of the disposition pathway mediated by CYP3A (DPI_{3A}) of victim drugs sorted by their CYP3A sensitivities.	Page 207
Table 7.2:	Calculated inhibitor (InR_{3A}) and inducer (IcR_{3A}) ratios sorted by their strengths.	Page 209

Classes at the University of Basel

Class name	Semester	Mark	Credit points
Advances in Infection Biology, Epidemiology and Global Public Health	FS 2017	PASS	1
Drug Sciences	FS 2017	PASS	1
Infection Biology – from in vitro models to human patients	HS 2017	PASS	1
Molecular Medicine	HS 2017	PASS	2
Introduction to R	HS 2017	PASS	2
Good Clinical Practice	HS 2017	PASS	1
Quantitative Systems Pharmacology	HS 2017	PASS	2
Good Scientific Practice	FS 2018	PASS	1
Translational Cancer Research	FS 2018	PASS	2
Applied Statistics Using R	FS 2018	PASS	1
Molecular Virology	HS 2018	PASS	2
Critical Appraisal of Published Clinical Studies	HS 2018	-	-
From Bench to Bedside	FS 2019	PASS	1
The Messenger is the Message	HS 2019	PASS	1
Making of a Drug	HS 2019	PASS	2
			20

Felix Stader

E-Mail: Felix.Stader@usb.ch

Address: Universitätsspital Basel
- Infektiologie und Spitalhygiene -
Petersgraben 4
4051 Basel
Switzerland

Professional Experience

since 04/2020:	Post-doc University Hospital Basel, Basel, Switzerland
02/2017 – 03/2020:	PhD candidate University Hospital Basel, Basel, Switzerland
03/2016 – 01/2017:	Research Associate Certara UK Ltd., Sheffield, United Kingdom
09/2014 – 02/2016:	Research Assistant Certara UK Ltd., Sheffield, United Kingdom
01/2014 – 05/2014:	Research Assistant Helmholtz-Institute of Pharmaceutical Research, Saarbrücken, Germany
03/2011 – 10/2013:	Several Student Assistant Posts Westfälische Wilhelms-University, Münster, Germany

Higher Education

- 03/2020: Doctor of Philosophy (PhD) in Medical Biological Research
University of Basel, Basel, Switzerland
- 02/2017 – 03/2020: Doctor of Philosophy (PhD) studies in Medical-Biological Research
University of Basel, Basel, Switzerland
- 09/2013: Master of Sciences in Pharmaceutical Science
- 10/2011 – 09/2013: Master studies in Pharmaceutical Science
Westfälische Wilhelms-University, Münster, Germany
- 08/2011: Bachelor of Science in Biology
- 10/2008 – 08/2011: Bachelor studies in Biology
Westfälische Wilhelms-University, Münster, Germany

Abilities

Knowledge of languages: German (native) and English (C1)

Knowledge in MS Office (very good), SimCYP (very good), Matlab (good), R (basic)

GCP certificate for investigators and study teams for Switzerland (acquired on the 19th of January 2018 in Basel)

Publications

Stader F, Courlet P, Kinvig H, Penny MA, Decosterd LA, Battegay M, Siccardi M, & Marzolini C.

Clinical data combined with modelling and simulation indicate unchanged drug-drug interaction magnitudes in the elderly.

Clinical Pharmacology & Therapeutics, 2020. [Epub ahead of print].

Marzolini C, **Stader F**, Stoeckle M, Franzeck F, Egli A, Bassetti S, Hollinger A, Osthoff M, Weisser M, Gebhard CE, Baettig V, Khanna N, Tschudin-Sutter S, Mueller D, Hirsch HH, Battegay M, & Sendi P.

Effect of systemic inflammatory response to SARS-CoV-2 on lopinavir and hydroxychloroquine plasma concentrations.

Antimicrobial Agents & Chemotherapy, 2020. [Epub ahead of print].

Stader F, Khoo S, Stoeckle M, Back D, Hirsch H, Battegay M, & Marzolini C.

Stopping lopinavir/ritonavir in COVID-19 patients: Duration of the drug interacting effect.

The Journal of Antimicrobial Chemotherapy, 2020. [Epub ahead of print].

Stader F, Courlet P, Kinvig H, Battegay M, Decosterd LA, Penny MA, Siccardi M, & Marzolini C.

Effect of ageing on antiretroviral drug pharmacokinetics using clinical data combined with modelling and simulation.

The British Journal of Clinical Pharmacology, 2020. [Epub ahead of print].

Pan X*, **Stader F***, Abduljalil K, Gill KL, Johnson T, Gardner I, & Jamei M.

Development and application of a physiologically based pharmacokinetic model to predict the pharmacokinetics of therapeutic proteins in neonates, infants, and children.

The AAPS Journal, 2020, [Epub ahead of print].

*contributed equally to this work

Stader F, Decosterd LA, Stoeckle M, Cavassini M, Battegay M, Saldanha SA, Marzolini C, Courlet P, & the Swiss HIV Cohort Study.

Aging does not impact drug-drug interaction magnitudes with antiretrovirals: a Swiss HIV Cohort Study. AIDS, 2020. 34(6): 949-952.

Stader F, Kinvig H, Penny MA, Battegay M, Siccardi M, & Marzolini C.

Physiologically based pharmacokinetic modelling to identify pharmacokinetic parameters driving drug exposure changes in the elderly.

Clinical Pharmacokinetics, 2020. 59(3): 383-401.

Courlet P, **Stader F**, Guidi M, Saldanha SA, Stoeckle M, Cavassini M, Battegay M, Buclin T, Decosterd LA, Marzolini C, & Swiss HIV Cohort Study.

Pharmacokinetic profiles of boosted darunavir, dolutegravir and lamivudine in aging people living with HIV.

AIDS, 2020. 34(1): 103-108.

Stader F, Penny MA, Siccardi M, & Marzolini C.

A comprehensive framework for physiologically based pharmacokinetic modelling in Matlab®.

CPT Pharmacometrics & Systems Pharmacology, 2019. 8(7): 444-459

Stader F, Siccardi M, Battegay M, Kinvig H, Penny MA, & Marzolini C.

Repository describing an aging population to inform physiologically based pharmacokinetic models considering anatomical, physiological, and biological age-dependent changes.

Clinical Pharmacokinetics, 2019. 58(4): 483-501.

Stader F, Kinvig H, Battegay M, Khoo S, Owen M, Siccardi M, & Marzolini C.

Analysis of clinical drug-drug interaction data to predict magnitudes of uncharacterized interactions between antiretroviral drugs and comedications.

Antimicrobial Agents & Chemotherapy, 2018. 62(7): 1-12.

Stader F, Wuerthwein G, Groll AH, Vehreschild JJ, Cornely OA, & Hempel G.

Physiology-based pharmacokinetics of caspofungin for adults and paediatrics.

Pharmaceutical Research, 2015. 32(6): 2029-2037.

Contributions to Scientific Conferences

Conference on Retrovirus and Opportunistic Infections (CROI), March 2020, Boston (MA), USA

Poster presentation: Aging does not impact drug-drug interaction magnitudes involving antiretroviral drugs.

Stader F., Courlet P, Kinvig H, Battegay M, Decosterd LA, Penny MA, Siccardi M, & Marzolini C.

European AIDS Clinical Society (EACS) Conference, November 2019, Basel, Switzerland

Mini lecture: Are there gender and age differences in antiretroviral pharmacokinetics?

Stader F.

American Conference of Pharmacometrics (ACoP), October 2019, Orlando (FL), USA

Poster presentation: Aging does not impact the magnitude of drug-drug interactions – a proof of concept study using physiologically based pharmacokinetic modelling.

Stader F., Kinvig H, Penny MA, Battegay M, Siccardi M, & Marzolini C.

Population Approach Group Europe (PAGE) Meeting, June 2019, Stockholm, Sweden

Poster presentation: Physiologically based pharmacokinetic modelling to identify pharmacokinetic parameters driving age-related changes in drug exposure in the elderly.

Stader F., Kinvig H, Penny MA, Battegay M, Siccardi M, & Marzolini C.

International Workshop on Clinical Pharmacology of HIV, Hepatitis and Other Antiviral Drugs, May 2019, Noorwijk, The Netherlands

Oral presentation: Physiologically based pharmacokinetic modelling to determine pharmacokinetic alterations driving ritonavir exposure changes in aging people living with HIV.

Stader F., Kinvig H, Penny MA, Battegay M, Siccardi M, & Marzolini C.

Conference on Retrovirus and Opportunistic Infections (CROI), March 2019, Seattle (WA), USA

Poster presentation: Drug interaction magnitudes in young vs. elderly: example of darunavir/r + rivaroxaban.

Stader F., Siccardi M, Kinvig H, Battegay M, Penny MA, & Marzolini C.

Population Approach Group Europe (PAGE) Meeting, June 2018, Montreux, Switzerland

Poster presentation: A population database for healthy elderly to inform physiologically based pharmacokinetic models considering anatomical, physiological, and biological system parameters.

Stader F, Siccardi M, Penny MA, Kinvig H, Battegay M, & Marzolini C.

European AIDS Clinical Society (EACS) Conference, October 2017, Milan, Italy

Poster presentation: Effective approach to predict CYP3A4-mediated drug-drug interactions between antiretroviral drugs and comedications to guide dosing recommendations.

Stader F, Kinvig H, Battegay M, Khoo S, Owen A, Siccardi M, & Marzolini C.

American Conference of Pharmacometrics (ACoP), October 2016, Seattle (WA), USA

Oral presentation: Physiologically based pharmacokinetic model of erythropoietin in neonates.

Stader F, Abduljalil K, & Johnson T.

Pharmacometrics NRW Meeting, October 2013, Cologne, Germany

Oral presentation: Physiologically based pharmacokinetic model of the antifungal agent caspofungin.

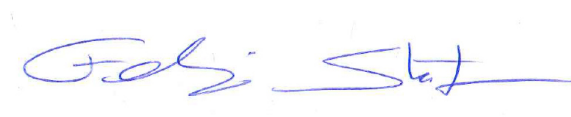
Stader F, Wuerthwein G, Groll AH, & Hempel G.

Awards and Grants

Best Poster Abstract Award from the International Workshop on Clinical Pharmacology of HIV, Hepatitis and Other Antiretroviral Drugs in May 2019

Young Investigator Scholarship, CROI 2019

Young Investigator Scholarship, CROI 2020.



08th of August 2020, Basel